GEOTECHNICAL PRACTICE PUBLICATION NO. 7

GeoChallenges

Rising to the Geotechnical Challenges of Colorado

Edited by
Christoph M. Goss, Ph.D., P.E.
Jere A. Strickland, P.E.
Richard L. Wiltshire, P.E.

ASCE

G-I GEO-INSTITUTE ASCE

GEOTECHNICAL PRACTICE PUBLICATION NO. 7

GEOCHALLENGES

RISING TO THE GEOTECHNICAL CHALLENGES OF COLORADO

PROCEEDINGS OF THE 2012 BIENNIAL GEOTECHNICAL SEMINAR

November 9, 2012
Denver, Colorado

SPONSORED BY
The Geo-Institute of the American Society of Civil Engineers

Geo-Institute Chapter of the Colorado Section of the American Society of Civil Engineers

Rocky Mountain Section of the Association of Environmental and Engineering Geologists

Colorado Association of Geotechnical Engineers

EDITED BY
Christoph M. Goss, Ph.D., P.E.
Jere A. Strickland, P.E.
Richard L. Wiltshire, P.E.

Published by the American Society of Civil Engineers

Cataloging-in-Publication Data on file with the Library of Congress.

American Society of Civil Engineers
1801 Alexander Bell Drive
Reston, Virginia, 20191-4400

www.pubs.asce.org

ISBN 978-0-7844-1263-3
Manufactured in the United States of America.

Preface

As geo-professionals, we are called to provide solutions for the many challenges that our earth presents in the areas we choose to work, play and live. From nature's geological features to our world's aging infrastructure, we are presented with the challenge of developing in areas and in ways that many thought were unbuildable or un-attainable. Yet, through the use of new technologies, modeling methods and visual mapping, geo-professionals have answered these many challenges by providing viable solutions. This book provides examples of how some in our profession have overcome these types of challenges in mining applications, tunneling, geological anomalies, alternative energy resources and infrastructure. This will highlight, again, how the geo-professional community provides solutions to the most challenging applications.

Since 1984, the Geotechnical Institute Chapter of Colorado (formally known as the ASCE Colorado Section's Geotechnical Group) in collaboration with the Rocky Mountain Section of the Association of Environmental and Engineering Geologists and the Colorado Association of Geotechnical Engineers, has organized a biennial series of geotechnical seminars on a wide variety of themes that have been attended by as many as 270 civil/geotechnical engineers, geologists, and other geo-professionals. The geotechnical seminars have been held at area universities or hotels and have offered the opportunity for sharing ideas and experiences among Colorado's diverse geo-disciplines. Since 2004, ASCE's Geo-Institute has published the papers of these seminars in Geotechnical Practice Publications, allowing the experiences to be shared with a worldwide audience.

The GeoChallenges Steering Committee convened in August 2011 and held monthly meetings to plan for the 2012 Biennial Geotechnical Seminar. The Steering Committee members included Joseph Kerrigan (Conference Chair), Dustin Bennetts, Mark Brooks, Robin Dornfest, Darin Duran, Dr. Christoph Goss, Joels Malama, Dr. Bill McCarron, Minal Parekh, Becky Roland, Keith Seaton, Jere Strickland, David Thomas, Mark Vessely Chris Wienecke, and Richard Wiltshire.

Christoph Goss, Jere Strickland, and Richard Wiltshire

Acknowledgments

The GeoChallenges Steering Committee wishes to take this opportunity to thank all of the authors and reviewers of our papers, which are herein presented as Geotechnical Practice Publication No. 7. The authors have spent many hours in preparing and finalizing their papers, which will be presented at the 2012 Biennial Geotechnical Seminar on November 9, 2012. These papers have been reviewed by a volunteer group of Denver area geo-professionals who put in their valuable time and helped make these papers even better. The Geo-Institute's Committee on Technical Publications completed its review of our GeoTrends papers in a very timely manner and their adherence to our aggressive publication schedule is greatly appreciated. We would also like to acknowledge the assistance of Donna Dickert of ASCE's Book Production Department for putting this publication together.

Author List

This page intentionally left blank

Contents

Constructing Challenges

Challenges for Debris-Flow Mitigation in Colorado: Helpful Ideas from Recent Research

Paul Santi[1], Ph.D., P.G.

[1]Professor, Department of Geology and Geological Engineering, Colorado School of Mines, 1500 Illinois St., Golden CO 80401, psanti@mines.edu

ABSTRACT: A large amount of recent research has focused on debris flow analysis, prediction, and mitigation, particularly in burned areas. Ten concepts from this work are especially applicable in Colorado. 1) Debris flows are larger and more likely to occur following wildfire, and the problem is getting worse due to climate change. 2) After wildfire, vegetation often recovers to pre-fire conditions in one to three years. 3) Volume measurement and related volume prediction methods for debris flows have much larger error ranges than is typically assumed. 4) Likewise, measurement and prediction of debris-flow velocities may easily include errors. 5) Impact forces from boulders carried by debris flows are typically overestimated. 6) Flows often occur in surges, probably from creation and breaching of small dams of material. 7) Flow paths on open slopes are unpredictable and may change rapidly following development of these small dams. 8) In burned areas, the occurrence of debris flows depends more on rainfall intensity bursts, with flows often occurring within a few minutes of 10-minute intensities exceeding threshold values, than on total storm rainfall. 9) A corollary is that debris-flow volume, as predicted from multiple-regression datasets, depends more on total rainfall than on shorter intensity ranges. 10) Many flows are comprised more of channel sediment than of materials mobilized from a single slide mass, meaning that they grow substantially in volume in transit.

INTRODUCTION

Debris flows are a common and destructive geologic hazard in Colorado. Recent debris flows have covered Interstate 70 in more than 7m of debris, have affected dozens of flow channels following alpine summer cloudbursts (e.g., Coe et al., 2007; Godt and Coe, 2007), and have influenced zoning and building locations in many mountain communities (such as Aspen, Vail, Glenwood Springs, Telluride, Ouray, and Georgetown). Recent wildfires have created conditions where numerous large and destructive debris-flow events have impacted Durango, Glenwood Springs, and Boulder (e.g., Cannon et al., 2003a; Cannon et al., 2008; Ruddy et al., 2010).

Mitigation for debris flows typically relies on systems to intercept debris, such as basins, walls, fences, and check dams; systems to guide debris past vulnerable structures, such as berms, levees and temporary barriers; and systems to reduce likelihood or volume of flows, such as mulching, revegetation after wildfire, and erosion barriers. Successful design and implementation of these systems depends on accurate estimates of a variety of debris-flow parameters, including volume, probability of occurrence, velocity, discharge rate, flow path direction and extent, triggering events, and fluid properties of the flow. Recent research has addressed many of these parameters, improving the accuracy of their prediction, raising awareness of typical pitfalls, and enhancing our understanding of the processes and our potential for influencing them. The goal of this paper is to review ten areas where recent research and field observations may be especially useful for mitigation of debris-flow hazards in Colorado.

1) THE GROWING, BURNING PROBLEM

Debris flows are larger and more likely to occur following wildfire, and the problem is getting worse due to climate change. Following wildfire, there is more erosion and runoff because of loss of vegetation (reducing interception, infiltration, root strength and resistance to raindrop impact), temporary development of hydrophobic and ash layers which further limit water infiltration, and heat fusing of soil into coarser and less cohesive aggregates that are more easily eroded (Martin and Moody, 2001; Shakesby and Doerr, 2006; Santi et al., in press).

NASA estimates that there are over 6000 fires burning every day in July, August, and September (NASA, 2012). Climate change over the latter half of the last century has led to an increase in the number of wildfires and the length of the fire season (2.5 months longer in 2006 than in 1987) (Westerling et al. 2006). Despite the possible influence of fire suppression, exclusion and fuel treatment, wildfire area burned is substantially controlled by climate (Littell et al. 2009). Grissino-Mayer et al. (2004) state that fire severity, frequency, and extent are expected to change drastically in coming decades in response to changing climate conditions.

Climate change models show an increase in temperatures that will lead to more wildfires, but they also show a significant change in the precipitation patterns with more intense storms that can trigger post-wildfire debris flows. For example, in climate model results presented by Snyder and Sloan (2005), the trends predicted specifically for California show that there will be large increases in intense precipitation. Heavy rainfall events have become more frequent over the past 50 years, even in locations where the mean precipitation has decreased or is unchanged (Chen and Knutson, 2008). Allen and Soden (2008) believe that this amplification of rainfall extremes is bound to be larger than that predicted by models, implying that projections of future rainfall extremes in response to anthropogenic global warming may be underestimated.

Debris flows in burned areas are larger than flows in the same areas before the burn or after recovery. For example, Figure 1 shows data from 276 sites in the Western U.S., compiled by Santi and Morandi (in review), where the median yield rate (volume of debris per unit area of drainage basin) for burned areas is over twice the rate for unburned areas. Debris flows can be triggered by much lower rainfall amounts and intensity in burned areas than in unburned areas, as shown in Figure 2 (Cannon and DeGraff, 2009).

2) THE PLANTS COME BACK

After wildfire, vegetation often recovers to pre-fire conditions in one to three years. For example, Figure 3 plots data showing vegetation represented as decreasing bare soil exposed for different burn severities (from Benavides-Solario and MacDonald, 2005). Assuming that typical Colorado mountain regions have a range of up to 20 to 30 percent bare soil, vegetative recovery appears to take approximately three years. As plant regrowth will reduce hillslope sediment erosion, researchers have shown that the sediment delivery returns to pre-fire rates within 2 to 4 years in the Rockies (Martin and Moody, 2001; Legleiter et al., 2003). Extending this concept further, Santi and Morandi (in review), found that debris flow volumes return to their pre-fire magnitudes in approximately 3 to 5 years (Figure 4).

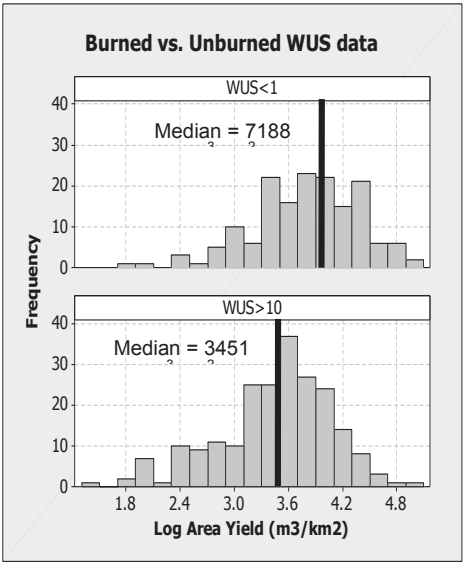

FIG. 1. Comparison of debris-flow area yield rates (volume of debris per unit area of drainage basin) for burned (WUS<1) and unburned (WUS>10) sites in the Western U.S. (Santi and Morandi, in review)

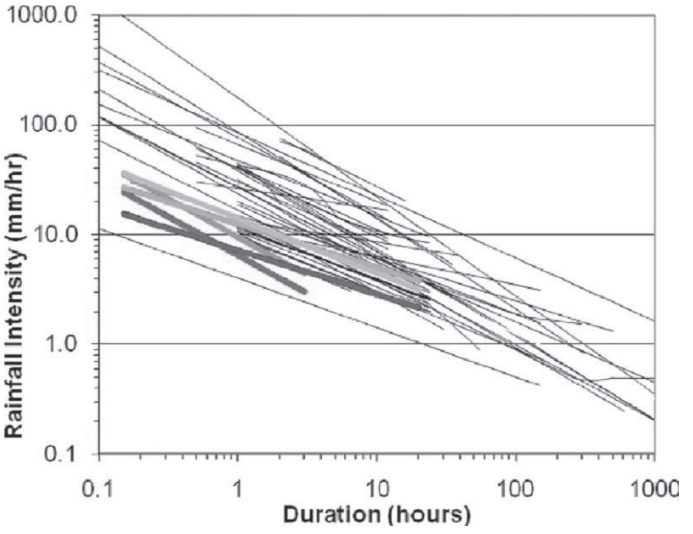

FIG. 2. Plot of various rainfall intensity/duration thresholds for unburned (fine lines) and burned (thick lines) sites worldwide (Cannon and DeGraff, 2009)

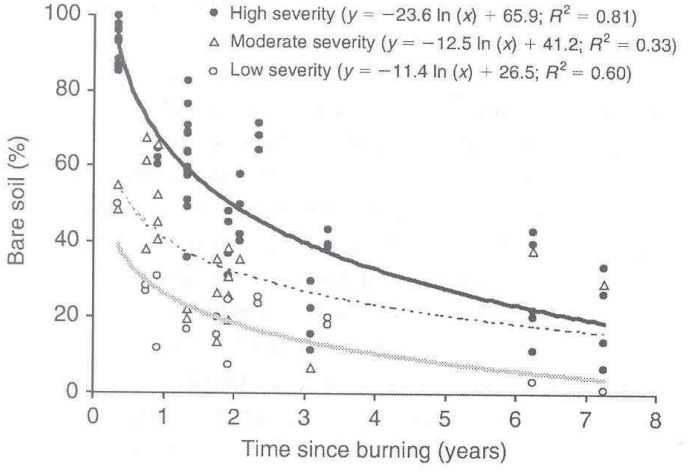

FIG. 3. Percentage of bare soil following a burn, as related to burn severity. Recovery to pre-burn conditions (70 to 80% vegetated) takes approximately 3 years (Benavides-Solario and MacDonald, 2005)

3) VOLUME PREDICTION IS HARD TO GET RIGHT

Volume measurement and related volume prediction methods for debris flows have much larger error ranges than is typically assumed. Most prediction methods are developed by creating predictive equations that best match the actual measured volumes in the database (e.g., Cannon et al., 2009). However, the error in the actual measured volumes is generally unaccounted for, and this error range is the minimum error inherent in the model.

For volumes measured by counting truck loads of removed debris, Santi and deWolfe (2005) showed that the error range is -45 to +80 percent, due to excavation of multiple events, digging below the bottom of the debris flow being measured, under- or over-loading trucks, and underestimation of the fluid portions of the flow that were carried beyond the deposit being excavated.

For debris-flow volumes measured by outlining map or air photo limits of the event by CAD and estimating the average debris thickness, Santi and deWolfe (2005) estimate error of -48 to +83 percent, due to error in judgment of flow boundaries and flow thickness, inclusion of previous events, and loss of fluid portions of the flow. Santi and deWolfe (2005) calculate an average relative percent difference of 28 percent between two agencies (U.S. Army Corps of Engineers and San Bernardino Flood Control District) that both used this method to independently measure volumes of the same ten debris flows.

Debris-flow volumes may also be measured by field GPS mapping, where errors are estimated at -27 to +37 percent (Santi and deWolfe, 2005), stemming mostly from inaccurate debris thickness estimates.

Researchers have also estimated debris-flow volumes based on channel erosion, using a series of cross-sections along the length of the flow channel (e.g., Hungr et al., 2005; Stock and Dietrich, 2006; Santi, et al., 2008). Santi and deWolfe (2005) calculate error from this method at ±23 percent, with a precision (reproducibility) of ±11 percent.

Because the input of measured debris-flow volumes is not well constrained, the output of predicted volumes using various published equations is also not well constrained. An example is shown on Figure 4, where a plot of measured versus predicted values has a range of approximately two standard errors.

4) VELOCITY PREDICTION IS ALSO HARD TO GET RIGHT

Measurement and prediction of debris-flow velocity is not as straightforward a process as it would initially appear to be. Prochaska et al. (2008a) showed that measurement of velocity in the field using superelevation (banking around bends) equations depends strongly on the scale of the media used (e.g., air photos, topographic maps, etc.) and the length of the channel section measured. Furthermore,

they note that many events reported in the technical literature would be classified as supercritical flows (Froude number, F>1), rendering the forced vortex equations inapplicable to individual cross-sections. Prochaska et al. (2008a) also show that information about material properties such as viscosity and yield strength needed for predictive equations is often very different for laboratory and field scale measurements.

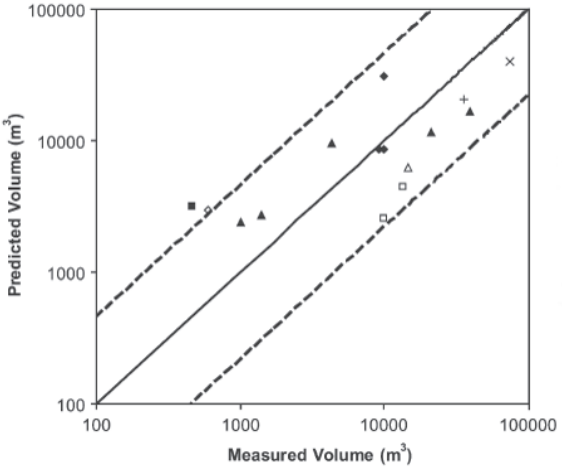

FIG. 4. Example of typical error range for predictive method to estimate debris-flow volume (Cannon et al., 2009). Solid line indicates perfect prediction and dashed lines indicate two standard errors

On the other hand, Prochaska et al. (2008a) show that because velocities are fairly consistent along the length of a debris-flow path, as is the ratio h^2S (where h is the flow depth and S is the channel slope), reasonable estimates of velocity can be made using Table 1, which was developed based on a set of reliable field velocity measurements.

Table 1. Summary of Velocity versus h^2S Data from Prochaska et al. (2008a)

Calculated Velocity Range	h^2S Range		
	$h^2S < 3\ m^2$	$3\ m^2 < h^2S < 6\ m^2$	$6\ m^2 < h^2S$
Mean – 1 Standard Deviation	3.7 m/s	4.5 m/s	7.0 m/s
Mean	6.0 m/s	6.8 m/s	10.4 m/s
Mean + 1 Standard Deviation	8.3 m/s	9.1 m/s	13.8 m/s
Mean + 2 Standard Deviations	10.6 m/s	11.4 m/s	17.2 m/s

5) IMPACT FORCES ARE NOT CONTROLLED BY THE BIG GUYS

Impact forces from boulders carried by debris flows are typically overestimated, meaning that deflection walls, bridge piers and beams, and structures may be overdesigned. Typical design guidelines recommend that impact forces should be calculated using a design boulder with a diameter equal to the predicted depth of the debris flow at that location, and traveling at the same velocity as the flow. Prochaska et al. (2008b) analyzed the size and speed of over 200 boulders in eight different video segments from around the world and found that the largest boulders in a debris flow travel at speeds less than the velocity of the flow (typically only 20 to 40 percent of the maximum flow velocity, although two videos showed velocities in the range of 60 to 70 percent of maximum). They showed that the maximum impact forces are generated by boulders approximately 45 to 85 percent of the largest particle size, and that these forces are typically 50 to 60 percent of the values calculated conventionally. These smaller boulders typically travel at 40 to 80 percent of the maximum velocity.

6) FLOWS DO NOT MOVE AS SINGLE EVENTS

Debris flows have been shown to occur in surges, probably from the creation and breaching of small dams of material in the flow channel. Using video equipment, pressure transducers, and rain gauges, McCoy et al. (2010) and McCoy et al. (2011) established three monitoring stations at Chalk Cliffs in central Colorado. During four separate storms, they tracked multiple surges within each resultant debris-flow event, where each surge had the characteristic steep bouldery snout and watery tail of a unique debris flow. One event had five surges pass an upper monitoring station, but none of these surges made it as far as a lower monitoring station, indicating that the material was deposited along some mid-channel reach. Another event produced 17 discernible surge fronts, and the deposit produced from this flow resulted in five distinct unstratified deposits. Videos of the events showed formation and rupture of in-channel debris dams that contributed to the surging nature.

These observations reveal important information about the nature of debris-flow processes. First, a given deposit is likely comprised of several surges, each which would have a lower discharge rate than a single surge producing the same total volume. Second, the formation and rupture of debris dams means that the sediment is delivered down-channel in an intermittent fashion, and that mitigation should take into account the apparent readiness of debris flows to move from a transport to a deposition regime.

7) FLOWS ON OPEN SLOPES FOLLOW UNPREDICTABLE PATHS

The propensity of debris flows to move in pulses and to create and rupture dams of material enhances the distributary nature of deposits on open slopes, where the flow has overflowed or travelled beyond a confined channel. This results in lobate deposits, even for a single debris-flow event, that spread over a debris fan into unanticipated areas. For example, Figure 5 shows two lobes of a branching debris-

flow deposit near Springville, Utah (from an event in 2003) and Figure 6 shows a flow which took an unpredictable right turn, even though it could have followed a straight, evenly-sloping paved road (from an event in Santaquin, Utah in 2002).

Similar behavior has been observed in Colorado. A debris flow in September 2002 in the Durango area, following the Missionary Ridge fire that summer, inundated a home that was located at least 62m from the an active, incised stream channel (Coe et al., 2007). A report following the event indicated that "evidence on the fan surface suggests that channels were blocked by large boulders and diverted many times during the event" (Coe et al., 2007).

While it may seem logical that a debris fan is created by migrating lobes of debris-flow deposits over time, it is easy to forget how quickly these lobes may jump from one sector of a fan to another.

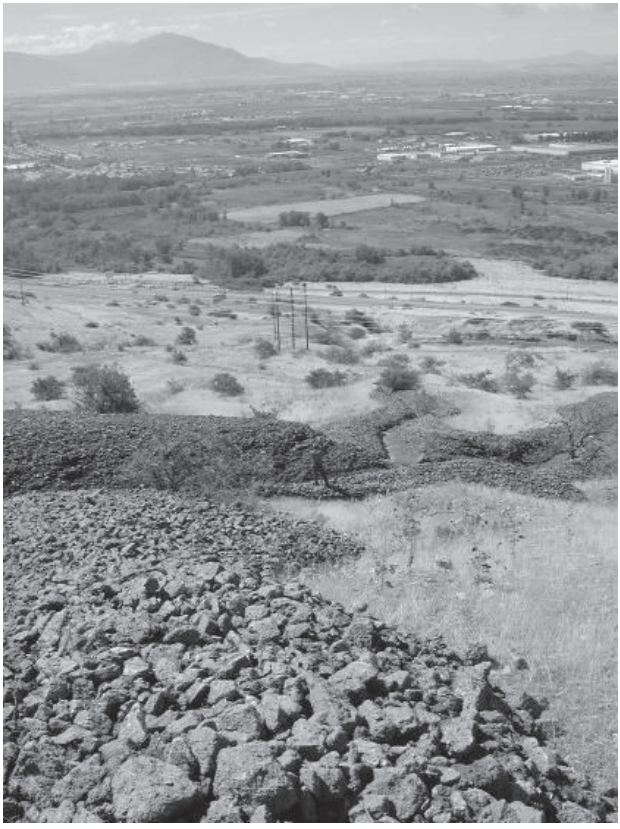

FIG. 5. Branching debris-flow deposit on open slope near Springville, Utah (photo by Rich Giraud, Utah Geological Survey)

FIG. 6. Random sharp turn in an open-slope debris flow in Santaquin, Utah in 2002 (photo by Date Deiter, USFS, originally published in Giraud, 2005)

8) INITIATION OF DEBRIS FLOWS DEPENDS ON INTENSE RAINFALL BURSTS

In burned areas, occurrence of debris flows depends more on rainfall intensity bursts, with flows often occurring within a few minutes of 10-minute intensities that exceed some threshold value, than it depends on total storm rainfall. That is, there is more than enough rainfall to provide the water needed for a debris flow, but initiating a flow requires a short and intense burst of rainfall.

Santi (2009) used a database of 46 debris flows following wildfires in California, Colorado and Utah to show that the rainstorms causing the flows generated a median of 14 times the amount of water needed to produce the typical sediment:water ratio for a debris flow (assuming the debris flows contain 20 to 40 percent water by volume, as suggested by Pierson and Costa, 1987 and O'Brien and Julien, 1985). He concluded that, even when accounting for typical infiltration rates, the supply of water to generate a debris flow was not the limiting factor.

The importance and magnitude of rainfall intensity spikes to initiate debris flows has been shown by McCoy et al. (2010), McCoy et al. (2011), Friedman and Santi (2011), and Friedman (2012), who used field instrumentation to record rainfall intensity and timing of debris flows. An example of these data is shown on Figure 7, where the time lag between rainfall intensity bursts and debris flow pulses is less than four minutes. Both Friedman (2012) and Kean et al. (in press) found that short periods of intense rainfall (typically 5-minute intensity) were responsible for debris-flow initiation. Similarly, Figure 2 shows the typical shorter and lower intensity threshold

values for debris flow initiation in recently burned areas when compared to unburned areas.

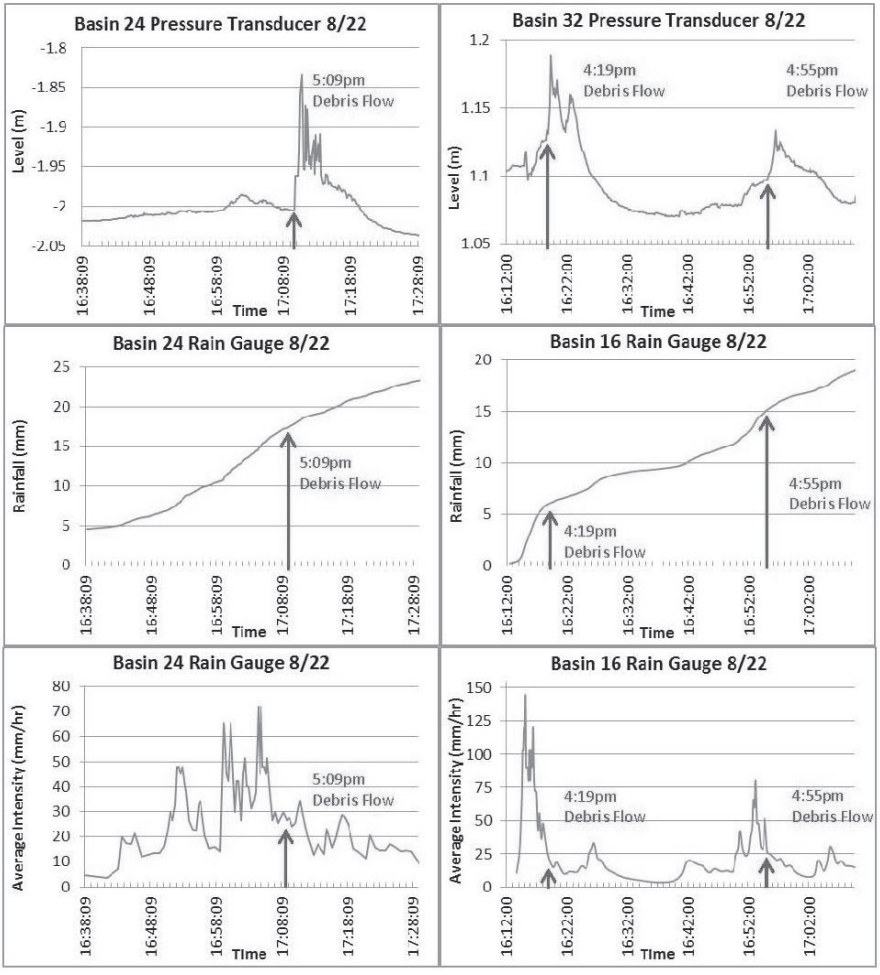

FIG. 7. Recordings of rain gauges and pressure transducers, at Medano Fire burn area, Great Sand Dunes National Park and Preserve, Colorado. Upper graphs show debris flow passage over in-channel pressure transducers. Middle graphs show cumulative rainfall and lower graphs show instantaneous rainfall intensity (Friedman, 2012)

9) TOTAL VOLUME SEEMS TO DEPEND ON TOTAL RAINFALL

A corollary to the previous observation of the role of rainfall intensity on debris-flow initiation is that debris-flow volume, as predicted from multiple-regression datasets, depends more on total storm rainfall than on shorter intensity ranges. For example, Cannon et al. (2009) recommend the following predictive equation for use in recently burned areas in the Intermountain West of the U.S.:

$$\ln V = 7.2 + 0.6(\ln A) + 0.7(B)^{1/2} + 0.2(T)^{1/2} + 0.3 \quad (1)$$

Where: V = volume (m^3)
A = drainage basin area (km^2)
B = drainage basin area burned at high and moderate severity (km^2)
T = total storm rainfall (mm)

This equation was developed using multiple regression techniques that included numerous measures of storm rainfall, including several short-term intensity values. However, the total storm rainfall was the rainfall measure that best predicted total debris-flow volume.

Another popular predictive method developed by multiple regression analysis, the Los Angeles District Debris Method (U.S. Army Corps of Engineers, 2000), is applicable to both burned and unburned areas. For smaller basins (0.25 to 7.8 km^2, or 0.1 to 3.0 mi^2), their equation relies on maximum 1-hour precipitation. While this is much shorter than total storm rainfall for many events, it is still a much longer measure than the 5- or 10-minute intensities related to debris-flow initiation. Furthermore, many of the storms that initiate debris flows are short in duration, so that maximum 1-hour precipitation levels are similar to total rainfall amounts. For example, the data presented in Gartner et al. (2005) shows 58 percent of the storms to be less than or equal to one hour in duration, and another 24 percent are between one and four hours in duration. Equations to predict debris-flow volume for larger basins using the Los Angeles District Debris Method use unit peak inflow, which is a function of average rainfall intensity over the length of the storm, also a longer term measurement of rainfall than those related to debris-flow initiation.

10) MUCH OF THE MATERIAL IS PICKED UP EN ROUTE

Many debris flows are comprised more of channel sediment than of materials mobilized from a single slide mass, meaning that they grow substantially in volume in transit. Coe et al. (2008) note that debris flows are typically mobilized in one of three ways: 1) from landslides, 2) from landslides that erode and entrain material from the hillside and flow channel as they move, and 3) from channel runoff that erodes and entrains enough sediment to become a debris flow. The authors noted that the second and third types of mobilization are quite common, they result in debris flows that are larger in volume and travel longer distances than the first type, and they are well documented in the technical literature (e.g., Rickenmann et al., 2003; Cannon et al.,

2003b; Berti and Simoni, 2005; Hungr et al., 2005; Stock and Dietrich, 2006). Figure 8 shows an example of the third mechanism, where incremental debris-flow volumes were measured by increments of channel erosion calculated from a series of channel cross-sections. In this example, the channel yield rate, measured in incremental added volume per unit channel length shows a dramatic increase partway down the channel. Santi et al. (2008) showed that these jumps in yield rate occurred in 87 percent of the 46 debris flows they measured, indicating that it is a very common phenomenon. They also noted that 52 percent of the flows had debris input from side channels that fed into the main channel, and that these side channels contributed an average of 23 percent of the total debris-flow volume. Therefore, about half of debris flows can be expected to have a branching source area and mitigation measures should take this into account.

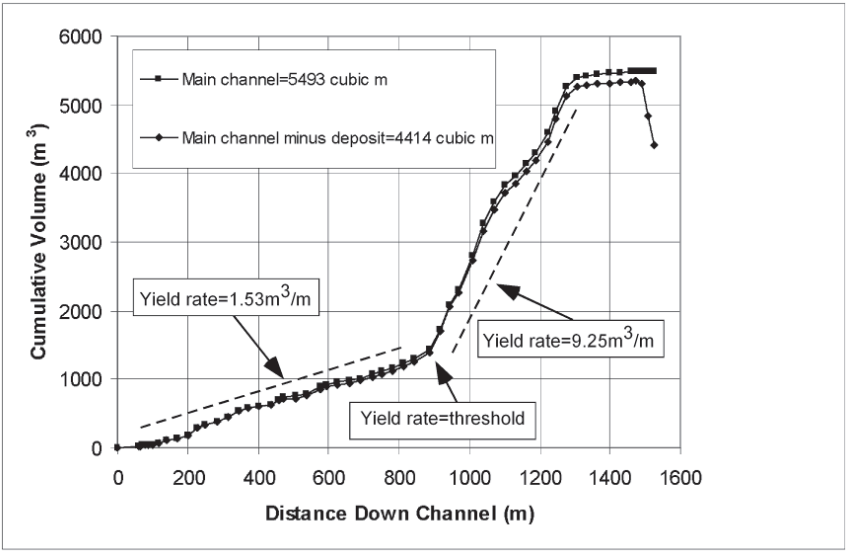

FIG. 8. Example graph showing cumulative debris-flow volume from Elkhorn Canyon near Durango, Colorado, following the 2002 Missionary Ridge Fire (Santi, 2008). Yield rate is calculated as the slope of the cumulative volume line

CONCLUSIONS: IMPLICATIONS FOR MITIGATION AND PLANNING

At present, and even more so in the future, debris-flow mitigation plans must account for the increase in likelihood and volume of events in recently burned areas, for at least a few years following the fire. Predicted debris-flow volumes and velocities for design should be done conservatively, recognizing the errors inherent in the predictive process, but prediction of impact forces can actually be done with less conservatism than is usually applied. Designers should recognize that debris flows move in multiple pulses, starting and stopping as flowpaths are dammed, broken through, and avulsed onto new paths. This problem is especially acute on open slopes

where debris flows are not channelized. It does not take a large rainstorm to initiate a debris flow, especially in recently burned areas, but larger storms tend to produce larger flows. Finally, it is important to recognize that a significant amount of debris will be entrained from channel and hillslope sediments, and possibly from side channels as well, and mitigation plans should control, reduce, and/or account for the increased volume from these sources.

ACKNOWLEDGMENTS

Much of the information research in this study was developed for projects funded by the Joint Fire Science Program (contract 03-1-4-14) and by the National Science Foundation (EAR-Geomorphology, award # 1118056), for which the author is grateful.

REFERENCES

Allan, R.P., and Soden, B.J. (2008). "Atmospheric warming and the amplification of precipitation extremes." *Science* Vol. 321: 1481-1484.

Benavides-Solario, J. and MacDonald, L.H. (2005). "Measurement and prediction of post-fire erosion at the hillslope scale, Colorado Front Range." *International Journal of Wildland Fire* Vol. 14: 1-18.

Berti, M., Simoni, A. (2005). "Experimental evidences and numerical modeling of debris flow initiated by channel runoff." *Landslides* Vol. 2: 171–182.

Cannon, S.H. and DeGraff, J.D. (2009). "The increasing wildfire and post-fire debris-flow threat in Western USA, and implications for consequences of climate change." In K. Sassa, P. Canuti (eds.), Landslides – Disaster Risk Reduction, Springer-Verlag Berlin Heidelberg, 177-190.

Cannon, S.H., Gartner, J.E., Holland-Sears, A., Thurston, B.M., Gleason, J.A. (2003a). "Debris flow response of basins burned by the 2002 Coal Seam and Missionary Ridge fires, Colorado." In: Boyer, D.D., Santi, P.M., Rogers, W.P. (Eds.), Engineering Geology in Colorado-Contributions, Trends, and Case Histories, AEG Special Publication 15 Colorado Geological Survey Special Publication 55. 31 pp., on CD-ROM.

Cannon, S.H., Gartner, J.E., Parrett, C., Parise, M. (2003b)."Wildfire-related debris flow generation through episodic progressive sediment bulking processes, western U.S.A." In: Rickenmann, D., Chen, C.L. (Eds.), Debris-Flow Hazards Mitigation: Mechanics, Prediction, and Assessment. Millpress, Rotterdam, 71–82.

Cannon, S.H., Gartner, J.E., Wilson, R.C., and Laber, J.L. (2008). "Storm rainfall conditions for floods and debris flows from recently burned areas in southwestern Colorado and southern California." *Geomorphology* Vol. 96: 250-269.

Cannon SH, Gartner, JE, Rupert MG, Michael JA, Rea AH, Parrett C (2009). "Predicting the probability and volume of post-wildfire debris flows in the intermountain western United States." *Geological Society of America Bulletin* Vol. 122: 127-144.

Chen, C-T., and Knutson, T. (2008). "On the verification and comparison of extreme rainfall indices from climate models." *Journal of Climate* Vol. 21, pp.1605-1621.

Coe, J.A., Godt, J.W., Wait, T.C., and Kean, J.W. (2007). "Field reconnaissance of debris flows triggered by a July 21, 2007, thunderstorm in Alpine, Colorado, and vicinity." U.S. Geological Survey Open-File Report 2007-1237, 25 p.

Coe, J. A., Cannon, S.H., and Santi, P.M. (2008). "Introduction to the special issue on debris flows initiated by runoff, erosion, and sediment entrainment in western North America." *Geomorphology* Vol. 96: 247-249.

Coe, J.A. (ed), Bigio, E.R., Blair, R.W., Burke, M., Cannon, S.H., deWolfe, V.G., Ey, J., Gartner, J.E., Gillam, M. L., Knowlton, N.D., Santi, P.M., and Schulz, W.H. (2007). "Mass wasting following the 2002 Missionary Ridge Fire near Durango, Colorado, a field trip guidebook." U.S. Geological Survey Open File Report 2007-1289 and AEG Special Publication No. 20, 54 p.

Friedman, E.Q. (2012). "Debris-flow hazard assessment and monitoring within the 2010 Medano Fire burn area, Great Sand Dunes National Park and Preserve, Colorado." unpublished MS thesis, Colorado School of Mines, 115 p.

Friedman, E.Q and Santi, P.M. (2011). "Debris-Flow Hazard Assessment for the 2010 Medano Pass Fire burn area, Great Sand Dunes National Park and Preserve, Colorado." Association of Environmental and Engineering Geologists 54th Annual Meeting Program with Abstracts, Anchorage, AK.

Gartner, J. E. , Cannon, S. H. , Bigio, E. R. , Davis, N. K. , Parrett, C. Pierce, K.L. , Rupert, M. G. , Thurston, B. L. , Trebish, M. J. , Garcia, S. P., and Rea, A. H. (2005). "Compilation of data relating to the erosive response of 606 recently burned." U.S. Geological Survey Open-File Report 2005-1218.

Giraud, R.E. (2005). "Guidelines for the geologic evaluation of debris-flow hazards on alluvial fans in Utah." Miscellaneous Publication 05-6, Utah Geological Survey, 16 p.

Godt, J.W. and Coe, J.A. (2007). "Alpine debris flows triggered by a 28 July 1999 thunderstorm in the central Front Range, Colorado." *Geomorphology* Vol.. 84: 80-97.

Grissino-Mayer, H.D., Romme, W.H., Floyd, L.M., Hanna, D.D. (2004). "Climatic and human influences on fire regimes of the southwestern San Juan Mountains, Colorado, USA." *Ecology* Vol. 85: 1708-1724.

Hungr, O., McDougall, S., Bovis, M. (2005). "Entrainment of material by debris flows." In: Jakob, M., Hungr, O. (Eds.), Debris-flow Hazards and Related Phenomena. Springer, Berlin Heidelberg, 135–158.

Kean J.W., Staley, D.M., Leeper, R.J., Schmidt, K.M., and Gartner, J.E. (in press). "A low cost method to measure the timing of post-fire flash floods and debris flows relative to rainfall." *Water Resources Research*.

Legleiter, C.J., Lawrence, R.L., Fonstad, M.A., Marcus, W.A., Aspinall, R. (2003). "Fluvial response a decade after wildfire in the northern Yellowstone ecosystem: a spatially explicit analysis." *Geomorphology* Vol. 54: 119-136.

Littell, J.S., McKenzie, D., Peterson, D.L., Westerling, A.L. (2009). "Climate and wildfire area burned in western U.S. ecoprovinces, 1916-2003." *Ecological Applications* Vol. 19: 1003–1021.

Martin, D.A. and Moody, J.A. (2001). "Comparison of soil infiltration rates in burned and unburned mountainous watersheds." *Hydrological Processes* Vol. 15: 2893-2903.

McCoy, S.W., Kean, J.W., Coe, J.A., Staley, D.M., Wasklewicz, T.A., Tucker, G.E. (2010). "Evolution of a natural debris flow: In situ measurements of flow dynamics, video imagery, and terrestrial laser scanning." *Geology* Vol. 38: 735-738.

McCoy, S. W. , Coe, J. A. , Kean, J. W. , Tucker, G. E. , Staley, D. M. , and Wasklewicz, T. A. (2011). "Observations of debris flows at Chalk Cliffs, Colorado, U.S.A.: Part 1, in situ measurements of flow dynamics, tracer particle movement and video imagery from the summer of 2009." in Genevois, R., Hamilton, D.L., and Prestininzi, A., eds., Proceedings of the 5th International Conference on Debris Flow Hazards Mitigation, Mechanics, Prediction and Assessment, Padua, Italy, June 14-17, 2011, Italian Journal of Engineering Geology and Environment and Casa Editrice Universita La Sapienza, Rome, Italy, 715-724.

NASA (2012). "Earth Observatory." http://earthobservatory.nasa.gov/, accessed May 3, 2012.

O'Brien, J. S. and P. Y. Julien. (1985) "Physical properties and mechanics of hyperconcentrated sediment flows." Proc. ASCE Hyd. Div. Spec. Conf. on Delineation of Landslides, Flash Flood and Debris Flow Hazards, Logan Utah, June 1984, 260-279.

Pierson, T.C., and Costa, J.E. (1987). "A rheologic classification of subaerial sediment-water flows." *Geological Society of America Reviews in Engineering Geology* Vol. 7: 1-12.

Prochaska, A.B., Santi, P.M., Higgins, J.D., and Cannon, S.H. (2008a). "A study to estimate debris flow velocity." *Landslides* Vol. 5: 431-444.

Prochaska, A.B., Santi, P.M., and Higgins, J.D. (2008b). "Relationships between size and velocity for particles within debris flows." *Canadian Geotechnical Journal* Vol. 45: 1778-1783.

Rickenmann, D., Weber, D., Stepanov, B. (2003). "Erosion by debris flows in field and laboratory experiments." In: Rickenmann, D., Chen, C. (Eds.), Debris Flow Hazards Mitigation: Mechanics, Prediction, and Assessment. Millpress, Rotterdam, The Netherlands, 883–894.

Ruddy, B.C., Stevens, M.R., Verdin, K.L., and Elliott, J.G. (2010). "Probability and volume of potential postwildfire debris flows in the 2010 Fourmile burn area, Boulder County, Colorado." U.S. Geological Survey Open-File Report 2010–1244, 5 p.

Santi, P.M. and deWolfe, V.G. (2005). "Comparisons of Debris Flow Volume Measurements and Predictions." Association of Environmental and Engineering Geologists 48th Annual Meeting Program with Abstracts, Las Vegas, NV.

Santi, P.M. and Morandi, L. (in review). "Comparison of Debris-Flow Volumes from Burned and Unburned Areas." *Landslides*.

Santi, P.M., Cannon, S.H., and DeGraff, J.D. (in press). "Wildfire and landscape change." in Shroder, J., ed., Treatise on Geomorphology, Elsevier.

Santi, P.M., deWolfe, V.G., Higgins, J.D., Cannon, S.H., Gartner, J.E. (2008). "Sources of debris flow material in burned areas." *Geomorphology* Vol. 96: 310-321.

Santi, P.M. (2009). "Water availability and debris flow generation in burned areas." Geological Society of America Annual Meeting Abstracts with Programs.

Shakesby, R.A. and Doerr, S.H. (2006). "Wildfire as a hydrological and geomorphological agent." *Earth Science Reviews* Vol. 74: 269-307.

Snyder, M.A., and Sloan, L.C. (2005). "Transient future climate over the Western United States using a regional climate model." *Earth Interactions* Vol. 9: 1-21.

Stock, J.D., Dietrich,W.E. (2006). "Erosion of steepland valleys by debris flows." *Geological Society of America Bulletin* Vol. 118: 1125–1148.

USACE (2000). "US Army Corps of Engineers Los Angeles District Debris Method." Los Angeles District Hydraulics and Hydrology Branch, 39 pp.

Westerling, A.L., Hidalgo, H.G., Cayan, D.R., Swetnam, T.W. (2006). "Warming and earlier spring increase western U.S. forest wildfire activity." *Science* Vol. 313: 940-943.

Debris-flow Hazard Assessment and Model Validation, Medano Fire, Great Sand Dunes National Park and Preserve, Colorado

Evan Friedman[1], E.I., and Paul Santi[2], Ph.D., P.G.

[1]Geotechnical Engineer, Hatch Mott MacDonald, 198 Union Blvd., Lakewood, CO 80401; efriedma@mines.edu
[2]Professor, Colorado School of Mines, 1500 Illinois St., Golden, CO 80401; psanti@mines.edu

ABSTRACT: A debris-flow hazard assessment was conducted for the Medano Creek Watershed, at Great Sand Dunes National Park and Preserve, in response to the 2010 Medano Fire that burned approximately 24 square kilometers (6,000 acres) in and around the preserve. Debris-flow probability and volume predictions were made using four empirical regression models and geographic information system (GIS) data and tools. Model parameters include burn severity, rainfall intensity, topographic characteristics, and soil properties. Data was collected and analyzed on the basin scale from burned tributaries of Medano Creek. Model results provided the park's resource managers with information on potential basin-specific hazards to roads, campsites, and park visitors. Monitoring of the first significant rainfall events following the fire and the resulting debris-flow responses throughout the spring, summer, and fall of 2011 provided means for model validation. Of the three probability models utilized, two predicted high probability of debris flow occurrence for all basins that produced debris flows, with numerous false positives, while the third failed to predict high probability in any of the basins. The volume model predicted volumes within approximately one order of magnitude higher than those measured.

INTRODUCTION

Debris flows are often observed in mountainous burned areas in response to rainstorms shortly after wildfires. Their increase in frequency can be attributed to increases in runoff and erosion of material affected by the fire, which are most dramatic in the year or two following the fire (Cannon and Gartner, 2005). The destructive power of debris flows poses a hazard to roads and structures, and can endanger human life. Rapid assessment of debris-flow hazards before the first intense rainfall events following a wildfire is important for planning efforts to avoid or mitigate potential hazards.

The Medano Fire occurred in June and July of 2010 in Medano Creek Watershed, burning approximately 24 square kilometers (6000 acres), mainly within the Great Sand Dunes National Preserve in the Sangre de Cristo Range of south-central Colorado (Figure 1). The wildfire occurred near the end of the summer rainfall season, and the rainstorms that followed were lower in average intensity than the 2-year recurrence interval, 1-hour duration storm for the area (Miller et al., 1973). These storms triggered minor ashy sediment-laden floods, which primarily transported fine sand (as mapped by Kirkham, 2010). An early thaw of the thin winter snowpack in the watershed, mainly before March 2011, was followed by a dry spring. In July 2011, approximately one year after the fire, a series of short-duration and high-intensity convective thunderstorms delivered rain to the watershed, triggering debris flows and ashy, sandy hyper-concentrated floods. Flow events occurred in response to several rainstorms during July and August, before storm intensity weakened in the fall. The spring, summer, and fall of 2011 provided an ideal opportunity to assess the debris-flow hazard in the burned area, and monitor flood and debris-flow activity in response to the first intense storms since the fire.

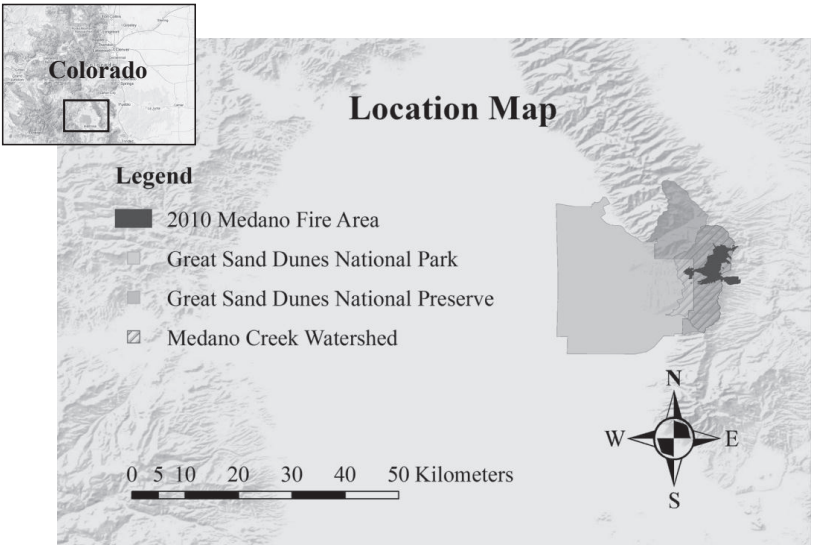

FIG. 1. Location map of the Medano Fire in the Sangre de Cristo Range, at Great Sand Dunes National Park and Preserve, Colorado

This research includes assessment of the debris-flow hazard in the burned tributary basins of Medano Creek Watershed (Figure 1), and monitoring of debris-flow activity in the spring, summer, and fall of 2011 following the fire to validate models used for hazard assessment. Debris-flow probability and volume predictions were made based on implementation of several empirical regression models developed by Gartner et al. (2008) and Cannon et al. (2009) for the intermountain western U.S., in a GIS

platform. The models integrate measures of burn severity, storm rainfall conditions, topographic characteristics, and soil properties to provide hazard estimates for the burned basins of Medano Creek Watershed. Model results provided the park's resource managers with information on potential basin-specific hazards to roads, campsites, facilities, and park visitors, and aided in selection of basins for installation of debris-flow monitoring equipment. Instrumented monitoring and field mapping of geomorphic response to rainfall events in the burn area provided a means for evaluating model validity in this setting, as well as documenting the hydrologic response of each basin.

BACKGROUND

Debris flows are transient mass movement events that involve the fluid movement of a large volume of highly concentrated viscous water-debris mixture down stream channels, generally in response to intense rainfall. Debris flows pose a greater hazard than other flows because of their unique destructive power (Cannon et al., 2003b). The large volumes of material generated from these flows can exert great impulsive loads (Cannon et al., 2003b) and can inundate areas downstream with sediment, damaging structures and endangering human life.

Much previous research has been focused on predicting the probability and potential volume of debris flows from both burned and unburned watersheds (e.g. Chen and Jan, 2000; Laigle and Marchi, 2000; Lin et al., 2000; Bianco and Franzi, 2000; Gartner et al., 2008; Rupert et al., 2008; and Cannon et al., 2009). Some of these efforts have produced multivariate regression models that can be used to predict the probability and potential volume of debris-flow occurrences in burned basins, using GIS tools and readily available data (e.g. Gartner et al., 2008; Rupert et al., 2008; and Cannon et al., 2009). In this study, debris-flow probability and volume models for burned areas in the intermountain western U.S., presented by Cannon et al. (2009), will be used to assess the hazards at a location with geologic and morphologic characteristics unlike those used to develop and test the model previously. Comparison of observed response with model results will provide feedback on the predictive ability of the models in this specific environment, and provide data for future development of regional or local scale models.

This is a unique geologic setting for this type of study, due to the influence of abundant eolian sand on the soil morphology. The study site is also a pristine natural watershed in a wilderness area, within a mountain range that has not yet been studied for debris-flow characteristics. This research presents an opportunity to validate regression models used for hazard assessment against a sample of basins outside the population used to develop the models, providing insight into their predictive accuracy and potential improvements.

Geologic Setting

The Medano Fire occurred almost entirely within the Medano Creek Watershed on the west side of the northern Sangre de Cristo Range. Medano Creek flows from headwaters on the east side of Mount Herard (4069 meters [13,350 feet] elevation), cutting into Proterozoic leucocratic gneiss then crossing over the Little Sand Creek Thrust Fault twice, first onto the overthrust Crestone Conglomerate Member of Permian and Pennsylvanian age, then back across onto Proterozoic gneiss intruded by various magma bodies (Johnson et al., 1989). Where the creek emerges from its canyon it turns south and runs between pediment surfaces to the east and the high dunes of the Great Sand Dunes complex to the west. Several kilometers further downstream, depending on the seasonal flow, the creek disappears into the eolian sand and thick basin sediments of the eastern San Luis Valley.

The large deposit of eolian sand at the Great Sand Dunes complex plays a significant role in the morphology and sediment transport processes of the Medano Creek Watershed. The same prevailing westerly winds that deposited the eolian sand at the embayment in the Sangre de Cristo Range, also transport sand up the valley of Medano Creek and over basin divides. The sand mantles the lee hillslopes of the watershed and collects in its drainage network, especially on the western end near the dune field. The transport of sand throughout the watershed by eolian and dry ravel processes has presumably been accelerated since the Medano fire due to the lack of vegetation on the slopes.

METHODS

Debris-Flow Probability and Volume Models

Three regression models developed by Cannon et al. (2009) were used to predict the probability of debris-flow occurrence, and one model developed by Gartner et al. (2008) was used to predict potential debris-flow volumes, for each of the 57 severely burned basins of the Medano Creek Watershed. The probability models used were created through multivariable logistic regression analysis of relevant data from recently burned basins in the U.S. intermountain west (California, Colorado, Idaho, Montana, and Utah) that did and did not produce debris flows, to identify the most significant variables for prediction of debris-flow occurrence. Five probability models, each using a combination of different parameters, were found to be statistically significant. The three models used for this analysis (models A, B, and C) were the strongest predictors of debris-flow occurrence in recently burned basins (Cannon et al., 2009). They are as follows:

$$\text{Probability} = e^x/(1+e^x) \quad (1)$$

$$\text{Model A: } x = -0.7 + 0.03a - 1.6b + 0.06c + 0.2d - 0.4e + 0.07f \quad (2)$$

a = Percent of basin area with slopes greater than 30 percent
b = Ruggedness (change in basin elevation divided by the square root of basin area)

c = Percent of basin area burned at moderate and high severity
d = Percent clay content of surface soils
e = Liquid limit in percent
f = Average storm intensity (mm/hr)

Model B: $x = -7.6 - 1.1a + 0.06b + 0.09c - 1.4d + 0.06e$ (3)
a = Ruggedness (change in basin elevation divided by the square root of basin area)
b = Percent of basin area burned at moderate and high severity
c = Percent clay content of soils
d = Percent organic matter of soils
e = Average storm intensity (mm/hr)

Model C: $x = 4.8 + 0.05a + 0.2b - 0.4c - 1.5d + 0.07e$ (4)
a = Percent of basin area burned at moderate and high severity
b = Percent clay content
c = Liquid limit in percent
d = Hydrologic group (based on soil infiltration rate and depth to confining layer)
e = Average storm intensity (mm/hr)

Volume models were developed using multivariable regression analysis of relevant data for recently burned basins in the intermountain western U.S., where volume of debris was quantified, to identify the most significant variables for prediction of debris-flow volume. The volume prediction model used for this analysis, from Gardner et al. (2008) and modified by Cannon et al. (2009), is as follows:

$\ln V = 7.2 + 0.6(\ln A) + 0.7(B)^{1/2} + 0.2(T)^{1/2} + 0.3$ (5)
V = Volume (m^3)
A = Area of basin with slopes greater than 30 percent (km^2)
B = Area of basin burned at moderate and high severity (km^2)
T = Total storm rainfall (mm)

For the initial hazard assessment, data for each of the variables above was collected for each basin burned severely by the Medano Fire using GIS tools and various input datasets, as described in the following section. Design values of average storm intensity and total rainfall were calculated from NOAA Atlas 2, Volume 3 for the area (Miller et al., 1973), to be used for hazard assessment. Short duration (less than 1-hour), intense convective storms were found to be the most common triggering events for debris flows in the intermountain U.S., based on precipitation data collected at debris-flow sites (Cannon et al., 2009). Design storms of 1-hour duration, and 2-year (18.9 mm) and 10-year (31.8 mm) return intervals were selected to provide storm rainfall conditions that represented likely magnitudes of summer thunderstorms.

Data Acquisition

Basins of Medano Creek Watershed with areas between 0.01 and 10 square kilometers (the range validated by Cannon et al., 2009) that were burned in the Medano Fire, were delineated above their confluence with Medano Creek, or above trail crossings in the case of the lower drainages near the park facilities, using GIS hydrology tools to extract data from the 10-meter digital elevation model (DEM) of the site. Model input data for 57 basins in Medano Creek Watershed that had greater than 1 percent of their area burned at medium and high severity was extracted using GIS spatial analyst tools. Burn severity was calculated from imagery generated by the Burned Area Emergency Response team (USDA Forest Service, 2010) using normalized burn ratio from Landsat mapping (Key and Benson, 2006). Basin morphological characteristics were calculated from the 10-meter DEM. Soils data were acquired from the NRCS STATSGO U.S. Soils Database (Soil Survey Staff, 2011). The range of values for representative soil types within each map unit was averaged, and weighted averages were calculated for basins that contained more than one soil unit. This data was manually input into regression equations described in the previous section.

Monitoring

Significant rainfall and runoff events were identified and characterized using the SNOpackTELemetry weather station on Medano Pass, the National Weather Service station at the park visitor center, the Colorado Department of Water Resources stream gaging station on lower Medano Creek, and from rain gauges and pressure transducers installed for this project. Field observations of erosion and deposition were documented and surveyed after significant rainfall events. Debris-flow volume estimates were made by measuring deposit area using handheld GPS surveys and estimating average deposit thickness. Thickness measurements were made from hand dug pits in new debris-flow deposits, and included debris deposited above the obvious burned upper layer of soils. Representative thickness measurements for each deposit were averaged, and the resulting average thickness multiplied by the area of each deposit to estimate deposit volumes.

RESULTS

Hazard Assessment

The initial hazard assessment was performed in the spring of 2011, prior to the summer storm season. The results of probability and volume models for each basin in response to the 1-hour, 2-year and 10-year design storms are presented in this section. The overall hazard rankings for the basins, calculated as the sum of probability and volume rankings, are also shown.

Model Results

Each of the three probability models resulted in a different range of values for the burned basins of Medano Creek Watershed. Model A resulted in the highest probabilities (1 to 96 percent), Model C the next highest probabilities (1 to 95 percent), and Model B the lowest range of probabilities (0 to 43 percent). Figure 2 shows the distributions of probability values among the basins for the three models, for both 2-year and 10-year return interval storms. Despite differences in the ranges of probabilities for the three models, they all tended to agree somewhat on the relative ranking of each basin. The probability values from all three models were averaged for each of the two design storms, and the resulting values were divided in to three probability categories: 0 to 33.3 percent, 33.4 to 66.6 percent, and 66.7 to 100 percent. The predicted volumes for each rainfall input were also divided into three categories: 0 to 1000 m^3, 1001 to 10,000 m^3, and 10,001 to 100,000 m^3. Figure 3 shows the distribution of the volume model results.

Individual maps were created showing the spatial distribution of the probability and volume categories for 1-hour, 2-year and 10-year return interval storms. Figures 4 and 5 show rankings for each basin based on the previously described probability and volume categories, using the 10-year return interval storm.

Hazard Ranking and Mapping

Integer rankings were assigned to each probability and volume grouping, respectively, from 1 (lowest) to 3 (highest). The probability and volume rankings were then summed to give an overall hazard rank for each basin. The rankings were divided into three categories: low (2-3), moderate (4), and high (5-6). Figure 6 shows the spatial distribution of overall hazard rankings for each burned basin, using the 10-year return interval storm. This hazard ranking, being the sum of the probability and volume rankings, represents the overall debris-flow hazard posed by each basin in response to the given rainfall event. These maps are the most significant product of the GIS-based hazard assessment in terms of resource management, policy decisions, or emergency planning. The basins mapped as high hazard can be prioritized for mitigation efforts, or in this case avoidance by closing campsites in the lower reaches of the basin.

Monitoring

The rainfall and debris-flow monitoring was broken down into five monitoring periods, between site visits, during the spring, summer, and fall of 2011: (1) March 14 through May 25, (2) May 25 through June 15, (3) June 15 through August 15, (4) August 15 through August 27, and (5) August 27 through October 17. During monitoring period 1 the SNOTEL rain gauge on Medano Pass was monitored remotely and recorded no significant precipitation. Site visits bounding the period consisted of field reconnaissance for installation of monitoring equipment in basins 7, 16, 24, and 32 (basin locations are shown on Figure 4) and observations of initial

geomorphic conditions of the post-fire landscape. Installation of monitoring equipment and recording of data began during the May 25, 2011 site visit, just before the start of monitoring period 2. Data collection from rain gauges and pressure transducers, observations of geomorphic response, and sampling of materials was conducted during monitoring periods 2 through 5.

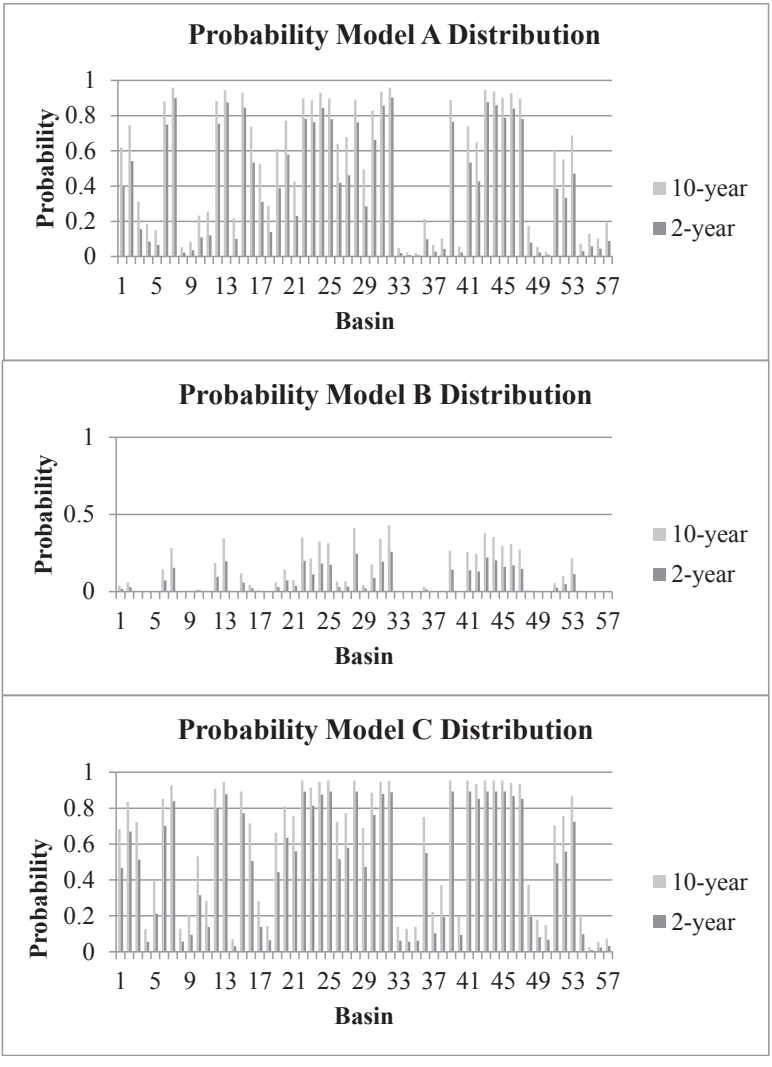

FIG. 2. Bar graphs showing distributions of probability values from models A, B, and C, respectively, for all basins in response to the 2-year and 10-year return interval storms

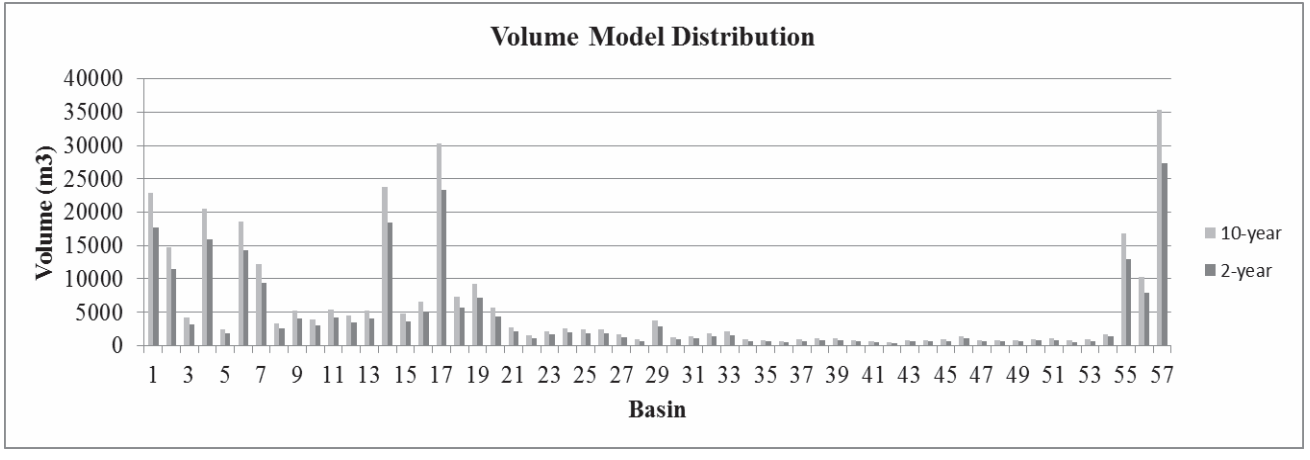

FIG. 3. Bar graph showing the distribution of values from the volume model for all basins in response to 1-hour, 2-year and 10-year return interval storms

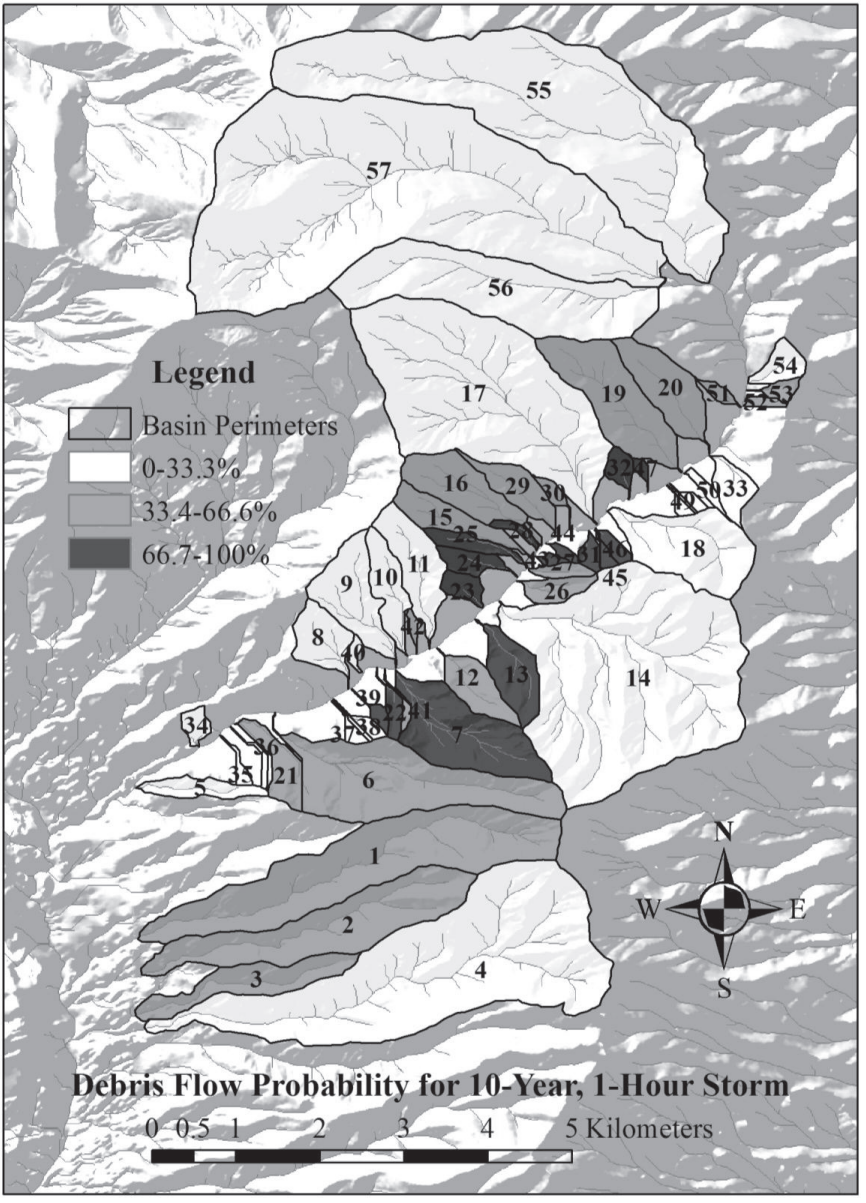

FIG. 4. Map showing spatial distributions by basin of debris-flow probability categories for a 10-year return interval, 1-hour duration storm

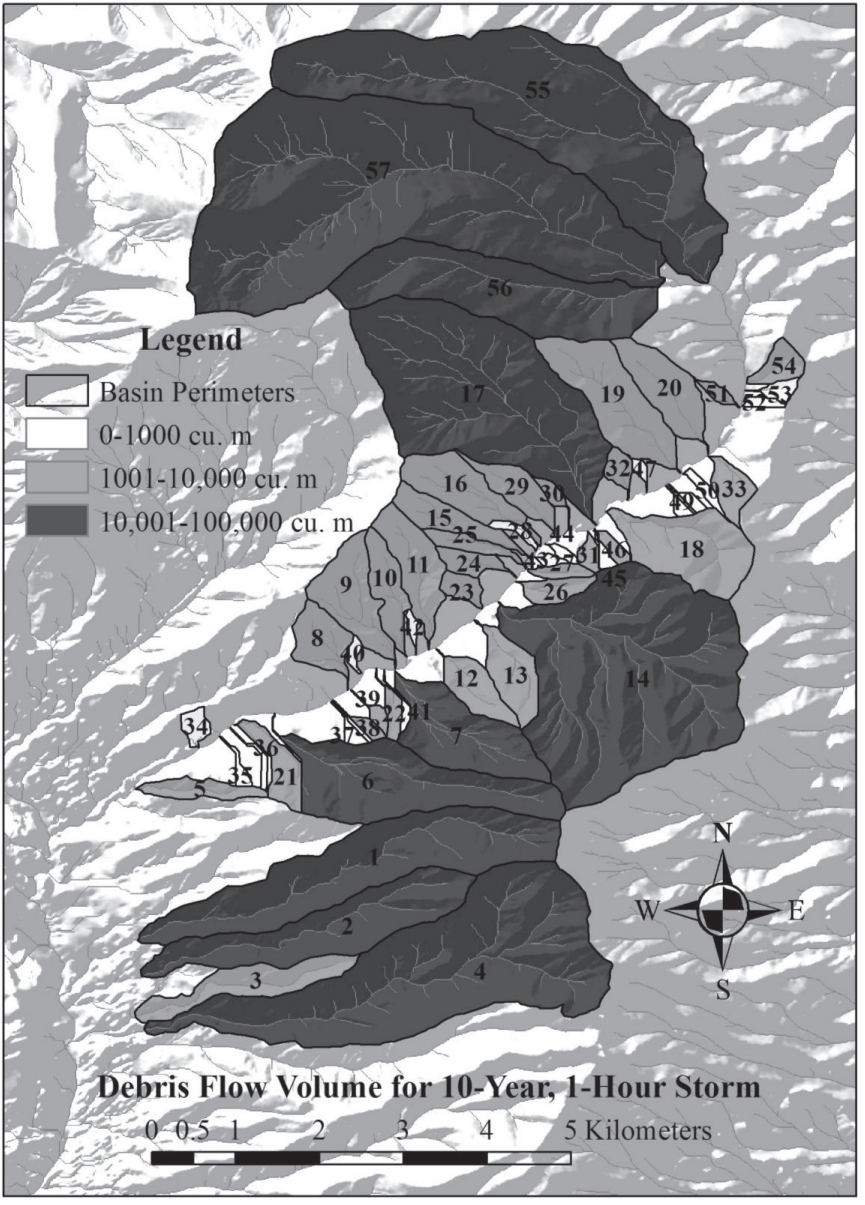

FIG. 5. Map showing spatial distributions by basin of debris-flow volume categories for a 10-year return interval, 1-hour duration storm

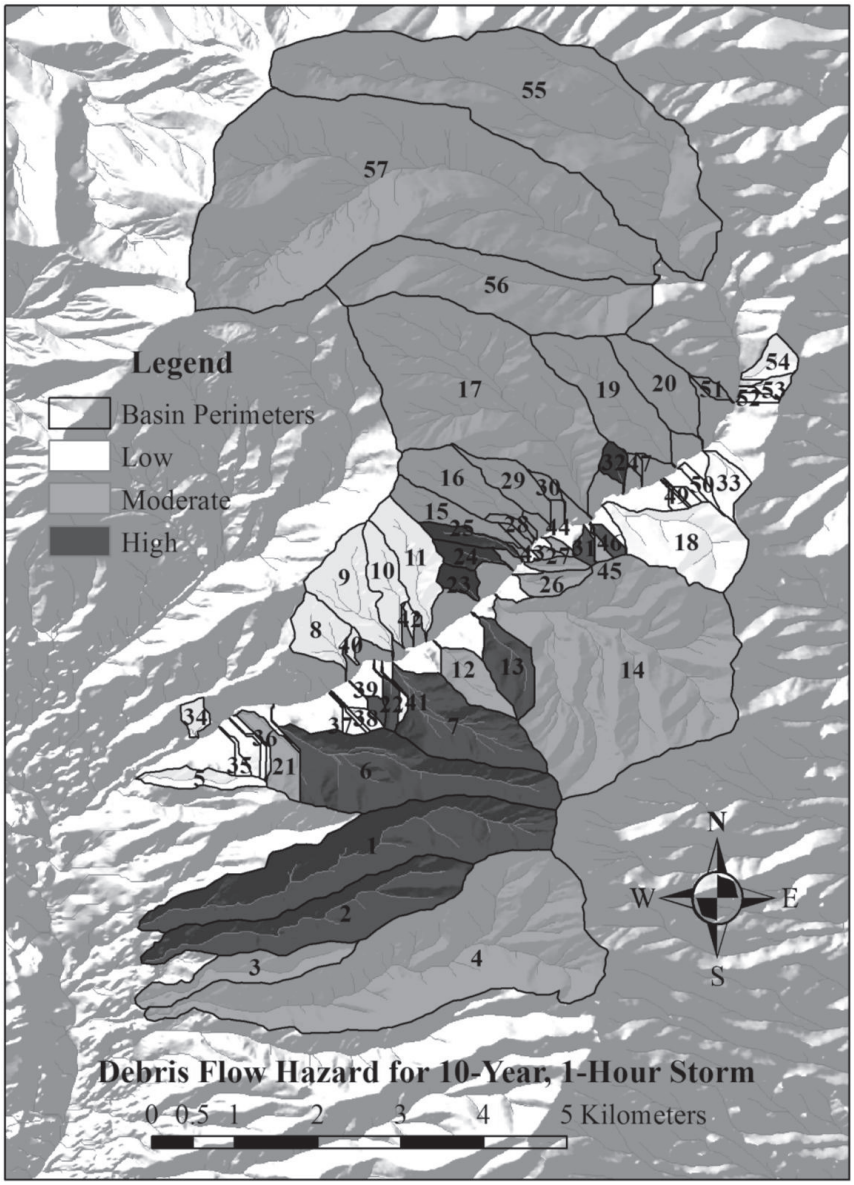

FIG. 6. Map showing spatial distributions by basin of debris-flow hazard categories for a 10-year return interval, 1-hour duration storm

Model Validation

In order to validate the models, actual rainfall conditions that resulted in debris flow occurrence recorded at the site during the monitoring period are input into debris-flow probability and volume models and compared to the observed basin responses. The timing of debris-flow events on August 22, 2011 is known from pressure transducer records in basins 24 and 32, as is the rainfall intensity throughout the storm from rain gauges in basins 16 and 24 nearby. This enables calculation of average intensity values up to the time of debris-flow initiation in these basins, which were between 19.7 mm/hr to 54.8 mm/hr. The timing of debris flows during the August 28, 2011 event is unknown, but the average storm intensities recorded on rain gauges in close proximity to debris flows (gauges in basins 7 and 24) were 15.6 and 20.5 mm/hr, respectively. Since both of these storms delivered high intensity rainfall to extensive areas throughout the watershed, and true intensity values are not known for the majority of the burned basins, the calculated mean of the recorded intensity values (26.3 mm/hr) from the debris flow triggering storms described above is used for probability model validation. For comparison, the mean of average storm intensity values for the full duration of all rain events that triggered debris flows (13.0 mm/hr), recorded on rain gauges in close proximity (in basins 7, 16, and 24) to debris flows is also used for model validation. The large difference between these two mean values can be attributed to the fact that the full duration of the August 22 storm event was significantly greater than the duration of rainfall before the debris flows occurred. Figure 7 shows the relationship between the recorded values for these two measures of average intensity, and those of the 1-hour, 2-year, 5-year, and 10-year design storms.

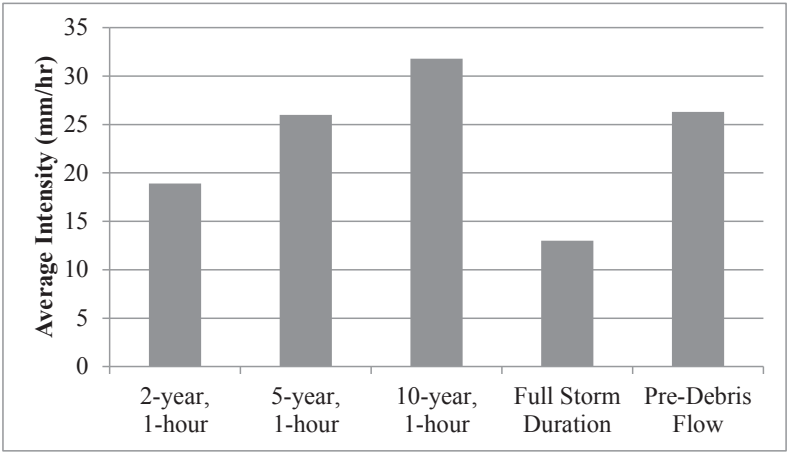

FIG. 7. Average intensity of rainfall for 1-hour, 2-year, 5-year, and 10-year design storms, and means of recorded average intensity values for storms that triggered debris flow

Probability Models

Debris flows were observed in seven basins (7, 12, 15, 23, 24, 25, and 32) in response to the August 22 and 28 storms previously described. Probability models A and C both predicted high probability of occurrence in all seven of the basins that produced debris flows, whereas Model B did not predict high probability of occurrence in any basins. Figures 8 and 9 present histograms of probability distributions among all basins for Models A, B, and C, with darker inset bars indicating the number of basins within each probability range that actually produced debris flows.

It is apparent that Model B severely under-predicted debris-flow probability in this setting. The highest probability values for the 13.0 mm/hr intensity were less than 20 percent, and the highest values for the 26.3 mm/hr intensity were less than 40 percent. Models A and C both predicted relatively high probability values (greater than 67 percent, based on the categories established in the hazard assessment) for all basins that produced debris flows, using both rainfall intensity values. Both models, however over-predicted the number of basins with high probability of debris-flow occurrence, compared to those that actually produced debris flows. At the low rainfall intensity input (13.0 mm/hr.), Model A predicted high probability of debris flows in 10 basins that did not produce debris flows, and by this criterion Model C returned 13 false positives. At the high rainfall intensity input (26.3 mm/hr.), Model A returned 13 false positives, while model C returned 21 false positives. Models A and C both performed well in terms of predicting high probability of debris-flow occurrence in all basins where debris flows occurred, but Model A performed slightly better in terms of resulting in less over-prediction.

The average of the three probability models predicted high probability in all but two of the basins where debris flows occurred using the high intensity value (26.3 mm/hr). The probability values assigned to the two under-predicted basins were 62 and 63 percent, which are relatively close to the high probability category minimum (67 percent). The average of the three models returned only 7 false positives at the high intensity value, which are fewer than models A and C. At the low intensity input (13.0 mm/hr), however, the average of the three models did not predict high probability of debris-flow occurrence in any basin. It appears that averaging the models improves accuracy in terms of predictive ability and decreases the number of false positives, but the influence of Model B lowers the probability values significantly. As a result, averaging the three models is only effective when relatively high intensity rainfall inputs are used. In this case, the 1-hour, 5-year or 10-year design storms (26.0 and 31.8 mm/hr., respectively) would have been the most accurate inputs if using the average of the three models. Using Model C alone appears to be the most conservative approach in this case, recognizing that it generates a high number of false positives, even at low levels of rainfall intensity (less than the 1-hour, 2-year storm). Using Model A alone is a slightly less

conservative approach, with slightly less over-prediction than Model C, and appears to be the most accurate at intensities less than or equal to the 1-hour, 2-year design storm in this case.

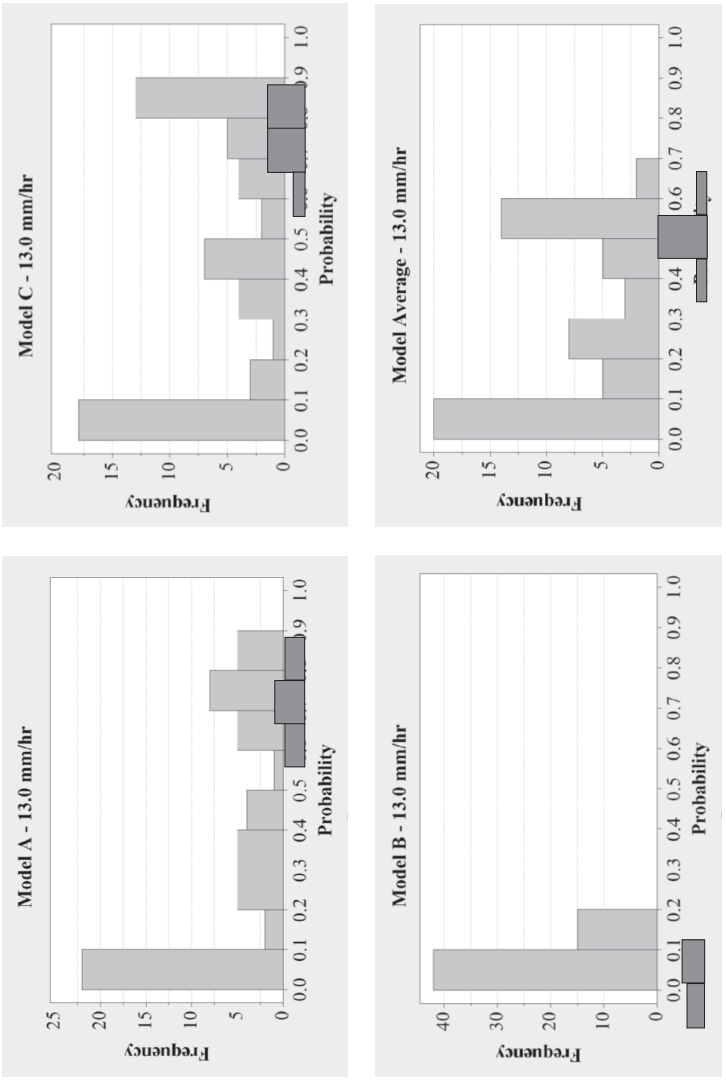

FIG. 8. Histograms of basin debris-flow probability distributions from models A, B, C, and the average of the three, for an average storm intensity of 13.0 mm/hr. Darker inset bars indicate the number of basins that produced debris flows in each bin of probability values

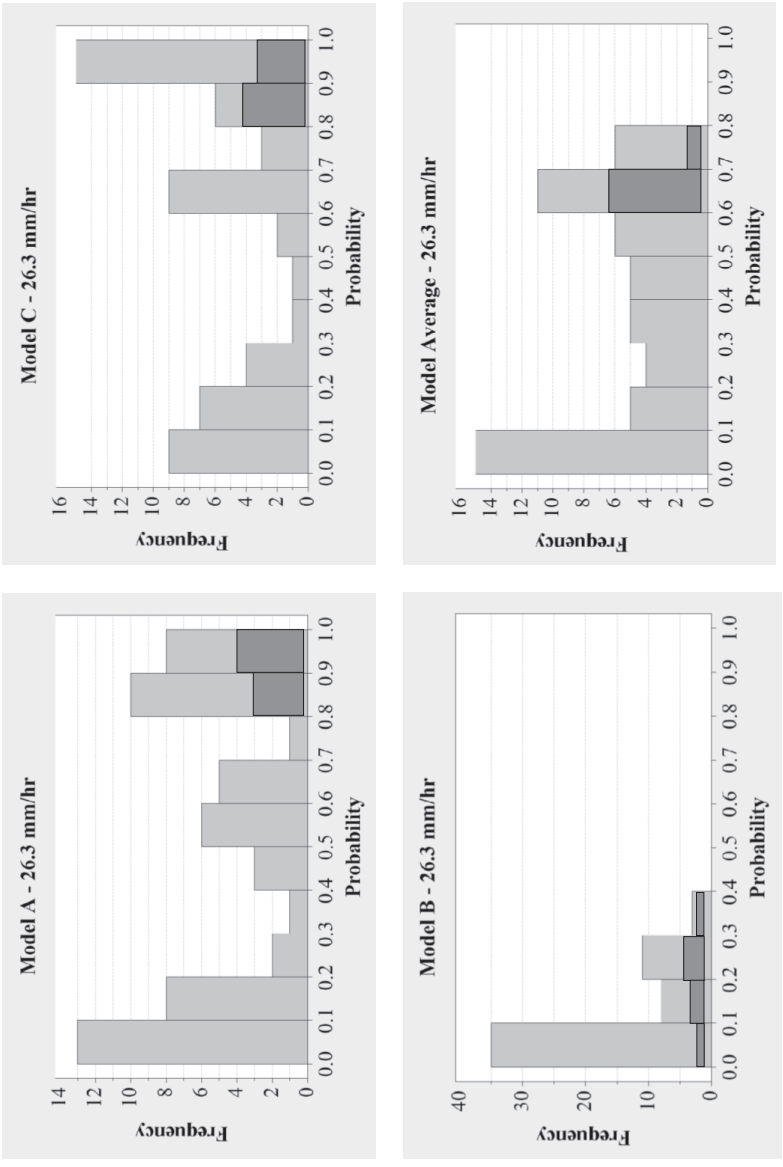

FIG. 9. Histograms of basin debris-flow probability distributions from models A, B, C, and the average of the three, for an average storm intensity of 26.3 mm/hr. Darker inset bars indicate the number of basins that produced debris flows in each bin of probability values

Volume Model

Measurements of deposit volumes were made after various debris-flow events. The total rainfall of the storm triggering the debris flow, as recorded in or near the basin that produced the debris flow, was used to calculate a predicted volume for comparison. Table 1 summarizes volume measurements from debris-flow deposits and predicted debris-flow volumes based on actual storm events.

Table 1. Predicted versus measured debris-flow volumes in response to various rainfall events

Basin	Area (km^2)	Volume Model (m^3)	Measured Volume (m^3)
7	1.17	9826	908
15	0.39	4265	759
23	0.13	1900	126
24	0.17	2268	855
25	0.17	2126	290

Volume measurements were within approximately one order of magnitude lower than model predictions. It should be noted that the accuracy of volume measurements themselves is poor due to variable thickness and loss of material into Medano Creek in some cases. It is likely that some sand was washed out of debris-flow deposits as they drained and was eroded by subsequent rainfall and runoff, which could contribute significantly to the overall measured volume of debris flows. However, it is assumed that this discrepancy does not completely account for the order of magnitude difference based on visual comparison of eroded volumes with measured volumes. Previous comparisons of predicted and measured volumes (Gartner, personal communication, March 1, 2012) suggest that this volume model tends to over-predict volumes of debris flows from small basins and under-predict volumes from large basins. The basins in Table 1 have relatively small areas compared to the range of basin areas used to generate the model, explaining the low predicted volumes.

CONCLUSIONS

- The three empirical debris-flow probability models found to be statistically significant predictors of event occurrence in previous analyses are not in agreement on the magnitude of probability estimates, and thus were averaged for initial hazard assessment. Relative probability rankings were consistent among all three models.
- Based on averaged model results, conditions in eleven basins (1, 2, 6, 7, 13, 22, 23, 24, 25, 32, and 39) burned by the Medano Fire resulted in relatively high debris-flow hazard estimates in response to a 1-hour duration, 10-year return interval storm, and three basins (2, 6, and 32) had relatively high

debris-flow hazard potential estimates in response to a 1-hour duration, 2-year return interval storm.

- The information from the hazard assessment was taken into consideration by the park's resource managers when closing campsites threatened by debris flow and flood hazards.
- Debris flows occurred in basins 7, 12, 15, 23, 24, 25, and 32 in response to multiple storm events throughout July and August of 2011.
- Of the three probability models used in the hazard assessment for the Medano Fire, models A and C were the most successful in predicting debris-flow occurrence, though they tended to over-predict probability of occurrence. Model B severely under-predicted probability of debris-flow occurrence in this setting. Models A and C are conservative models that will likely perform well for debris-flow hazard assessment in similar settings within the intermountain western U.S. with 1-hour, 2-year or possibly lower intensity design storms.
- An average of the results from the three probability models was also successful in predicting relatively high probability values for basins that produced debris flows, and over-predicted fewer basins than either of models A or C. This average of probability model results is advisable for use in hazard assessment in similar settings only if used with relatively high intensity design storms (5-year to 10-year or greater return interval storm).
- The volume model over-predicted volumes of debris-flow deposition, though they were within an order of magnitude. The discrepancy is consistent with previous observations of volume over-prediction for relatively small basins using similar models in other settings.

ACKNOWLEDGMENTS

The authors appreciate the support of the National Science Foundation (award EAR-1118506) and the U.S. Geological Survey Geologic Hazards Science Center.

REFERENCES

Bianco, G., and Franzi, L. (2000). "Estimation of debris-flow volumes from storm events." In: Wieczorek, G.F. and Naeser, N.D., eds., *Debris-Flow Hazards Mitigation: Mechanics, Prediction, and Assessment*, Balkema, Rotterdam: 441-448.

Cannon, S.H., Powers, P.S., and Savage, W.Z. (1998). "Fire-related hyper-concentrated and debris flows on Storm King Mountain, Glenwood Springs, Colorado, USA." *Environmental Geology*, 35 (2-3): 210-218.

Cannon, S.H. (2001). "Debris flow generation from recently burned watersheds." *Environmental and Engineering Geoscience*, 7 (4): 321-341.

Cannon, S.H., Gartner, J.E., Holland-Sears, A., Thurston, B.M., and Gleason, A.J. (2003a). "Debris-flow response of basins burned by the 2002 Coal Seam and Missionary Ridge fires, Colorado." In: Boyer, D.D., Santi, P.M., and Rogers, W.P., eds., *Engineering Geology in Colorado-Contributions, Trends, and Case*

Histories, Association of Engineering Geologists Special Publication 14, Colorado Geological Survey Special Publication 55 (CD-ROM), CGS, Denver, CO.

Cannon, S.H., Gartner, J.E., Parrett, C., and Parise, M. (2003b). "Wildfire-related debris-flow generation through episodic progressive sediment bulking processes, western USA." In: Rickenmann, D., and Chen, C.L., eds., *Debris-Flow Hazards Mitigation: Mechanics, Prediction, and Assessment*, Millpress, Rotterdam: 71-82.

Cannon, S.H. and Gartner, J.E. (2005). "Wildfire-related debris flow from a hazards perspective." In: Hungr, O. and Jacob, M. eds., *Debris-Flow Hazards and Related Phenomena*, Springer-Praxis Books in Geophysical Sciences: 321-344.

Cannon, S.H., Gartner J.E, Wilson, R.C., Bowers, J.C., and Laber, J.L. (2008). "Storm rainfall conditions for floods and debris flows from recently burned areas in southwestern Colorado and southern California." *Geomorphology*, 96: 250-269.

Cannon, S.H., Gartner, J.E., Rupert, M.G., Michael, J.A., Rea, A.H. , and Parrett, C. (2009). "Predicting the probability and volume of postwildfire debris flows in the intermountain western United States." *Geological Society of America Bulletin B26459.1*, September, 2009: 127-144.

Coe, J.A., Kinner, D.A., Godt, J.W. (2008). "Initiation conditions for debris flows generated by runoff at Chalk Cliffs, central Colorado." *Geomorphology*, 96: 270-297.

Coussot, P., and Meunier, M. (1996). "Recognition, classification and mechanical description of debris flows." *Earth-Science Reviews*, 40: 209-227.

Chen, J.C., and Jan, C.D. (2000). "Debris-flow occurrence probability on hillslopes." In: Wieczorek, G.F. and Naeser, N.D., eds., *Debris-Flow Hazards Mitigation: Mechanics, Prediction, and Assessment*, Balkema, Rotterdam: 411-416.

Cipra, J.E., Kelly, E.F., MacDonald, L., and Norman, J. (2003). "Part 3: Soil Properties, Erosion, and Implications for Rehabilitation and Aquatic Ecosystems." USDA Forest Service Gen. Tech. Rep. RMRS-GTR-114: 204-219.

Deganutti, A.M., Marchi, L., and Arratano, M. (2000). "Rainfall and debris-flow occurrence in the Moscardo basin (Italian Alps)." In: Wieczorek, G.F. and Naeser, N.D., eds., *Debris-Flow Hazards Mitigation: Mechanics, Prediction, and Assessment*, Balkema, Rotterdam: 67-72.

Gartner, J.E., Cannon, S.H., Santi, P.M., and deWolf, V.G. (2008). "Empirical models to predict the volumes of debris flows generated by recently burned basins in the western U.S." *Geomorphology*, 96: 339-354.

Gartner J.E., personal communication, March 1, 2012, U.S. Geological Survey, Golden, CO.

Johnson, B.R, Bruce, R.M., and Lindsey, D.A. (1989). "Geologic map of the Medano Pass Quadrangle and part of the Liberty Quadrangle, Alamosa, Huerfano, and Saguache Counties, Colorado." U.S. Geological Survey, Miscellaneous Field Studies Map MF-2089, scale 1:24000.

Key, C.H., and Benson, N.C. (2006). "Landscape assessment (LA): Sampling and analysis methods." USDA Forest Service Gen. Tech. Rep. RMRS-GTR-164-CD (CD-ROM).

Kirkham, R.M. (2010). "Surficial deposits and preliminary assessment of the potential for flows in the area burned by the 2010 Medano Fire, Great Sand Dunes National Park and Preserve, Colorado." *Report*, GeoLogical Solutions: 40 p.

Laigle, D., and Marchi, L. (2000). "Example of mud/debris-flow hazard assessment, using numerical models." In: Wieczorek, G.F. and Naeser, N.D., eds., *Debris-Flow Hazards Mitigation: Mechanics, Prediction, and Assessment*, Balkema, Rotterdam: 417-424.

Lin, P.S., Hung, J.C., Lin, J.Y., and Yang, M.D. (2000). "Risk assessment of potential debris-flows using GIS." In: Wieczorek, G.F. and Naeser, N.D., eds., *Debris-Flow Hazards Mitigation: Mechanics, Prediction, and Assessment*, Balkema, Rotterdam: 431-440.

Miller, J.F., Frederick, R.H., and Tracy, R.J. (1973). Precipitation-Frequency Atlas of the Western United States, NOAA Atlas 2, Volume III-Colorado, National Weather Service: 47 p.

Moody, J.A., and Martin, D.A. (2001). "Initial hydrologic and geomorphic response following a wildfire in the Colorado Front Range." *Earth Surface Processes and Landforms*, 26: 1049-1070.

Ruleman, C. and Machette, M.N. (2007). "An overview of the Sangre de Cristo fault system and new insights into interactions between Quaternary faults in the northern Rio Grande Rift." In Ruleman, C., M. N. Machette, M-M. Coates, and M. L. Johnson, eds., *2007 Rocky Mountain Section Friends of the Pleistocene Field Trip—Quaternary Geology of the San Luis Basin of Colorado and New Mexico*, September 7–9, 2007, U. S. Geological Survey Open-File Report 2007-1193: 187-197.

Rupert, M.G., Cannon, S.H., Gartner, J.E., Michael, J.A., and Helsel, D.R. (2008). "Using logistic regression to predict the probability of debris flows in areas burned by wildfires, Southern California 2003-2006." U.S. Geological Survey Open-File Report 2008-1370: 9 p.

Soil Survey Staff (2011). "Natural Resources Conservation Service, United States Department of Agriculture. U.S. General Soil Map (STATSGO2)." Available online at http://soildatamart.nrcs.usda.gov. Accessed 5/16/2011.

USDA Forest Service (2010). "BARC Data Bundle for the Medano Fire occurring in Great Sand Dunes National Park – 2010." U.S. Forest Service. Available online at http://activefire maps.fs.fed.us/baer/download.php?year=2010. Accessed 3/3/2011.

Use of Rockfall Rating Systems in the Design of New Slopes

Scott A. Anderson[1], M. ASCE, P.E. and Matthew J. DeMarco[2], M. ASCE

[1]Manager, Geotechnical Engineering Technical Service Team, Federal Highway Administration, 12300 West Dakota Ave, Suite 340, Lakewood, CO 80228; scott.anderson@dot.gov
[2]Central Federal Lands Geotech Team Lead, Federal Highway Administration, 12300 West Dakota Ave, Suite 210, Lakewood, CO 80228; matthew.demarco@dot.gov

ABSTRACT: One typically uses different means to evaluate a highway rock slope depending on whether it exists currently or is in design. For example, the Rockfall Hazard Rating System (RHRS) and derivatives are commonly used to evaluate existing slopes and inform decision makers who are managing rock slope inventories. In contrast, kinematic and limit equilibrium analyses and methods based on observation and probability, such as Ritchey Ditch Criteria, Rockfall Catchment Area Design (RCAD), and the Colorado Rockfall Simulation Program (CRSP), are typically used to provide information for decision making when designing new slopes. Is there good reason for this difference? This paper raises this challenge and proposes that rating systems are not just good for existing inventories; they are good tools for design of new and rehabilitated slopes. Some of the challenges in using a rating system for design are addressed and the importance of distinguishing risk from hazard is highlighted. Finally, the paper demonstrates how rating systems can help us move towards and define a standard of practice for rock slope design in Colorado and other mountainous environments, and it discusses the challenge of establishing and applying an appropriate standard.

INTRODUCTION

This paper is written from the perspective of the highway industry though the points made are more broadly applicable and may have relevance to other owners of infrastructure and facilities, especially in mountainous terrain. Public highway agencies usually have a few goals that define their mission, often including the following:

- Provide safe highways;
- Provide highway systems that meet the broad range of user needs, ensuring consistent availability of transportation corridors;
- Provide highways with operation and maintenance costs that can be anticipated and planned for;

- Be good stewards of natural and scenic resources; and
- Be good stewards of public funds (financial resources).

Decisions regarding rock slopes should be and usually are based on these goals, satisfying each to some extent. It is recognized that these goals cannot all be optimized individually because they sometimes pull in different directions. Rather, there is a balance that is strived for that represents the optimum design for a project, a transportation corridor or system, and/or an owner.

One typically uses different means to evaluate a highway rock slope depending on whether it exists currently or is in design. The Rockfall Hazard Rating System (RHRS) (Pierson and Van Vickle, 1993) and many derivatives are used to evaluate existing slopes and inform decision makers who are managing rock slope inventories. In contrast, kinematic and limit equilibrium analyses and methods based on observation and probability, such as Ritchey Ditch Criteria (Ritchie, 1963), Rockfall Catchment Area Design Guide (RCAD) (Pierson et al., 2001), and the Colorado Rockfall Simulation Program (CRSP) (Jones et al., 1999), are typically used to provide information for decision making when designing new slopes. The thesis presented here is that rating systems are not just good for evaluating and managing existing inventories; they are good tools for design of new and rehabilitated slopes. Rating systems can help us define and move towards a standard of practice for rock slope design that is based on risk, and will help agencies balance their efforts on divergent goals. This is true whether the slope already exists or is in design. Throughout this paper RHRS, RCAD and CRSP are used to represent certain tools for convenience and simplicity. These are publically available in some form but this is not an endorsement of these products over others. Similar products could be substituted wherever these titles are used.

BACKGROUND

It is not practical to prevent all rocks on slopes (cut or natural) from falling, to prevent all falling rocks from reaching highways, or to immediately remove fallen rocks from highways. Therefore, rocks will impact vehicles, either moving or stopped, and vehicles will impact rocks. Programmatically, a certain low level expectation of this must be tolerated. Furthermore, highways below cut or natural rock slopes will have rock removal and repair as a maintenance need. In other words, it is not a question of "if" rockfall will occur; it is a question of how much is acceptable, or tolerable. One can measure this in terms of hazard or risk. Hazard and risk definitions vary but generally *hazard* is a measure of the likelihood of rockfall occurrence; whereas, r*isk* is a measure of likelihood and consequence of occurrence. Figure 1 shows an example where the consequence could be considered high.

FIG 1. Rock slope at Glacier National Park where rockfall is expected to reach the travel lanes of the road (courtesy of Cornforth Consultants, Inc.)

Risk is the measure that best addresses our objectives because it includes consequences and can potentially be used to compare rockfall risks with other risks owned by the agency. Hazard is important to characterize because it must be represented in the calculation of risk, but knowing hazard alone only goes so far. Consequences must also be characterized. Consequences used in the calculation of risk include, for example: none, increased maintenance, public or private property damage, and injury or death, to one or many (both motorists and pedestrians).

The highway industry follows a loosely defined standard-of-practice, tempered with the specific needs of our projects, such as minimizing environmental impact and considering cost in proportion to the type and volume of traffic along the road. The standard of practice uses analysis methods that address hazard and consequence, but often not together, or in a systematic way. Risk is seldom explicitly addressed and, as such, is not part of a current standard.

Standards would allow us to explain to our multi-disciplinary teammates, project managers, partner land management agencies, and the public, in a consistent manner, why certain decisions are made. Standards would also explain that there is always maintenance and safety risk associated with rockfall, and would allow for characterization of that risk in a systematic way. In addition, they would also frame desired performance objectives in a manner allowing comparison to broader route or corridor objectives, including environmental, capacity, and operating cost issues. As such, the criteria used to define a standard should be with respect to risk; not factor of safety, percent retained in ditch, or hazard, so our goal is to use our analysis methods to provide us a measure of risk.

ANALYSIS METHODS

In current practice, various methods are used to analyze rockfall hazard and consequences. Each method has strengths and weaknesses, and in their own way contributes to an understanding of risk. To understand this contribution it is important to have a consistent definition of the failure event and the risk associated with it. If we define failure as the event of a rock starting to fall from a slope and evaluate the definition of "risk" the following relationships and influences are observed:

$$\text{Risk} = f\{\text{Probability of Failure, Consequence of Failure}\}$$

Probability of Failure	= *f*(site conditions); which include geology, climate, presence of water, construction techniques, slope angle/aspect, reinforcement, retention, etc.
Consequence of Failure	= *f*(proximity to people/property, potential energy of rock/debris mass); which are affected by catchment width/depth (effectiveness), height to failure, size/volume of rock, slope angle, surface attenuation, retention/attenuation measures, etc.

Figure 2 shows an example where steps are taken to reduce probability of failure. Figure 3 shows (a) a case where the ditch and run out area is far from the road, and (b) where a barrier is used on the same road to contain rockfall in the ditch. In both cases, the consequence of failure is reduced. With these definitions in mind, the common tools for analysis are described below and reference is made to how they contribute to understanding risk.

FIG 2. Hand-scaling of a cut after construction to reduce probability of failure (hazard)

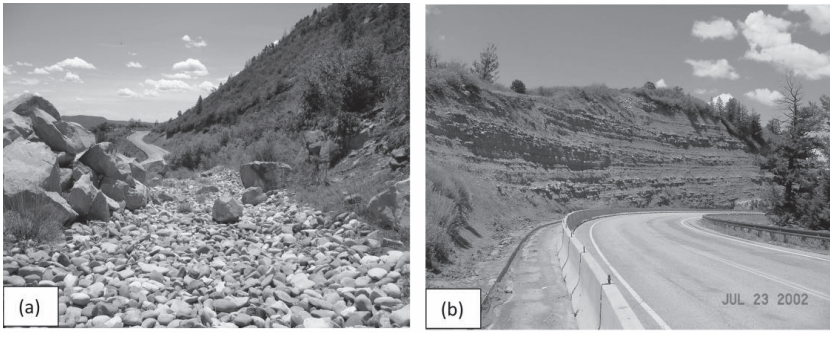

FIG 3. Examples at Mesa Verde National Park where ditch effectiveness and distance from travel lanes effectively confines rockfall to the fallout area, reducing the consequence of failure

Rock Slope Stability Analysis

Kinematic and limit equilibrium analyses can be used to calculate rock slope stability (Wyllie and Mah, 1998). These techniques are used to provide an assessment of hazard unique to a specific slope or site. Unfortunately, slopes are often found to be theoretically unstable or to have an unacceptably low factor of safety, when such is not actually true. This is because the analyses assume that discontinuities do intersect, are planar, and have largely frictional strength characteristics absent of any cementation or intact rock strength. These are reasonable and cautious assumptions given the uncertainty in the data that usually exist (mostly related to few, widely scattered measurements), but they combine to produce conservative solutions, not a best estimate of the average. Often it is assumed that kinematically feasible failures extend the full height of the cut; another cautious, conservative assumption, but not a best estimate of failure size and location, and therefore, not a good basis for estimating consequences which are related to volume and fall height.

Though an analysis of this type is usually deterministic and results in a factor of safety, there is an implicit relationship between factor of safety and probability of failure. In other words, these methods establish an estimated probability of failure implicitly and they could be modified to do so explicitly. The probability of failure is the measure of hazard and one of the two key inputs for calculating risk. These methods do not address failure consequence such as travel distance and bounce heights. As described above, they can be used to estimate volume and, through that prediction, a measure of consequence of failure, but these methods are generally best suited for analyzing failure probability and not consequence. A calculated factor of safety (or estimate of failure probability) is not an estimate or measure of risk because it does not address consequence.

Rockfall Catchment

These methods provide rational and statistical means of estimating ditch effectiveness and the effectiveness of other mitigation measures, such as fences, barriers and attenuators. They are usually used alone to calculate the percent of rocks that would reach the road if a given shape/size distribution were to fall, given a certain geometry of ditch and other mitigation measures. The ditch is then designed to meet a certain retention criteria. Other means of retention can be added to the design if needed, such as barriers, fences and attenuators. We have two types of tools in this area: those that are based on observation, such as RCAD, and those that are based on mechanical or numerical simulation, such as CRSP and RocFall (RocScience, 2012).

The RCAD empirical methodology is simple and powerful, yet results can be misleading if applied to conditions different than those from which the data were obtained (e.g., rock type and shape, slope geometry, slope-rock interaction). In the RCAD design charts for slopes of certain heights and slope ratios, each of the charts provides the percent retained per ditch geometry for a drop height equal to the slope height. Note, however, if some portion of the total rockfall hazard initiates lower on

the slope those rocks have a higher percentage of being retained – as shown in the RCAD charts for shorter slope heights. Therefore, if an entire cut or a section of cut with similar characteristics is considered as a unit, it may be appropriate to explicitly state that the catchment design for a certain percent retained includes the integrated retention of rockfall for the entire slope – not just the retention based on the highest rockfall initiation. For example, consider a triangular-shaped cut with a maximum height of 24 meters (80 feet). If the catchment is designed for 95 percent retention based on the 24-meter RCAD design charts, the actual percent retained assuming equal likelihood of rockfall initiating anywhere on the slope could be over 99 percent. If 95 percent catchment retention is actually the performance target for the slope, the catchment area should be designed to about 60 percent retention based solely on the design charts. This type of integration is typically not done with RCAD analysis or with CRSP type analysis so reported analyses are generally for a 'design event', not a statistical measure of expected performance.

CRSP, RocFall and other analytical/mechanical methods have different limitations and do not exactly replicate the observations at the RCAD study quarry (where the RCAD data are absolutely correct), but they may offer the best way to extrapolate RCAD findings to different rock and site conditions and evaluate the importance of parameters not varied in the RCAD work, including variable slope materials and geometries. They also provide for the rapid assessment of retention for a defined distribution of rock sizes and shapes initiating over a delineated initiation area. The level of uncertainty in the predictions is considerable and care should be used in their application.

RCAD and CRSP are examples of tools used for consequence management – evaluating the outcomes of falling rocks, rather than the probability for rock failure resulting in rockfall – either in the design of new slopes, evaluation/maintenance of existing slopes, or analysis of specific rockfall events. Consequence is directly but not completely addressed by RCAD (and CRSP, etc.) because proximity is also dependent on average daily traffic, vehicle speed, sight distance, highway maintenance, roadway width, shoulder area(s), clear zones, etc., which are independent design considerations.

In summary, RCAD, CRSP, and other run-out and energy prediction tools are only effective in understanding and managing part of one of the key variables affecting risk: the consequence of failure. Estimating rockfall retention is only part of the process. Therefore, it is not good risk management to fix a standard retention criterion of, for example, 90 percent retained, as a goal for design and maintenance when what is desired is a certain acceptable level of risk.

Hazard Ratings

The RHRS and many State derivatives (Drumm et al., 2005; NYDOT, 2007), are used to evaluate rockfall hazard. For the RHRS, ten factors are scored on an

exponential scale (of approximately 1 to 100) and summed to produce an overall slope rating that primarily indicates the likelihood of impact between a moving car and a fallen rock. A score in the range of 500 would typically indicate a very high hazard.

The RHRS is often used as though it were rating risk, not hazard, which is not too surprising because it includes factors that address both probability of failure and consequence of failure. In fact, defining failure as we have, as the event of a rock starting to fall, the RHRS has four of ten factors addressing hazard (failure probability) and six factors addressing consequence. The four factors primarily addressing the probability of failure are:

- Geologic Character Case 1 – Structural Condition/Rock Friction (failure along structural discontinuities);
- Geologic Character Case 2 – Differential Erosion Condition/Erosion Rate (failure due to erosion);
- Slope Water and Ice Conditions (climate-related slope water occurrence contributing to regular or seasonal rockfall); and
- Rockfall History (approximate frequency of occurrence).

The six factors primarily addressing consequence of failure are:

- Slope Height (potential energy contributing to severity of rockfall impacts and roll-out distance);
- Ditch Effectiveness (degree to which rock does not make it onto the travelway);
- Average Vehicle Risk (opportunity for vehicles to engage fallen rock or be struck by falling rock);
- Percent Decision Sight Distance (opportunity to avoid fallen rock on the roadway based on posted speed limit);
- Roadway Width (opportunity to avoid fallen rock within the travelway); and
- Block Size/Volume per Event (severity of impact to vehicles/structures, degree of roadway coverage with fallen rock, potential to close the roadway, etc.).

That the RHRS is referred to as a hazard rating has more to do with the fact that the risk is evaluated in a qualitative way, not in a way based on probability. For example, note that “Ditch Effectiveness”, as one of ten equal factors, is only one-tenth of the ‘hazard’. Thus, if a ditch is perfectly effective versus perfectly ineffective, it could make a difference of as little as 10 percent on the RHRS. With respect to public safety risk, this is counter-intuitive because if all rock is held within a ditch there is no risk of impact (or other safety consequences).

Nevertheless, the presentation here shows that we have methods that address probability of failure, methods that address consequence of failure and methods that address both probability and consequence. None of the methods are perfect but progress towards a goal of risk-based standards is best made from the methods that consider both probability and consequence of failure, which are rating systems like the

RHRS. Note that rating systems also present a logical way to capture kinematic/limit equilibrium and fall trajectory and catchment calculations so the analysis tools and methods would still be an important part of the risk-based design process.

DESIGN OF NEW SLOPES

There are two types of "new" slopes often encountered. One is a significant widening or improvement of a cut that currently exists (Figure 4). This often results in an increase in cut size and height. The second type is a new alignment where no current exposure of the rock exists. In either of these cases the design could be developed to result in a level of risk that is set by the owner. The risk could be set to be equivalent to an average level of risk for a corridor or road system or, for example, it could be set to a lower level so that in time the risk posed by rock slopes system-wide would drop. If the risk assessment is quantitative, the risk could also be set with reference to other risks assumed by the owner. This approach is consistent with steps being taken in other parts of highway design where owners are balancing their investments in a corridor to lower risk for the whole corridor, not just for certain elements (e.g., improvements to safety geometrics).

FIG 4. New slope created by widening and straightening to increase roadway capacity and traffic safety

In order to move in this direction, the first step is to start using analysis methods that address both of the two key components of rockfall risk: hazard and consequence. As discussed above, the RHRS addresses both of these components and if it were used instead or in addition to kinematic and limit equilibrium analyses (which address probability of rockfall) and CRSP and RCAD (which address consequence of rockfall), for example, then one could solve for a rating that would be expected after construction. The rating would be a function of the geometry of the cut and the roadway design, the site conditions, and the construction techniques. The geometry of the cut and roadway template are known definitively in advance and the site conditions are predicted based on site investigation during the design phase. Construction techniques specified as part of the construction contract, as they typically are, allow one to predict the condition of the new slope after blasting and excavation.

There are some challenges to using rating systems to design new slopes. The primary challenges are with respect to giving an assessed RHRS rating to a slope that can't be observed because it doesn't exist yet, and using existing rating systems that are based on summations, not products, and thus don't capture the conditional probability that is required in a risk assessment.

For consideration of the first challenge, the RHRS factors are presented in Table 1 along with the general process for evaluating and scoring, as well as ways during the design phase that the design could be modified to change the RHRS score. As can be seen from the table, some of the factors are evaluated and scored based on line and grade on plan sheets and on routine information normally in the hands of the design team. Other factors provide an opportunity to incorporate the results of CRSP and RCAD, and of kinematic and limit equilibrium analysis methods, which are the more common analysis methods for new slopes. Figure 5 shows where observations and investigations, and certain specific analysis methods, contribute to the RHRS factors and also how the RHRS and other factors contribute to risk.

Other factors are going to require predictions be made based on limited information and site observation. Interestingly, this is no different than most geotechnical designs, wherein limited explorations are used to predict capacity and performance – it is just unusual from a rockfall perspective. It is easy to imagine how the predictions could be tested (re-rated) after construction to confirm what was discovered in construction was as envisioned in design.

The second big challenge to using the RHRS in this way is that RHRS is based on the summation of factor scores, not the determination of conditional probability. For example, a decision tree for the calculation of rockfall risk might be something like this:

(1) Probability of rockfall initiating = A (based on four RHRS failure factors, possibly supplemented by kinematic analyses);

(2) Given rockfall initiates, the probability that it is not retained by the ditch = B (based on three RHRS factors related to ditch effectiveness, possibly supplemented with RCAD/CRSP analyses); and
(3) Given that rockfall escapes the ditch, the probability that the rockfall and vehicle collide = C (based on three RHRS factors related to hazard avoidance by motorists).

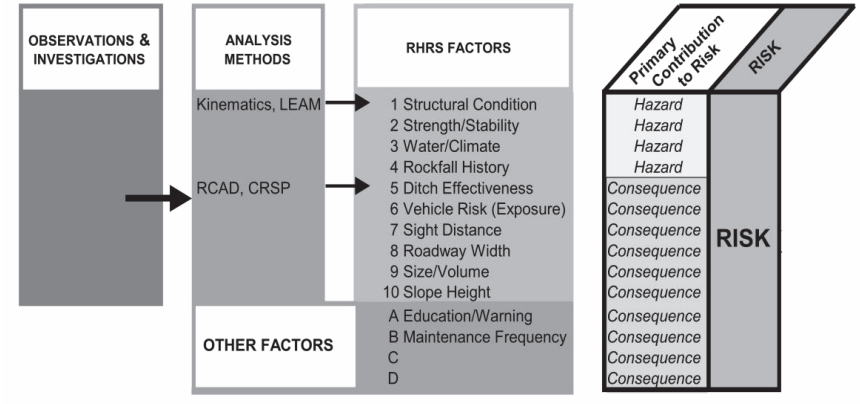

FIG 5. The evaluation of risk through observations, analysis rating system and other factors

In this example, B and C are conditional probabilities and the probability that rockfall and vehicle collide is the product, A x B x C. From this it is clear that if the ditch was essentially 100 percent effective the risk of a rockfall – vehicle collision is effectively zero. This challenge is most notable for the ditch effectiveness factor but one can envision its impact on other factors as well. Ideally, this challenge would be dealt with by converting the RHRS to a system based on multiplication of factors from one based on summation. Until that can happen it is suggested here that other criteria be used in addition to a RHRS rating to evaluate suitability of a rock slope design. For example, the owner might specify that regardless of the calculated RHRS rating for the slope in design, a certain percent retention from the maximum slope height is required.

Table 1. Evaluation of RHRS scores in the rock slope design phase

RHRS Rating Element	Evaluation and Scoring Option	Alteration Options
Consequence Related Elements		
Slope Height	• Based on planned road grade, slope angle and topography	• Alter road grade or slope angle • Add benches or measures such as bolts, mesh or attenuators to change effective height
Ditch Effectiveness	• Use CRSP or RCAD to evaluate effectiveness in terms of percent retained	• Change ditch geometry • Add barriers
Average Vehicle Risk	• Rate based on design sources	• Design to prevent traffic slowing and increase speed limit
Percent Decision Sight Distance	• Rate based on roadway design	• Work with geometrics and clear zones to increase decision sight distance • Reduce speed limit
Roadway Width	• Rate based on roadway design	• Consider shoulder or non-travel lanes as available for retention.
Consequence Related Elements		
Block Size/Event Volume	• Use adjacent sites for reference, rock cut mapping • Borehole information • Kinematic or limit equilibrium analysis	• Mesh, bolts or other measures to reduce the size or volume of material that could fail • Specify scaling
Probability of Failure Related Elements		
Geologic Character Case 1 Structured Rock Geologic Character Case 2 Differential Erosion	• Use adjacent sites for reference, rock cut mapping • Borehole information • Kinematic or limit equilibrium analysis	• Alignment changes
Water and Ice Condition	• Use adjacent sites for reference, rock cut mapping • Borehole information	• Install drainage
Rockfall History	• Base on regional experience and construction method • Borehole information	• Specify construction method, scaling

BENEFITS OF RATING SYSTEMS

Rating systems embrace the other analysis methods often used in design and they address risk because they capture both hazard and consequence. Their use gives an owner the ability to manage risk and gives the potential for establishing a standard of practice, even if only loosely defined.

Risk Management

Risk management is an ultimate objective of an owner whether looking from the perspective of public safety, performance of the system or financial and/or natural

resource stewardship. However, getting to a comprehensive suite of risk management tools is a long term objective for most and not something that can be done right away. Additionally, one needs to consider subjective elements in the formulation as well. For public owners there certainly are public tides that need to be heeded and there are ranges in the tolerability of risk. For instance, rockfall fatalities comprise only about 0.005 percent of highway fatalities nationally yet they have a public interest that far exceeds that, perhaps because of expectations we have set for roads free of these risks coupled with the often dramatic nature of fatal rockfall events.

On the other hand, managing agencies may have greatly diverging risk tolerances from the expectations of the traveling public, as well as within and amongst interagency entities. For example, the consequences of rockfall may be far greater when considering the direct and indirect costs of road closures, including maintenance, repair, alternative route capacity, socio-economic impacts, etc., and these may be the broader-view risks to be managed by public highway agencies. In contrast, natural resource management entities may consider preservation of the corridor viewshed a priority, resulting in a higher risk tolerance for rockfall and justification for routine roadway maintenance and repair expenditures and inconvenience.

Moving rock slope design to a framework that estimates risk will help owners set priorities based on these costs. The initial steps proposed in this paper will not result in a quantitative risk calculation that could be compared to other risks on the system, such as pavements and bridges, but it is a step in that direction. This type of analysis is also a positive step in that it will allow owners to evaluate the risk reduction benefits of some measures and design alternatives with respect to their life cycle costs and broader corridor management objectives. We are starting to build more and more mitigation measures directly on rock slopes and are getting information not just on how they can reduce the hazard and the consequence of rockfall, but on how long they last and how much they cost to own and maintain.

Standard of Practice

A precise standard of practice for rock slope design and rockfall mitigation will be difficult and perhaps impossible to define, even using risk as its measure, as there are many intangibles. Nevertheless, it is envisioned that if designs and assessments of existing slopes are evaluated with respect to risk in consistent ways, a band of practice can be established as shown in Figure 6. Quantifying slope performance somewhere within this band establishes the standard of practice for a given roadway or section and will assist owners in balancing the five goals listed in the introduction to this paper.

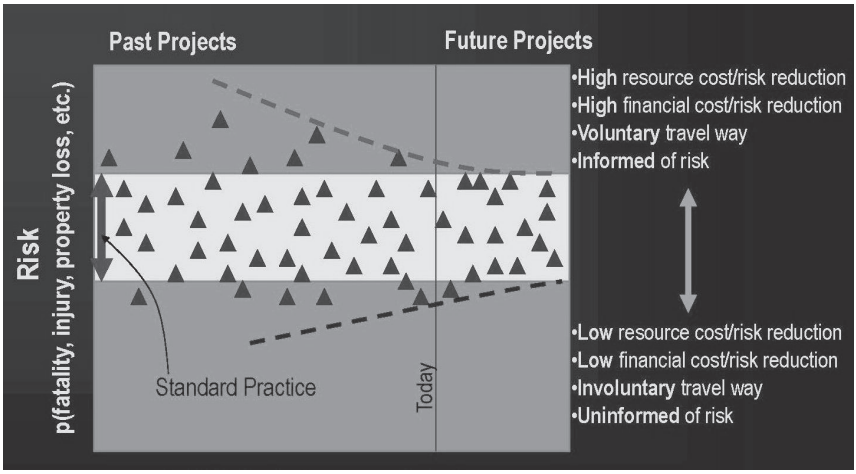

FIG 6. The evolution of a band of standard practice

An established range of practice would be useful for owners and responsible professionals engaged with the owners in setting expectations. Establishing the current range of practice, as well as future targets for slope performance, allows owning agencies to manage internal expectations as well, identifying when competing mission priorities fall within or outside accepted performance levels. The proposed risk-based approach to designing new slopes or mitigating old ones would provide a framework for setting a standard for a particular route or region and in evaluating alternative designs, such as ditch width versus scaling or mesh installation in a rational way. Having a standard for a given project will help the appropriate allocation of resources targeted at route-appropriate performance objectives and avoid "worst-first" management of existing slopes and over-/under-design of new or rehabilitated slopes.

CONCLUSIONS

One typically uses different means to evaluate a highway rock slope depending on whether it exists currently or is in design. For example, the Rockfall Hazard Rating System (RHRS) and derivatives are commonly used to evaluate existing slopes and inform decision makers who are managing rock slope inventories. In contrast, kinematic and limit equilibrium analyses and methods based on observation and probability, such as Ritchey Ditch Criteria, Rockfall Catchment Area Design (RCAD), and the Colorado Rockfall Simulation Program (CRSP), are typically used to provide information for decision making when designing new slopes. The shortcoming of all of these methods is that they only address probability of failure or consequence of failure. As such, if they are used alone or not in some consistent combination, they lead to new slopes that are not designed on the basis of risk.

Existing rockfall hazard rating systems such as the RHRS and others that have been developed similarly, or from the RHRS, provide an opportunity to design new slopes on the basis of risk. These rating systems currently have their own limitations in that they are based on the summation of factor scores and this prevents them from being used to actually calculate risk based on conditional probabilities of events, such as rockfall initiating, then escaping a ditch, then coming in contact with a car. Nevertheless, with some additional design criteria to be used in conjunction with a targeted rating value, these systems could allow owners to design new slopes to meet certain approximate risk standards. The FHWA is interested in exploring this idea further and in exploring the development and deployment of true risk-based rating systems for the future.

It is unlikely that this development will result in a singular expectation of risk associated with rockfall on highway slopes, or a precise standard of practice because of the many factors considered in design. These factors were all part of the recent reconstruction of Guanella Pass Road in Colorado and the varied rockfall mitigation measures that were included (example shown in Figure 7), and they include the goals to:

- Provide safe highways;
- Provide highway systems that meet the broad range of user needs, ensuring consistent availability of transportation corridors;
- Provide highways with operation and maintenance costs that can be anticipated and planned for;
- Be good stewards of natural and scenic resources; and
- Be good stewards of public funds (financial resources).

It is expected that the development of a risk-based design approach will result in improved communication of the desires and expectations of highway owners, highway designers, and highway users. Such an approach will facilitate management of the performance of a system of highways – something of great interest to highway owners. It is also likely that other public and private entities with interests on or near rock slopes will find this of value for the same general reasons.

FIG 7. A rockfall fence installed on Guanella Pass Road

REFERENCES

Brown, D.Z. and Vinson, R.J. (2006). "Stiffness parameters for a strong and colorful aeolian soil." G*eomaterial Characterization* (GSP 199), ASCE, Reston/VA: 12-22.

Cimponella, G.R. and Rubertsen, K.P. (1999). "Common problems with conventional testing." *J. Geotechnical & Geoenv. Engrg.*, Vol. 181 (9): 1193-1199.

Drumm, E.C., Mauldon, M., Dunne, W.M., Bateman, V.C. and McCarter, B. (2005). Rockfall Management System for Tennessee: Final Report—Phase II. Tennessee DOT, Nashville. www.tdot.state.tn.us/longrange/reports/res1189.pdf.

Jones, C.L., Higgins, J.D. and Andrew, R.D. (1999). "Colorado Rock-Fall Simulation Program, Version 4.0." Available through Colorado Geological Survey, http://geosurveystore.state.co.us/p-676-colorado-rockfall-simulation-program-version-40.aspx.

NYDOT (2007). Geotechnical Engineering Manual: Rock Slope Rating Procedure. Geotechnical Engineering Bureau, State of New York DOT, GEM-15, rev. 1. https://www.dot.ny.gov/divisions/engineering/technical-services/technical-services-repository/GEM-15b.pdf

Pierson, L.A. and Van Vickle, R. (1993). Rockfall Hazard Rating System. Federal Highway Administration Publication No. FHWA-SA-93-057, 104 pp.

Pierson, L.A. (1991). "The Rockfall Hazard Rating System." Oregon Department of Transportation, Federal Highway Administration Publication No. FHWA-OR-GT-92-05, 16 pp.

Pierson, L.A., Gullixson, C.F. and Chassie, R.G. (2001). Rockfall Catchment Area Design Guide – Final Report. Oregon Dept. of Transportation Research Group pub. No. SPR-3(032), pp.92.

Ritchie, A.M. (1963). "Evaluation of Rockfall and Its Control." Highway Research Record, No. 17, pp. 13-28.

RocScience (2012). RocFall v.4.055. RocScience Inc., 31 Balsam Avenue, Toronto, Ontario M4E 3B5.

Wyllie, D. and Mah, C.W. (1998). Rock Slopes – Reference Manual. Federal Highway Administration Publication No. HI-99-007, 393 pp.

Evaluation of Sinkhole at Beaver Park Dam, Colorado Guided By Risk Analysis

John W. France [1], M. ASCE, P.E., Bill McCormick[2], M. ASCE, P.E., and Matt Gavin [2], M. ASCE, P.E.

[1]Vice President, URS Corporation, 8181 East Tufts Avenue, Denver, CO 80237; john.france@urs.com
[2]Colorado Division of Water Resources, 7405 South Highway 50, Salida, CO 81201; bill.mccormick@state.co.us
[3]Colorado Division of Water Resources, 160 Rockpoint Drive, Suite E, Durango, CO 81301; matthew.gavin@state.co.us

ABSTRACT: Beaver Park Dam, originally constructed between 1912 and 1914, has a long history of seepage through the left abutment. In the spring of 2010, a sinkhole was observed on the downstream left abutment, near the dam, in a location of prior seepage concerns. After an initial evaluation, the Colorado State Engineer's Office (SEO) restricted storage in the reservoir to 6 m (20 feet) below the spillway crest. A facilitated, expert elicitation, risk analysis was conducted to estimate failure probabilities and risks for: 1) the existing facility under normal operation, 2) the existing facility under the currently restricted operation, and 3) a potentially rehabilitated facility under normal operations. The results of the risk analysis helped the owner in understanding the significance of the existing conditions, the risk reduction benefits resulting from the current restriction, and the need to pursue dam safety modifications for the facility. The results also helped provide the Colorado SEO with a sound basis for the magnitude of the interim reservoir restriction.

INTRODUCTION

Beaver Park Dam is a large, High Hazard dam owned and operated by the Colorado Division of Parks and Wildlife (CPW), located near South Fork, Colorado, as shown in Figure 1. In the spring of 2010, a sinkhole was observed on the downstream left abutment of the dam, near a location of prior seepage concerns. After an initial evaluation, the Colorado State Engineer's Office (SEO) restricted storage in the reservoir to 6 m (20 feet) below the spillway crest. A facilitated, expert elicitation, risk analysis was conducted to estimate failure probabilities and risks for: 1) the existing facility under normal operation, 2) the existing facility under the restricted operation, and 3) risk reduction alternatives. The scope of the risk analysis was limited to static, internal erosion failure modes. The results of the risk analysis were compared to the risk guidelines being used at that time by the Department of Interior,

Bureau of Reclamation (Reclamation, 2003). This paper describes how the risk analysis was used to support dam safety decisions for the facility.

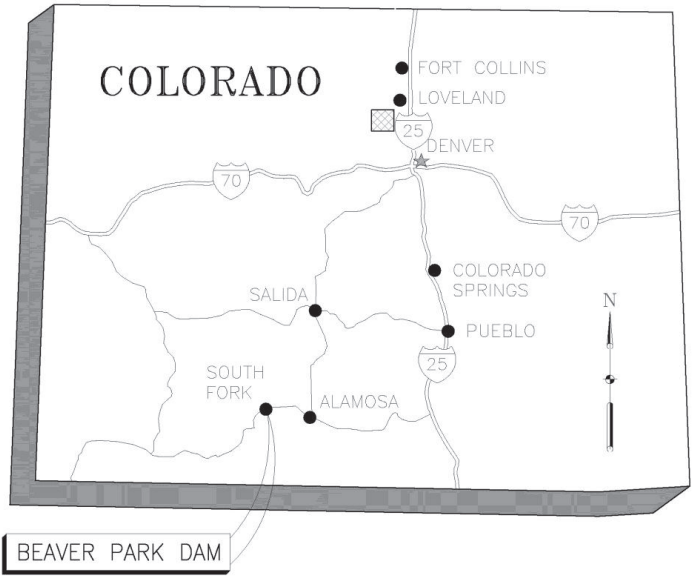

FIG. 1. Beaver Park Dam Location Map

DAM DESCRIPTION AND CONSTRUCTION HISTORY

The project was originally constructed between 1912 and 1914 as a 26.5 m (87-foot) high concrete-faced rockfill structure. A low level outlet tunnel was constructed through the left abutment with a gate chamber located at the upstream dam toe, and a masonry overflow spillway channel was constructed over the dam crest near the maximum section, as shown in Figure 2.

The geology at the dam site consists of latite and fractured latite of volcanic origin beneath the original dam and on both abutments. The rock has thick bedding of several tens of feet and prominent jointing, probably associated with the cooling of tuff layers following deposition. However, the latite rock on the left (looking downstream) abutment is only a knob of limited extent, flanked further to the left by a large hill of glacial moraine deposits, which form the abutment/reservoir rim for about 610 m (2,000 feet) to the west (left) of the original dam. The dam site geology is illustrated in plan and profile in Figures 3 and 4.

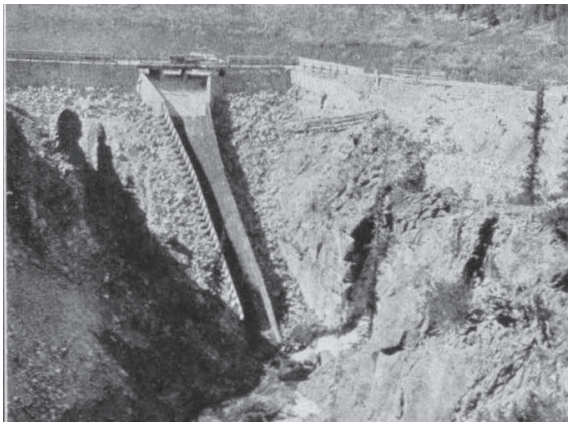

FIG. 2. Downstream Face of Original Dam

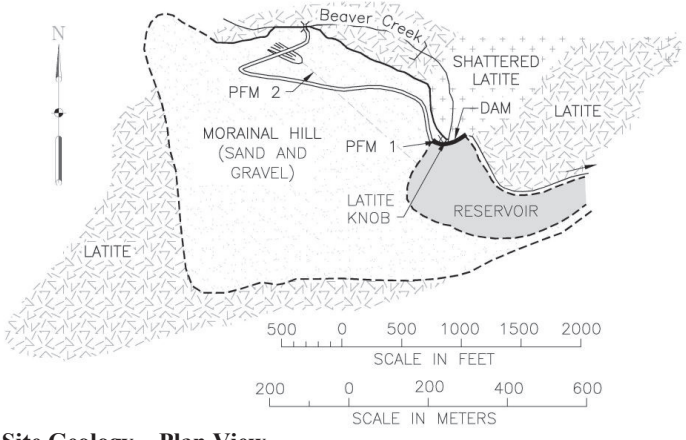

FIG. 3. Site Geology – Plan View

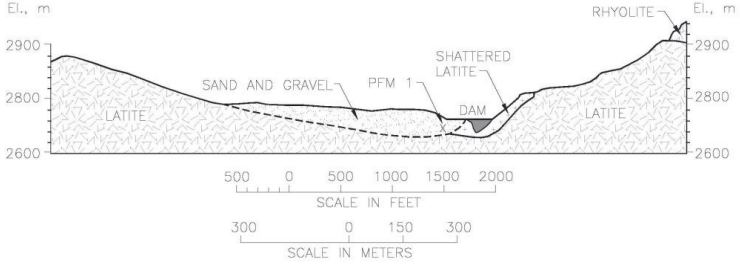

FIG. 4. Site Geology – Profile View

Because of significant seepage through the left abutment noted during first filling, a drainage tunnel was excavated from the downstream slope at the base of the left abutment. The exact location and extent of the tunnel are unknown. The drainage tunnel was later backfilled with rockfill in 1938, following the appearance of a sinkhole above the presumed location of the tunnel.

Between 1915 and 1916, grouting and reservoir puddle lining operations were performed. In addition, rock-filled cribbing was constructed across the downstream slope of the left abutment near the dam, in the general location where seepage had been observed during first filling. The cribbing extended across glacial moraine material in a V-shaped gap in the left abutment latite rock knob.

Between 1947 and 1953, major modifications to the dam were completed, including a 3 m (10 feet) dam raise, with significant earthfill placed upstream and downstream of the original dam and significant earthfill placed on and upstream of the left abutment moraine. The spillway was removed from the crest and downstream slope of the dam, and a new side channel spillway was constructed on the right abutment. A reinforced concrete seepage wall was placed across the old spillway entrance. The inlet to the outlet works was extended upstream, as necessitated by the upstream fill, the gate tower and controls were raised 3 m (10 feet) to match the dam raise, and repairs were made in the outlet tunnel. The raised crest elevation was 2681 m (8,794 feet). The right abutment spillway crest elevation is 2677 m (8,782 feet).

Between 1966 and 1969, additional modifications were made to the outlet tunnel and right abutment spillway. Further modifications were made to the outlet tunnel between 1970 and 1971. The modifications to the outlet tunnel included constructing a steel liner in the tunnel, with the annular space between the liner and the tunnel grouted full.

Between 1987 and 1988, modifications were completed to raise the dam and excavate an auxiliary spillway to the right of the then existing side-channel spillway on the right abutment. The dam raise was to elevation 2686.4 m (8811.5 feet). The raised embankment section is shown on the drawings as an impervious zone with rockfill on both the upstream and downstream sides.

The evolution of the cross section of the dam is shown on Figure 5.

Because of concern about potential failure of the crib structure and the slope above the crib structure, rockfill was placed at the toe of the slope of the left abutment moraine in 1978, covering some of the cribbing and the location of the left abutment drainage tunnel. Additional rockfill was placed in the area of the cribbing during the 1988/1989 dam raise/spillway enlargement work.

In 2009, a collapsed section of the steel liner in the outlet tunnel on the downstream side of the gate chamber was repaired on an emergency basis.

The normal maximum surface area of Beaver Park Reservoir is approximately 38 hectares (93 acres) at spillway crest elevation 2677 m (8,782) feet. The gross storage capacity of the reservoir at the spillway crest is approximately 5.8 million m^3 (4,700 acre-feet). The reservoir level and downstream releases are controlled by the side channel spillway and the outlet works. The reservoir typically fills and spills in the spring. To facilitate conservation pool agreements, there is typically a period of deeper drawdown late in the irrigation season. During this time (September through October), reservoir levels are lowered to about 6 m (20 feet) below the spillway crest. The drawdown is typically short-lived, as the gates are normally closed by October 31.

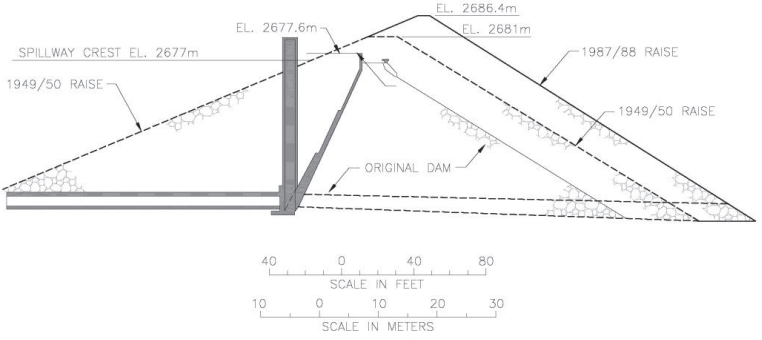

FIG. 5. Evolution of Cross Section of the Dam

Brief History of Dam Performance

The dam has experienced seepage-related performance issues throughout its history, starting with first filling in 1914. Observed incidents related to seepage include the following highlights:

- Immediately upon initial filling in 1914, seepage was observed around the latite rock knob on the left abutment, through the moraine in the gap in the left abutment rock. Before the reservoir was two-thirds full, the "fine till" began to wash out.
- When the water was allowed to rise in the reservoir for a second time in 1914, a much larger leak developed at a point about 240 m (800 feet)[1] from the reservoir, in the hillside formed by the moraine above the stream as it trends west, downstream of the dam. A washout at this location formed a gully as deep as 6 m (20 feet) and created a fan of eroded material that extended to the valley bottom.

[1] The downstream distance for this failure mode was believed to be about 460 m (1,500 feet) based on information available during the initial risk analysis. Subsequently, survey data collected for modification designs indicated that the actual distance is about 240 m (800 feet). An earlier publication on this risk analysis (France et al, 2011) included reference to the 460 m (1,500 feet) distance.

- During a third reservoir filling attempt in 1916, a serious leak occurred near the east end of the drainage tunnel then under construction in the left abutment. The seepage reportedly carried sands and gravels, and a large mass collapsed at the end of the tunnel.
- Around 1921/1922, the reservoir stood at a gage height of 18 m (60 feet) (approximate elevation 2671 m (8,760 feet)), and, within thirty days, reportedly fell to a gage height of 9 m (30 feet). Based on written descriptions, the seepage did not appear to flow through the dam embankment, but rather through the left abutment. This water loss rate indicates more than 0.6 m^3/s (20 ft^3/s) leakage.
- In 1938, a sinkhole or depression was observed in the area above the cribbing on the left abutment. The sinkhole or depression was reportedly 3.7 m (12 feet) in diameter and 6 m (20 feet) deep. It was also noted that the drainage tunnel was blocked by failed timbers and rock 7.6 m (25 feet) from the entrance. The drainage tunnel was backfilled shortly after the occurrence of the sinkhole or depression.
- In 1941, significant seepage in the area of the left abutment rock knob was reported.
- In 1958, seepage areas were observed on the face of the dam. A sinkhole approximately 3 m (10 feet) in diameter and 3.4 m (11 feet) deep adjacent to the gate tower was noted. Another area was noted, in which 11 to 15 m^3 (15 to 20 yd^3) of material had slumped or slipped, approximately 15 m (50 feet) from the crest of the spillway at the right abutment.
- In 1961, internal erosion of material into the gate tower was reported.
- In 1975, internal erosion into the outlet works gate tower was again noted as muddy leakage through cracks in the tower structure.
- In 1976, failure of the cribbing, which had initiated a few years earlier, was worsening. Reports noted that a hole was found in the upstream face of the dam, described as being approximately 11 m (37 feet) above the invert of the outlet and approximately 30 m (100 feet) to the left of the outlet trash rack. The hole was 1 m (3 feet) wide, approximately 1.5 m (5 feet) deep, and more or less cylindrical.
- In 2010, a sinkhole was observed in the moraine in the left abutment to the left of the rock knob and downstream of the embankment on the left abutment. This sinkhole may be in the same area as the 1938 sinkhole.

RISK ANALYSIS

Methodology

At the suggestion of URS Corporation (URS), the CPW decided to complete a quantitative risk analysis to better understand the issues related to the observed sinkhole. The risk analysis was completed in general accordance with the methods

presented in "Dam Safety Risk Analysis Best Practices" (Reclamation, 2010)[2]. This risk analysis effort was limited to consideration of only seepage and piping (internal erosion) risks for normal operations. Other static loading risks and hydrologic (flood) and seismic (earthquake) loading risks were not considered in this effort.

The risk analysis was accomplished by assembling a group of experienced engineers and geologists from CPW, URS, and the Colorado SEO in a facilitated workshop setting, using the expert elicitation process described in Reclamation, 2010. The process consisted of: a) identification and qualification of potential failure modes, b) estimation of dam failure consequences, c) development of failure event trees, and d) estimation of nodal probabilities for the event trees. For this process, risk is defined as:

$$ALL = P_L \times P_F \times C \quad (1)$$

where ALL = annualized life loss risk
P_L = probability of load
P_F = probability of failure, given the load
C = consequences

All elements of the risk analysis process are discussed below.

Potential Failure Modes

The risk analysis began with a potential failure modes analysis. The risk analysis team identified three potential failure modes (PFMs), which were judged to be sufficiently significant to justify quantitative risk estimation. These three potential failure modes, designated as PFM Nos. 1 through 3, are described in detail below. In addition, the team identified three other PFMs, which were judged to be significantly less likely than PFM Nos. 1 through 3. These three other PFMs are described briefly and the principal reasons for the judgments that they are very unlikely are given. These three less likely PFMs were not carried through to a quantitative risk analysis.

PFM No. 1 – Internal Erosion of the Left Abutment Moraine Exiting Along the Downstream Abutment Face. This potential failure mode would occur through the development of the following events:

1. Seepage gradients through the abutment are sufficient to initiate erosion of the moraine that forms the foundation of the left portion of the dam embankment.
2. The eroding moraine material exits downstream through one of the following paths: into the abandoned drainage tunnel, through the cribbing and rockfill buttress, or along the outer contact of the rock knob.

[2] The referenced Reclamation document, "Dam Safety Risk Analysis, Best Practices Training Manual," has been revised and updated numerous times, including some revisions after the referenced date; however, the subsequent revisions have not been substantial relative to the application to Beaver Park Dam.

3. The gradation of the downstream rockfill materials is insufficient to provide adequate filtering of the eroding material.
4. A pipe (cavity) forms in the moraine abutment and extends upstream toward the embankment and puddle liner.
5. Embankment/liner material begins to erode into the abutment, further progressing the pipe upstream toward the reservoir.
6. The pipe connects to the reservoir, resulting in a direct, open seepage path downstream. The pipe continues to enlarge.
7. Intervention fails.
8. Rapid erosion of the embankment and foundation occurs, leading to breach development and release of the reservoir.

The location of the pathway for this failure mode is illustrated on Figures 3 and 4.

PFM No. 2 – Internal Erosion of the Left Abutment Moraine Exiting Approximately 240 m (800 feet) Downstream. This potential failure mode is similar to PFM 1 in that it involves internal erosion of the moraine comprising the left abutment. This potential failure mode would occur through the development of the following events:

1. Seepage gradients through the abutment are sufficient to initiate erosion of the moraine that forms the foundation of the left portion of the dam embankment.
2. The eroding moraine material exits approximately 240 m (800 feet) downstream of the dam into the area where there was a washout during initial filling of the reservoir.
3. No downstream material is present to adequately filter the eroding material.
4. A pipe forms through the moraine foundation and extends 240 m (800 feet) upstream toward the embankment and puddle liner.
5. Embankment and puddle liner material begin to erode into the abutment, further progressing the pipe upstream toward the reservoir.
6. The pipe connects to the reservoir, resulting in a direct, open seepage path 240 m (800 feet) long. The pipe continues to enlarge.
7. Intervention fails.
8. Rapid erosion of the embankment and foundation occurs, leading to breach development and release of the reservoir.

The pathway for this failure mode is illustrated on Figure 3.

PFM No. 3 – Internal Erosion of Embankment Into Discontinuities in the Left Abutment Rock Knob - This potential failure mode would occur through the development of the following events:

1. Concentrated seepage through weak joint infilling material or open joints in the rock knob initiates erosion of the adjacent embankment material.
2. Embankment material begins to erode and is carried through the rock knob along the discontinuities.

3. Eroded material exits along the downstream exposed face of the rock knob or into the rockfill in the embankment.
4. A pipe forms in the embankment and progresses upstream.
5. The pipe connects to the reservoir, and the pipe enlarges.
6. Intervention fails.
7. Erosion of the embankment progresses, leading to breach development and release of the reservoir.

Less Likely Failure Modes

Internal Erosion Through the Right Abutment. This failure mode is similar to PFM No. 3 and involves internal erosion of embankment material into voids and discontinuities of the abutment rock. Open joints along the foundation of the right abutment allow concentrated seepage that could initiate erosion of the adjacent embankment material, which could then progress as a pipe upstream, intersecting the reservoir. Due mainly to the erosion-resistant bedrock, which would restrict lateral progression or widening of the erosion path, along with the erosion resistant rockfill limiting upstream progression, it was judged that it is difficult to conceive of this mechanism developing into a catastrophic release of the reservoir.

Erosion Through the Concrete Face. This failure mode consists of open joints, cracks or other defects in the concrete facing of the original dam, allowing concentrated seepage paths through the facing and into the downstream rockfill. These concentrated seepage paths could initiate erosion of the earthfill that was placed immediately adjacent to the facing during the dam raise in the 1947-1953 timeframe. The coarse rockfill downstream of the facing would not provide filtering of the eroding embankment material. Erosion could progress upstream, intercepting the reservoir. Seepage may be occurring through the concrete face and may pose maintenance issues if the seepage is significant enough to disrupt the upstream earthfill material. However, based on the likely small size of cracks in the concrete face and the high discharge capability of the downstream rockfill shell, it was difficult to conceive that this failure mode would lead to a catastrophic dam failure.

Uncontrolled Release of Reservoir Through Failed Outlet Gate Tower. This failure mode consists of embankment material eroding into defects or open joints in the outlet gate tower, or alternatively structural collapse of a portion of the tower inducing significant inflow of material and seepage through the outlet tunnel/conduit.

Muddy leakage into the tower has been observed in the past indicating adjacent earthfill material was eroding into the tower. Repairs were performed in response to the leakage and no other occurrences have been noted in the last 35 years. Since the installation of the gate in the downstream face of the tower, the tower has operated as a wet well. This results in minimal to no seepage gradient into the tower, resulting in a very low likelihood of the initiation of erosion. These considerations limit the feasibility of this piping failure mechanism.

The following considerations were noted in regard to the potential of developing a dam breach due to a structural collapse of the tower. The tower, which was part of the original construction, was not modified during the 1947-1953 dam modification, and, therefore, may have inadequate strength for the modified loading conditions induced by the additional earthfill. Although some cracking has been observed in the tower over the 50 plus years since the additional earthfill placement, no significant or severe defect indicating a loss of structural integrity has been observed. There was likely some reserve structural capacity of the tower based on historically conservative design procedures.

Regardless of the mechanism, the downstream gate would provide a means of controlling reservoir release if it is not made inoperable by debris in the tower. A structural collapse of the tower would impact the upstream gate, but would not likely inhibit the use of the downstream gate. Even if the downstream gate were to fail, or was otherwise disabled, the discharge would be limited to the capacity of the outlet tunnel, which is about 17 m^3/s (600 ft^3/s). The steel lining and rock tunnel would restrict any further progression of the release. Therefore, this failure mode was considered very unlikely to result in a catastrophic dam failure or a large release flow.

Consequences

Beaver Park Dam is classified as a High Hazard facility. The dam is located on Beaver Creek, where the creek runs generally in a northerly direction about 1.6 km (1 mi) to its confluence with the South Fork of the Rio Grande. Immediately downstream of the dam, the creek cuts a deep channel through near vertical rock cliffs. Downstream of the narrow canyon, the creek emerges into the broad V-shaped valley of the Rio Grande.

A detailed inundation study has not been performed for the dam. However, a simplified HEC-RAS study was recently performed to provide a screening level assessment of the potential inundation and downstream flooding. The peak breach discharge due to dam failure was estimated to be on the order 1,400 m^3/s (50,000 ft^3/s), based on a simplified procedure to estimate breach geometry and assuming a rapid release. Floodwaters from a dam failure would flow through Beaver Creek Canyon and along the South Fork of the Rio Grande for a total distance of approximately 6 km (4 mi) before entering the Rio Grande valley near South Fork, Colorado. From there, flow levels would begin to attenuate as the channel becomes wider. Flood flows would continue down the Rio Grande through the South Fork population center. Population centers within the inundation zone include a popular recreational area, which accommodates overnight campers, located approximately 3 km (2 mi) downstream of the dam, within the relatively narrow canyon, and homes in South Fork constructed along the riverbank. In addition, a U.S. Highway 160 bridge would likely be inundated by the flood wave.

The camping area downstream of the dam has on average 50 to 75 people seasonally. A preliminary and qualitative estimate of inhabited homes and recreationalists who may be within the inundation area near South Fork indicates approximately 200 to 400 people (approximately 100 homes) could be within the flood zone. Several of these structures are RV or mobile trailer type homes, which would be easily damaged in a flood. A detailed evaluation of fatality rates for these populations at risk was not performed due to limited information. However, in consideration of likely flood severity and ability to evacuate, a loss of life estimate ranging from 10 to 50, with a best estimate of 25 people, was assumed for the purposes of this risk analysis. In light of the lack of an inundation-mapping-based loss of life estimate performed for this dam, this life loss estimate is believed to be conservative (i.e., high).

Event Trees

Once the potential failure modes had been defined and thoroughly understood, the team began the process of discussing each step of the failure mechanism and estimating probabilities. Probabilities of failure were estimated for the three previously described potential failure modes that were considered plausible enough to contribute significantly to the overall risk of failure of the dam. The series of events to fully develop the three internal erosion failure modes were based on Reclamation's Best Practices Guidance (Reclamation, 2010) and generally included the following sequence of events:

- Reservoir At or Rises Above Threshold Level
  - Erosion Initiates
    - Erosion Continuation (lack of filtering)
      - Progression Step 1 (roof forms to support a pipe)
        - Progression Step 2 (upstream zone fails to fill crack)
          - Progression Step 3 (constriction or upstream zone fails to limit flows)
            - Unsuccessful Intervention
              - Catastrophic Breach

Risk Estimates – Existing Conditions

This risk analysis initially considered normal operating conditions (without the current reservoir restriction). Therefore, the probability of the reservoir rising to normal pool level was considered to be 100 percent (or P = 1.0). The risk team thoroughly discussed the factors and considerations that would be relevant to each event node prior to estimating probabilities for each of the subsequent events. If there was significant uncertainty in the probability of a given event, the team estimated a range of probabilities, selecting a value within the range as the "best estimate." In assigning probabilities to the various events, the risk team used the verbal probability

descriptors given in Table 1, which are a slight modification of the verbal descriptor scheme given in Reclamation (2010). The modification is the addition of a descriptor "inconceivable" with an associated probability of 0.0001.

Table 1. Verbal Probability Descriptors

Descriptor	Probability
Virtually Certain	0.999
Very Likely	0.99
Likely	0.9
Neutral	0.5
Unlikely	0.1
Very Unlikely	0.01
Virtually Impossible	0.001
Inconceivable	0.0001

PFM No. 1 – Internal Erosion of the Left Abutment Moraine Exiting Along the Downstream Abutment Face. Table 2 summarizes the factors that make this failure mode more likely or less likely and the assigned probability of occurrence for each step in the event node series. The mean (best estimate) annualized probability of failure estimate for this potential failure mode is $\mathbf{1.5 \times 10^{-2}}$. Combined with the mean loss of life estimate of 25 people, the estimated annualized life loss (ALL) risk for this potential failure mode is $\mathbf{3.8 \times 10^{-1}}$. This life loss risk is greater than 1×10^{-2}, which indicates justification for taking expedited action to reduce risk, according to the Reclamation guidelines used for this analysis.

The most influential factors increasing the risk estimate for this potential failure mode are the lack of a downstream filter, lack of an upstream crack stopper or constriction, and limited ability to detect the erosion because of the relatively concealed locations of the exit points. A significant event node probability is the 0.05 probability estimated for the initiation node. The information presented in Reclamation (2010) indicates that the experience for Reclamation's portfolio of dams suggests a best estimate range of probability for initiation for seepage and piping through the foundation is 2×10^{-3} to 1×10^{-2}. Evidence of sinkholes potentially related to this potential failure mode at Beaver Park Dam has been observed two to three times in the almost 100 year history of this dam; this corresponds to a recurrence rate of about 2/100 to 3/100 (0.02 to 0.03). Based on the Reclamation guidance and the observed frequency of sinkhole occurrence, the team estimated the probability of initiation as a best estimate of 0.05 and a range of 0.01 to 0.1; the best estimate being five times higher than the upper end of Reclamation's estimated range.

PFM No. 2 – Internal Erosion of the Left Abutment Moraine Exiting Approximately 240 m (800 ft) Downstream. Event node probabilities for this PFM were estimated using the same tabular format presented in Table 2 for PFM No. 1. Space limitations do not allow inclusion of that information in this paper. The resulting mean annualized probability of failure estimate for this potential failure

mode is **4.0 x 10^{-6}**. Combined with the mean loss of life estimate of 25 people, the estimated annualized life loss risk for this potential failure mode is **1.0 x 10^{-4}**. This annualized probability of failure and life loss risk are within the range of Reclamation's risk guidelines indicating a reduced justification to take action to reduce risk.

Similar to PFM No. 1, the most influential factors increasing the risk estimate for this failure mode are the lack of a downstream filter and lack of an upstream crack stopper or constriction. However, the factors that significantly reduce the risk of this potential failure mode in comparison to PFM No. 1 were the reduced probability of erosion initiating due to the relatively low average seepage gradients as well as the low probability that the glacial moraine material could sustain a roof for such a long distance (240 m (800 feet)), considering the lateral variability of the moraine deposit. The probability of sustaining a roof for this potential failure mode was estimated at 0.05, compared to 0.5 for this event node for PMF No. 1. In addition, intervention for this potential failure mode was judged to be more likely than for PFM No. 1, due to: a) the improved detection ability if specific monitoring of the area was conducted and b) the extended period of time that would be needed for this potential failure mode to fully progress. Finally, development of the breach was estimated to be slightly less likely for this potential failure mode compared to PFM No. 1 (0.9 compared to 0.99), because of the larger volume of material that would need to be removed for breaching to occur in this PFM.

Table 2. Probability of Failure of Beaver Park Dam, PFM No. 1

PFM NO. 1: FAILURE DUE TO INTERNAL EROSION OF MORAINE OF LEFT ABUTMENT FOUNDATION INTO THE FOLLOWING FEATURES: CRIBBING/ROCKFILL BUTTRESS, DRAINAGE TUNNEL, OR ALONG CONTACT AT ROCK KNOB				
Node Description	**Likely/Unlikely Factors**	**Probability Descriptor**	**Probability Estimate**	
			Best	**Range**
Reservoir at or Above Threshold Level (normal pool)	Assume reservoir is brought back into normal operating conditions		1.0	

Table 2. Probability of Failure of Beaver Park Dam, PFM No. 1

PFM NO. 1: FAILURE DUE TO INTERNAL EROSION OF MORAINE OF LEFT ABUTMENT FOUNDATION INTO THE FOLLOWING FEATURES: CRIBBING/ROCKFILL BUTTRESS, DRAINAGE TUNNEL, OR ALONG CONTACT AT ROCK KNOB				
Node Description	**Likely/Unlikely Factors**	**Probability Descriptor**	**Probability Estimate**	
			Best	**Range**
Initiation – Erosion Starts (considers re-initiation)	More Likely Factors: 1. Moraine and embankment are erodible (SM-ML) 2. Evidence that erosion has occurred (sinkholes in 1938 and 2010) 3. Steep exit slope encourages movement of material 4. Muddy flow reported in one instance (1938) out of drainage tunnel (but may be due to timber decay) 5. Washout occurred in this area during first filling attempt 6. High gradients possible (into upstream end of tunnel could be 0.5 or higher) 7. Material reportedly washed into drainage tunnel and collapsed a portion of tunnel during filling Less Likely Factors: 1. 1938 and 2010 sinkholes may be caused by presence of an open shaft (timber seen in sinkhole in 1938) and not seepage 2. Since initial filling, evidence of development of this failure mode has been limited to the observed sinkholes 3. Average gradient is not high (estimated to be 0.15 to 0.20)	Unlikely – Very Unlikely	0.05	0.01 – 0.1
Continuation – Unfiltered Exit	More Likely Factors: 1. Exits: into drainage tunnel or cribbing and out rockfill buttress 2. Limited info on cribbing backfill, drainage tunnel backfill, rockfill placed in 1978 and 1988 3. Low probability of filter compatibility of moraine with tunnel backfill Less Likely Factors: 1. Photos and exposed rockfill indicate some zones may contain well-graded material with smaller particles. However, these zones are not continuous and therefore unlikely the full face is filtered	Likely	0.9	

Table 2. Probability of Failure of Beaver Park Dam, PFM No. 1

PFM NO. 1: FAILURE DUE TO INTERNAL EROSION OF MORAINE OF LEFT ABUTMENT FOUNDATION INTO THE FOLLOWING FEATURES: CRIBBING/ROCKFILL BUTTRESS, DRAINAGE TUNNEL, OR ALONG CONTACT AT ROCK KNOB				
Node Description	**Likely/Unlikely Factors**	**Probability Descriptor**	**Probability Estimate**	
			Best	**Range**
Progression – Roof Forms	More Likely Factors: 1. Moraine is a layered and non-uniform deposit. Braided channel of coarse material with less than 10% fines within a finer-grained mass. Fine-grained deposits possible in the glacial outwash deposit 2. Drainage tunnel was excavated in the moraine – evidence of some cohesion possibly as the result of high density 3. Very steep (> 1:1) exit slope indicating cohesion 4. One lab test indicated 9% clay-sized particles Less Likely Factors: 1. Need continuous, cohesive layer over several hundred feet and greater than ~ 0.3 m (1 foot) thick 2. The tunnel collapse that previously occurred did not result in a progression (but reservoir was quickly lowered)	Unlikely - Likely	0.5	0.1 – 0.9
Progression – Upstream zones fails to fill pipe	More Likely Factors: 1. Homogenous embankment 2. Upstream material (embankment and moraine) is a sandy silt (SM-ML). Would be difficult for this material to plug large hole	Very Likely	0.99	
Progression – Constriction or upstream zone fails to limit flows	More Likely Factors: 1. Large deposit of sandy silt 2. Reservoir blanket likely similar material as moraine and likely thin and deteriorated	Very Likely	0.99	
Intervention fails	More Likely Factors: 1. Rockfill hinders observations at downstream toe 2. Limited monitoring instrumentation/locations (1 downstream flume). Downstream gauge could measure increased flow, but would be a delayed detection 3. Rockfill also may block the interface on which it is desired to place reverse filter in a response 4. Access to downstream toe and material placement would be difficult and take time 5. Sinkholes are the most readily detectable (as compared to irregular discharge), but a sinkhole may not form Less Likely Factors: 1. Visited by staff about 1-2 times weekly during normal operations (year round) and will do walk through inspection 2. Rapid drawdown capacity (can significantly lower reservoir in a few days) 3. Gates operated frequently, but aging	Neutral - Likely	0.7	0.5 – 0.9

Table 2. Probability of Failure of Beaver Park Dam, PFM No. 1

PFM NO. 1: FAILURE DUE TO INTERNAL EROSION OF MORAINE OF LEFT ABUTMENT FOUNDATION INTO THE FOLLOWING FEATURES: CRIBBING/ROCKFILL BUTTRESS, DRAINAGE TUNNEL, OR ALONG CONTACT AT ROCK KNOB				
Node Description	**Likely/Unlikely Factors**	**Probability Descriptor**	**Probability Estimate**	
			Best	**Range**
Dam Breaches	More Likely Factors: 1. Embankment and abutment materials are erodible and without intervention would continue to erode until the full breach is developed		0.99	
Estimated Annualized Probability of Failure			**1.5×10^{-2}**	4.4×10^{-4} - 7.1×10^{-2}

PFM No. 3 – Internal Erosion of Embankment Into Discontinuities In The Left Abutment Rock Knob. Event node probabilities for this PFM were estimated using the same tabular format presented in Table 2 for PFM No. 1. The resulting mean annualized probability of failure estimated for this potential failure mode is **2.5×10^{-7}**. Combined with the mean loss of life estimate of 25 people, the estimated annualized life loss risk for this potential failure mode is **6.3×10^{-6}**. This annualized probability of failure and life loss risk are within the range of Reclamation's risk guidelines indicating a reduced justification to take action to reduce risk.

The most influential factors increasing the risk estimate for this potential failure mode are the ability to sustain a roof through the rock knob as well as through the limited thickness of overlying embankment material, the erosion susceptibility of the embankment material, and the lack of a downstream filter. However, the fact that seepage in this potential failure mode would be through a jointed rock mass significantly reduced the overall risk. The limited size of the joints and the high resistance to enlarging the crack through the rock allow an improved ability of self-healing or plugging of the joints as well as providing an effective constriction to uncontrolled progression. Furthermore, there is a high probability of detection and intervention given the visibility of the exit point and the long duration to fully develop the failure mode. There is also improved erosion resistance at the downstream exit for those exit points that are under rockfill, which would reduce the probability of fully developing a dam breach through this seepage path, even if intervention was unsuccessful.

Risk Estimate – Current Reservoir Restrictions

In order to evaluate the justification and effectiveness of the current 6 m (20-foot) reservoir restriction imposed by the Colorado SEO, the team estimated the risk of the highest risk potential failure mode, PFM No. 1 (erosion through the left abutment moraine, exiting at the downstream abutment face), under the restricted pool conditions. The probabilities of two of the event nodes were judged to be affected by the restriction and were modified; all other probability estimates remained unchanged.

Erosion Initiates. The probability that erosion would initiate under the lowered pool was considered to be significantly reduced in comparison to the normal operating conditions. The lower pool results in at least a 25 percent reduction in the average seepage gradient. In addition, the restricted pool level is significantly lower than the normal operating level since the 1950s. Based on these considerations, the probability of the occurrence of this event node was reduced from 0.05 under normal operating conditions to 0.002 under the restricted pool. The estimated value of 0.002 is the lower end of the initiation range probability indicated in Reclamation (2010).

Intervention Fails. The probability that intervention would fail under the lowered pool was also considered to be significantly reduced in comparison to the normal operating conditions. Daily dam inspections are being conducted during the reservoir restriction period. This improves the probability of detection of sinkholes, vortexes or muddy discharge in the downstream channel, even though the immediate exit points are relatively concealed. Furthermore, the reservoir can be drawn down more quickly in the event intervention was required, due to the reduced storage volume in the reservoir. Based on these considerations, the probability of intervention failing was reduced from 0.7, under normal operating conditions, to 0.1 under the restricted pool.

Overall Risk Reduction. Based on the reduction of estimated probabilities for these two nodes, the overall annualized probability of failure for this potential failure mode was reduced to $\mathbf{8.7 \times 10^{-5}}$ under the restricted pool. This results in a mean annualized life loss risk of $\mathbf{2.1 \times 10^{-3}}$. The reservoir restriction reduces the risk by slightly over two orders of magnitude into the range designated in Reclamation's guidelines as justifying long-term risk reduction actions instead of the range indicating the need for expedited action. Therefore, the reservoir restriction appears to be a reasonable and prudent measure until such time that more permanent remediation can be implemented.

Risk Estimate – Risk Reduction Alternatives

The following three alternatives were considered for reducing the risk for PFM No. 1:

- A filtered seepage collection system on the left abutment
- A diaphragm wall in the left abutment
- A low permeability blanket on the upstream slope and in the reservoir on the left abutment

The risks were re-evaluated for these three alternatives for a return to normal reservoir operations.

The filtered seepage collection alternative (No. 1) would be expected to slightly increase the probability of intervention, as a result of the ability to monitor the seepage flows from the filter and drain system. The probability for the unsuccessful intervention node was changed from 0.7 to 0.5. The major effect of the filtered

seepage collection alternative would be to provide a low probability of an unfiltered seepage exit. The probability for this node was reduced from 0.9 to 0.005. The resulting estimated annualized probability of failure for this potential failure mode with the filtered seepage collection system on the left abutment is **6.0×10^{-5}**.

The diaphragm wall in the left abutment (No. 2) would slightly reduce the probability of initiation, as the result of potentially reduced exit gradient. The probability for the initiation node was changed from 0.05 to 0.03. It would also be expected to moderately reduce the likelihood of breach formation, because it might constrain any pipe to such a long path that the reservoir would drain without forming a full breach. The probability for this node was reduced from 0.99 to 0.5. The major effect of this alternative would be a much lower probability of progression as the result of flow being limited by a well-constructed wall, tied into bedrock and having no significant windows. The probability for the third progression node was reduced from 0.99 to 0.005. The resulting estimated annualized probability of failure for this potential failure mode with the construction of the diaphragm wall in the left abutment is **2.4×10^{-5}**.

The low permeability blanket on the upstream slope and in the reservoir (No. 3) would be expected to have only a minor affect on the probability of initiation, as the result of potentially reduced exit gradients. The probability for the initiation node was changed from 0.05 to 0.03. This alternative would not be expected to have any effect on any of the other event nodes. The resulting estimated annualized probability of failure for this potential failure mode following the construction of the low permeability blanket is **9.0×10^{-3}**, only slightly less than the estimated **1.5×10^{-2}** for the existing conditions under normal operations.

The low permeability blanket provides very little risk reduction and was eliminated from further consideration. Preliminary designs and estimated costs were developed for the other two alternatives. The estimated cost was much higher for the diaphragm wall than for the filtered seepage collection system, while the risk reduction was only slightly greater for the diaphragm wall. In addition, it was judged that the confidence level in successful construction of the diaphragm wall was less than that for the filtered seepage collection system. Therefore, the seepage collection system on the left abutment was selected as the preferred alternative.

SUMMARY OF RISK ESTIMATES

Table 3 summarizes the "best estimates" of annualized probability of failure, loss of life consequences, and annualized life loss risk for each potential failure mode evaluated. These results are also presented graphically on an *f*-N chart in Figure 6. The *f*-N chart is a plot of the annualized probability of failure (*f*), on the vertical axis, versus the estimated loss of life consequences (N), on the horizontal axis. Both axes are logarithmic scales. The diagonal lines on Figure 6 are lines of equal annualized life loss risk, with the corresponding annualized life loss risks noted on the right side of the figure.

It should be noted that the risk estimate results for Alternative No. 1 plot slightly above the guideline for diminishing justification to take action to reduce risk. However, in this instance, this was judged to be acceptable because the life loss estimate of 25 people is believed to be conservatively high and modification to the alternative to further reduce the probability of failure would be very expensive.

Table 3. Summary of "Best Estimates" of Risks

Potential Failure Mode	Description	Annualized Probability of Failure	Estimated Loss of Life	Annualized Life Loss Risk
PFM No. 1	Normal Operations - Piping of Moraine along the Left Abutment Exiting at the Downstream Abutment Face	1.5×10^{-2}	25	3.8×10^{-1}
PFM No. 2	Normal Operations - Piping of Moraine along the Left Abutment Exiting 1,500-ft Downstream of the Dam	4.0×10^{-6}	25	1.0×10^{-4}
PFM No. 3	Normal Operations - Piping Into Discontinuities in the Left Abutment Rock Knob	2.5×10^{-7}	25	6.3×10^{-6}
PFM No. 1-Restricted	PFM No. 1 Under Current Reservoir Restrictions (20 feet below the spillway crest)	8.7×10^{-5}	25	2.1×10^{-3}
PFM No. 1-Modified – Alternative 1	PFM No. 1 Under Normal Operations with a Left Abutment Filtered Seepage Collection System	6.0×10^{-5}	25	1.5×10^{-3}
PFM No. 1-Modified – Alternative 2	PFM No. 1 Under Normal Operations with a Left Abutment Diaphragm Wall	2.4×10^{-5}	25	6.0×10^{-4}
PFM No. 1-Modified – Alternative 3	PFM No. 1 Under Normal Operations with a Left Abutment Upstream Blanket	9.0×10^{-3}	25	2.3×10^{-1}

SUMMARY AND CONCLUSIONS

Six potential failure modes were identified for the Beaver Park Dam under normal operating conditions, reservoir elevation 2677 m (8,782). Of the six PFMs, three were considered highly unlikely and were not carried forward to the quantitative risk analysis. A quantitative risk analysis was completed for the remaining three potential failure modes, all relating to internal erosion of the embankment and/or foundation moraine materials on the left abutment.

Based on a simplified approach used to estimate loss of life consequences in the event of a dam breach, a mean loss of life estimate of 25 people was assumed for the purposes of the risk analysis. Based on the results of the risk analysis, PFM No. 1 was identified as the most critical potential failure mode, with the highest level of estimated risk. PFM No. 1 considers the potential of internal erosion of the moraine material along the left abutment, exiting the downstream face of the abutment near the downstream toe of the dam, and progressing upstream to the reservoir, resulting in a dam breach.

The mean annualized probability of failure for PFM No.1 under existing conditions was estimated by the team to be $\mathbf{1.5 \times 10^{-2}}$. The estimated mean annualized life loss risk for PFM No. 1 under existing conditions was $\mathbf{3.8 \times 10^{-1}}$, which is the product of the annualized probability of failure and the estimated loss of life consequences. The most influential factors increasing the risk estimate for this failure mode are the lack of a downstream filter, lack of an upstream crack stopper or constriction, and limited ability to detect the erosion due to the relatively concealed locations of the exit points. The combination of the annualized probability of failure and the mean annualized life loss risk for PFM No. 1 under existing conditions significantly exceeds (by more than an order of magnitude) Reclamation's guidelines for expedited risk reduction actions, according to their Public Protection Guidelines [Reclamation, 2003][3]. Based on these estimated risks, expedited risk reduction actions are justified. The risk estimates for PFM No. 2 and PFM No. 3 under existing conditions are below Reclamation's guidelines, indicating a reduced justification for risk reduction action related to these potential failure modes.

The reservoir is currently under a maximum normal high pool restriction to 6 m (20 feet) below the normal spillway crest. This is considered an interim risk reduction action. The team also estimated the risks of the dam under the restricted operating conditions. The mean annualized probability of failure for PFM No.1 under the restricted pool was estimated by the team to be $\mathbf{8.7 \times 10^{-5}}$. The estimated mean annualized life loss risk for PFM No. 1 under the restricted pool was $\mathbf{2.1 \times 10^{-3}}$, which is below the expedited action range, but still within Reclamation's range of justification for long-term risk reduction action. Based on the results of the risk analysis, maintaining the restricted pool level as an interim means of risk reduction is a prudent measure until a permanent remediation for the dam can be developed and implemented.

An alternatives analysis was completed to evaluate three alternatives to reduce the seepage and piping risk associated with PFM No. 1. Risks were re-evaluated for the three alternatives. Based on the risk analysis results, estimated construction costs, and an assessment of the reliability of construction, a filtered seepage collection system on the left abutment was selected as the preferred alternative.

[3] In August 2011 Reclamation issued Interim Dam Safety Public Protection Guidelines, which are intended to replace the 2003 Public Protection Guidelines. The 2003 Guidelines were the agency's guidance at the time of the work reported in this paper. The conclusions presented in this paper are generally consistent with the new, 2011 guidance.

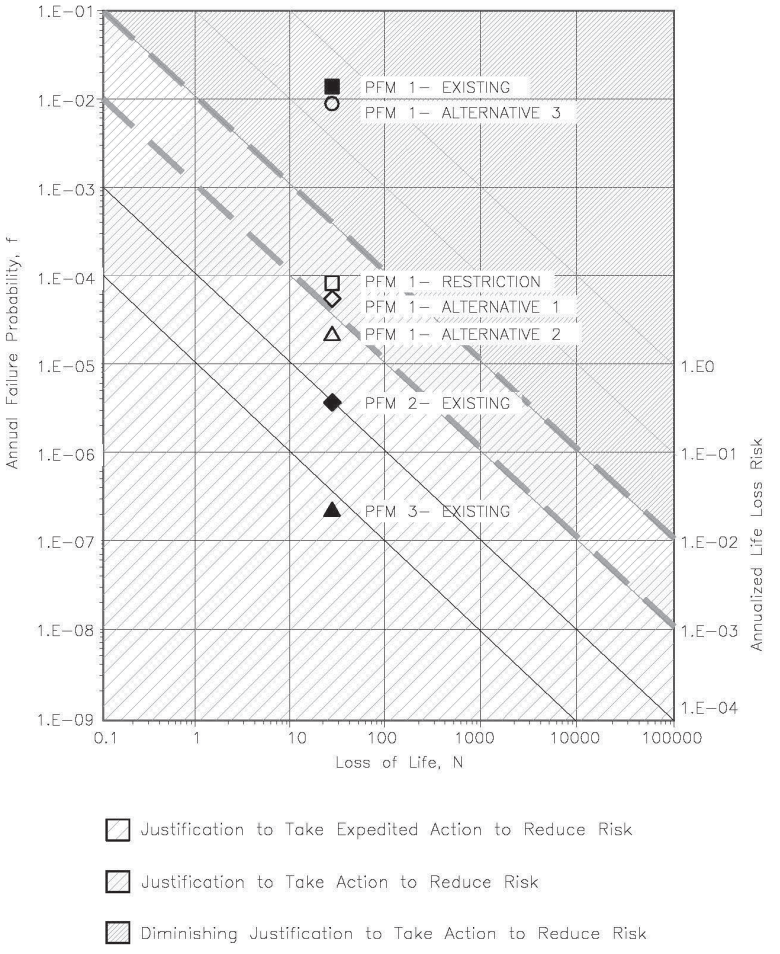

FIG. 6. *f*-N Plot of Results

ACKNOWLEDGEMENTS

The authors gratefully acknowledge the Association of State Dam Safety Officials and the United States Society on Dams for permission to republish figures, tables, and some text from papers previously published in Dam Safety 2011, the Proceedings of the Annual Conference of ASDSO (France et al, 2011) and the Proceedings of the 32nd Annual Meeting and Conference of USSD (France et al, 2012).

REFERENCES

France, John W., Bill McCormick, and Matt Gavin, "Risk Analysis Provides Support for Dam Safety Decisions for Beaver Park Dam, Colorado," Proceedings of Dam Safety 2011, Annual Conference of the Association of State Dam Safety Officials, Washington, DC, September 2011.

France, John W., Bill McCormick, and Matt Gavin, "Risk Analysis Guides Dam Safety Decisions for Beaver Park Dam, Colorado," Proceedings of the 32nd Annual Meeting and Conference of the United States Society on Dams, New Orleans, LA, April 2012.

U.S. Department of Interior, Bureau of Reclamation (Reclamation), 2003, "Guidelines for Achieving Public Protection in Dam Safety Decision Making," Technical Service Center, Denver, Colorado, June 15, 2003.

U.S. Department of Interior, Bureau of Reclamation (Reclamation), 2009, "Dam Safety Risk Analysis Best Practices, Version 1.3" Technical Service Center, Denver, Colorado, February 2010.

Seismic and Electrical 3D Imaging to Aid in Landslide Remediation Design, East Fork Landslide, Wolf Creek Pass, Colorado

Phil Sirles[1], Khamis Haramy[2], M. ASCE, Rick D. Andrew[3], M. ASCE, P.G., and Roger W. Surdahl[4], M. ASCE., P.E.

[1]Managing Geophysicist / VP, Zonge International, Inc., 7721 W. 6th Ave., Suite G, Lakewood, CO 80214; phil.sirles@zonge.com
[2]Sr. Geotechnical Engineer, Central Federal Lands Highway Division, FHWA, 12300 W. Dakota Avenue, Suite 210B, Lakewood, CO 80228; khamis.haramy@dot.gov
[3]Vice President, Yeh and Associates, 5700 East Evans Avenue Denver, CO 80222; randrew@yeh-eng.com
[4]Technical Delivery Engineer, Central Federal Lands Highway Division, FHWA, 12300 W. Dakota Avenue, Suite 210B, Lakewood, CO 80228; roger.surdahl@dot.gov

ABSTRACT: 3D geophysical investigations were performed on an active landslide in southwestern Colorado, south of Highway 160 on the west side of Wolf Creek Pass. The landslide impacted a major natural gas line and forced closure of an important forest access road. Two geophysical methods, seismic and electrical, were selected to optimize subsurface volumetric evaluation and supplement conventional geotechnical field investigations. The primary purpose of this study was to evaluate the value of wide-area surface geophysical surveys, using new 3D technologies, to better characterize the landslide mass and improve remediation designs. The purpose and project objectives were met with this study. Results indicate the 3D seismic survey delineated soft materials within the landslide mass and the landslide slip plane depth, as it correlated with borehole results. 3D electrical resistivity results, when compared to areas outside the most the recent movement of the landslide and borehole results, showed anomalies of lower resistance that correlate well with areas of higher water content. In addition, 3D induced polarization results indicate materials within the landslide mass that have high chargeability which appear to correlate with higher clay content.

INTRODUCTION

The project site is located in southwestern Colorado, on the west side of Wolf Creek Pass (Figure 1). The East Fork landslide, reactivated in 2009, with a 183 m (600') wide by 610 m (2000') upslope disturbance is outlined on the aerial view of the area in Figure 2. The

2009 movement displaced a National Forest Service access road (seen as the light brown line in Figure 2) about 46 m (150') downslope, where the landslide terminated in the East Fork of the San Juan River. This slide continued to move at a rate of several feet per day in the area of the access road which forced a road closure. The slide continued to move with a decreasing rate for the next two months. Most of the measured movement occurred below the roadway and up to 152.5 m (500') above the roadway. However, lateral shear, expressed as pressure ridges, existed along both the eastern and western flanks of the landslide and could be observed over 610 m (2000') feet above the road. Extensional features such as sag ponds were also observed at various locations, some of which contained water. Large pine and aspen trees were downed and toppled, and some were leaning precariously due to the movement (inset photos). A primary natural gas pipeline located along the access road ruptured during the event; the pipeline services the San Luis Valley and other areas, including Vail and Aspen. Re-establishing safe access through the National Forest was a high priority for public and private land access, and the gas pipeline needed immediate repair.

Figure 1. Location map for East Fork landslide 3D geophysics project

East Fork slide is characterized as a translational landslide with signs of minor rotational sliding below the access road. These types of landslides can exhibit sudden, rapid failure, are relatively shallow-seated, and are typically composed of loose, highly disturbed saturated soils. Movements of these masses commonly occur along depositional boundaries that dip parallel to the slide surface, as observed on both sides of the slide, but may also occur along the upper portions of larger, deeper-seated, ancient landslide regions. The total slide, including the previously active area is about 457 m (1500') wide by 762 m (2500') upslope. Figure 2 shows the approximate outline of the landslide as mapped in 2009.

Although the slide mass reached a relatively stable condition by the fall of 2009 when the geophysical surveys were conducted, several hazards still exist including **(1)** reactivation of the highly disturbed, unconsolidated slide mass during winter/spring snow melts and seasonal late-summer monsoon rains; **(2)** surface and groundwater drainage and impounding problems within the disturbed ground mass potentially contributing to slide reactivation; **(3)** river damming if large volumes of materials are transported into the narrow East Fork of the San Juan river channel at the toe of the slide during low flows; **(4)** leaning and falling trees along the roadway alignment; and **(5)** sliding and/or significant consolidation settlement of loose, saturated, near-surface soils within the larger slide mass.

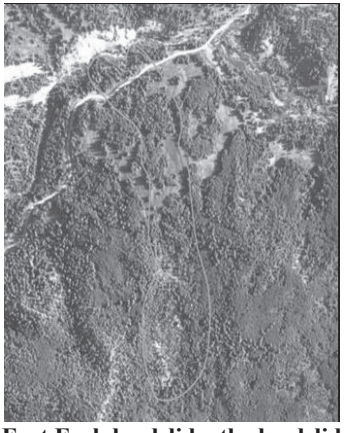

Figure 2. Aerial view of East Fork landslide, the landslide mass is outlined (approximately) in orange. North is to the top of the image. The East Fork of the San Juan River is near the top edge of the photo which bounds the north side of the landslide

Site investigations focused on evaluating current surface conditions, identifying and assessing factors potentially contributing to slide reactivation, determining subsurface lithology and material properties, identifying slip plane and ground water elevation and developing recommendations for mitigating landslide impacts in the immediate vicinity of the roadway. Due to difficult terrain and access restrictions related to working within the boundaries of a remote National Forest, very few borings could be drilled at this site.

GEOLOGIC SETTING

The general geologic conditions at the site consist of Upper Cretaceous sedimentary formations such as the Mancos and Mesa Verde (e.g., shale and sandstone, respectively) overlain by more recent Tertiary volcanic rocks consisting of basalt flows, lahar deposits, ash layers and breccia. The regional geologic setting is the San Juan Volcanic field, which has recently been very well mapped and documented by Lipman (2006), where multiple volcanic centers (i.e., calderas) were active in the

Tertiary Period. Existing site terrain is characterized by steep slopes, hummocky ground, and shallow depressions indicative of ancient landslides that have been oversteepened due to Pleistocene glaciation. The top of these landslides exhibit graben-like headscarp features, where unstable ground has pulled away from stable ground causing the head of the unstable slope to subside. Slope movement was accelerated by continual undercutting at the toe of the slide by the East Fork of the San Juan River.

The East Fork Landslide, in the East Fork Valley, is an example of part of a much larger complex of prehistoric landslides as described by Lipman (2006). Lipman mapped massive landslides complexes all along the south and western flanks of the San Juan volcanic field. The recent East Fork slide is evidenced by an extensive and prominent 100 m (330') high headscarp in volcanic bedrock covering approximately 121.5 hectares (300 acres) several thousand feet upslope from the roadway (see Figure 2). An ancient slide purportedly extends eastwards approximately one mile along the current Forest Service road. The toe of the 2009 landslide is bound by the East Fork of the San Juan River, which continued to undercut the materials during renovation of the National Forest Service access road.

The landslide debris is a heterogeneous mix of clayey soil derived from the local weathered volcanic- and sedimentary-rock formations. Due to weathering and exposure during extreme wet and dry seasonal cycles, these soils exhibit very low shear strength and have become prone to slope instability (Lipman, 2006). It is likely that there are water bearing pockets of fractured bedrock that are recharged by surface water (e.g., snowmelt and/or rain) surrounded and isolated by impermeable clayey soil deposits within the landslide (soil) mass.

The initiation trigger for the slide is due to a high accumulation of groundwater for several years, during which high winter snow packs and substantial summer monsoon rains recharged the landslide mass faster than it could drain. Additionally, the stability of the slope is compromised by a poorly drained sag-pond headscarp area that contributes groundwater recharge at the top of the sliding soil mass. A small rotational-type movement, located between the toe and the access road, may have started the larger translational movement. The progressive translational failure further up the slope were likely triggered because the resisting forces of a surcharged landslide mass were removed by this rotational event. Geotechnical investigations at the East Fork slide indicate the subsurface can be subdivided into three generalized material layers:

(1) 0 to 17.7 m (58') includes soft, low density, medium plasticity clays with low shear strength;
(2) 17.7 to 25 m (58' to 82') includes hard, dense claystone with low plasticity; and,
(3) below 25 m (82') hard volcanic breccia (bedrock).

GEOPHYSICAL METHODS

The purpose of this project was to investigate if surface geophysical methods – 3D seismic and 3D electrical tomography techniques are effective in characterizing the subsurface conditions beneath a large active landslide. Typically, landslide conditions are investigated with geologic observations and geotechnical investigations; that is, standard engineering and geologic mapping, drill holes, test pits, sampling, and laboratory testing. Wide-area surface geophysical techniques were chosen for this investigation because they are non-intrusive and cost- and time-effective field methods; considering the site-specific constraints of working on an active landslide. Geophysical techniques provide 3D volumetric images in comparison to borings that only provide point measurements. Specific objectives are outlined below, with the emphasis on use of 3D acquisition, processing, interpretation, and visualization of 3D seismic, resistivity, and induced polarization data.

Seismic Tomography (ST)

The 3D-ST method is based on the fact that seismic waves travel at different velocities as the waves move radially outward through materials with different density and/or stiffness. The method used for this study measured the 3D compressional (P-) wave velocity distribution of subsurface units. In general, low P-wave velocities are indicative of loose materials, semi-consolidated sediments, or highly weathered rock. Conversely, high velocities are indicative of competent bedrock, dense or highly compacted soils and sediments.

Seismic waves are generated by an energy source, typically by a sledge hammer striking a plate or small explosive charges, and travel through the subsurface layers at some particular velocity until an interface with different acoustic properties is encountered. Some of the energy passes through the interface and some is transmitted along the interface. As the refracted wave travels along the interface a portion of the seismic energy is redirected upward to the surface and is detected by geophones placed on the ground. In order to be successful and adhere to physical principles, seismic refraction surveys require that deeper layers have faster velocities than the overlying layers. As the geology of landslides is complex and likely does not always consist of distinct '*layers'* with successively higher velocities, use of advanced and recently developed 3D-ST modeling can produce volumetric subsurface images and 2D cross-sections (i.e., standard seismic traverses) for better characterization of the entire slide mass. For further details about the use of advanced 3D seismic imaging using the refraction method refer to Sirles and Haramy (2006), and Sirles and Rock (2006).

Electrical Resistivity (ER) and Induced Polarization (IP)

ER and IP are geophysical data that can be acquired simultaneously using the same 3D array of electrodes. ER is a commonly used to assess properties of the subsurface such as moisture content, fines content, and the presence of voids (e.g., karst). IP is an extension of the ER method, where it is also used to determine the distribution of

subsurface electrical properties. In general, resistivity measures the ability of earth materials to conduct electricity while IP measurements determine the ability of earth materials to store electric charge and release it over time; analogous to a leaky capacitor.

The primary difference is that IP values represent a set of readings that are acquired *after* the measurement of each resistivity value has been obtained for a particular set of electrodes. Therefore, both data sets are acquired (in 3D) with the same field equipment and set-up positioned on the ground surface. For the dipole-dipole electrode array used at the East Fork landslide site, current is introduced into the ground at two (current) electrodes and the resulting electric field is measured at two (potential) electrodes. No trenching, drilling, site grading or access road construction was involved for placement of transmitter or receiver electrodes. Both 3D-ER and 3D-IP data sets were collected, processed, interpreted, and are presented in FHWA final report (2011).

Resistivity variations in rock or soil are caused by the degree of saturation (i.e., moisture content), conductivity of the pore fluids, grain size, porosity and permeability, and resistivity of the rock or soil framework, in approximately that order. Cultural features (i.e., man-made objects such as fences, power lines, pipelines, etc.) can affect ground resistivity measurements.

When current induced into subsurface rock formations or soil deposits is interrupted, the time-rate of decay is measured. The chargeability, or time-rate of decay, that occurs in the subsurface is dependent on the: **(1)** lithology – particularly clay content; **(2)** type of clay (e.g., montmorillonite versus bentonite); and, **(3)** mineralization. Mineral content in rock or clay content and type in soils have shown to dramatically increase the IP response. Some clays significantly contribute to an IP effect, commonly referred to as the membrane polarization, due to their ionic charges at the particle interfaces. However, the IP effect is most commonly caused by an overvoltage due to the presence of metallic minerals in rock formations where it produces a much higher IP response than those measured in soil deposits. Thus the IP electrical method is a standard geophysical approach used for mineral exploration. For additional information on the IP effect and its use see Trip et.al., (1984). At the East Fork landslide site there is minimal mineralization in the colluvial soils overlying volcanic or sedimentary bedrock so the IP effect is attributed to soil lithology, primarily the presence and type of clay.

DATA COLLECTION

To produce 3D-ST, 3D-ER, and 3D-IP results that would be useful for remediation design, the geophysical surveys were performed within an area defined by FHWA and National Forest personnel to be the most critical portion of the landslide. This survey area is primarily where the roadway and pipeline were compromised; that is, the lower 152 m (500') of the 2009 East Fork slide. A 3D grid was established with GPS, and the same grid was utilized for both the seismic and electrical surveys. One piezometer

and two inclinometers were also installed within the investigated area of the East Fork landslide. The geologic and geotechnical information obtained in these three borings were used as ground-truth for verification of the geophysical results. Within this area defined as critical the outline of the landslide and the area covered by the 3D grid of receivers, either seismic or electrical, are shown on Figure 3. Also shown are the three borings, from which geologic and geotechnical data were used to calibrate the geophysical results. The gas pipeline is also depicted on the site plan (Figure 3); it generally follows and is located just uphill of the National Forest Service access road.

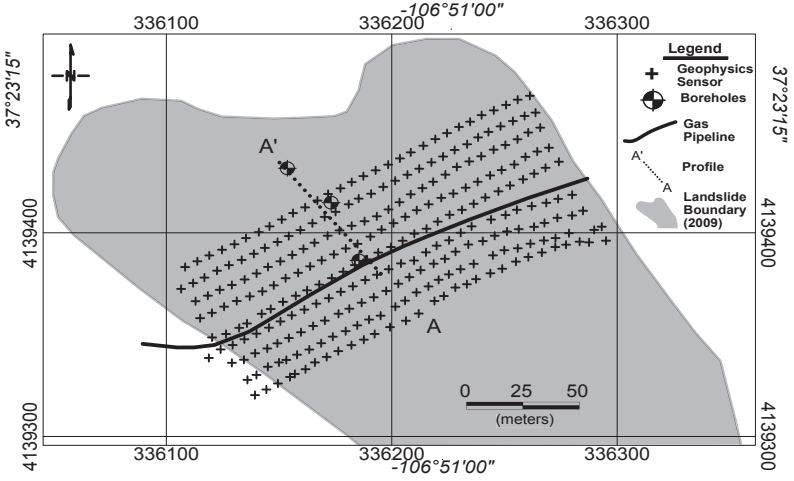

Figure 3. East Fork landslide (gray shaded area) and the 3D geophysical grid layout. Landslide movement was to the northwest with the East Fork of the San Juan River being the northwest (rounded) boundary of the landslide mass

Seismic

A 3D seismic survey was acquired using 14 Hz vertical component geophones spaced 6.1 m (20') apart along nine lines spread approximately 9.1 m (30') apart. The grid was established to be a long and narrow strip, with the long line direction placed perpendicular to slope movement (Figure 3). Shot points were placed off the end of lines, and interior to the grid at even intervals. Seismic data were recorded using the Seistronix EX-6 capable of recording over 350 channels at one time; 310 active channels were deployed at the East Fork site. P-wave seismic energy was generated by impacting a 9 kg (16-pound) sledge hammer on a metal plate and also by using small explosive charges. Hammer impacts were primarily used in the interior of receiver grid where the shot to geophone (i.e., receiver) distances were small. Small explosive charges were also used as a seismic source, both in and out of the 3D grid. The Poulter method was used, which creates a seismic signal when an airborne shockwave strikes the ground. The Poulter method is safe and very useful technique for small explosive / seismic sources in mountainous and wooded terrain. One line was extended eastward about 165 m (540') out of the 3D grid. The longer 2D line was used for comparison of

subsurface 3D geophysical data acquired on the slide to the data acquired outside the sliding soil mass.

Electrical

3D-ER and 3D-IP surveys were acquired using a Zonge Electrical-resistivity Tomography Acquisition (ZETA) system. The ZETA is a 31-channel geophysical data acquisition system which allows for 30 transmit-receive pairs of electrodes to be acquired. All the electrodes were placed in the same position as the geophones had previously been placed (i.e., the grid size and shape were the same). As such, the electrode stations were laid out in the form of nine lines laid perpendicular to the flow direction of the landslide (Figure 3). Since there has not been much 3D-ER work performed on landslides, therefore each line of electrodes was also acquired as an individual standard 2D-ER line. Then the entire 3D grid, or electrode array, was used as a 3D pattern of transmit-receive electrode pairings in the grid. In 3D mode one line would be used as the transmitter (*current*) electrodes and an adjacent line was used as the receiver (*potential*) electrodes. The current dipole was thus alongside the line of receiver rather than inline as conventionally 2D ER is performed. Using this 'broadside' dipole-dipole configuration the 3D subsurface volume of soil and/or rock beneath the lines and in between the lines is affected by the changes in the electric field.

For the landslide field work the electrode lines were divided into groups of three with first and third lines being active. To obtain the desired lateral separation the middle line of each triple was inactive. The pairing were L1-L3, L4-L6, and L7-L9. To correspond to the seismic data acquisition, an extension of Line 8 was also occupied for both ER and IP measurements to provide subsurface data both inside and outside of the known landslide.

DATA ANALYSIS

Both seismic and electrical data were analyzed using 3D tomographic inversion modeling/analysis packages.

Seismic

Refracted, or first-break arrival times for each seismic source-receiver pair, and associated source and receiver coordinates, were processed using a 3D seismic refraction tomography inversion program developed by GAP Engineering, Inc. (*not commercially available*). The GAP software is a 3D numerical modeling code which utilizes the discrete element method and particle flow code to produce 3D P-wave velocity images. Several inversions were performed on the data using various groups of shot-receiver pairs and initial velocity models to reduce error with the inversion fit and to ensure validity of the results. The final modeling runs utilized nearly all shot-receiver pairs. Once the data are completely processed in 3D, 2D cross-sections in any direction and at any point in the grid space can be produced. The 3D modeling

program can also plot 3D constant velocity-slice images, similar to a velocity iso-surface, from the 3D volume. The final 3D seismic velocity model was generated and plotted, and the results were compared to the electrical (resistivity and IP) results for interpretation in the 2011 FHWA (CTIP) report.

Electrical

Electrical data were processed with the commercially available inversion code ERT-Lab (2007). ERT-Lab is capable of processing the resistivity and IP data separately, in either 2D or 3D analysis modes. Either the ER or IP data set cans then be visualized in formats similar to the seismic data: (1) 3D volumes; (2) 2D slices (cross-sections); (3) 2D plan view maps; or (4) constant resistivity and/or chargeability slices (i.e., iso-surfaces). The final presentation formats, presented in the 2011 FHWA report, are conducive for comparison and correlation with each set of geophysical data, and also incorporation of the geotechnical data acquired at the site.

GEOPHYSICAL RESULTS

Seismic

The 3D seismic results are revealing in that four primary observations can be made: (1) the slip plane is correlative with a P-wave velocity of about 1220 meters per second (m/s) (4000 ft/s); (2) the surface of the slip plans is undulatory and extends beyond the 3D grid area in two places; (3) depth to the slip plane varies between 1.5 m (5') and 18 m (60') depending on location within the geophysical grid; and, (4) the materials below the slip plane are interpreted to be represent a two-layer bedrock structure.

Because a significant number of (*color*) figures are produced during 3D tomographic analyses, it requires extensive visualization to *see* the 3D results obtained by this study. However, for the purpose of this paper, a single example 2D cross-section has been selected (A-A' identified on Figure 3). This profile was chosen for two reasons: 1) because it represents the direction of movement or translation of materials downslope; and, 2) it contains the only borehole control at the site. Velocity data in Figure 4 are presented with a 200 m/s (656 ft/s) contour interval.

Although it is just one example, the seismic profile extracted from the 3D volume presented on Figure 4 indicates the seismic results correlate well with the depth of the slip plane, as defined by geotechnical data from the two slope indicator (SI) borings. Depth to the slip plane derived from the SI borings (shown on the profile A-A') is about 17.7 m (58') below ground surface. This depth is also coincident with the claystone layer encountered in each boring. It is not clear if the sliding soil mass moved along the top of the soil / claystone interface, or if the materials in the soil sliding mass are also composed of claystone. Several examples of intact claystone blocks can be observed on the landslide as prominent rock-like outcrops with internal sedimentary structure, but very little or no lateral uniformity; therefore, they are considered remnant intact bedrock blocks within the materials translated downslope.

It is reasonable to believe that these big claystone blocks moved with the soil sliding mass.

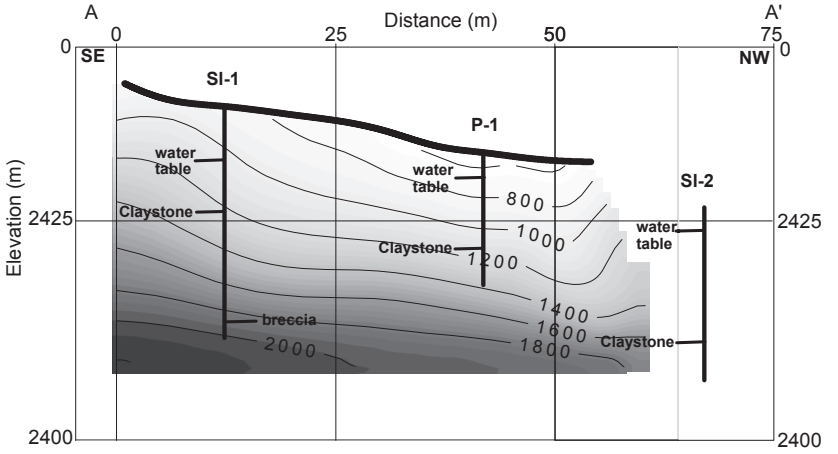

Figure. 4. Seismic profile along borehole section A-A' (contour interval equals 200 meters/second, 656 feet/second)

The P-wave velocities obtained in the landslide mass range from very slow (275 m/s – 900 ft/s) to just less than 1220 m/s (4000 ft/s). This range is typical for unconsolidated, non-indurated soils; also, soils which are unsaturated. Although there is considerable P-wave velocity variation laterally and vertically within the landslide mass the velocities, in general, increase gradually with depth to the slip plane. The overall gradual increase can likely be attributed to overburden pressure. 3D velocity variations are very difficult to present using a single 2D profile (Figure 2).

Below the slip plane, the velocities are representative of hard, laterally uniform bedrock materials with two layers: the claystone bedrock layer with P-wave velocities ranging from 1220 m/s (4000 ft/s) to 1900 m/s (6250 ft/s); and, the breccia with P-wave velocities above 1900 m/s (6250 ft/s) to the total depth of investigation for the seismic survey (approximately 45 m (150'). Both of these velocity ranges are typical for semi-indurated claystone and indurated or cemented volcanic breccia.

Electrical

Similar to the discussion of seismic results in Section 6.1, 3D-ER and 3D-IP analyses produce a significant amount of (*color*) figures; however, for this paper only the single example 2D cross-section A-A' identified on Figure 3 has been extracted for discussion. This 2D profile contains the three geotechnical borings, and is in the direction of slide movement.

ER and IP data are presented in 2D profile format in Figures 5 and 6, respectively. Resistivity data are contoured at 4-ohm-meter intervals; and, the IP data are contoured at 1 millisecond intervals. These two figures are representative of most of the 3D-ER, 3D-IP data obtained at the East Fork landslide.

3D-ER results indicate that the lateral variation of both moisture content and clay content in the soil sliding mass is high above the slip plane at a depth of about 18 m (60'). The resistivity values are all very low, ranging from 5 to 40 ohm-m. This range is typical of saturated to partially saturated, fine-grained soils. Figure 5 shows this wide range of low resistivity values to the uphill side (left) in the undrained soil sliding mass, while the downhill side (right) has higher ER values. Generally, the high ER values are confined to the upper 5 m (16.5') of soil and were obtained over or near the reconstructed access road where dry course-granular materials were placed and good drainage had occurred in the subsurface.

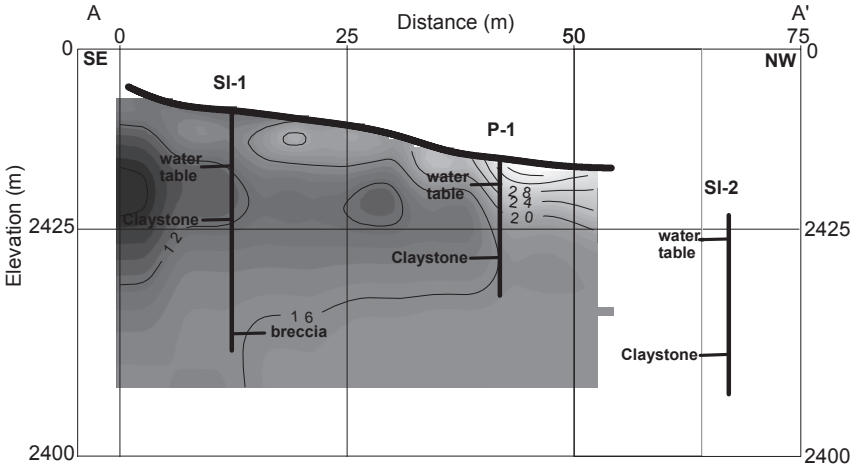

Figure. 5. ER profile along borehole section A-A' (contour interval equals 4 ohm-meters)

Within the landslide mass 3D–ER values vary greatly. There tend to be pockets of very high resistivity (near the repaired road) but also very low, in areas that are interpreted as poorly drained and as such have high moisture content beneath what are interpreted as (dry) sag ponds. Borehole logs for the soil sliding mass materials indicate the soils are generally clayey, which correlates to the overall low ER values throughout the site. Beneath the slip plane, the ER data become much more uniform and less variable with mid-range ER values (i.e., 14-16 ohm-m). These values are what would be anticipated for claystone bedrock.

A profile extracted from the 3D-IP volume is presented in Figure 6. The IP data are indicative of a chaotic or jumbled soil configuration within the soil sliding mass; that is, no original bedding or layers exist after movement of the slide. Since IP is affected by the water content and presence of clay, we anticipated a relatively close relationship between the ER and IP results. However, the IP data are very irregular and have a large range of chargeability values over a very short distance. Figure 6 is generally representative of the results observed from the IP survey. Very close and tight bulls-eye contours, indicative of laterally heterogeneous clay and water contents within the landslide mass. The range of IP values within the landslide mass range from 0 to about 5 milliseconds (ms), but no uniformity exists. Beneath the interpreted slide plan (at 18 m (60')), the IP values appear to be much more regular and uniform at about 1-2 ms. Therefore, the ER and IP generally match in that above the slip plane their character is irregular representative of a jumbled soil mass, and below the slip plane they are more uniform and representative of layered bedrock.

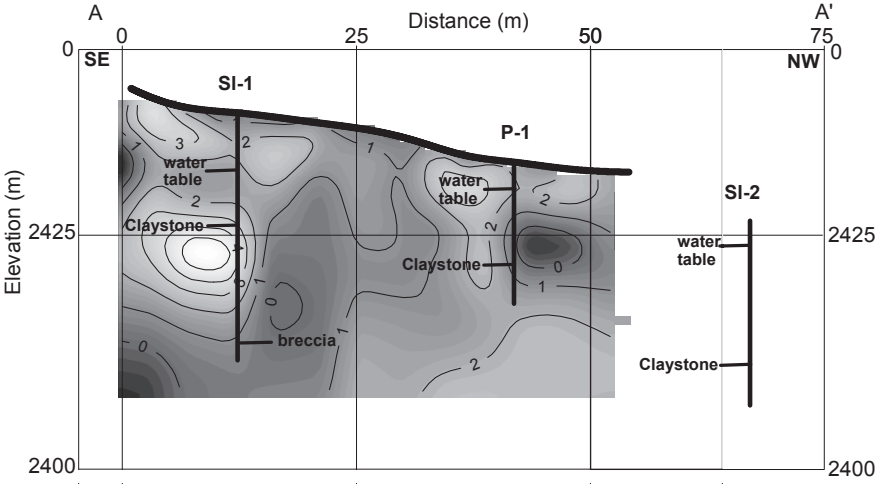

Figure. 6. IP profile along borehole section A-A'(contour interval equals 1 millisecond)

SUMMARY AND CONCLUSIONS

This geophysical study was intended to determine the viability of deploying 3D surveys (*seismic*, *resistivity and IP*) on an active landslide. The 3D surveys were designed to cover a large area, approximately 1951 m^2 (21,000 ft^2). The 3D data were acquired relatively quickly for each method requiring only a few days per method. The geophysical data show good correlation with the geotechnical data available, and the individual 3D data sets show good correlation with each other. That is, these independent data sets correlate with the three-layer geologic setting of a jumbled set of poorly drained, variable sandy and clayey deposits in the sliding soil mass, weathered claystone below the slip plane, and deeper more sound volcanic bedrock at depth. The following conclusions can be drawn from the 3D surveys:

1) 3D seismic data provided information regarding the density and/or stiffness of the landslide mass and appears to be very helpful in showing the undulations and inconsistent depth of the slip plane below this slide (*in the area investigated*); and,
2) 3D resistivity and IP data provided information regarding the relative moisture and lithology within the landslide mass, but also help define the slip plane because they both become much more uniform below the slip plane.

The geophysical data were acquired in the area of greatest concern, as defined by FHWA and National Forest staff, but these data represent only a small portion of a much larger landslide. Correlations with ground conditions and borehole data reveal that the geophysical results obtained are quite promising for use in engineering design. The following recommendations can be made regarding the use of these geophysical data for engineering remediation:

1) 3D data need to be processed quickly following the slide event to optimize the drilling and other field investigations, or possibly the remediation design; and,
2) Field data acquisition should follow the slope failure as soon as possible; yet safely, on an active slide.

The geophysical data presented herein were obtained five to six months after the 2009 movement. Timing of data acquisition would clearly be affected by moisture content and site conditions that change from spring when the slides occurred to fall when the data were acquired. Although there is good correlation, if the 3D measurements had been made sooner after failure of the slope, we feel confident the resultant 3D seismic, resistivity and induced polarization data would have been more useful for engineering remediation design, and at a minimum could have optimized follow-on geotechnical field investigations (i.e., drilling, sampling, and laboratory testing).

ACKNOWLEDGMENTS

The authors appreciate the support of personnel from Yeh and Associates, specifically from the Durango office; staff at Central Federal Lands Highway Division of the FHWA whom aided with the logistics and coordination of other agencies for the field work; and, the Zonge staff who acquired the geophysical data under difficult field conditions.

REFERENCES

ERT Lab, (2007), Geostudi Astier, S.R.L. and Multiphase Technologies – Version 1.1.0 (*a commercially available software package*).

Federal Highway Administration, Central Federal Lands Highway Division CTIP (Coordinated Technology Implementation Program), 2011, Publication No. FHWA-CFL/TD-11-006.

Lipman, P.W., (2006) Geologic Map of the Central San Juan Caldera Cluster, Southwest Colorado, Geologic Investigation Series I-2799, Version 1.0, U.S. Geological Survey

Sirles, P. & Haramy K. (2006) Advancements in 3D Subsurface Modeling using Seismic Refraction Data – A New Perspective, in Proceedings for GEOPHYSICS 2006, the 3rd International Conference on Applied Geophysics, St. Louis, MO.

Sirles, P. & Rock A. (2006) Advancements in Subsurface Imaging Using 3D Seismic Refraction, in Proceedings for SAGEEP, Philadelphia, PA.

Tripp, A., Hohmann, G., & Swift, C., 1984, Two-dimensional Resistivity and IP inversion: Geophysics, **49**, 1708-1717.

Photogrammetric Methods, Geologic Discontinuity Mapping For Spillway Modifications, Pathfinder Dam, Wyoming

Bryan K. Simpson[1], P.G., P.E.

[1]Engineering Geologist, U.S. Department of the Interior, Bureau of Reclamation, Denver Federal Center, Building 67, P.O. Box 25007, Denver, CO 80225-0007; bksimpson@usbr.gov

ABSTRACT: This paper provides an illustration of recent photogrammetry methods used in support of geologic mapping for the design of a new spillway at Pathfinder Dam, located in the central portion of Wyoming.

Terrestrial-based photogrammetry was successfully used in conjunction with field geologic mapping. The collections methods included collection of topographic data, and measurement of both joint and shear orientations in order to develop a comprehensive three-dimensional (3-D) model for analysis and foundation documentation and acceptance purposes. The photogrammetric work performed consisted of rapid data collection using an off-the-shelf digital camera. Collection of field digital photographs was accomplished by the use of a camera mounted atop a 12-foot-long survey staff and a wireless shutter trigger system. The new spillway foundation was approximately 750 feet in length, and 20 feet in width. The geology of the foundation consisted primarily of granitic bedrock that is cut by several prominent generally continuous joint sets, local joint sets, and shear zones.

The software available to construct 3-D models using ordinary digital images is being developed and improving at a rapid rate. Processing methods used Adam Technologies 3DM Mine Mapping Suite software to construct this project's photogrammetric model. Processing was performed in a reasonable timeframe, constructing approximately 150 Digital Terrain Models (DTM) pairs, and included statistical analysis of joint sets and presentation of stereoscopic pole plots. Lessons learned regarding the processing challenges of specific field conditions, including scaling and lighting variations, will be discussed.

INTRODUCTION

Geologic mapping of foundations for dam structures is one of the most important tasks that an engineering geologist performs. It is the responsibility of the engineering geologist to properly characterize and accept the foundation as suitable for support of the structure(s), knowing that failure of the foundation could result in significant property damage and more importantly, loss of life. Historical tried and true methods for geologic mapping have consisted of traditional graph paper and a Brunton

compass. This mapping method is very effective; however, the final foundation acceptance map is lacking as to what the foundation materials actually looked like visually, just prior to construction. Recent technological improvements in both digital cameras and photogrammetric processing software have resulted in another tool at the disposal of the engineering geologist for use in geologic mapping. The purpose of this paper is to illustrate how photogrammetry has been successfully used to enhance the level of geologic mapping for foundation acceptance and to provide concise archival documentation.

PROJECT

Pathfinder Dam is located on the North Platte River southwest of Casper, Wyoming. The dam was constructed between 1903 and 1909 as part of the North Platte Project. Operations and maintenance activities for the project were provided by the U.S. Reclamation Service, which became the Bureau of Reclamation (in 1923). Pathfinder Dam is a cyclopean masonry, thick arch dam fashioned from massive blocks of locally quarried granite. The dam is founded on coarse grained, massive granitic bedrock. The existing spillway crest extends from the left abutment of Pathfinder Dam further left to a granite rock outcropping located to the north/northeast. The existing spillway crest is a concrete flat-crested weir at an elevation of 5850.1 feet.

The primary purpose of the new spillway crest modification is to restore the lost storage volume from the deposition of sediment within the reservoir. Approximately 54,000 acre-feet (ac-ft) of sediment has accumulated within the reservoir since the construction of Pathfinder Dam in 1909. The additional storage will be obtained by constructing a new reinforced concrete ogee spillway structure with a crest elevation of 5852.49 feet resulting in an approximate raise of 2.4 feet. The new ogee spillway is approximately 750 feet in length and 20feet in width.

PURPOSE

Geologic Mapping and Foundation Acceptance

The purpose of the geologic mapping is to document the geologic discontinuity conditions exposed during excavation and cleaning of the foundation for the proposed new ogee spillway. The granitic bedrock comprising the foundation is cut by frequent discontinuities. Photogrammetry was used to capture the planer features and the statistical features of the software were used to rapidly quantify the discontinuity data. To ensure an adequate foundation, the foundation geology is inspected and formally approved by the designers, geologists, and construction engineers.

METHODS

Data Collection

Geologic mapping on conventional photographs of the foundation was performed in the field by a team of geologists. Geologic mapping included characterization of

discontinuities within the exposed granitic bedrock consisting of joint dip, dip direction, continuity, roughness, moisture, hardness, weathering, openness, thickness, and joint healing/infilling characteristics. Areas of exposed bedrock within the foundation footprint that were deemed unsatisfactory with regard to detached blocks, drummy materials, joints openness, poor infilling conditions, or poor orientation to the proposed foundation were marked for removal or slush grouting. Survey stationing, centerline of the spillway alignment, and limits of the spillway were painted on the exposed foundation surface for control in both the conventional photographs and photogrammetric images. Temporary survey targets were also placed on the foundation surface and surveyed using GPS methods.

Once geologic mapping on conventional photographs was completed, equipment was set up to capture photogrammetric images of the foundation. An "off-the-shelf" Nikon D700 camera was mounted atop a 12-foot-long survey staff, used in conjunction with a wireless shutter trigger system for collection of field digital images. Photographs were taken along the centerline of the foundation alignment at 5-foot intervals as shown in Figure 1.

FIG. 1. Photogrammetric image being taken along the spillway foundation

Once all the foundation had been completely accepted, mapped, and photographed, the photogrammetric images and geology mapped on field photos were collected for office work.

Processing of Data

Processing of the photogrammetric images was performed using proprietary

Adamtech software. The Adamtech software is comprised of two different program applications. The initial Calibcam program is used to calibrate the camera being used and to compile the photogrammetric images together. The software identifies unique points on each image initially, and then determines common points between images. Provided that enough common points are identified between images, a resection and bundle adjustment can be accomplished by the software, thus creating a spatial relationship for all images. This is referred to as a "relative only" model. At this point, the survey information from the temporary photogrammetric targets captured in the photogrammetric images was imported into the model. Once the survey information has been imported into the model, and related to the survey targets identified in the photographs, then a successful resection and bundle adjustment will result in a simplified final three-dimensional model in real world space. At this time, distance measurements can be made from any specific location to another in the model. Digital terrain models (DTM) of any number of specific photogrammetric stereo pairs can be generated at this time to import into the second Adamtech application, 3DMAnalyst, which will create the final three-dimensional model. See Figure 2 for an example of a photogrammetric model illustrating the Pathfinder Spillway Modification overall orthorectified site plan by station.

The accompanying Adamtech software program, 3DMAnalyst, can then be used to load the previously constructed DTMs into a final three-dimensional model that includes detailed three-dimensional photo texturing. Once the final three-dimensional model is operating, a number of different useful applications can be performed that include the following:

- Contouring by elevation of the three-dimensional surface can be performed at a contour interval selected by the user (example, 1-foot minor contours with 5-foot major contours)
- Mapped geologic discontinuity data, such as jointing, faulting, shear zones, etc., can be defined and input into the three-dimensional model.
- Planes/faces identified in the three-dimensional model can be recognized by the user or automatically detected using the software face recognition. The faces in the model have real world control and orientation expressed as dip and dip direction. The dip and dip direction of the faces as determined by the software can be compared (ground truthed) to the geology mapped in the field to verify accuracy.
- The software will automatically plot the pole of the joint planes by stereonet projections, Equal Angle (Wolff) or Equal Area (Schmidt). This powerful discontinuity statistical tool is already included in the Adamtech software, that otherwise would need to be exported into other types of statistical software such as Dips.

An example of the final Pathfinder photogrammetric product for geology mapping and foundation acceptance is shown in Figure 3.

FIG. 2. Example of photogrammetric model of the new Pathfinder ogee spillway foundation illustrating the overall orthorectified site plan by station

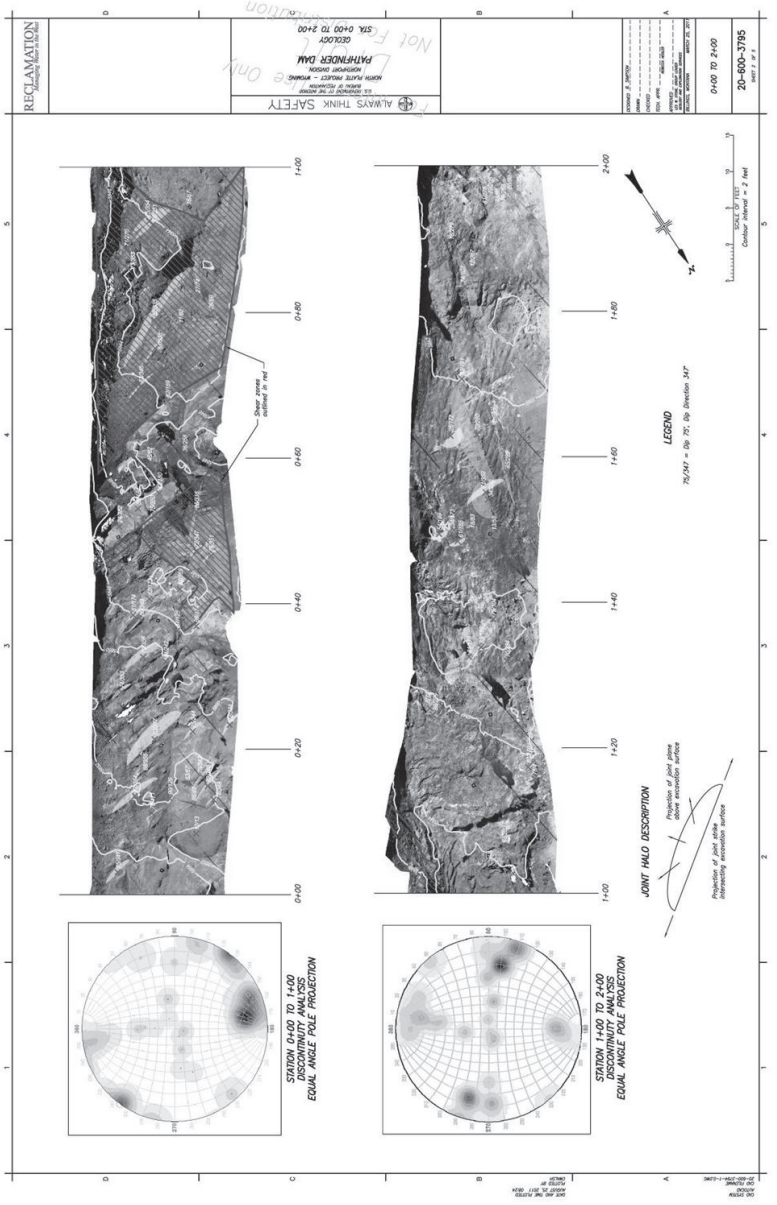

FIG. 3. Geologic maps and stereonets of the new Pathfinder ogee foundation using the processed photogrammetric models

CONCLUSIONS

Photogrammetry is a tool, just like many other above-ground remote sensing methods such as LIDAR or synthetic aperture radar. Advantages for use of photogrammetry include:

- Ability to quickly obtain data in the field.
- Visual identification of the geology is documented in the model and additional mapping can be verified from the user's desk.
- Digital cameras can be "off-the-shelf" as opposed to specialized for photogrammetric use.
- Archival of photogrammetric images is invaluable for future use, regardless of technology advances.

Photogrammetric mapping is not only applicable to existing dams, but also of great importance for new construction to assure the details of the geology, concrete structures, and embankments are quickly and accurately obtained for current and future use. With photogrammetric models, it can be very practical to obtain remarkably accurate data, and these methods have many advantages over traditional surveys.

LESSONS LEARNED

The photogrammetric images were taken using a 12-foot-long survey staff. In order to maintain a preferred camera height to camera spacing distance ratio, this limited the camera stationing to a maximum spacing of 5 feet along centerline. This process worked well but required having to take 150 photographs to capture the entire footprint, and required additional software processing time. In retrospect, the use of a mast system that would allow for greater camera height would allow for greater spacing between camera stations. This would have reduced the total number of images taken, thus reducing the overall software processing time. The increased camera height would also reduce the potential of scaling problems between photographs that can be associated with a foundation that has an undulatory surface, such as in the case of Pathfinder's spillway.

Processing of the photographs with different light conditions (due to the construction schedule) proved to be a challenge within the Adamtech software, but was not insurmountable. Having the ability to take the photographs sequentially, or at specific times to minimize different lighting conditions, would result in easier processing and an overall better product.

The project survey data used GPS technology (specifically for the survey targets used in the photogrammetric model) that contained some erroneous survey points. When placing survey targets in the models for control, be cognizant that survey targets placed near obstructions may result in erroneous data due to poor satellite coverage.

Having a surplus of survey targets in the model allows the user the luxury of removing erroneous survey target information from the model and while maintaining adequate control.

ACKNOWLEDGMENTS

The author appreciates the mentoring and support of the Bureau of Reclamation Photogrammetry Team Program Managers, Rebecca Heisler, Engineering Geologist, and Joseph Kottenstette, P.E.

REFERENCES

ADAM Technology, 2012, "*3DM Analyst Mine Mapping Suite, 3D Measurement, Camera Calibration and Block Adjustment Software*" User Guide, Suite 3, 41 Belmont Avenue, Belmont WA 4104, Australia.

Bureau of Reclamation, November 25, 1983. "*SEED Examination Report for Pathfinder Dam* – North Platte Project, Wyoming,"

Bureau of Reclamation, Denver, Colorado, November 25, 1983. "*SEED Examination Report for Pathfinder Dam* – North Platte Project, Wyoming,"

Bureau of Reclamation, Denver, Colorado, February 1, 1989. "*Modification Decision Analysis – Pathfinder Dam – North Platte Project*," Decision Memorandum No. PF-3110-1

Bureau of Reclamation, Denver, Colorado, December 3, 1993. "*Preferred Corrective Action Alternatives for the North Platte River System Dams, Seminoe, Kortes, Pathfinder, Alcova, Glendo, and Guernsey Dams – Kendrick, Pick-Sloan, and North Platte Projects*," Decision Memorandum No. NPRS-3110-CAS-DM-1-93, Bureau of Reclamation, Denver, Colorado, December 3, 1993.

Bureau of Reclamation, Technical Service Center, Denver, Colorado, January 2000 "*Performance Parameters for Pathfinder Dam*," Technical Memorandum No PFD-8130-PP-TM-98-1.

Bureau of Reclamation, Denver, Colorado, July 16, 1990, "*Foundation Stability Analysis at Pathfinder Dam"*, North Platte Project, Technical Memorandum No. PF-3620-2,

Fiedler, William, R., 2000, "*Comprehensive Facility Review – Pathfinder Dam*, North Platte Project, Wyoming.

Garfield, James Rudolph, March 14, 1907, "*North Platte Project, Nebraska-Wyoming, Pathfinder Dike*," Specifications No. 129, United States Reclamation Service.

Mares, Dan and Torres, Roger Torres, May 26, 2004. "*Pathfinder Dam Spillway Modification, Addendum to the 2003 Risk Analysis Report*", TM-PA-8130-2004-1, Pathfinder Dam, North Platte Project, Great Plains Region,

Taucher, G., 1979 "*Safety Evaluation of Existing Dams Program"*, Pathfinder Dam, Lower Missouri Region.

Use of Photogrammetric Measurements in a Concrete Damage Survey Guernsey Dam South Spillway

Joseph Kottenstette[1] P.E.

[1]Geotechnical Engineer, Technical Service Center, Bureau of Reclamation, Denver Federal Center, Bldg 67 (86-68312), Denver, CO 80225-007; jkottenstette@usbr.gov

ABSTRACT: The Bureau of Reclamation (Reclamation) uses Close-Range Digital Photogrammetry to obtain three-dimensional (3D) digital measurements. The rapid acquisition of photographs and the effectiveness of the photogrammetry software has revolutionized the evaluation of issues that are affected by these measurements. These methods have improved both the quality and quantity of data obtained and enhanced the ability to visualize complex geometry and evaluate related issues.

Reclamation has applied photogrammetric measurement technology to obtain geologic and topographic mapping of exposed abutments and excavated foundation surfaces, and to measure joint surface roughness, and to monitor rock erosion, concrete spalls, changes to sediment beds of scale hydraulic models as they are exposed to various stream flow conditions.

This paper presents an example of concrete spall measurements at Guernsey Dam's south spillway. The spillway tunnel was being evaluated for possible use after being unused for many years. Initial judgments indicated a need to replace a significant portion of the tunnel lining after years of freeze thaw damage. The damaged area and depth were not well defined, and the high cost associated with replacing a significant portion of the tunnel lining justified additional study to quantify the extent of the damage and evaluate the need for repairs. Photogrammetric methods were used to develop an accurate, scaled 3D model of the tunnel lining. This resulted in a better evaluation and more specifically quantified the areas needing repair, leading to a much less expensive solution.

INTRODUCTION

Close Range Digital Photogrammetry is a relatively new technology. The photogrammetry method has proven useful in the medical field, forensic site investigations, the manufacturing industry, and no doubt many other fields. This paper presents an example of measuring concrete deterioration at the Guernsey Dam's south spillway.

Reclamation has been developing its expertise in applying this technology to a variety of issues where 3D measurement data are needed. Reclamation is using this technology in a vast range of areas including: geologic mapping, design and evaluation of hydraulic models, measuring blast damage, concrete crack mapping, archeological site mapping, changes in river channel, rock erosion, excavation quantities, and concrete deterioration.

ANALYSIS APPROACH

The photogrammetric results and the challenges that the Guernsey Dam site presented for photogrammetric analyses make this project an interesting one to focus on. This paper focuses exclusively on terrestrial (ground-based) photogrammetric methods because they provide unique advantages at Reclamation's dam sites where the steep topography and confined spaces (such as the Guernsey Dam south spillway) as well as the need for detailed mapping of the geologic structure pose unusual challenges. (While mapping the geologic structure is often the focus of photogrammetry efforts, this was not the case at Guernsey Dam). This paper is based on the authors' experience with the 3DM Analyst Mine Mapping Suite, an ADAM Technology product. This software has been useful for Reclamation as:

- Camera stations are effective even when located on moving platforms such as a boat in the reservoir. Camera station locations and orientation are not required as they are resolved from fixed common image control points.
- Multiple cameras and a large number of photos in the same bundle adjustment can be included. Several hundred photos are not uncommon for many of Reclamation's sites.

SITE DESCRIPTION

Guernsey Dam is an embankment structure on the North Platte River, about 2.4 km (1.5 miles) north of the town of Guernsey and 25.75 km (16 miles) downstream from Glendo Dam in southeastern Wyoming. The dam is a feature of the North Platte Project, and was constructed by Reclamation between 1925 and 1927. There are two spillways at Guernsey Dam, the south spillway and the north spillway.

The south spillway at Guernsey Dam has not been needed since the 1958 construction of Glendo Dam. However, hydrologic loadings on the North Platte River Basin and related risks have since led to modifications at Glendo Dam upstream of Guernsey Dam. These modifications will increase discharges from Glendo Dam and thus increase flows into Guernsey Dam. These increased flows cannot be handled by the north spillway alone. The south spillway tunnel would provide the required discharge capacity for these new flow conditions, but would require some repairs and modifications to bring it back into service.

The south spillway at the right abutment, centered approximately 51.8 m (170 feet) upstream from the dam axis, consists of a crest/drum gate structure, two drum gates, a vertical shaft, and tunnel. A warped concrete structure that transitions to a 9.45 m

(31-foot) diameter vertical shaft is located immediately downstream from the drum gates. The shaft then transitions through a vertical curve to a concrete-lined horseshoe-shaped tunnel with a 4.57 m (15-foot) crown radius above the spring line and 9.14 m (30-foot) radius walls and floor below spring line. The tunnel is about 220 m (723 feet) long with a constant invert elevation of 1316 m (4319.0 feet). A discharge channel excavated into rock is located downstream from the tunnel outlet portal (**Figure 1**).

The concrete around the intake structure and in the upstream half of the tunnel has deteriorated over the past 50 years. The concrete spalling is attributed to many years of freeze thaw damage (**Figure 2**). The amount of concrete deterioration and the existing conditions of the concrete are important design and cost considerations for the south spillway modifications.

GENERAL PHOTOGRAMMETRY PROCESS

Photogrammetry provides methods to determine 3D locations of objects from two-dimensional (2D) images. Improvements in computer software and hardware coupled with the improvements in digital cameras have made terrestrial photogrammetry an ideal tool for structural geologic mapping of steep rock slopes and dam abutments.

Pictures of the feature or site to be measured are taken from a series of camera stations; at least two stations are required. The images must overlap so that the same objects ("common points") are captured from at least two locations. Working with these common points and camera calibration data, the software determines the relationships between all of the images and the data in the scene (bundle adjustment). The resulting 3D model can be a "relative only" or an "absolute" model. The relative only model is provided in an arbitrary scale with an arbitrary location and coordinate system. The absolute model needs several common points with known locations (surveyed "control points") captured in the scene. Photogrammetric software is available from multiple vendors.

While the basic photogrammetric principles are the same, implementing these principles can be quite different, particularly when comparing terrestrial (pictures taken from camera station on the ground) versus aerial (pictures taken from an airplane) methods.

OVERALL PHOTOGRAMMETRIC PROCESS

This section has been adapted from Adam Technology, 2010 and Birch, J.S., 2006, and augmented by the author's experiences. The process includes the following steps:

- Conduct an initial site visit to plan the approach to determine equipment, photo, and analysis requirements.
- Take the initial photos.
- Evaluate the resolution, coverage, overlap, base-to-height ratios, and target resolution and location.

- Decide on the best location for targets and mount them. Targets can be surveyed at any time before or after photographs are obtained.
- Adjust the camera locations and/or lens selection.
- Print and evaluate the preliminary photographs if time and resources allow or if the complexity and experience demand this for a successful project.
- Check that the targets are captured at appropriate resolution.

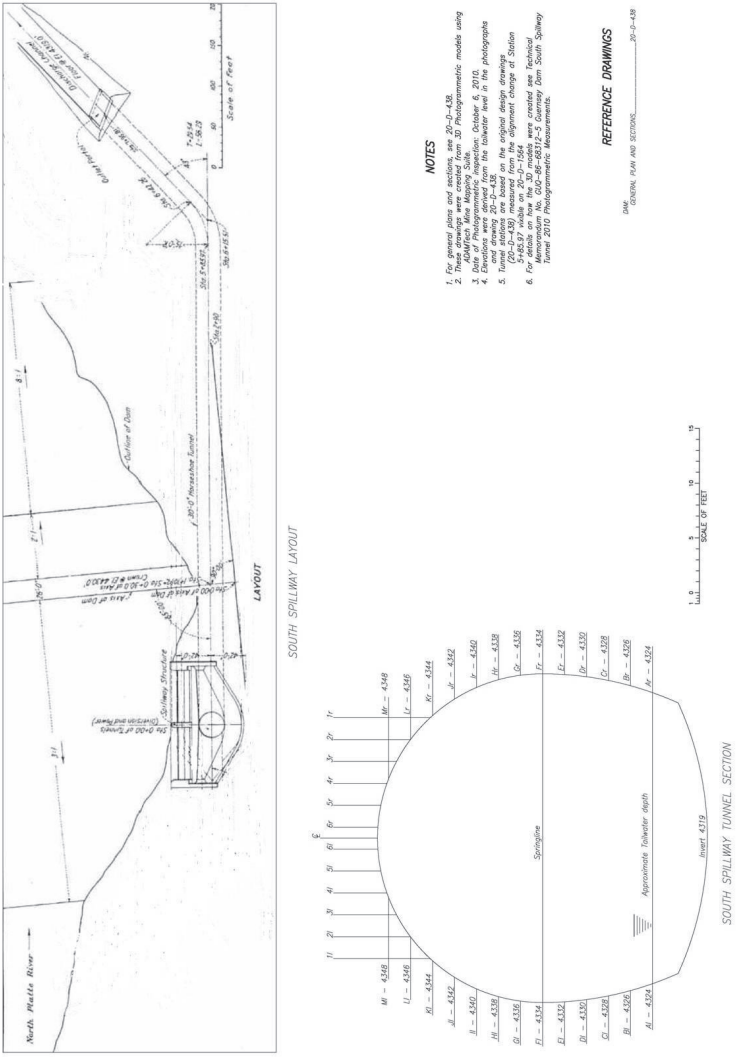

FIG. 1. South spillway plan and tunnel section

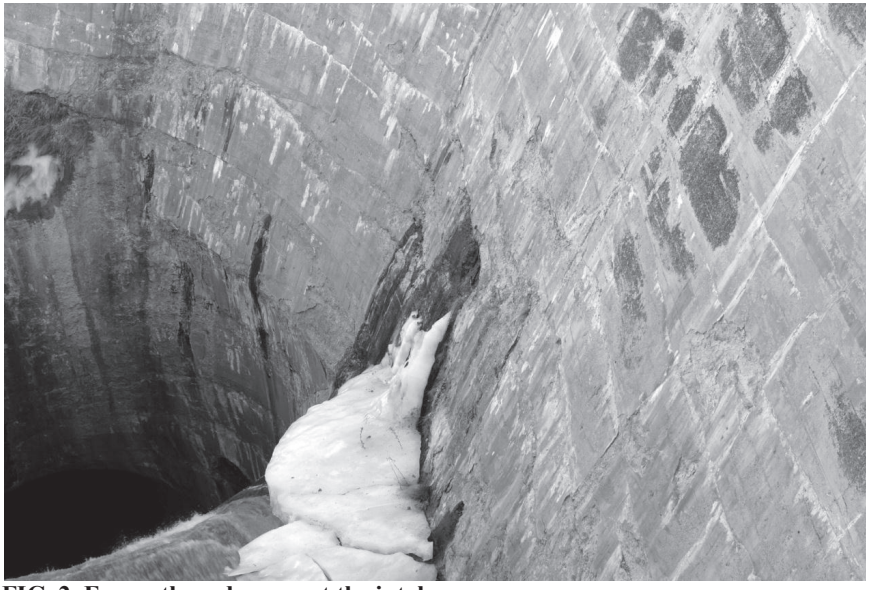

FIG. 2. Freeze thaw damage at the intake

Perform an initial bundle adjustment to check that the desired features are captured from two stations with the appropriate base-to-height ratio.

- Calibrate the camera.
- Check that the images capture the appropriate angles between the camera shooting direction and the feature being captured. For example, joints that strike parallel to the camera shooting direction will be difficult or impossible to measure. Several sets of photos from different angles to the ground surface may be needed to adequately characterize the orientations of all discontinuities.
- Take the final photographs.
- Use the bundle adjustment process to provide data for the 3D models.

With experience, this process can be streamlined.

FIELD TRIP PLANNING AND EXECUTION

Planning is needed to determine the equipment, photograph, and analyses requirements. The survey efforts and control requirements need to be coordinated with the survey crew. It is helpful to have the survey crew at the site at the beginning of the field work so that they can see what is needed and provide suggestions for the target locations. Considerations include:

- **Resolution requirements.** The resolution requirements for the project must be defined early, as this impacts the layout and equipment selection for the

project. The size of survey targets also depends on the resolution set for the project. Different locations in the project area may have different resolution requirements.

- **Target locations.** Target locations should consider access and visibility issues along with the requirements for survey stations and the tie points needed. Tie points are used to tie the photographs to other data, such as tying the mapped geology in the new photos to the existing design drawings and models. Initial target locations should be established based on existing site topography and conditions. The final target locations will be established in the field.
- **Coordinate systems.** Reclamation's older dam sites often use more than one coordinate system. This issue needs to be resolved first so all data can be easily integrated into the same coordinate system.
- **Lens focal length.** The resolution requirements and access constraints will determine the lens focal length and camera locations. Complex jobs can require a variety of lens focal lengths.
- **Camera locations.** The camera locations must be selected carefully. Selecting camera locations is a balancing act between competing parameters such as access constraints, resolution requirements, orientation, base to height ratios (i.e., ratio of distance between camera stations to distance from rock surface), surface geometry, and target locations. Initial camera locations could be estimated based on the existing site topography and conditions. The final camera locations require adjustment at the site. Having a variety of lenses allows for flexibility when establishing camera stations.

  The lighting and sun angle affect the timing for the photograph. Lighting is influenced by the time of day, time of year, weather, etc. Direct sunlight can be more challenging as it can produce high contrast between shaded and non-shaded areas. Shadows change with the sun angle and camera position. In extreme cases, this may prevent the photogrammetry software from matching pixels from overlapping photographs.

  Photographs can be taken from separate locations, or multiple photographs can be taken from a single station with a tripod in a "fan" method. If the fan method is not used and the shutter speed is high, then hand-held cameras can be used. Using a tripod and the fan method requires less skill and makes it possible to merge multiple images captured at the same camera station.
- **Printing on site.** Printing the images while at the site or at the end of each day can improve the chances for a successful field session. A portable printer or a local l-hour photo prints provider can serve this purpose. A laptop for viewing, storing, renaming, and checking the photographs is important. Time for reviewing the day's work and renaming image files is important on large, complex projects. It is easy to lose track of the station that the images were captured from. Shooting data typically saved with the image automatically provides information needed to select the proper calibration file. However, it is much easier to process the images when the image file name references the calibration file and the station number. Photographs should be grouped by camera station and calibration data, so the sorting and bundle adjustment can be constructed properly. Review photographs and complete the bundle

adjustment before concluding the field trip to reduce the need to return to the site. Bundle adjustments can fail due to poorly captured images.

DIGITAL CAMERA PROCEDURES WITH 3DM CALIBCAM

With a little experience, capturing the photographic images that result in good photogrammetric models is relatively simple for small jobs. For larger jobs with difficult access and lighting issues, the process becomes more challenging, and it is not easy to provide a guideline to deal with these more complex geometries. Experience plays a bigger role in large, more complex projects. Variables to consider include the size of the feature, the geometry of the surface, and/or the type of discontinuity exposure (whether you are mapping a joint trace or an exposed plane).

Three steps are required to acquire photogrammetric data with a digital camera:

1. **Acquire images**. Careful planning for the correct resolution settings, minimal convergence angles, and overlap between successive images will result in ideal 3D models.
2. **Calibrate the digital camera or develop the interior orientation.** The interior orientation refers to the parameters inside the camera that are not affected by the camera's position in the world. This is performed using the interior orientation bundle adjustment method to compensate for the effects of lens distortions. The camera's position and rotation are known as the exterior or outer orientation.
3. **Establish location and orientation of cameras.** The known coordinate locations of control points within each model and/or the surveyed camera station positions are used in the least squares bundle adjustment to calculate the exterior orientation of the model. This will enable 3D observations to be recorded from any location within the stereo model.

CAMERA CALIBRATION USING 3DM ANALYST

Achieving high accuracies requires accurate camera calibration. High-quality camera calibrations are important to maintain the accuracy of the 3D model. Without calibration, the "correct" location of an object in an image can be dozens of pixels away from the perceived position. With calibration, the location should be accurate to about 1/10 of a pixel. Camera calibration is much more significant for projects that have more than two camera locations.

The 3DM-Calib-Cam software can calibrate digital cameras and accepts standard camera and lens calibration information for film cameras. The 3DM-Calib-Cam software also provides the bundle adjustment of large projects containing multiple photographs.

With careful planning, the camera can be calibrated using the project photographs (and the 3DM-Calib-Cam software). Alternatively, a previously obtained calibration file can be used. It is important to keep the camera focus and aperture settings the same for both the calibration images and the project images.

LEAST SQUARES BUNDLE ADJUSTMENT

The bundle adjustment process resolves all camera locations and orientations for use in 3D models and includes the following steps:

- Develop a file structure and naming system that helps keep the data organized. File names should indicate: location, camera, and image number. Sort the photographs, rename them, and save them in the file structure.
- Import the photographs into Calibcam.
- Import the appropriate existing calibration files or create a field calibration with the appropriate images.
- Mark the control points on all images in the project.
- Execute the program "generate relative only points."
- Execute the resection exterior adjustment program and continue to refine the bundle adjustment as outlined in the program procedure.
- Verify that the field data can be successfully bundle adjusted before the field trip is concluded.
- Create merged images as needed for geologic mapping, volume calculations, or other needed measurements.
- If the bundle adjustment is not successful and the problem is with inadequate image data, it may be necessary to re-photograph some areas.

GUERNSEY DAM SOUTH SPILLWAY TUNNEL ANALYSIS

To determine the extent of freeze thaw damage in the Guernsey Dam south spillway, Reclamation performed a photogrammetric analysis of the intake structure, vertical shaft, and tunnel. This analysis required measuring the concrete surface of the tunnel between Station 0 + 00 and 6 + 00, as well as the large area of concrete around the intake structure and in the vertical shaft.

CHALLENGING SITE CONDITIONS

The work required photographing from ropes in the shaft, from a boat in the spillway tunnel, and with fall protection measures from the top of the spillway gates. The wet tunnel walls created several issues.

The confined space limited the distances between the camera and the surface being captured. This geometric constraint, along with the proper layout geometry required by the photogrammetric method, led to a large number of photographs and some extra steps in processing the photographs.

SETTING UP THE PHOTOGRAMMETRIC SURVEY

A critical initial step is to define the measurement requirements. Relating the measurements to a global coordinate system was not required for this damage survey, thus, survey control was not needed. Note: establishing survey control inside this tunnel with the access limited to a small boat would have been very difficult as the true scale and a local coordinate system related to the tunnel axis and stationing was required.

Scale bars were needed along the tunnel walls to provide a metric (**Figure 3**). The spillway intake required scale bars and three constant elevation targets on the back wall opposite the spillway gates (**Figure 4 and 5**). Typically, scale bars are provided for every 5th or 6th photograph (every 20 meters along each tunnel wall). However, the wet tunnel walls and boat access limitation made it difficult to attach the scale bars. The boat was not a stable platform for drilling anchors for the targets, and the wet walls prevented the use of glue to mount the scale bars. The scale bars were attached to metal washers by strong magnets. The metal washers were set in place using a ramset to shoot concrete nails into the tunnel lining 1 meter (a few feet) above the waterline.

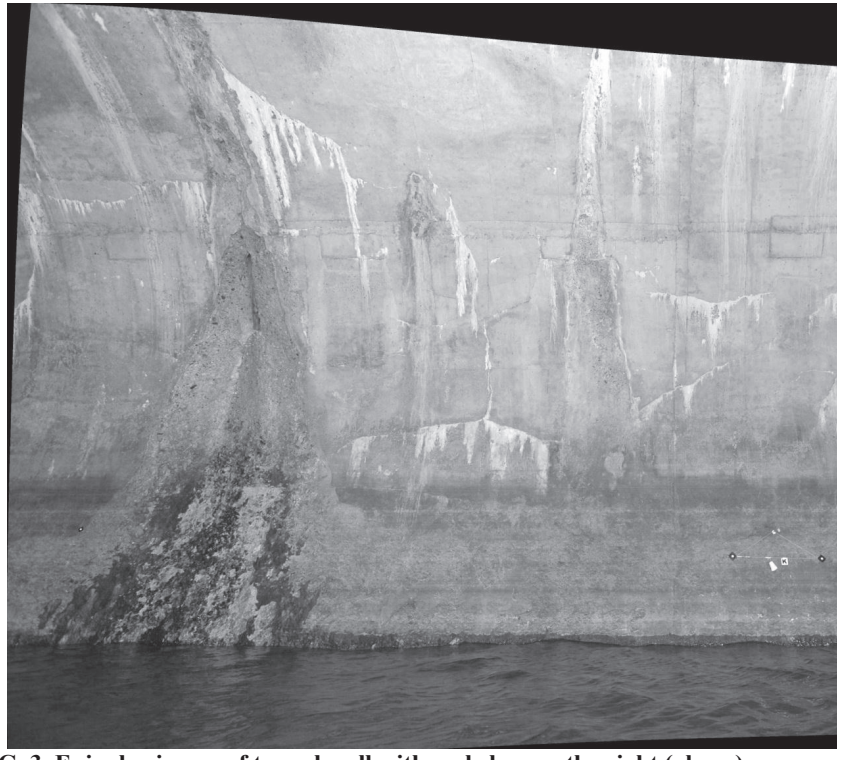

FIG. 3. Epipolar image of tunnel wall with scale bar on the right (above)

FIG. 4. Scale bars on the intake back wall (right)

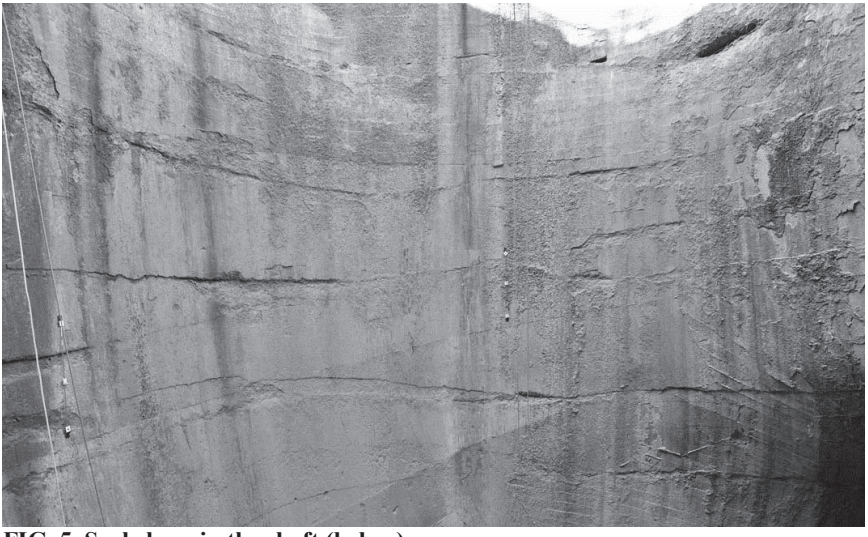

FIG. 5. Scale bars in the shaft (below)

The limited access forced scale bars to be established in a horizontal line. However, control features that are all along a single line do not provide sufficient control to correctly solve the model geometry. The proper nonlinear control system requires establishing two lines one on each tunnel wall at about the same elevation. Establishing scale bars for the set of crown photographs was not possible with the limited access available. An accurate 3D model of the tunnel lining could only be provided when the bundle adjustment included all the three tunnel strips (the left, right, and crown). Thus, the control lines (the two rows of scale bars—one on each side of the tunnel) needed to be connected to each other by the crown photographs. See the section on processing tunnel images below for more information on this.

Establishing global control in the tunnel was not required and would have been difficult without a stable platform. Global control is typically provided by surveyed control points. Local coordinates were based on known tunnel features such as the contraction joints and the tail water line. Elevations were determined using the water level elevation in the tunnel and constant elevation targets at the intake and shaft. If the state plane coordinates of the damaged concrete were needed, survey control points would have been required, one for every 5^{th} or 6^{th} photograph (every 20 meters along each wall) in each set of photos.

ACCESS LIMITATIONS

The tunnel access was limited to a small boat (**Figure 6**) by the tail water condition. The water depth in the tunnel was between 1.5 and 3 meters. The tunnel size and limited boat access precluded reaching the crown to mount scale bars.

The limited access at the intake and the vertical shaft required the photographer to be trained in rope access techniques (**Figure 7**). The support of a three-member rope access team was needed to safely take the photos in the shaft and around the intake.

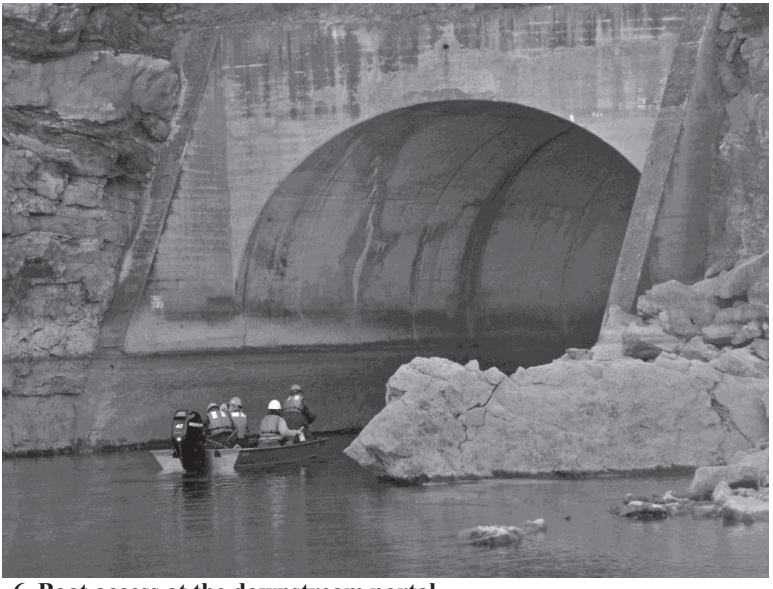

FIG. 6. Boat access at the downstream portal

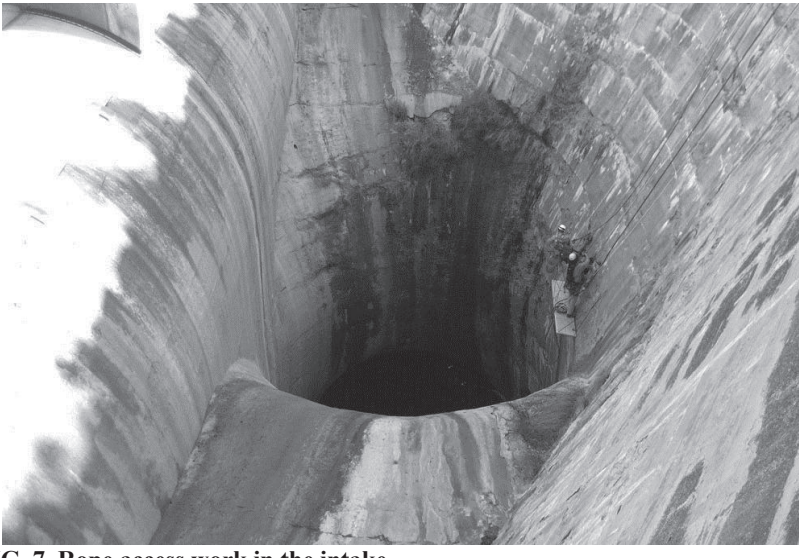

FIG. 7. Rope access work in the intake

LIGHTING CHALLENGES AND PROPER EXPOSURE IN THE TUNNEL

A small boat provided access to the tunnel. However, the dark tunnel and the unstable boat platform made it difficult to get sharp properly exposed image pairs. Initially, a single flash on the camera was used. The single flash provided a nice exposure with sharp images even though the boat was always moving. But this created a problem for the software. The software requires two overlapping images from different locations with the same light exposure. With a single flash on the camera, the light moved with the boat to the next camera position. The exposures for each photo looked good, but they each had a unique light condition that made it impossible for the software to define matching points on the adjacent images. A synchronized pair of flashes, one mounted at the stern and the other at the bow, solved this lighting problem. The photographs were retaken from the middle of the boat. The boat was about 20 feet long and camera stations were required every 10 feet, so as the boat moved and photographs were taken every 10 feet, the flashes replaced each other, keeping the lighting about the same for each adjacent photograph. The software recognized common points in adjacent images as long as the exposures were similar. This solution allowed the program to get the required match points.

A typical Nikon flash system was used in the tunnel; however, the requirements for taking the tunnel photographs was not typical. The batteries could not deliver the power needed to keep up with demand required by the quick succession flashes and large number of exposures. This caused the batteries to overheat and the flash system to fail before the set of photos were completed. The photo session was stopped and restarted after changing the batteries. It was not obvious that the flash system failed until both flashes quit working. This led to some areas of the tunnel crown not being captured completely. Additional crown photographs were required and this created some interesting challenges during processing.

CAPTURING STEREO IMAGE PAIRS IN THE TUNNEL

Photographs were taken every 3.04 m (10 feet) along the tunnel length to maintain the proper base to height ratio. Three lines of photos were required: two lines from the boat moving along a wall focusing on the opposite wall and the third line from the boat moving along the tunnel axis focusing on the crown of the tunnel. The proper base to height ratio controlled the spacing. The 3.04 m (10 foot) spacing with the 20mm lens on the Nikon D-700 provided plenty of overlap and more than enough accuracy. **Figures 8, 9, and 10** show 3D views of the camera locations relative to the automatically generated relative only points from the bundle adjustment for the tunnel and the intake. Approximately 180 photographs were bundle adjusted for the final tunnel project between stations 0+20 and 6+00. Intake photographs were captured from the gates looking toward the back wall. Photographs of the vertical shaft were obtained from ropes. Stations were selected based on the proper base to height ratio. The 50 mm lens with the D-700 camera was selected for the intake and shaft to deliver accuracies similar to the accuracy achieved in the tunnel with the 20 mm lens and the D-700 camera.

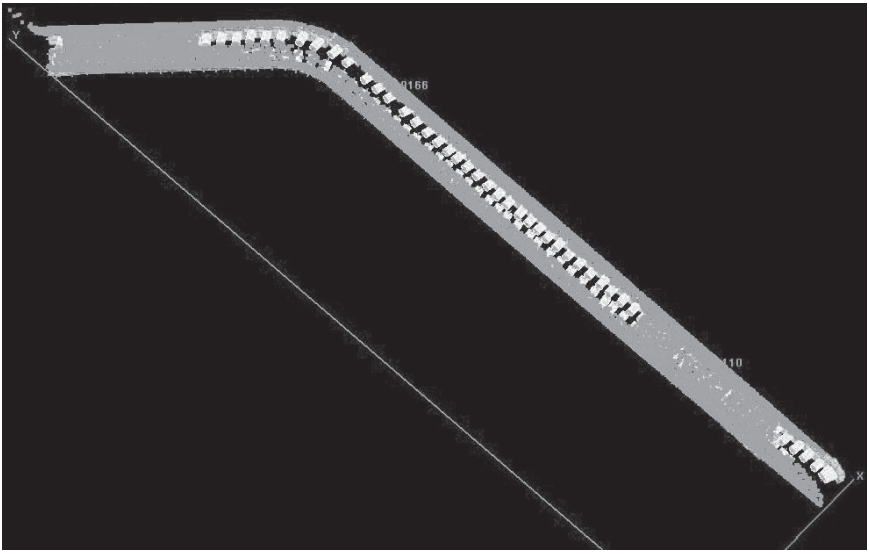

FIG. 8. Calibcam view of relative only points on the tunnel lining and camera stations from the boat

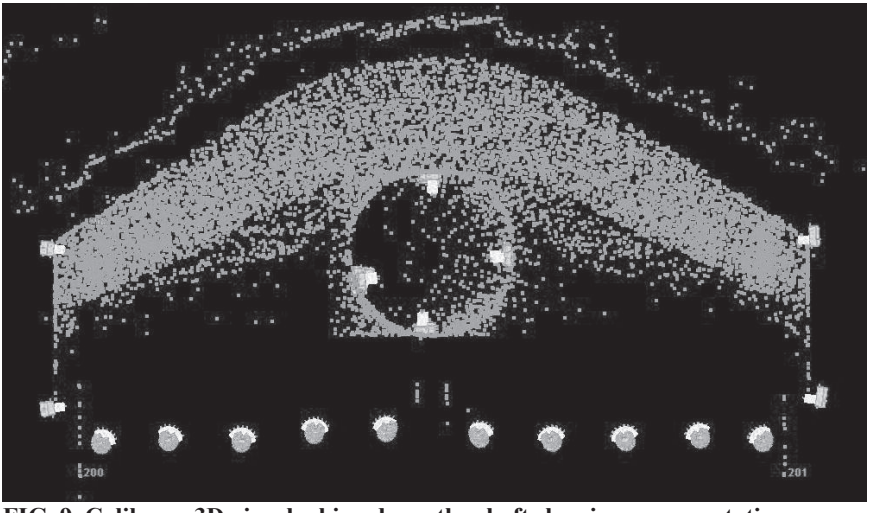

FIG. 9. Calibcam 3D view looking down the shaft showing camera stations on the spillway gates and in the shaft, only relative points are also shown

FIG. 10. Calibcam 3D view of camera stations and relative only point for the intake and shaft

PROCESSING THE IMAGES WITH 3DM CALIBCAM TO SOLVE THE EXTERIOR ORIENTATION

The third line that focused on the tunnel crown did not include the scale bars as there was no easy way to reach the crown to attach them. This meant that the crown could only be included in the model if it could be connected to each wall in the photogrammetric model by proper overlap in the image set. The correct 3D scale model that included both walls and the crown could only be resolved by combining all the photographs into one bundle adjustment.

The bundle adjustment of three independent tunnel strips (the left wall, the right wall, and the crown), while possible, would not be correctly located relative to each other. The crown would have no control and the two rows of scale bars would only provide scale information for each side. The relative location of the three tunnel strips could only be resolved when all three were included in one really large bundle adjustment. The control or scale bars are not linear when both sides of the tunnel are included with the crown. This system of control has 2 lines of control separated by the tunnel width. During processing, the need to get all the images and the scale bars from both sides of the tunnel into one bundle solution became obvious. The initial bundle adjustments included both walls from station 0+00 to station 6+00. However, when the crown was included only for station 6+00 to about 5+60, the tunnel walls started to converge as photos progressed from 5+60 upstream toward 0+00. This was because the crown photos were not included. The crown photos need to be included, as they provide the data that connects the walls to each other so that the proper

relative geometry can be determined. After including a few crown photos in the bundle adjustment near the upstream end (Station 0+00), the walls no longer converged and the correct relative only scale model was resolved.

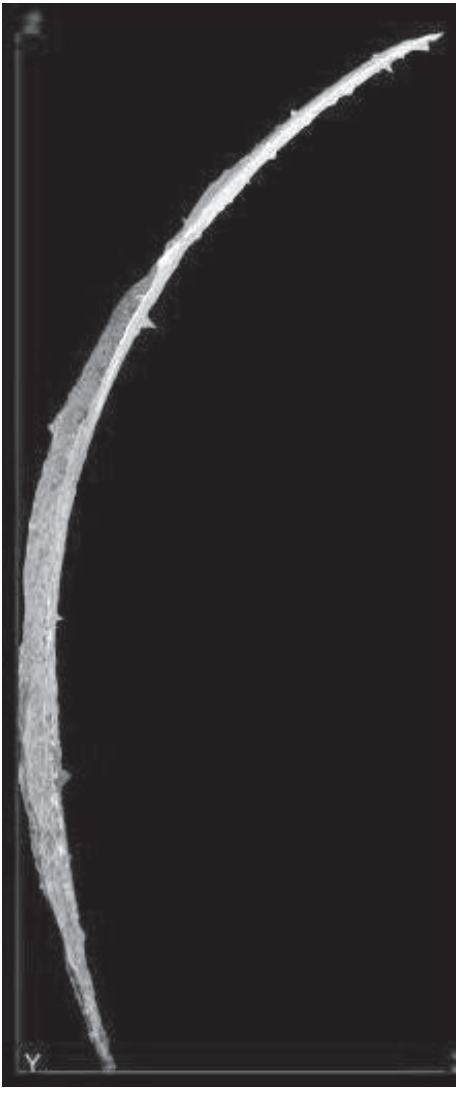

FIG. 11. 3D view of textured DTM looking down the tunnel axis (left)

PROCESSING IMAGE PAIRS WITH 3DM ANALYST

Image pairs from the image pair list that had the desired coverage and a good base to height ratio (1:3 to1:5) were selected for the Digital Terrain Model (DTM) generation. The DTMs were trimmed and merged to cover the desired area. Sections, profiles, and ortho-photos were generated in 3DM analyst. These were exported for post processing in ARC GIS and AutoCAD. **Figures 11 thru 14** show 3D views of the 3DM Analyst results for a few image pairs where significant freeze thaw damage can be seen along the tunnel walls. These areas are readily apparent by the bulges and other anomalies in the detailed surface. **Figures 15 and 16** show the plan and elevation respectively of 3D model for the intake structure. This model is a merged DTM of the entire back wall of the intake and shaft structure. Many image pairs were required to create the intake model. This model was used to generate damage profiles (contours of the surface) for the concrete in the back wall and the ortho-photo used in the final damage map created in AutoCAD Civil 3D.

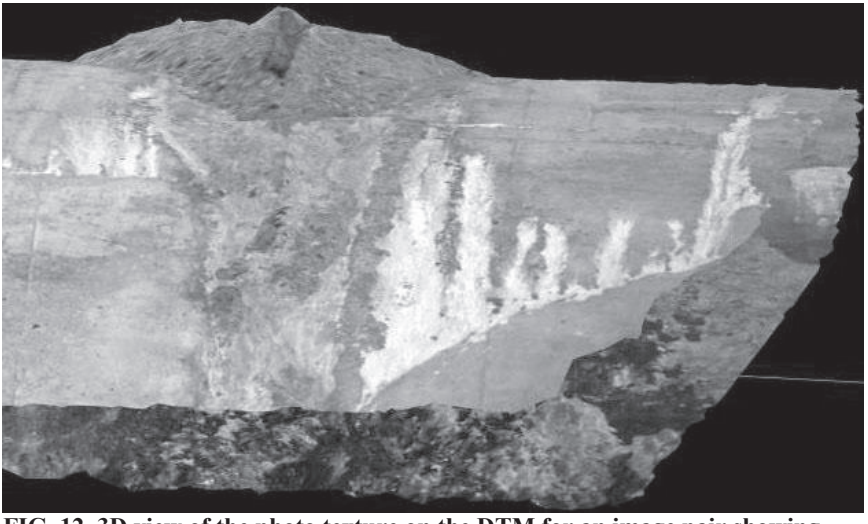

FIG. 12. 3D view of the photo texture on the DTM for an image pair showing significant tunnel lining damage (above)

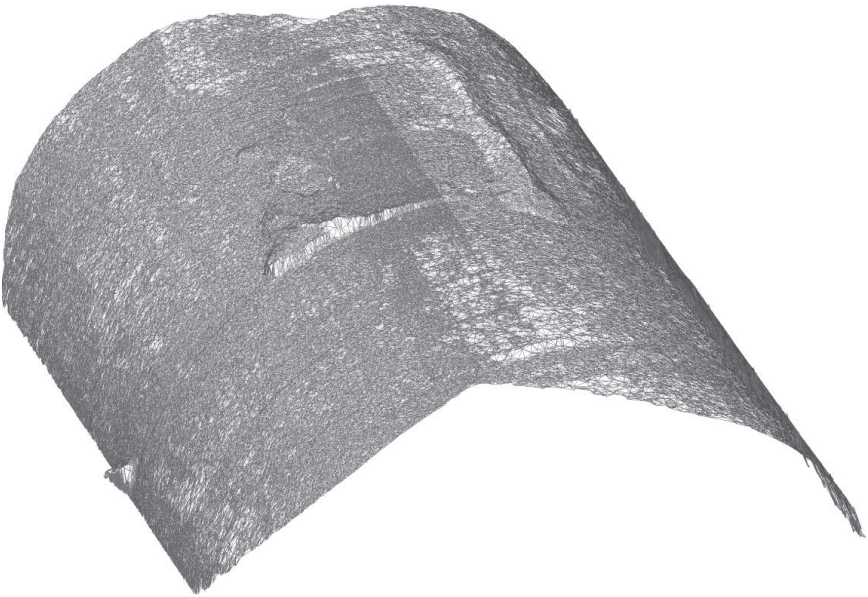

FIG. 13. DTM mesh of the tunnel lining

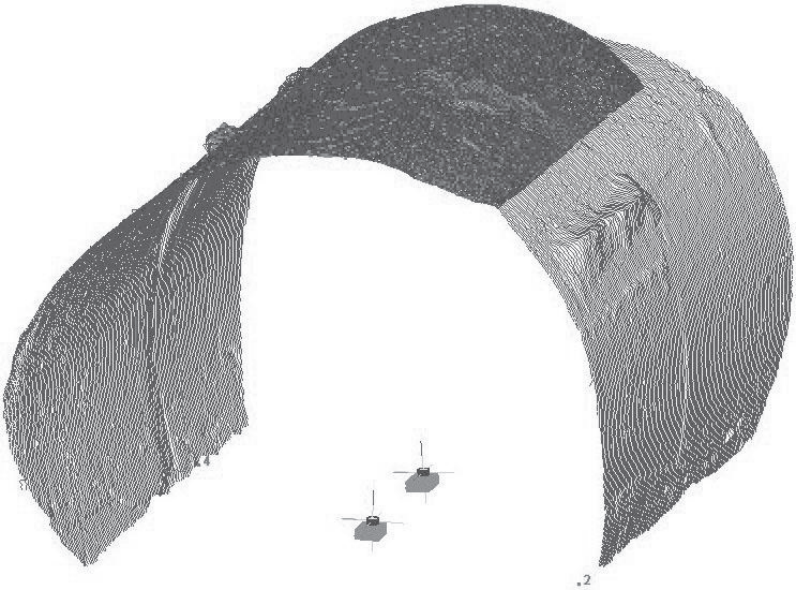

FIG. 14. Closely spaced tunnel sections showing damage areas and camera locations for the crown DTM

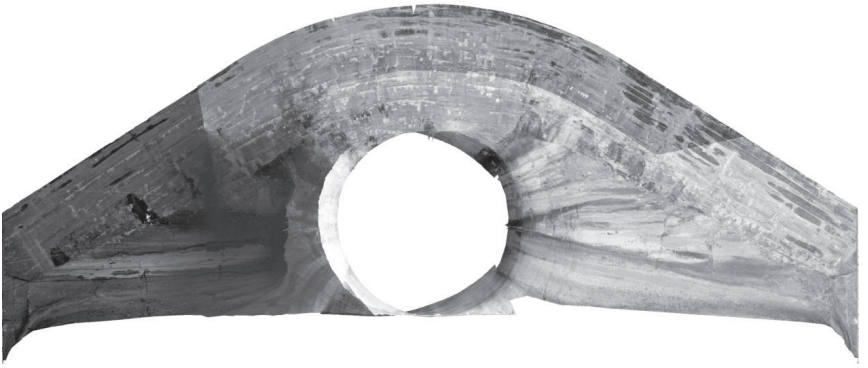

FIG. 15. Textured plan map of intake structure back wall

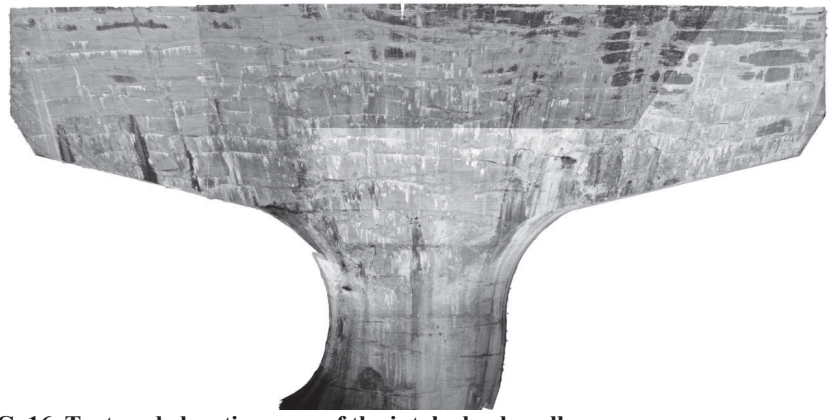

FIG. 16. Textured elevation map of the intake back wall

POST PROCESSING AND RESULTS ACHIEVED

The tunnel and intake structure models provided a set of damage profiles that could be referenced by elevation and tunnel station. These profiles were exported into AutoCAD along with the tunnel station and elevation so a detailed map of the damage could be seen relative to the tunnel station and intake elevation. **Figure 17** shows the final damage map for the tunnel between stations 0+20 and 2+00. **Figure 18** shows the final damage map for intake structure back wall. The depth of the damage was also measured and recorded on the final map. This was done for the upstream 182.9 m (600 feet) of tunnel. The downstream 38.1 m (125 feet) of the tunnel were also captured, but not processed in detail, as the damage in this reach was relatively minor. The roughness of the damaged zones was evaluated for the potential to induce cavitation under the new flow conditions. The 3-D surface model and the photographs provided the data needed to evaluate quantitatively the need for tunnel repairs. This resulted in a significantly smaller repair effort and saved significant construction

costs. The photographs and the 3D models provide a quantitative record of the tunnel and intake conditions at the time the photographs were taken. This will be a valuable record that can be used as a baseline for future evaluation after the tunnel is put into service and experiences floods.

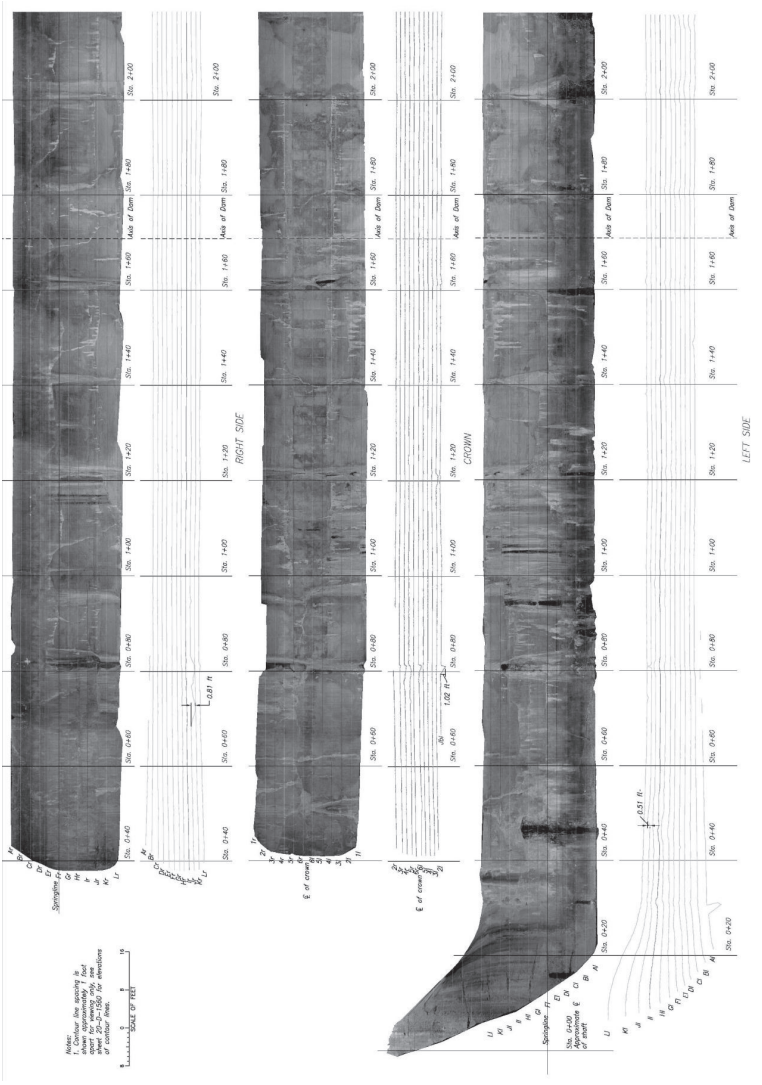

FIG. 17. Damage map with profile lines and ortho-photo of the tunnel lining between stations 0+20 & 2+00

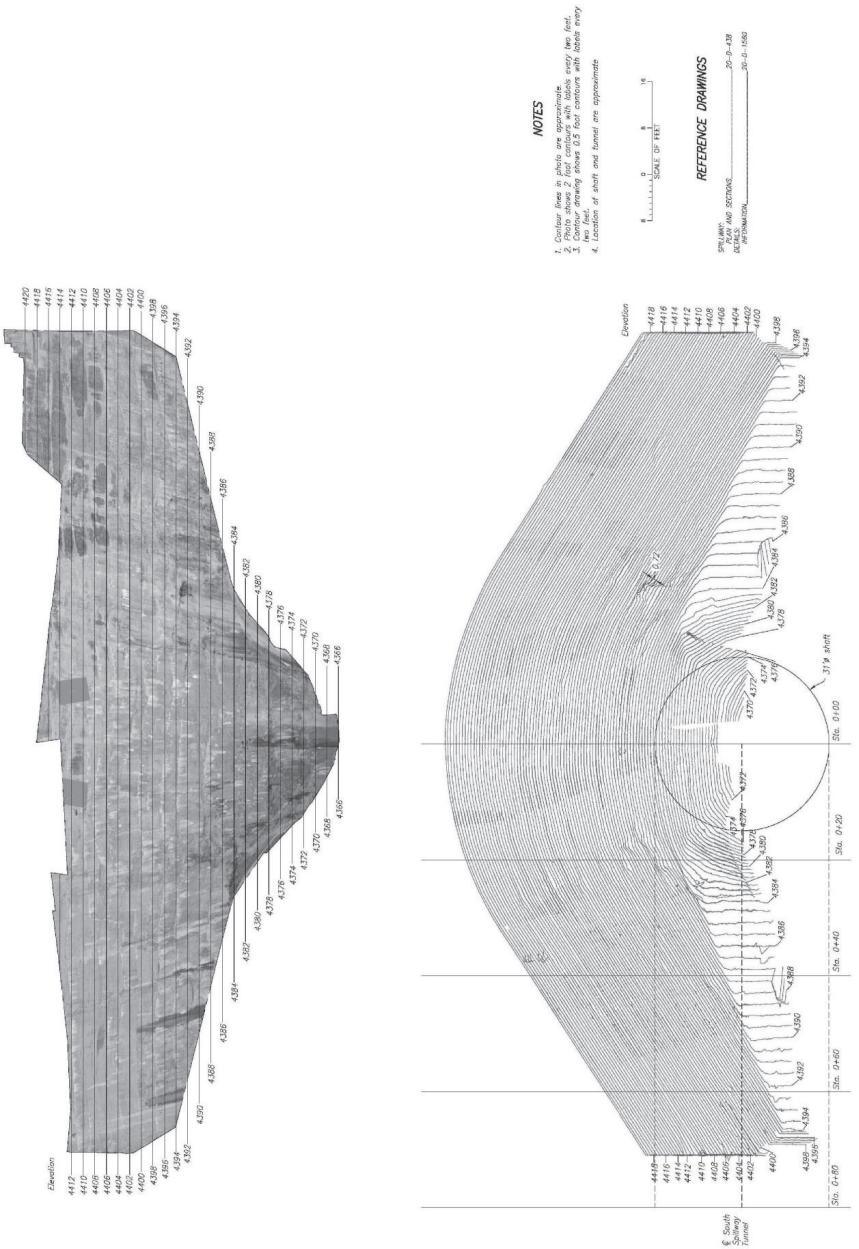

FIG. 18. Damage map with profile lines and ortho-photo elevation of the intake structure back wall

CONCLUSIONS

Our capability to understand, monitor, and analyze dam behavior is often influenced by our ability to perform accurate measurements. Digital close range (terrestrial) photogrammetry offers an exciting new method for measuring that is limited only by our imagination. This paper provides one example of a recent photogrammetry applications performed by Reclamation.

This paper discusses issues we resolved so that other photogrammetry projects can take advantage of these innovations, including:

- Using magnets to attach the scale bars to the sides of the tunnels allowed us to provide a scale, but forced the scale bars to be established in a line.
- Providing a set of crown photos allowed the control lines to be connected to each other.
- Putting all three strips into one bundle solution resolved problems with walls converging.
- Using synchronized flashes on each end of the boat to solve lighting issues, enabling all the photographs to be captured in a few hours. Most other methods for capturing this type of measurement data (conventional survey and LIDAR scans) require a stable platform and the limited access (small boat) would not work. These other methods would be much more costly and time consuming and may even require dewatering the tunnel.

Advantages to using photogrammetric measurements include:

- Once a metric has been established, the actual size and extent of the damage can be determined from the 3D model.
- Field work is limited to setting up and taking the photographs; actual damage measurements takes place in the office.
- Photographs remain as a permanent record of structural condition at the time of the survey and can always be revisited to look for changes based on subsequent surveys following significant flood events.

FUTURE PLANS

Many other Reclamation projects have been supported by these methods. The 3D imaging and measurement capabilities of photogrammetry will improve and become even simpler as software development progresses, and digital camera resolution improves. It is already possible to construct an accurate 3D computer model of a complex structure using only photographs. It is easy to foresee a day in the near future where photogrammetry modeling will be a standard tool offering great improvements in measurement capabilities in many industries, including dam design, analysis, and construction. It would be extremely difficult to produce the level of 3D data achieved with close range photogrammetry at this site by any other means.

ACKNOWLEDGMENTS

The author appreciates the support of Sheena Barnes and Dom Galic in Reclamation, who helped with the field collection and image processing. In addition, Reclamation's Science and Technology Program and Dam Safety Technology Development Program provided funding.

REFERENCES

ADAM Technology (2010) *3DM Analyst Mine Mapping Suite 2.3.4 User's Manual,* ADAM Technology, Suite 3, 41 Belmont Avenue, Belmont WA 6104, Australia, http://www.adamtech.com.au.

Birch, J. S. (2006) "Using 3DM Analyst Mine Mapping Suite for Rock Face Characterization." *Laser and Photogrammetric Methods for Rock Face Characterization Workshop*, 13-32.

Bureau of Reclamation (2009). *Guernsey Dam Hydrologic Risk Analysis North Platte Project, Wyoming*, *Technical Memorandum No. GUI-8130-IE-2009-2* Denver, Colorado.

Bureau of Reclamation (2011). *Corrective Action Alternatives Guernsey TM No. GUE-8130-CAS-2011-1* Denver, Colorado.

Balloon Photogrammetry along the Middle Fork John Day River, Oregon

Kendra Russell[1]
[1]Hydraulic Engineer, Bureau of Reclamation,Technical Service Center, Denver Federal Center, Bldg 67 (86-68240), Denver CO 80225-007; krussell@usbr.gov

ABSTRACT: Low altitude balloon photogrammetry has been used to obtain high-resolution photographs and detailed topographic information of large wood restoration projects on the Middle Fork John Day River in Oregon. These data can be used to monitor changes in channel morphology. Overlapping photographs and ground survey control points are input into a photogrammetry software program to produce orthophotographs and digital terrain model elevation points. To acquire the photos, a remote controlled digital camera is attached to a 2.4 meter diameter helium balloon. The balloon is tethered to the ground and flown above the location of interest. Ground survey control is established by using global positioning system (GPS) equipment to survey ground targets placed within the photographed area.

Photographs of the large wood structures were obtained in November 2008 and September 2009. The photographs were used quantitatively to determine the exact location of each log within the structure, log lengths, structure extent into channel, and area of bars formed downstream of structures. Qualitatively the photographs were used to see how much hydraulic cover for aquatic species was being provided, find the formation of pools and bars that created habitat, and planform locations. Elevation data were accurate on exposed land and but not in vegetated areas. Below water topography is not accurately captured in the processed elevations. There are limitations to a balloon-based data collection process. Data collection is very weather dependent. Photo processing can be time intensive. Site conditions also determine the feasibility: power lines, trees, and steep embankments can cause difficulties maneuvering the equipment.

INTRODUCTION

Several large wood (LWD) restoration projects have been installed on the Middle Fork John Day River near John Day, Oregon. LWD sites were visited to record an "as-built" of the structure configuration and monitor morphological changes resulting from structure installation. In addition, detailed topographic information was desired to look at wood characteristics such as length, diameter and rootwad size. The quantity of structures, time allotted for the field investigation, and poor satellite coverage made

a detailed topographic survey with a total station or GPS equipment at each structure not feasible. Therefore, two projects were flown at low altitude using a tethered balloon.

LWD structures were installed on The Nature Conservancy property (TNC) in July–August, 2007 and July-August, 2008. These structures were photographed in November, 2008. Seventeen total structures were installed; seven were designed as collector v-logs, four were designed as scouring v-logs, and six were designed as deflector v-logs (MWH 2006). The structures are split into two groups separated by approximately one mile: the upstream section has ten structures and the downstream section has seven structures. Scouring v-logs were intended to provide salmonid resting habitat and depth cover as well as physical cover and shade. Deflector v-logs were meant to create friction within the structure and cause the river flow to go around the structure, resulting in narrowing and deepening of the channel. Instream cover and habitat diversity were anticipated to be created by these structures. Collector v-logs were designed to collect woody debris in the channel and create cover, resting, and hiding refuge for adult and juvenile fish. The scouring v-logs have a pre-excavated pool unlike the deflector and collector v-logs. All log members of the structures are bolted together. All structures are similar in size, spanning approximately 10.7 meters (35 feet) along the river bank and extending roughly 6.1 meters (20 feet) into the river.

The largest peak flow the 2007 structures had experienced by November, 2008 was approximately 34 to 42.5 meters^3/sec (1,200 to 1,500 cubic feet per second (ft^3/s)) based on 65.1 meters^3/sec (2,300 ft^3/s) measured 48.3 kilometers (30 miles) downstream from the structures (recorded at USGS 14044000 Middle Fork John Day River at Ritter, Oregon). This flow is between a 2-year and 5-year event for the Middle Fork John Day River based on a recent hydrologic analysis (Reclamation, 2008). The 2008 structures had only experienced base flow conditions (less than 2.8 meters^3/sec (100 ft^3/s)) between the time of their installation and the site visit.

LWD structures were also installed between Beaver Creek and Ragged Creek in summer 2009. Fifteen structures were installed over 914.4 meters (3,000 ft) of river channel. Structures were comprised of two to ten key log members. Scour pools were pre-excavated around the structures. Key members were pinned and ballasted as minimally as possible. Smaller logs were placed without anchoring to allow for mobilization and natural deposition downstream. These log structures were placed to improve fish habitat conditions and promote floodplain connectivity. One structure was placed at the inlet of a side channel to promote backwaters and deflect flow into the side channel. Potentially, this structure could redirect all main channel flow into the historical side channel. This reach, photographed with the balloon in September 2009, had been recently constructed and had only experienced base flow conditions.

INSTRUMENTATION

Low altitude balloon photogrammetry is an emerging technology. Originally, photogrammetry was limited to professionals with the required training, equipment, and software. However, with the development of high quality digital cameras,

photogrammetry software programs have been developed that are accessible to anyone with a camera. A digital camera and a mechanism, such as a tethered balloon, to lift the camera above the object of interest, such as a river corridor, is all that is needed to collect the photographs to be processed in a photogrammetry software program.

To acquire photographs for mapping ground surfaces and in-channel features, a digital camera (Nikon D300) is attached to a 2.4 meter-(8 ft) diameter helium balloon. The balloon is controlled by manually tethering it to reels held by two people on the ground. The balloon can be moved along the river by the people who are standing on opposite banks. Pan and tilt camera movements were remotely controlled using a control unit designed for flying small airplanes and helicopters. The live image from the camera was transmitted to a receiver on the ground, enabling the operator to see directly through the camera lens and remotely trigger the camera at specific overlapping intervals for development of accurate terrain models. In the field investigation of the Middle Fork John Day River, the balloon was approximately 100 to 45.7 meters (150 ft) above the ground for the photographs. Figures 1a and 1b show the balloon and camera used to take photographs of the LWD structures.

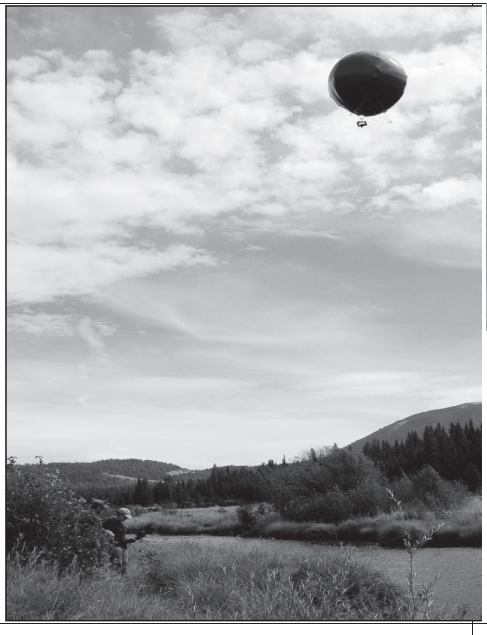

FIG. 1a. Helium balloon used to carry digital camera. The balloon can carry approximately 12 pounds

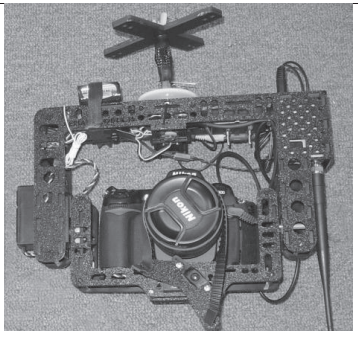

FIG. 1b. D300 Nikon camera mounted to frame with pan (360° rotation) and tilt (from horizontal to straight down) servo motors to control orientation

The low altitude balloon digital photogrammetry provides high resolution spatial information in a fraction of the time it would take to survey the same number of points using traditional methods. Ground survey control is established by using GPS equipment to survey ground targets placed within the area to be photographed. Targets have a white background with a black circle and are large enough to be located in the photos. Targets are spaced semi-randomly along the river corridor to improve the spatial and vertical accuracy of the orthophotographs. In general, at least two targets were placed in the vicinity of objects of concern. In addition to the target survey points, GPS survey was completed on top of and adjacent to the log structures to compare with the photogrammetry results.

PHOTOGRAMMETRIC PROCESSING

Photographs acquired from the helium balloon were imported into Adam Technology's 3DM Analyst Mine Mapping Suite (Birch, 2006). An example photograph is shown in Figure 2. Using the software, images were paired, and common points were generated between the images. The software experienced difficulty finding common points within the river channel, and therefore, multiple points were added manually to accurately match the images. Control points and associated GPS information were added to the targets in the images to orient the photos spatially.

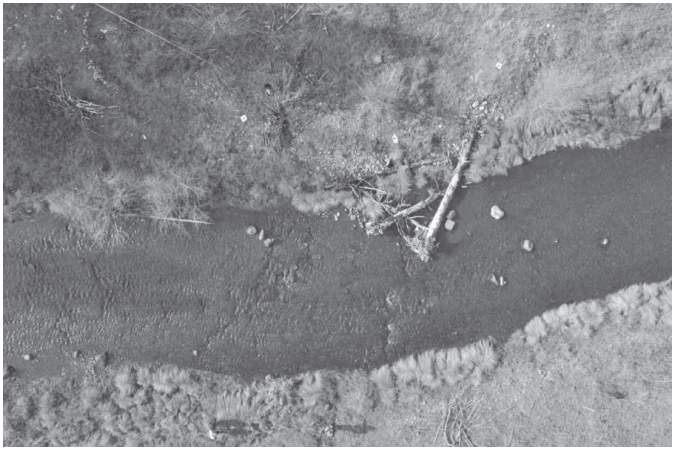

FIG. 2. View of an engineered LWD structure in the Middle Fork John Day River as seen from a helium balloon about 36.6 meters (120 ft) above the ground (flow is from left to right)

The software needs at least three control points with known locations to form an absolute orientation (Birch, 2006). For the TNC project, four targets were placed at each structure, and overlapping images were taken from one structure to the next to orient the entire project in the State Plane coordinate system. For the Beaver Creek to

Ragged Creek project, targets were placed along the entire reach. Figure 3 shows a structure from the TNC project with the four targets labeled.

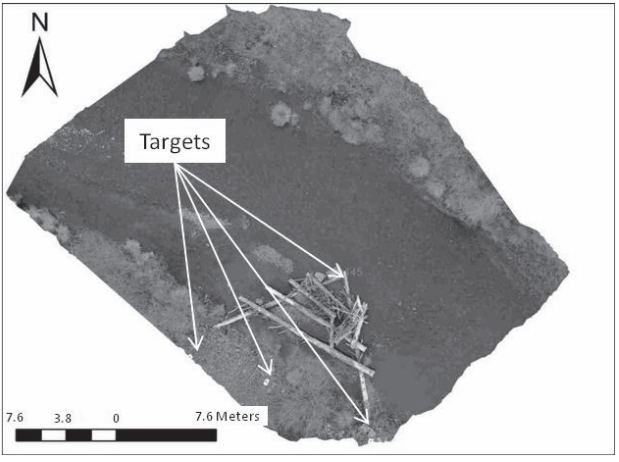

FIG. 3. Structure from the TNC project with four targets labeled

The digital terrain model (DTM) generator within the Adam Technology software was used to create spatial points with elevation and orthophotographs. Figure 4 shows the same structure from Figure 3 with the DTM points overlaid. There are over 50,000 points generated for the one orthophotograph. As seen from the DTM points, the software had difficulty in generating elevation points across the water surface and also in locations with trees.

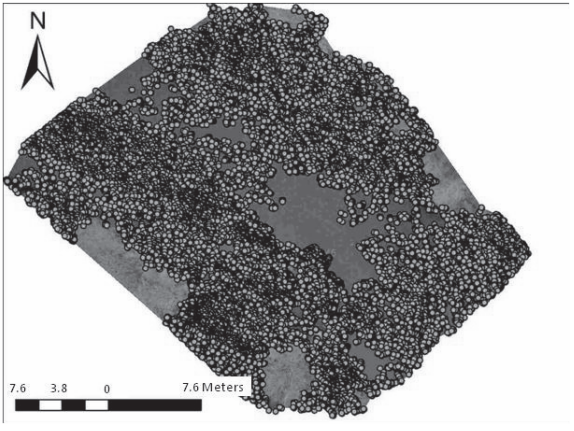

FIG. 4. Orthophotograph of LWD structure on TNC project with elevation points from Adam Technology software processing overlaid

Since there were multiple structures in series the orthophotographs were merged to create a continuous image. Three of the downstream site structures (AA, BB, and CC) are shown in Figure 5. Continuous images can be used to evaluate changes in morphology upstream and downstream of the structure as well as the interaction between the structures. For example, bars are beginning to form between the structures illustrated in Figure 5.

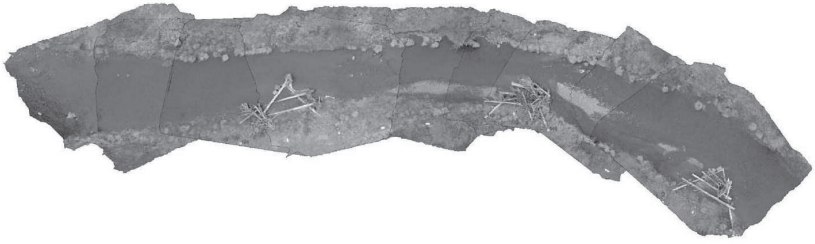

FIG.5. Ten merged orthophotographs generated from Adam Technology software that cover a portion of the downstream site from LWD structure AA (right-most feature) to CC (left-most feature). Flow is from right to left

RESULTS

The accuracy of the elevation data results is extremely important if these data are being used to build numerical models or track sediment volume changes. The software program produces error residuals for the ground targets based on the input GPS survey information. Table 1 shows the average and maximum error residuals for both projects surveyed.

TABLE 1. Average and maximum error residuals for ground targets

	TNC Project		Beaver to Ragged Project	
	Average Error Residual m (ft)	Maximum Error Residual m (ft)	Average Error Residual m (ft)	Maximum Error Residual m (ft)
X Direction	0.01 (0.04)	0.06 (0.19)	0.02 (0.07)	0.06 (0.19)
Y Direction	0.01 (0.05)	0.06 (0.21)	0.02 (0.06)	0.08 (0.28)
Z Direction	0.02 (0.08)	0.13 (0.43)	0.02 (0.06)	0.07 (0.23)

The accuracy of the DTM points also varies within each photo-image pair of the projects. For the Middle Fork John Day River, the accuracies of the digital elevation data were tested with an additional bathymetric survey. Underwater ground truthing survey points were collected for the 2008 photos and showed little agreement between GPS points and the processed DTM elevations in the channel. One issue was that the processed photos did not have dense elevation points in the wetted portions of the

channel. Therefore, of the surveyed bathymetric points collected, only 18 of 62 were within 0.30 meters (1 ft) of a DTM point. Figure 6 compares the surveyed points to the calculated DTM points. On average, the DTM point elevations were different by 0.30 meters (1 ft). It is noted that all of the DTM points have a higher elevation than the surveyed points. This could potentially indicate that the DTM points are actually representative of the water surface elevation or of some other elevation in the water column. Based on these results, the in-channel points are considered inaccurate bed elevations and were not used in any further analyses. However, qualitative information on bed material sizing and relative depth (for pool locations) may be visually ascertained from the photograph, depending on the clarity of the photograph, along with clarity and depth of water. The Middle Fork John Day River was relatively shallow and clear but this information would be difficult to obtain on a more turbid or deep river.

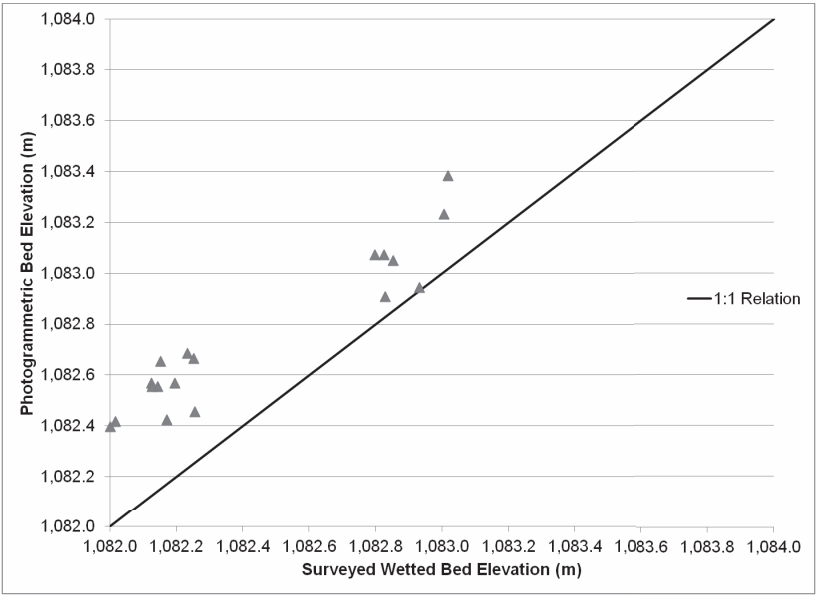

FIG. 6. Comparison of bathymetric survey points to DTM points

Additional ground truthing points were surveyed on a variety of surfaces (logs, bare ground, vegetation mats, and vegetation or brush) during the 2009 visit to the Middle Fork John Day River. Vegetation mats are strips of black tarp where specific riparian plant species have been planted for restoration. Figure 7 shows the comparison of the ground truth points and the calculated DTM points plotted by distance apart. For this comparison, the closest DTM elevation was differenced from the survey elevation. Points that were not within 0.5 meters (1.6 ft) of each other were not included in this comparison. The bold black dashed lines represent 0.15 meters (0.5 ft) of elevation difference. The logs, vegetation mats, and bare ground do not appear to have any bias.

However, the vegetation or brush points show that the DTM points are biased higher than the surveyed points. This is likely because the DTM points are from the top of the vegetation rather than the ground beneath. This is similar to a "first return" acquired from LIDAR data.

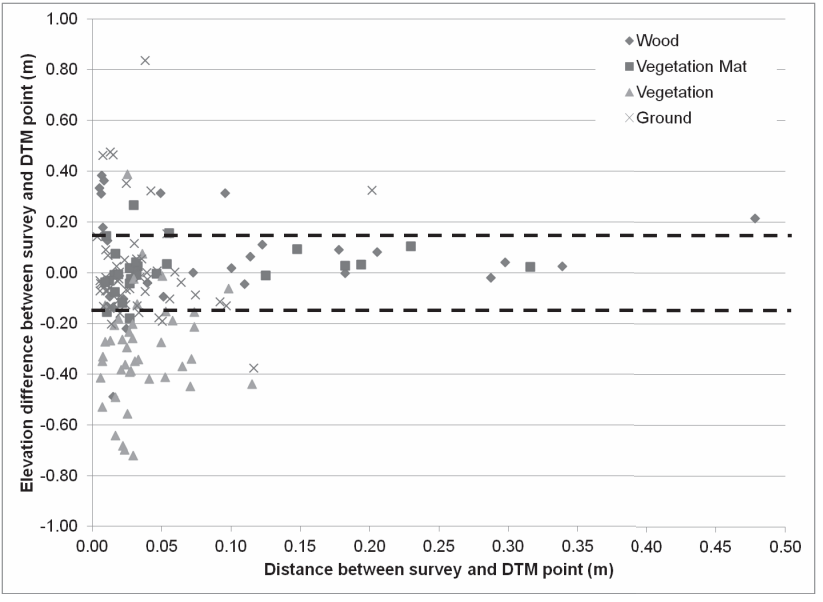

FIG. 7. Comparison of surveyed ground truth points and computed photogrammetry elevation points

Photogrammetry produces a very dense set of DTM points (see Figure 4). Figure 8 shows the comparison of the closest surveyed values from each of the ground truth types to the DTM points. To determine if any of the points in the vegetated areas were able to "see" through the vegetation and pick up ground elevations, the minimum elevation was selected from DTM points that were within 0.15 meters (0.5 ft) of the vegetation points. The vegetation plot includes the minimum and closest elevation values. The minimum elevations are still biased higher than the surveyed elevations. Although the minimum elevation does improve the relationship slightly, it is not adequately capturing the ground elevation. Therefore, the DTM points in vegetated areas should not be utilized in other analyses. This should be reevaluated at a different site where the vegetation may be less dense than what was seen on the Beaver to Ragged project. For the wood, vegetation mats, and bare ground DTM points, the average elevation difference (absolute value) is 0.16, 0.09, and 0.12 meters (0.54, 0.30 and 0.38 ft), respectively.

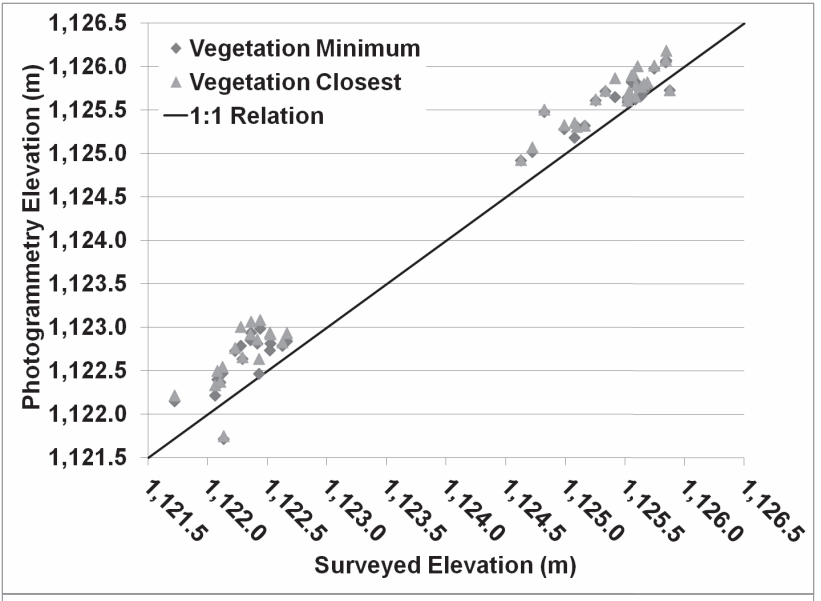
Vegetation Minimum
Vegetation Closest
1:1 Relation
Photogrammetry Elevation (m)
1,126.5
1,126.0
1,125.5
1,125.0
1,124.5
1,124.0
1,123.5
1,123.0
1,122.5
1,122.0
1,121.5
1,121.5 1,122.0 1,122.5 1,123.0 1,123.5 1,124.0 1,124.5 1,125.0 1,125.5 1,126.0 1,126.5
Surveyed Elevation (m)

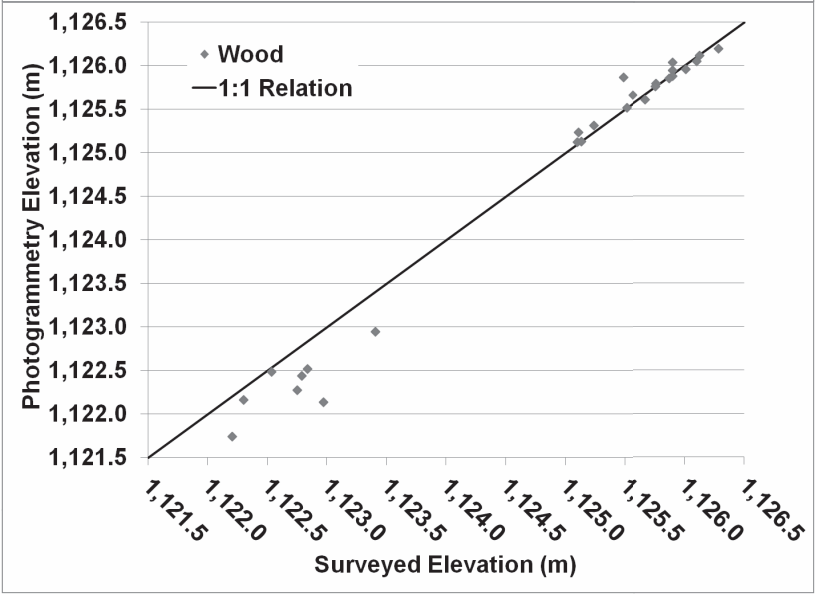
Wood
1:1 Relation
Photogrammetry Elevation (m)
1,126.5
1,126.0
1,125.5
1,125.0
1,124.5
1,124.0
1,123.5
1,123.0
1,122.5
1,122.0
1,121.5
1,121.5 1,122.0 1,122.5 1,123.0 1,123.5 1,124.0 1,124.5 1,125.0 1,125.5 1,126.0 1,126.5
Surveyed Elevation (m)

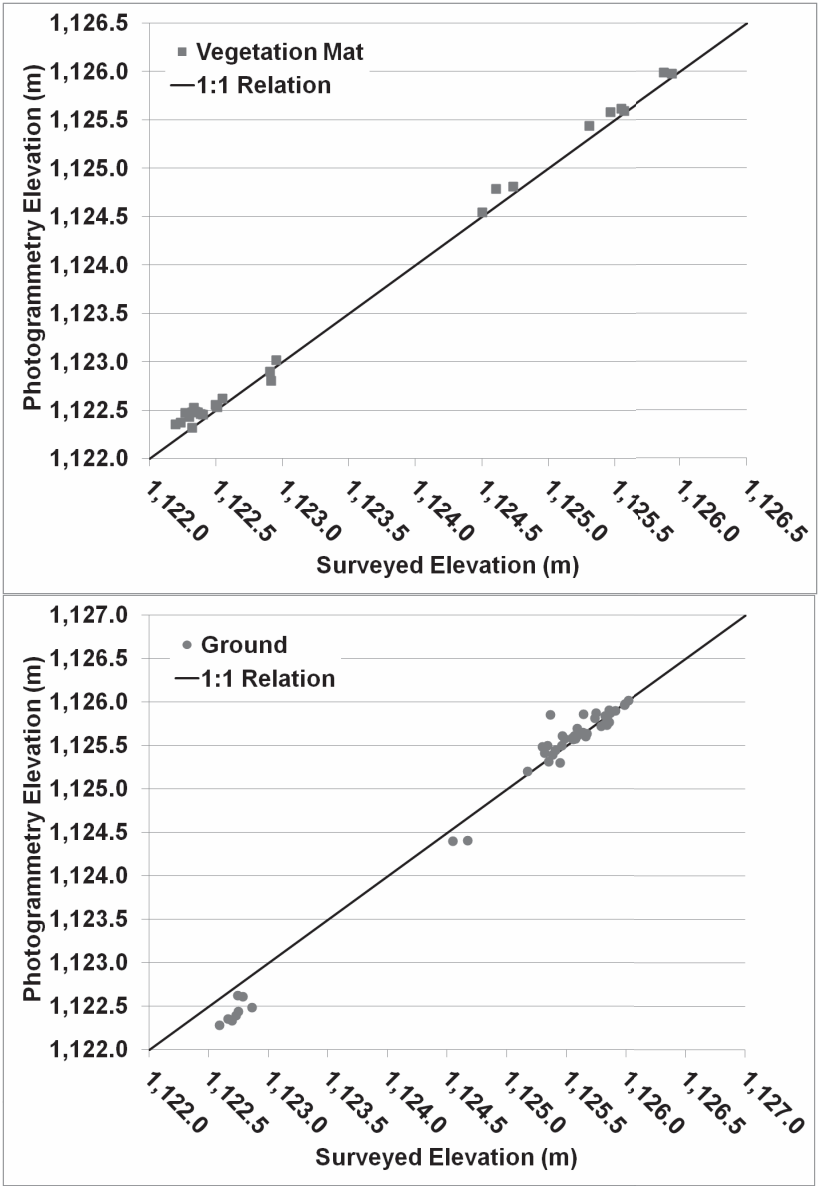

FIG. 8. Comparison of different ground cover survey points and DTM elevations

DISCUSSION

There are many different applications for which the orthophotographs and DTM elevation points can be utilized. For the two Middle Fork John Day River projects, characterizing the large wood structures and the morphological changes caused by the structures were the main purpose of the flights. For these projects, the orthophotographs were used to determine log lengths, determine the exact location of each log within a structure, quantify the structure extent into the channel, determine the cover provided and map pools, bars, and banklines. Interactions between multiple structures can also be discerned. For example on the TNC project, bars building between the structures were captured in the balloon photographs. In addition, the bed material type could be assessed using a photosieving software (where exposed above water). In conjunction with previous surveys or future balloon flights, the orthophotographs can be used to monitor changes in banklines, side channels, and log movement. The elevation information can be used to measure aggradation and degradation of exposed sediment deposits and to monitor vegetation changes such as height and density.

As an example, on the TNC project, survey data had been collected in 2005 prior to the large wood structure installation. The survey data were manipulated to create a channel bed surface. This surface was compared to the above water, unvegetated 2008 DTM points. Figure 9 shows the map of areas with erosion and deposition between the two survey dates. Using this, the volume of the bar downstream of the large wood structure can be calculated. In order to use this method, having similar types of topographic information would be useful. In this example, the 2005 data were heavily interpolated to create a continuous surface for comparison.

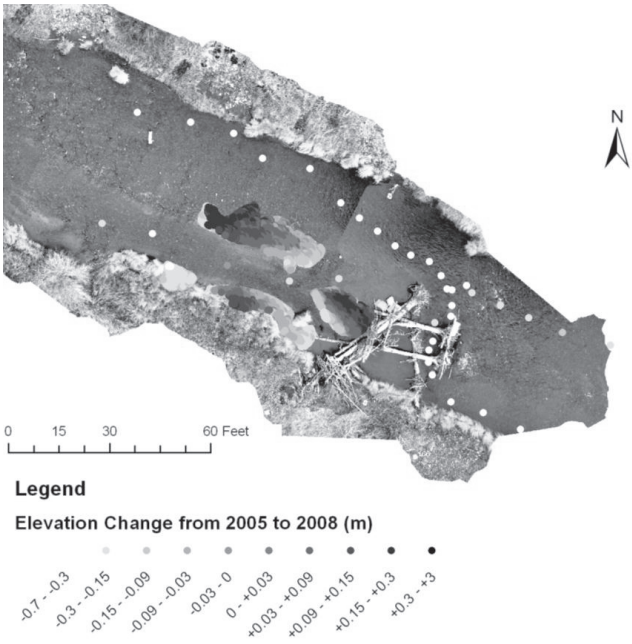

FIG. 9. Elevation change from 2005 to 2008 using calculated DTM points

There are advantages and disadvantages to using low altitude balloon photogrammetry. One of the advantages is that collection of the data is quick. Photographs can be obtained as quickly as you are able to maneuver around your area of interest. However, the processing of the photographs can be time intensive, especially if you have poor control of where and at what angle your photographs are obtained such as in a case with high winds. Another advantage is that the topographic information provided is detailed, accurate, and can be oriented in world coordinates. The accuracy and detail of the information are limited by the height of the tethered balloon, which affects pixel size. The larger the pixel size, the less resolution available in the elevation data. Also, not all of the elevation information is usable. The photogrammetry process used for these two projects was unable to capture below water topography. Also, the topographic information represented a "first return" rather than bare earth information in vegetated areas.

Data collection is very weather dependent; too much wind causes the balloon to be unstable. It is ideal to have the photos with the same orientation (parallel or perpendicular to the channel depending on how much of the floodplain is desired) for ease of processing. Therefore, control of the balloon and camera mount must be maintained. Power lines, trees, and steep embankments can cause difficulties

maneuvering the balloon. The width of the river corridor of interest may require multiple photograph strips across the channel or flying the balloon at a height that will not provide the desired accuracy in elevation data or photographic resolution.

CONCLUSIONS

Low altitude balloon photogrammetry has been used to obtain high-resolution photographs and detailed topographic information of large wood restoration projects on the Middle Fork John Day River. Overlapping photographs and ground survey control points are input into a photogrammetry software program to produce orthophotographs and digital terrain model elevation points. To acquire the photographs, a remote controlled digital camera is attached to a tethered 2.4 meter-(8 ft) diameter helium balloon.

Photographs of the large wood structures were obtained in November 2008 and September 2009. One of the biggest advantages to a low altitude balloon flight is the ability to produce high resolution photographs and topographic data that may be unsafe or extremely time consuming to collect with traditional ground survey methods. There are multitudes of uses for these products. The flights can be repeated and used to monitor planform changes of a river. In addition, bed material sizing can be assessed on exposed sediment deposits. Elevation data were accurate on bare ground and solid surfaces such as logs, but not in vegetated or below water areas. For the wood, vegetation mats, and bare ground DTM points, the average elevation difference (absolute value) is 0.16, 0.09, and 0.12 meters (0.54, 0.30 and 0.38 ft), respectively. There are limitations to the process such as site conditions and processing time.

ACKNOWLEDGMENTS

The author appreciates the support of Elaina Gordon and Mark Croghan of Bureau of Reclamation (Reclamation) who helped with the field collection. In addition, Joe Kottenstette, Rebecca Heisler, Carly Wegher and Sean Kimbrel of Reclamation processed the 2008 and 2009 photographs using Adam Technology software.

REFERENCES

Birch, J. S. (2006) "Using 3DM Analyst Mine Mapping Suite for Rock Face Characterization." *Laser and Photogrammetric Methods for Rock Face Characterization Workshop*, 13-32.

Bureau of Reclamation (2008). *Middle Fork and Upper John Day River Tributary Assessments, Grant County, Oregon*, Denver, Colorado.

MWH (2006). *Middle Fork John Day Habitat Improvement Conceptual Design Report.*

Templeton Gap Floodway Levees, Investigation and Mitigation of Mine Subsidence

Nathan Soule, M.ASCE, P.E., P.G.[1], Minal L. Parekh, M. ASCE, P.E.[2], Steven Kuehr, M. ASCE, P.E.[3], Al Amundson, P.E. [4], Kanaan Hanna, P.E.[5], Dan Bare, P.E.[6], Chris Pauley, M. ASCE, P.E., CFM[7]

[1]Senior Engineer, Brierley Associates, Denver, Colorado, 110 16th St., Suite 700, Denver, CO 80202
[2]Department of Civil and Environmental Engineering, Colorado School of Mines, Golden, Colorado, 1500 Illinois St., Department of Civil and Environmental Engineering, Golden 80401
[3]Chief Operating Officer, Brierley Associates, Denver, Colorado, 110 16th St., Suite 700, Denver, CO 80202
[4]Engineer, State of Colorado Division of Reclamation, Mining and Safety Colorado, 1313 Sherman St., Denver, CO
[5]Senior Mining Engineer, ZAPATA, Incorporated, Golden, Colorado, 301 Commercial Road, Suite B Golden, CO 80401
[6]Senior Civil Engineer, City of Colorado Springs, 30 S. Nevada Ave., Suite 502 P.O. Box 1575, Mail Code 520, Colorado Springs, CO 80901-1575
[7]Senior Project Manager, Anderson Consulting Engineers, Inc., 375 E. Horsetooth Road, Bldg. 5 Fort Collins, CO 80525

ABSTRACT: As part of FEMA's Digital Flood Insurance Rate Map (DFIRM) conversion project for El Paso County, Colorado, the Templeton Gap Levee (TGL) System required certification. The purpose of levee certification is to provide FEMA with documentation that areas behind the levees are protected from the 1% annual chance of exceedance flood event and may be accredited as such by FEMA on the DFIRM. Without certification, property owners behind the TGL could be required to purchase flood insurance, potentially costing the community millions of dollars annually in insurance premiums. During preliminary exploration and literature review, the engineering team found evidence of historic coal mining, predominantly room and pillar type mines with approximately 9 to 30 meters (30 to 100 feet) of cover over the coal seams under and around the TGL. Subsequent targeted drilling, geophysical surveys using DC resistivity and reverse vertical seismic profiling, and subsurface sonar and video void imaging confirmed that open mine voids exist under the levee, placing the structure at risk for future subsidence that could threaten the integrity of the TGL. The geophysical investigation: 1) provided detailed information on the subsurface characteristics beneath the TGL; 2) mapped possible mine workings beneath and adjacent to the levee; and 3) provided information for assessing risk for potential subsidence or sinkhole development associated with abandoned mines. Mitigation measures consisted of grouting the areas considered at high risk of

subsidence, using staged sanded cement grout injection into open mine voids. The Colorado Division of Reclamation, Mining and Safety finalized the mitigation plan and performed the work under the Inactive Mine Program. This paper describes the geotechnical and geophysical investigation and subsidence mitigation, as well as the agency partnership which developed to facilitate completion of this work.

INTRODUCTION

The Templeton Gap Flood Control Channel includes approximately 3.2 kilometers (2 miles) of earthen levee in the heart of the city of Colorado Springs. As part of FEMA's Digital Flood Insurance Rate Map (DFIRM) conversion project for El Paso County, Colorado, the Templeton Gap Levee (TGL) System required certification in order for it to be shown as a protective structure. The purpose of levee certification is to provide FEMA with documentation that areas behind the levees are protected from the 1% annual chance of exceedance flood event and may be accredited as such by FEMA on the DFIRM. Without certification, property owners behind the TGL could be required to purchase flood insurance, potentially costing the community millions of dollars annually in insurance premiums. During preliminary exploration and literature review, the engineering team found evidence of historic coal mining, predominantly room and pillar type mines with approximately 9 to 30 meters (30 to 100 feet) of cover over the coal seams under and around the TGL. With the discovery of the mine voids, the engineering team was concerned about possible mine subsidence affecting the integrity of the levee. In a collaborative effort, the project partners developed a plan to further evaluate the extents of the potential subsidence area, qualify the risks to the levee structure, and develop and fund a mitigation plan that would satisfy both the City of Colorado Springs and FEMA.

BACKGROUND

The Templeton Gap Flood Control Channel was constructed by the United States Army Corps of Engineers (USACE) in 1949 to provide flood protection for the central area of Colorado Springs, Colorado. The channel included approximately 3.2 kilometers (2 miles) of earthen levee and redirects surface rainwater flows from Templeton Gap drainage basin and Templeton Gap Wash away from downtown Colorado Springs. The Flood Control Channel is owned and operated by the City and extends from approximately 3.5 meters (1,000 feet) upstream of Union Blvd. downstream to Monument Creek, passing under Union Blvd., Hancock St., the Burlington Northern Santa Fe (BNSF) Railway Bridge, and Nevada Ave., as shown in Figure 1. The Flood Control Channel is approximately 3.2 kilometers (2 miles long), with elevation ranging from 1,897 to 1,867 meters (6,224 to 6,125 feet) above mean sea level (USACE, 1948). The Flood Control Channel traverses primarily between residential and commercial areas and drains approximately 22 square kilometers (8.5 square miles) northeast of downtown Colorado Springs.

The Flood Control Channel is inspected by the USACE as part of the Inspection of Completed Works Program. The 2008 inspection resulted in a "Minimally

Acceptable" rating, which indicates that the USACE concluded that "the project will function as designed and intended, but with a lesser degree of reliability than the project should provide" (USACE, 2009). The inspection noted primarily maintenance issues which the City addressed at the time. However, certification requires an evaluation of present day hydrologic, hydraulic, and geotechnical conditions to demonstrate that the area behind the levee is protected from the 1% annual chance of exceedance flood event. Often times and as was the case with TGL, rehabilitation and/or improvements are required before the levee can be certified.

Templeton Gap levee is underlain by bedrock of the Laramie, Fox Hills, and Pierre Shale Formations as well as the Louviers, Piney Creek, and Post Piney Creek Quaternary Alluvium. Aeolian and colluvium deposits cover the Fox Hills and much of the Laramie Formations in the local area. Bedrock strikes in the northwest-southeast direction and dips moderately to the northeast. Perched water tables within the bedrock are found in these formations (Lincoln DeVore, 1977). From well logs, it appears that the depth to water varies from 6 to 11.9 meters (20 to 39 feet) below ground surface. Excerpts from the original design report (USACE, 1948) indicated that groundwater was not encountered in the design-phase investigations.

Coal mining was a large industry surrounding the project site from the late 1800s to the mid-1900s. All of the coal produced in the area has been from the Upper Cretaceous Laramie Formation, which has coal bed thickness ranging from 1.5 to 3 meters (5 to 10 feet). Because of this, many abandoned mines are located within the project right-of-way, namely the Busy Bee Mine, Patterson Mine, "New" Slope Mine, Climax Mine No. 2, City No. 3 Mine, and the Danville Mine. Land subsidence has been reported across much of the region (Murray-Williams, 1983). Documents indicate that old trash and mine dumps have existed within the right-of-way of the Templeton Gap Flood Control Project, and may underlie the levee. Past reports note that mine openings have reduced the flow of water in the channel, especially east of Hancock Street to the entrance of the channel (Lincoln DeVore, 1977).

The area around the Templeton Gap Flood Control Project was relatively undeveloped until the late 1940s. Aerial photographs from 1949 indicate there was little residential development in the area. Construction of the channel is evident in aerial photos, as well as dirt roads, possibly leading to mine portals in the area. Nichols Airfield lies to the southwest of the project site. Aerial photos show that residential development construction is apparent between the years of 1953 and 1956, and steadily increases through the year 1980. From aerial photographs and historic topographical maps, Union Boulevard was constructed just west of Templeton Gap Rd. between 1975 and 1986.

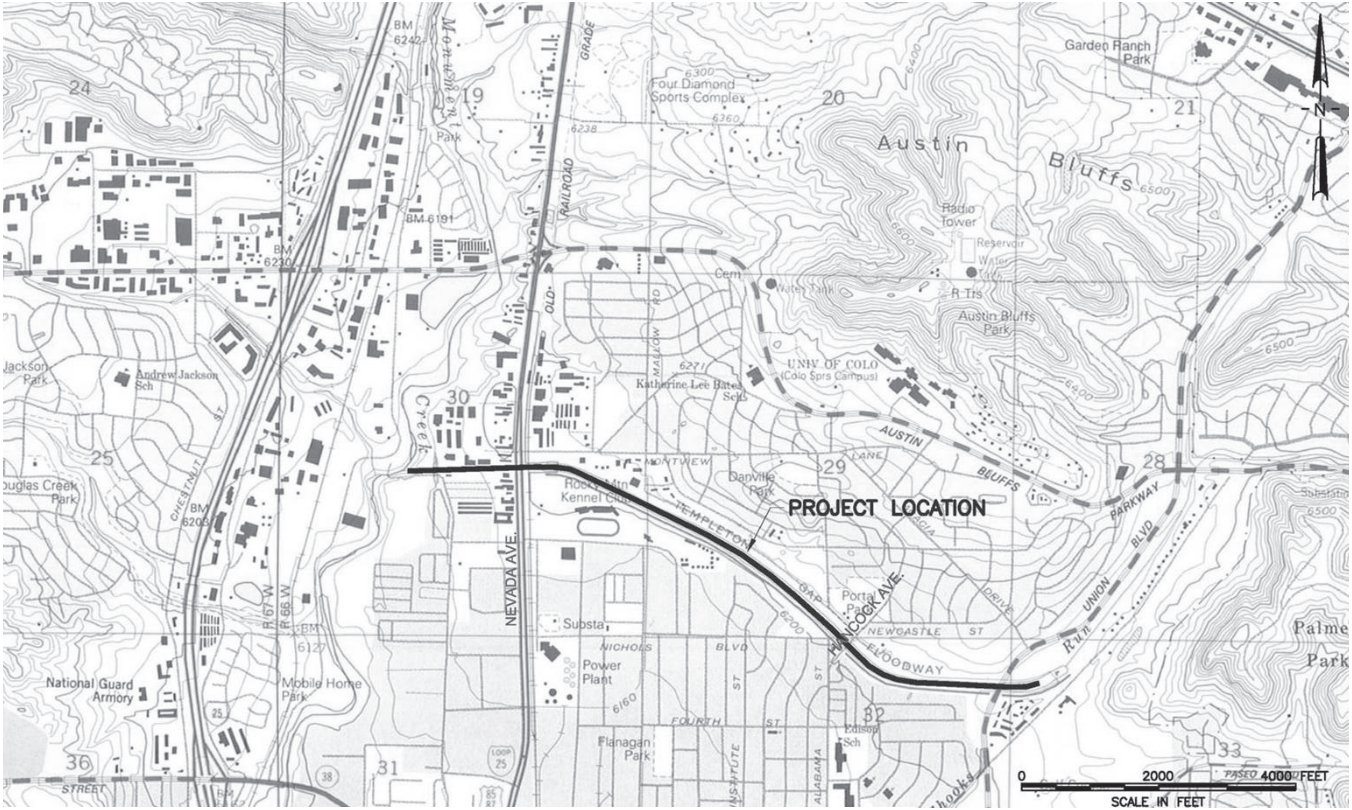

FIG 1. Project Location (Map Source: USGS Pikeview Quadrangle, CO (revised 1994)

SUBSIDENCE: INITIAL GEOTECHNICAL STUDY

Mine subsidence occurs due to underground excavation and collapse of mine workings. Eventually the collapse migrates upward and results in a depression or sinkhole at the ground surface. The severity of the subsidence depends on the size of the mine workings and the volume of the collapse, as well as the depth of the workings and the soil or rock situated between the ground surface and the mine. Templeton Gap Flood Control Channel is underlain in part by coal mine workings, which are predominantly room and pillar type mines with approximately 15 to 30 meters (50 to 100 feet) of cover over the coal seams (Figure 2) (Dames and Moore, 1985). Mine slopes/adits cross under the Flood Control Channel between Union Blvd. and Hancock St. (Amundson, 2006). The coal in the vicinity of the levee may occur in two seams, the A Seam and the B Seam, with the upper A Seam as shallow as 3 meters (10 feet) below grade. Review of published mapping of the area indicates subsidence events in the 1960's and 1970's in the area directly north of the Flood Control Channel, on Magnolia and Mariposa Streets and at Portal Park, and south of the Flood Control Channel near Union Blvd (Amuedo and Ivey, 1980).

The Flood Control Channel design identified undermined areas between the inlet and approximately Union Blvd. and included mitigation measures in the construction documents (USACE, 1948). The mitigation required in the design documents involved blasting in the mined areas to collapse the underground workings. However, the actual implementation and/or effectiveness of the mitigation measures cannot be confirmed from other project documentation.

The risk for future subsidence is rated as high hazard for uncollapsed or partially collapsed mine workings. High hazard is defined as: "Zone of highest potential for future subsidence", essentially meaning that 85 percent of future subsidence events were predicted to occur in this area with a probability of future subsidence of about 40 percent over room and pillar mining and 25 percent over extraction areas, with damage predicted to vary from very slight to very severe. (Dames and Moore, 1985).

Drilling performed as part of the initial investigation, encountered loose and/or lignitic zones below the embankment. The zones were considered to be abandoned mine workings or disposal areas, likely to include voids. The extent of these zones was not fully defined from the historic documents or from the initial investigations. The certification team considered future or continued subsidence resulting from the collapse of historic coal mine workings as a potential impact to the future freeboard, seepage, and slope stability of the levee embankment. Subsidence events are unpredictable in terms of size, extent, and rate. Room and pillar subsidence events have been occurring in the Country Club Circle area approximately 1,005 meters (3,300 feet) southeast of the TGL up through recent years, where mining methodology, depth of cover to the mined seams, and general hydrogeologic conditions are similar to those at the levee. After the initial investigation, the geotechnical lead, Lyman Henn, Inc. (now Brierley Associates, LLC) recommended additional investigation in the form of deep borings and geophysical investigation to

identify historic mine workings under the Flood Control Levee and to resolv mine maps available from CDRMS with the field conditions.

FIG 2. Mine Locations with Respect to the TGL (ZAPATA, 2010)

ADDITIONAL GEOTECHNICAL INVESTIGATION AND GEOPHYSICAL CHARACTERIZATION

Brierley contracted Zapata Incorporated, Blackhawk Division (ZAPATA) to map possible mine workings beneath and adjacent to the levee and to assess relative risk for potential subsidence or sinkhole development associated with abandoned mines in the "A" coal seam beneath the sites west and east of Union Boulevard. ZAPATA carried out the geophysical and geotechnical investigation in three phases along a 630-meter (2,067-foot) section of the waterside toe of the levee, extending from approximately 285 meters (935 feet) west of Union Blvd. to approximately 345 meters (1,132 feet) east of Union Blvd., and approximately 381 meters (1,250 feet) along the landside toe of the levee west of Union Blvd. Phases I and II identified the main areas of subsidence risk with potential to damage the levee and involved: 1) geophysical surveys using DC-Resistivity (DC-Res) and reverse vertical seismic profiling (RVSP) methods; 2) exploratory borings and sampling; 3) down hole sonar and video camera void imaging; and 4) a preliminary geotechnical site evaluation. The fieldwork for Phases I and II was carried out intermittently between September and December 2009, and January 2010. Phase III refined the areas recommended for mitigation. The findings were:

- Drilling: The 18 boreholes drilled as part of the geotechnical investigation encountered open subsurface voids or rubble zones, and solid coal associated with stable and unstable mine workings. All mine workings were flooded. Groundwater was encountered at depths ranging from 2.1 to 5.8 meters (7 to 19 feet) below ground surface (bgs).
- Sonar and Camera: The sonar and borehole camera tools provided detailed information on the existing condition and geometry of the mine workings encountered in the boreholes as shown on Figure 3.
- DC-Res characterized shallow subsurface conditions, and identified anomalies associated with Patterson mine workings (west of Union) at a depth of approximately 15 to 18 meters (50 to 60 feet) bgs. The suspected mine workings anomalies were used to identify the locations for the targeted exploratory borings as shown in Figure 4.

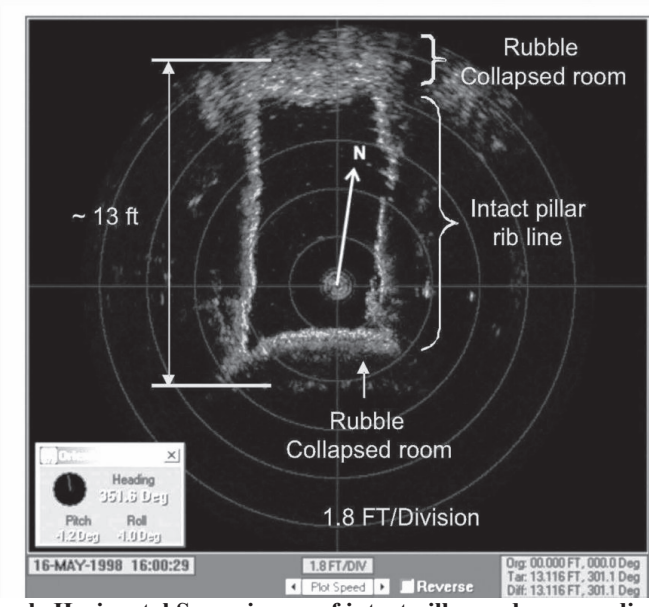

FIG 3. Example Horizontal Sonar image of intact pillar and surrounding rubble (ZAPATA, 2010)

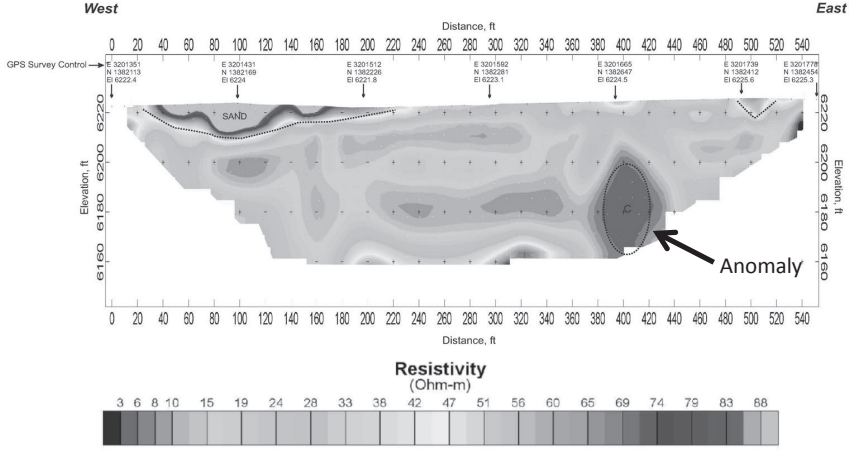

FIG 4. Plot of DC Resistivity along the Templeton Gap Floodway (ZAPATA, 2010)

- RVSP characterized subsurface conditions associated with City No. 3 mine workings (east of Union) at depth of approximately 30 meters (100 feet) bgs. The method identified void/rubble versus intact coal, providing information for subsequent boring confirmation, and geo-referencing the historical mine map with the ground surface as shown in Figure 5.

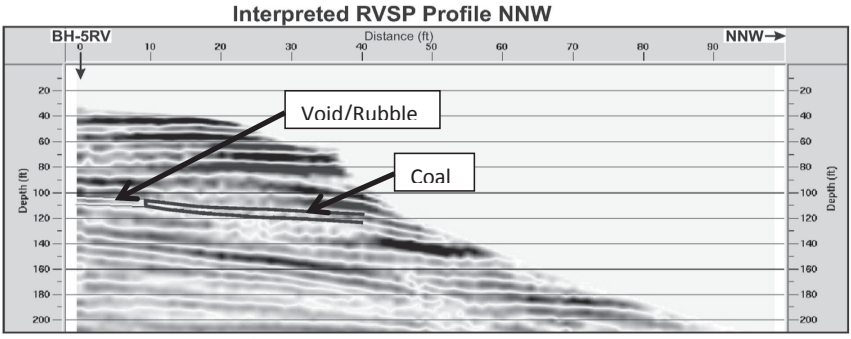

FIG 5. RVSP Profile from the Templeton Gap Floodway (ZAPATA, 2010)

The combination of data from the sources outlined above enabled ZAPATA to translate and orient the historic mine map to agree with the subsurface findings. The mine maps were determined to be fairly accurate with respect to the layout of the mine workings, but not with respect to how the layout is situated in the current surface coordinate system. The properly oriented map was a valuable tool in designing and implementing the mitigation scheme.

Based on geotechnical evaluation of the subsurface physical conditions within and above the mined A seam horizon, the team evaluated the subsidence failure mechanism and four related failure modes with various risk levels. Failure Mode 1 represents conditions of thick intact overburden/bedrock units, and stable mine workings (as seen along the waterside of the levee east of Union Blvd.), with an assigned risk level of "negligible". Failure Modes 2 and 3 represent various ground conditions ranging from relatively stable to spalling pillars, open voids with rubble, and thin (< 1.5 meters (5 feet) hard to soft immediate roof (as seen along the landside toe of the levee west of Union Blvd.), with the assignment of respective risk levels ranging from "low to moderate to high". Failure Mode 4 represents poor roof ground conditions, unstable pillars, loose coal, and voids/rubble (as seen along the waterside toe of the levee west of Union) , with an assigned risk level of "high". As the results of the subsidence failure mechanism/failure modes evaluation, ZAPATA concluded the following:

- The geophysical surveys and borehole investigations conducted in this study support the findings that past subsidence/sinkhole events are likely a function of localized mine roof failure and inflow of

unconsolidated near-surface aeolian sand, forming roughly circular sinkholes;

- The combination of shallow overburden (~ 12 meters (40 feet) along with settling of unconsolidated aeolian sand from the upper 9.1 to 12.2 meters (30 to 40 feet) into mine voids is expected to be the predominate cause of sinkhole events occurring along the waterside toe and the landside toe of the levee west of Union Blvd.; and
- The combination of thick overburden (~ 30 meters (100 feet) and the intact overlying bedrock unit along with stable mine workings will result in minimal and/or no sinkhole development east of Union Blvd.

Based on the integrated results of the multi-phase investigation combined with assessment of the risk levels, the team identified an area for mitigation work west of Union Blvd. as shown on Figure 6.

In summary, the impact to the levee was:

- East of Union Blvd.: The occurrence of future subsidence and/or sudden sinkholes to occur in this area was determined to be minimal, which led to the assignment of *risk level of negligible. This area will not require any further investigation or mitigation*;
- West of Union Blvd. waterside toe: The presence of unstable mine workings in this area presents a *high risk level* for subsidence and/or a sudden sinkhole to occur; and
- West of Union Blvd. landside toe: The risk of subsidence and/or a sudden sinkhole to occur along this area was determined to be less than the risk at the waterside toe area. The subsurface physical conditions in this area led to the assignment of respective *risk levels of low to high.*

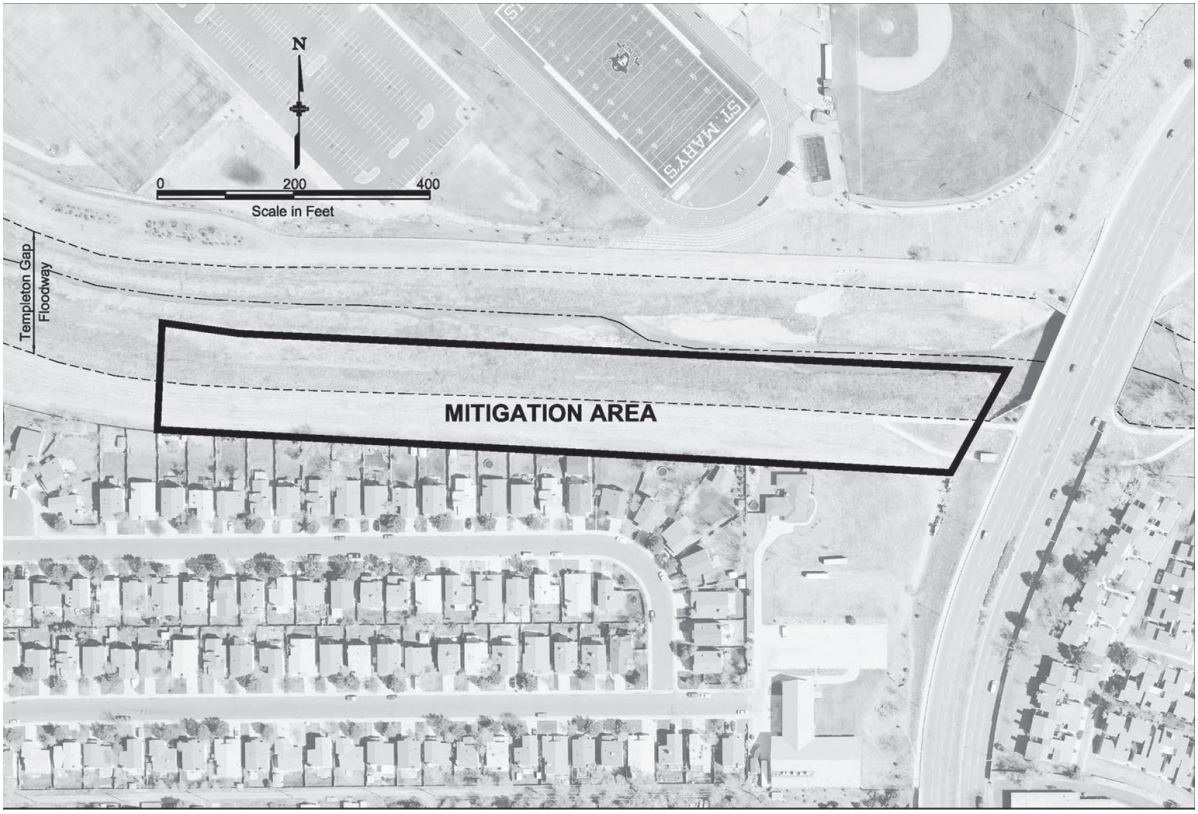

FIG 6. Selected Mitigation Area

AGENCY PARTNERING

In order to allow the FEMA certification process to move forward, the areas identified as having a high risk of future subsidence under the TGL needed to be mitigated. The City of Colorado Springs was interested in alternative methods to fund the mitigation work due to short term budgetary constraints. Brierley Associates, while researching potential mitigation options, met with the Colorado Division of Reclamation, Mining and Safety (CDRMS). The CDRMS had a current initiative for mine closure projects throughout the State of Colorado and was actively seeking appropriate projects to use its funding. Brierley Associates put the CDRMS in touch with the City and the CDRMS agreed to fund the design and construction of the mine void mitigation. Since Brierley Associates would remain the Geotechnical Engineer of Record for the FEMA levee certification, the CDRMS agreed to allow Brierley to review and provide input to the design and contract documents, as well as be present during construction.

MITIGATION DESIGN

The mitigation of the mine voids under the TGL was ultimately designed by the CDRMS; however, mitigation options were being explored by Brierley Associates and ZAPATA prior to official involvement from the CDRMS. At Country Club Circle, discussed above, mine voids were partially filled using a mixture of foam and sand. Foam, with the proper consistency has been shown be able to entrain sand allowing it to flow long distances with an angle of repose between 3 and 5 degrees. After a short period of time, a few hours to a few days depending on the chemistry of the foam, the foam dissipates leaving the mine void filled with sand.

However, unlike Country Club Circle, the mine voids under the TGL are filled with water. Case studies using foamed sand for applications under water were limited and the project team had concerns about its applicability at the TGL site. In order to test how the foamed sand would behave under water, Hayward Baker, Inc. and Cellular Concrete, Inc. agreed to perform a demonstration to test the product. A trench approximately 1 meter wide, 1.8 meters deep and 23 meters long (3 feet wide, 6 feet deep, and 75 feet long) was excavated and filled with water at Hayward Baker's property. Foamed sand was poured into the trench at the midpoint and the distance of spread was mapped using ZAPATA's sonar system to determine the surface profile of the sand. Additional profiles of the surface were taken 3 days and 11 days after initial placement. The final spread of the sand was measured between 7.3 and 8.5 meters (24 and 28 feet) with an angle of repose of 4.7 degrees.

The demonstration of the foamed sand under water was judged to be successful for areas of water-filled mine void that had uncollapsed rooms relatively free of rubble. Concerns remained whether the material would maintain its homogeneity and be able to effectively transport the sand through areas in the mine that contained a substantial amount of rubble and debris. When the CDRMS officially accepted the design responsibility, it included in the bid package line items for both cementitious grout

and foamed sand. The cementitious grout would be used if the mine voids were judged to contain rubble, and the foamed sand would be used if the mine rooms were judged to be relatively open.

The final CDRMS bid schedule contained 805 linear meters (2,640 linear feet) of borehole for grout injection, 3211 (cubic meters (4,200 cubic yards) of compaction grout, 268 linear meters (880 linear feet) of borehole for foamed sand injections, and 765 cubic meters (1,000 cubic yards) of foamed sand. Angled boreholes would be drilled on both the waterside and landside of the TGL to inject grout and foamed sand under and adjacent to the TGL.

MITIGATION IMPLEMENTATION

The void filling construction work was awarded to Nicholson Construction. The void filling program consisted of drilling a series of holes on the waterside and landside of the TGL over a distance that spanned approximately 366 meters (1,200 feet) west of the western edge of Union Boulevard and injecting the holes with grout until a prescribed pressure was reached. The majority of the void filling program started on August 8th, 2011 and continued through December 13th 2011. 70 holes were drilled on the waterside and 62 holes were drilled on the landside of the levee. On March 22, 2012 Nicholson grouted an additional two holes on the waterside of the levee to finish the void filling program. In total the void filling program utilized 1,863 cubic meters (2,436.9 cubic yards) of grout to stabilize the voids that were a result of the mining activities; 1,589.7 cubic meters (2079.2 cubic yards) were used on the landside and 273.5 cubic meters (357.7 cubic yards) were used on the waterside. The large discrepancy between the grout take on the landside versus the waterside was most likely due the fact that the landside work was completed first and filled the majority of the subsurface voids.

Foamed sand was not used in the actual mitigation. According to the CDRMS, based on the drilling of the grout holes, the mine voids appeared to contain rubble such that the foamed sand may not have adequately filled the voids.

During the construction work, a total of seven sinkholes occurred on or near the TGL. The cause of the sinkholes is not completely understood, but appears to be a result of the drilling and/or grout injection work. One potential cause discussed amongst the team involves perforation of the mine roof with the grout injection drill holes. The contractor drilled multiple injection holes before returning to inject grout. It is plausible that the open injection holes created a conduit for loose sand above to flow into them before grout was injected to fill the void.

All seven sinkholes occurred in the vicinity of the active work. Six of the sink holes were on the landside of the levee near or south of the levee toe and one sinkhole occurred on the waterside levee slope. Each sinkhole was filled by drilling into the sinkhole and injecting grout into the subsurface to fill voids and stop the sinkhole from expanding.

CONCLUSION

The discovery, characterization, and mitigation of the coal mine voids under the Templeton Gap Levee are examples of thorough implementation of multi-discipline engineering practice and out-of-the-box problem solving. Characterization of past mine workings is commonly a difficult undertaking. Existing mine maps, if they even exist, are often incomplete and difficult to accurately position spatially. Through research, geotechnical, and geophysical techniques, the project team was able to determine: 1) subsidence presented a risk to the levee, 2) the location of high risk areas, and 3) a method to mitigate that risk. Project challenges including finding a funding source for the mitigation work and evaluating alternative options for mitigating the voids led to collaboration between numerous agencies. The successful conclusion to the work is a testament to the willingness of all the project participants to work together to solve a shared and unique problem.

REFERENCES

Amuedo and Ivey, (1981) Inactive Mine Reclamation Program; Extent of Mining Map Showing Associate Hazards and Subsidence Features, Pikeview Quad.

Amundson, Al, (2006), Report of Abandoned Coal Mine Subsidence Occurrences in Colorado, Colorado Division of Minerals and Geology, Inactive Mine Program.

Dames and Moore (1985), Volume II, Excerpts from Final Report, Colorado Springs Subsidence Investigation, completed for the Colorado Division of Mined Land Reclamation.

Murray-Williams L., Turney, J.E, (1983) "Colorado Front Range Inactive Coal Mine Data and Subsidence Information, El Paso County, Colorado" Colorado Geologic Survey.

Lincoln DeVore (1977), "Engineering Study and the Revision of the North Shook's Run – Templeton Gap Drainage Basin".

United States Army Corp of Engineers letter to Dan Bare, (January 29, 2009)

United States Army Corp of Engineers (1948), Excerpts from "Definite Project Report on Templeton Gap Floodway at Colorado Springs, Colorado, Appendices II, III, and VI".

Zapata Incorporated, Blackhawk Division, (2010). "Geophysical-Geotechnical Investigation to Map Coal Mine Workings Beneath a Templeton Gap Floodway Levee in Colorado Springs, Colorado," Prepared for Lyman Henn, a division of Brierley Associates, LLC.

The Misbehavior of the Laramie Formation Claystones

Roy H. Spitzer[1], P.G. and Don W. Deere[2], P.E.

[1]Principal, Deere & Ault Consultants, Inc., 600 South Airport Road, Suite A-205, Longmont, CO 80503; roy.spitzer@deereault.com
[2]Chairman, Deere & Ault Consultants, Inc., 600 South Airport Road, Suite A-205, Longmont, CO 80503; don.deere@deereault.com

ABSTRACT: The Laramie Formation is the near-surface bedrock over much of the northern Front Range of Colorado. The Late Cretaceous bedrock is characterized by complexly interbedded sandstones and claystones with numerous vertical and lateral facies changes. The Lower Laramie also has coal beds that were mined in the areas near Marshall, Louisville, Lafayette, and the Tri-Towns. However, the main Laramie Formation lithology is claystones.

In general, claystones are in the "gray" area between soil and rock, and can be described as highly over-consolidated, very stiff, fissured, clays. Claystones generally have the following properties:

1. Low strength and are prone to landsliding
2. Are compressible under high structure loads
3. Are expansive and swell and shrink with changes in moisture contents
4. Are prone to slaking and break down readily when exposed to air and water
5. Are erodible when exposed to water

The Laramie claystones have caused numerous problems for civil structures and much of the construction in the northern Front Range area encounters this formation. The behavior, or rather the misbehavior, of the Laramie claystones largely results from its mineralogy. Laramie claystones are a smectite-rich (bentonite) mixed layer clay of illite/smectite with lesser amounts of kaolinite and illite. The Laramie claystones are a very low strength bedrock with low to very high swell potential. Plasticity Indices typically range from mid-20 percent to 50 percent and higher.

The stress history of the claystones also has contributed to the properties and behavior of the Laramie claystones.

This paper presents short examples and case histories which illustrate the properties of the Laramie claystones as encountered in civil projects.

INTRODUCTION

The Laramie Formation is the near surface bedrock beneath much of the northern metropolitan area that lies east of the Colorado Front Range. Figure 1 shows the general extent of the Laramie Formation in the Denver Structural Basin. In the southern part of the outlined area, the Laramie beds lie beneath younger bedrock strata. In the northwestern part of the outlined area, in parts of Boulder, Broomfield, Adams, and Weld Counties, the Laramie Formation beds subcrop are typically blanketed only by surficial soils. Therefore, the Laramie bedrock is encountered on most construction projects in this area and is the foundation for most civil structures. Over the past 30 years, there has been extensive growth and development on the northern Front Range area.

The Laramie Formation is Late Cretaceous in age, deposited approximately 70 million years before present (BP). The Laramie Formation beds were deposited in a non-marine alluvial plain/coastal plain setting along the western margin of the Western Interior Seaway (Roberts, 2007). The beds range from 107 to 304 meters (250 to 1,000 feet) thick and consist mainly of sandstones, siltstones, claystones, and carbonaceous shales or lignite beds. The Lower Laramie (the bottom approximately 91 meters (300 feet) includes seven coal beds that were mined in the areas near Lafayette, Louisville, Marshall, and the Tri-Towns (Dacono, Fredrick and Firestone) in the late 1800s, continuing up to approximately 1968.

Claystone is the dominant bedrock lithology, especially in the Upper Laramie Formation. The various lithologies in the Laramie Formation are complexly interbedded with numerous lateral and vertical facies changes.

The claystones are the focus of this paper. The claystones can be described as being in the gray area between soils and rock. They are essentially a bedrock of compaction rather than cementation, and are highly over-consolidated, very stiff to hard (soils descriptions), and can be termed “stiff, fissured clays”. The Laramie claystones have the following general behaviors:

1. Very low strength and are prone to landsliding
2. Are compressible under high structural loads
3. Expansive, swelling and shrinking with changes in moisture content
4. Slake and breakdown readily when exposed to air and water
5. Erode easily when exposed to water flows

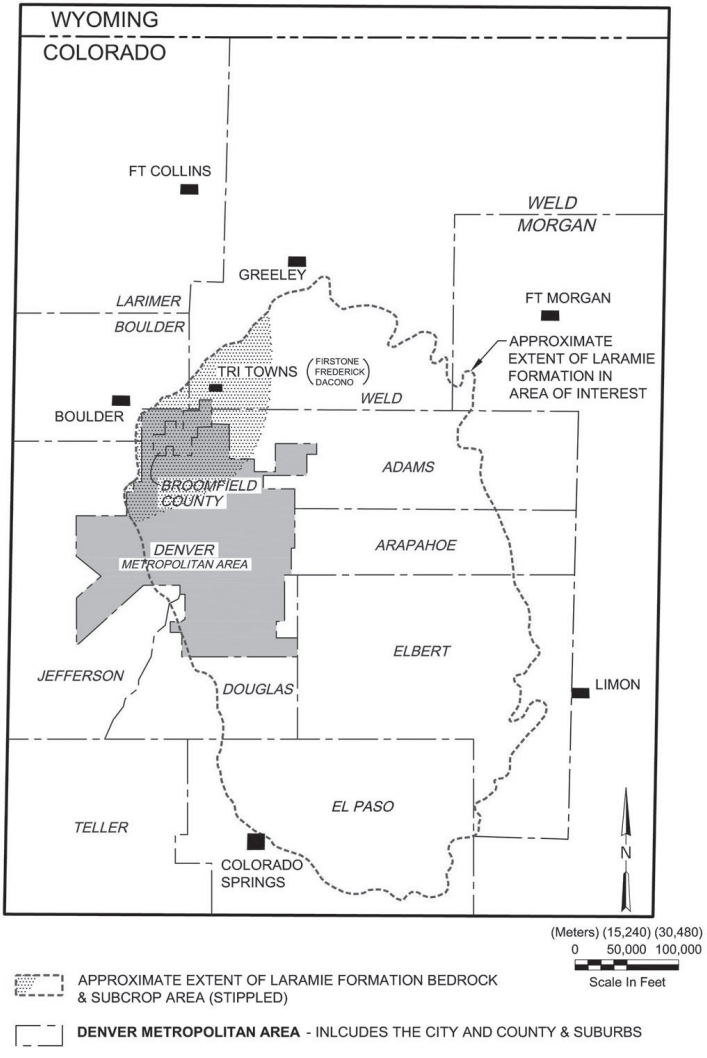

FIG. 1. Approximate extent of Laramie Formation bedrock

Because of these behaviors, the Laramie claystones have caused numerous problems for civil structures, beginning with the earliest development and construction on the Laramie claystone. It is because of the claystone properties and construction problems associated with the claystones that this paper is entitled, "*The Misbehaviors of the Laramie Formation Claystones*."

PHYSICAL AND ENGINEERING PROPERTIES OF THE LARAMIE CLAYSTONE

Primary Properties

There have been many geotechnical investigations that have encountered the Laramie claystones and documented some of the localized properties. However, most investigations penetrate only 1.5 to 3 meters (5 to 10 feet) of the bedrock strata. The investigations for the Standley Lake new outlet works (Spitzer and Deere, 2003) (CH2M Hill, 2001) provide a pretty fair inventory and range of laboratory index test results for the claystones encountered in an approximately 30-meter (100-foot) thick section of the Laramie bedrock strata. The index properties for the Laramie claystones from this site are summarized on Table 1.

Table 1. Laramie Claystone Index Properties

Test	Number of Tests	Minimum	Maximum	Average
Moisture Content	32	9.1%	17.9%	13%
Dry Density	32	1.74 g/cc (108.8 pcf)	2.12 g/cc (132.4 pcf)	1.94 g/cc (120.8 pcf)
Gradation, % Fines (silt and clay), -200 Sieve	31	57%	100%	92%
Hydrometer, % Clay (-2 micron)	4	43%	63%	50%
Liquid Limit	31	31%	67%	52%
Plastic Limit	36	12%	39%	19%
Plasticity Index	36	16%	44%	33%
Swell 4,890 kg/m^2 (1,000 lbs/ft^2)	17	0.1%	7.5%	2.1%
Unconfined Compressive Strength	29	0.18 MPa (25 psi)	6.33 MPa (893 psi)	1.42 MPa (200 psi)

The bedrock is typically moist, but with natural water contents significantly below the plastic limit. The bedrock dry densities typically range between about 1.76 to 1.92 g/cc (110 and 120 pcf). Though some zones can be quite sandy, the claystones are made up mainly of silt and clay sized materials with about 50 percent being clay. The Atterberg limits indicate the material is classified as a high plasticity clay (CH) in accordance with the Unified Soils Classification System. The swell/consolidation test results indicate very low to very high swell potential. The compressive strength tests indicate the claystones are a very low strength rock.

Our experience indicates these test results are generally typical for the Laramie claystones. In some locations, however, the claystones have higher swell potential with swell test results in the range of 8 to 12 percent. Some sites have extremely high swell pressures, estimated to be as high as 20,500 kg/m^2 (100,000 psf).

Six Laramie claystone samples from the Standley Lake Project were tested for slake durability. The test results gave slake durability indices ranging from 0.09 to 48.6 percent; but of the six samples, four were less than 1 percent which means the samples totally disintegrated on exposure to wetting and drying cycles. This results in the claystones being very erodible when exposed to air and water.

Two Laramie claystone samples from the Standley Lake project were tested by x-ray diffraction for clay mineralogy. The major clay component was identified as a smectite rich mixed layer clay of illite/smectite. Lesser clay components included illite and kaolinite. Smectite is a general term for moisture sensitive clay minerals. These are minerals that expand when wetted and shrink when dried. Smectites include sodium montmorillonite, which is commercially known as bentonite which is used for drilling mud, slurry wall construction, and pond liners; the first two because of its thixotropic behavior when mixed in a slurry and the last because of its low permeability.

Stress History

Laboratory test results demonstrate that the Laramie claystones are very low strength, fine grained bedrock composed in a large part of moisture sensitive clay minerals with significant swell potential when wetted. The composition of the Laramie claystones, however, accounts only for part of the behavior and properties of the claystone. The second major factor is the stress history of the Laramie beds. The Laramie claystones have been highly over-consolidated over a long period of geologic time. The claystones were consolidated under overburden pressures which were much in excess of those present today. Part of this compression of soils is recoverable. "*The recoverable portion increases with the content of the clay particles, and in plastic clays it forms an appreciable part of the total compression*" (Bjerrum, 1967). This is because of the platey structure and elastic nature of the clay minerals.

During compression over geologic time, diagenetic bonds were created between the soil particles. Although these bonds are not well understood with clay minerals, they probably involve bonds of a molecular nature. So without further compression or consolidation, the diagenetic bonds resulted in the Laramie claystones becoming more brittle and stronger. Part of the elastic compression thus becomes "locked in" the claystones by the diagenetic bonds like a compressed spring.

Removal of the overburden pressure by subsequent erosion has released some of the elastic compression from the beds. Differential rebound in the vertical direction with the unloading resulted in slickensides and fissures, and joints developing in the bedrock. In the weathered zones, breakdown of the diagenetic bonds resulted in a lower strength zone, a few centimeters to a meter (a feet inches to 3 feet) thick, generally parallel to the bedrock surface. However, the horizontal stresses induced by the over-consolidation of the claystone remains "locked in" and has not been relieved by the vertical unloading. Unless tectonic stresses are expected to be present, horizontal stresses are usually estimated to be approximately one-half of the vertical

stresses. However, because the horizontal stresses from the over-consolidation have not been relieved by the vertical unloading, the horizontal stresses in over-consolidated claystones can be significantly higher. For underground structures, this means there can be relatively high horizontal stresses around underground openings.

Stress history of claystones also comes into play with the shear strength of claystones due to the breakdown of the diagenetic bonds. The diagenetic bonds that have developed over geologic time as a result of the over-consolidation created a more brittle, higher strength material. Upon unloading, the diagenetic bonds breakdown over a relatively short period of time in comparison to geologic time. This is an important factor, especially beneath a structure that imposes shear loading like a dam, or in natural slopes or excavated slopes like road cuts.

Our experience with the Laramie claystones indicates the peak unweathered strength will have an effective friction angle (Φ') of approximately 21 degrees and effective cohesion (C') of approximately 102.4 to 204.8 kg/m^2 (500 to 1,000 psf). The high cohesion is mainly a result of the diagenetic bonds. The breakdown of diagenetic bonds results in the reduction of strength to the "fully softened" strength having an effective cohesion for design proposes assumed to be equal to 0. The effective friction angle remains approximately 21 degrees for the fully softened case.

If there is shear movement through the claystones on a discrete surface, the clay minerals become aligned, forming a surface with severely reduced strength that is termed "residual strength". For the Laramie claystones, estimates of residual strength are approximately C' = 0 and Φ' = 13 to 15 degrees (Dewoolkar and Huzjak, 2005; Deere, 2012).

These estimated strengths for the Laramie claystone are summarized in Table 2.

Table 2. Estimated Laramie Bedrock Strength Parameters

Strength Condition	Effective Cohesion (C')	Effective Friction (Φ')
Peak	102.4 to 204.8 kg/m^2 500 - 1,000 psf	21°
Fully Softened	0	21°
Residual	0	13 - 15°

CONSTRUCTION IMPACTS AND CASE HISTORIES

The Laramie claystones have impacted all types of construction.

Structure Foundations and Slabs

The most common impact of the Laramie claystones is probably due to the swelling properties of the claystones when wetted. As development occurs in an area, landscaping, irrigation and paved areas that concentrate runoff and intercept

evapotranspiration invariably result in increases of the moisture content in the subgrade soils and bedrock. The resulting swelling of the claystones results in structural damage to buildings, slabs, pavements, and utilities. Over the years there have been multiple approaches to attempt to mitigate the impacts swelling properties of the Laramie beds on structures. The most common approach is to found buildings on drilled piers using grade beams to concentrate the building loads. The drilled piers extend to a depth in the claystones that is presumed to be below the depth of seasonal moisture change. The building loads are concentrated on the piers by the grade beams in an attempt to resist the swell pressures. Void form is used to prevent swelling of the soils from acting on the grade beams.

Building floor slabs present a more difficult problem. Since they cover broad areas and are lightly loaded, differential swelling of the bedrock often results in cracking of the slabs. Approaches to mitigate the problem with floor slabs has included over-excavation and replacement with low permeability non-swelling soils, isolating the floor slabs from walls and utilities, and letting the slab "float" with respect to the rest of the building; and constructing structural floors supported on piers and grade beams with a void space between the soils and slabs. Post tensioned "waffle" slabs have also been used. All of these approaches have met with varying degrees of success, but still the swelling Laramie claystones have caused severe structural damage, especially to lightly loaded residential structures or structures with large slab areas, like schools.

Vista Ridge is a relatively new subdivision in the Laramie Formation in the town of Erie, north of State Highway 7. Some of the residential damage due to the swelling soils has been so severe that extensive remedial work has been required. Figure 2 below shows a Bobcat excavating beneath the garage floor slab inside a residence. Several other residences in the immediate area were also receiving similar extensive remedial work. Figure 3 shows the excavation of claystones around the foundation of another house. We have no details on the original construction or mitigation designs. However, the extensive remedial work clearly illustrates the impacts of the swelling properties of the Laramie claystones.

FIG. 2. Vista Ridge, Erie, Colorado. Bobcat excavating under garage slab

FIG. 3. Vista Ridge, Erie, Colorado. Excavating around house foundation (note the ladder)

Builders in another nearby residential development in the city of Broomfield have taken a different approach to residential construction on the Laramie bedrock. Rather than relying on a structural system or design to mitigate the effects of the swelling bedrock, this approach seeks to modify the bedrock behavior. In the Wildgrass and Silverleaf Subdivisions, the entire development area for each lot is being excavated to depths of approximately 6 meters (20 feet). The excavated bedrock is then moisture conditioned to near optimum Proctor moisture content and recompacted on-site. Figure 4 shows the extent of bedrock excavation on one of the sites and the bedrock strata excavated.

FIG. 4. Silverleaf Subdivision next to the Wildgrass Subdivision, Broomfield, Colorado. Deep excavation of Laramie claystones with sandstone beds and lenses

Each building envelop is then investigated by an exploratory boring to evaluate the remaining swell potential. Conceptually, the over-excavation, moisture conditioning and recompaction should act to reduce the swelling potential of the bedrock in three ways. First, compacting the bedrock at a lower density than the intact bedrock should reduce the swell potential by somewhat decompressing the elastic "spring" of the over-consolidated clay particles. Second, increasing the moisture content with the moisture conditioning results in swelling of the clays, reducing the remaining amount of swelling that can be expected after placement. And third, excavation and recompaction of the claystone disrupts the parallel platelet structure of the claystones potentially further reducing the swelling potential.

The effectiveness of this "behavior modification" approach to dealing with the Laramie claystones is still questionable, even though the concepts appear reasonable. Review of the post-placement soil testing indicates moisture contents ranging from 7 to 21 percent, dry densities ranging from 1.63 to 2.0 gm/cc (102 to 125 pcf), and swells ranging from 0 to 6 percent (Wildgrass Subdivision Filing No. 3). These test results appear to indicate quite variable moisture conditions, densities, and swell potential. This causes concern that wetting of the recompacted bedrock during the life of the structures could result in significant differential swelling and movements of slabs or foundation elements.

Slope Stability and Dams

The Laramie claystone is a weak slope former, and shallow landslides are evident in the natural slopes wherever there is significant topographic relief. For instance, numerous landslides can be seen in the area south of Superior. Slides also occur in road cuts in this area. The road cuts were typically stable for a period time after being excavated only to fail at a later date in shallow slumps. Excavation of road cuts relieves the horizontal stresses from over-consolidation, resulting in subtle strains and eventual breakdown of the diagenetic bonds. The claystone strength is reduced from peak to fully softened, and finally residual strength along the discrete landslide surfaces. Often there is water present in the claystones carried by thin lignite beds and stringers, which hastens the breakdown of the bonds and the reduction in strength.

In Louisville an overlot grading plan developed for a residential development resulted in relatively flat 4:1 (horizontal to vertical) Laramie claystone cut slopes made in accordance with the City's development standards. Approximately three months after the cuts were made, three shallow landslides developed across the slope. Test pits found seepage in the slope along some thin lignite beds. When drainage failed to stabilize the slopes, toe buttresses were constructed. These failures were probably caused by breakdown of the diagenetic bonds and reduction of the claystone strength from peak to fully softened.

Figure 5 shows a landslide that occurred in 2011 on a relatively gentle claystone slope above Colorado Highway 128 at Interlocken in Broomfield. The top of the slope was surcharge loaded with a very high reinforced earth (MSE) retaining wall

constructed by the FAA to allow extension of the runway at the Rocky Mountain Metropolitan Airport. Under the added load, the slope failed with the toe of the landslide bulging the highway payment upward as shown on Figure 6. While we are not aware of the design strength parameters used for this project, it is our opinion that the fully softened condition was probably present in the slope bedrock at the time of failure.

FIG. 5. Rocky Mountain Metropolitan Airport landslide

FIG. 6. Toe of Rocky Mountain Airport landslide in State Highway 128

Dam embankment foundation failures have also occurred on the shallow Laramie claystone beds. Great Western Dam, approximately 15.2 meters (50 feet) high, just north of Standley Lake, experienced a foundation failure in 1958. The landslide was

characterized as a deep downstream slide (Sherard, et.al., 1963). The landslide included the entire dam crest extending to the upstream slope. The slide parted the low level outlet conduit eliminating the ability to draw down the reservoir with the gravity outlet works. Figure 7 shows the slope failure on the dam. The dam was eventually stabilized with a downstream berm and the water level was safely lowered using a siphon. Analysis of the dam embankment in the 1990s using Laramie claystone residual strengths indicated that the embankment was still only marginally stable and an additional berm was added in 1995 to enhance the stability.

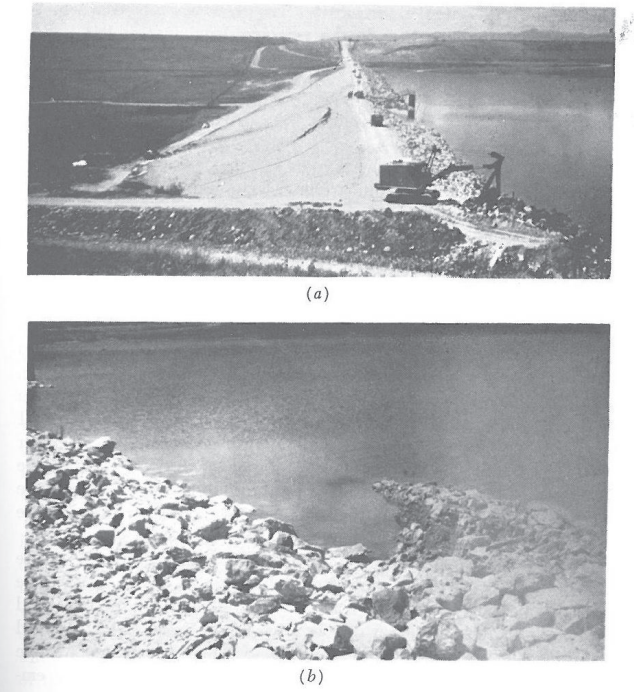

(*a*)

(*b*)

FIG. 7. Great Western Dam slope failure extending to upstream slope

A more recent slope failure in the Laramie claystones occurred at the Woman Creek Reservoir, also on the Laramie Formation bedrock near Standley Lake. Woman Creek Reservoir is a water quality reservoir with three separate long and narrow internal cells. The cells were excavated in the Laramie claystones, and the dikes separating the cells were constructed in part by excavating 3:1 (horizontal to vertical) slopes in the Laramie claystones and capping the bedrock with compacted claystone fill.

The reservoir was completed in 1996 and went into operation. Typically, the reservoir does not store water over long periods of time, but is used to detain water from Woman Creek and runoff from Rocky Flats. The detained water is pumped out to Woman Creek after sediments are allowed to settle. The water level in the cells

fluctuates based on runoff and the reservoir management practices. However, the stored water levels are typically low.

In the late fall of 2011, a large slump occurred in one of the internal dikes. The location of the failure is shown on Figure 8. At the location of the failure, most of the separation dike consists mainly of undisturbed Laramie claystones. Figure 9 shows the landslide.

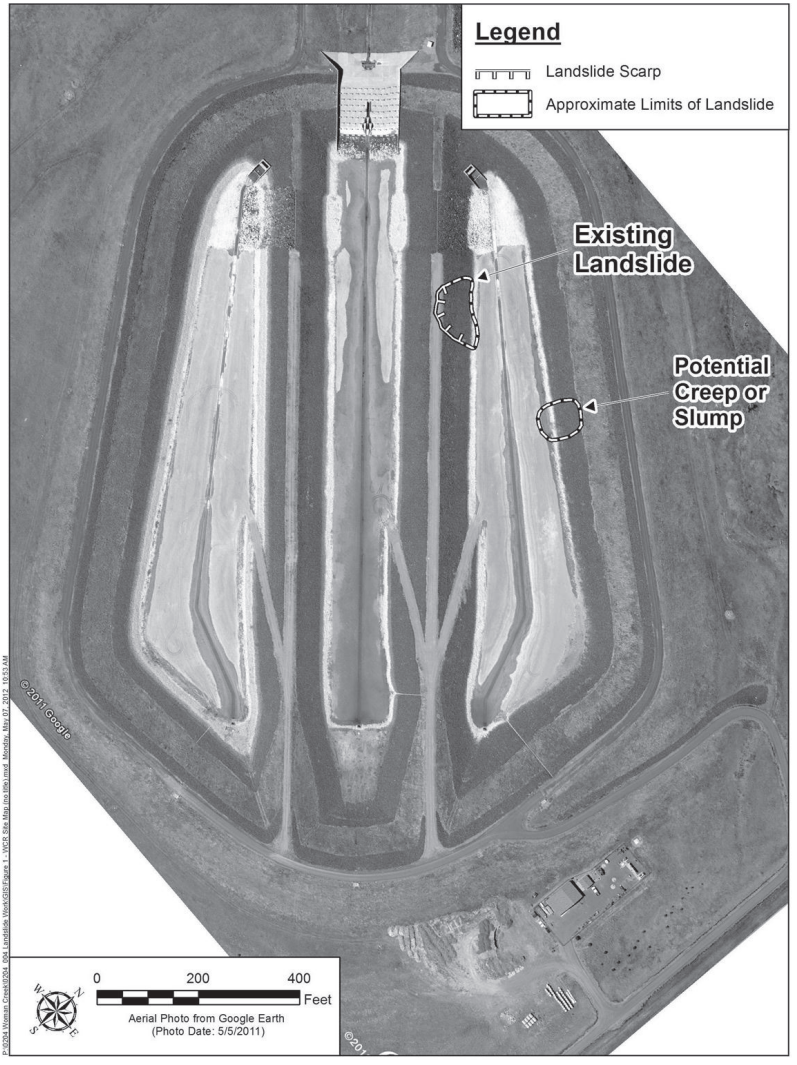

FIG. 8. Woman Creek Reservoir site map showing location of landslide

FIG. 9. Laramie claystone landslide on internal dike

The original stability analysis for the design used an effective friction angle of 21 degrees and an effective cohesion of 123 kg/m^2 (600 psf). Back calculation of the failed slope with the factor of safety set equal to 1, using the groundwater conditions from a nearby monitoring well, gave an effective friction angle of 21 degrees with an effective cohesion equal to zero.

This appears to be a case where upon excavation and relief of confining stresses on both the vertical and horizontal directions, the diagenetic bonds within the claystones began to breakdown, eventually approaching the fully softened conditions, which resulted in the slope failure 15 years following construction.

Underground Construction

The Standley lake Dam Rehabilitation Project included construction of a downstream outlet tunnel from the valve shaft to a downstream outlet conduit. The outlet tunnel was constructed 3.5 meters in diameter (11.5 feet) and 292 meters (962 feet) long through the Laramie claystones (Deere, et.al., 2005). The tunnel was mechanically excavated using a roadheader tunneling machine. The tunnel was supported by 10 centimeters (4 inches) of steel fiber reinforced shotcrete. Near the portal and in more problematic ground, the support included lattice girders and 15 centimeters (6 inches) of steel fiber reinforced shotcrete.

Figure 10 shows the bare claystones with a slickenside and overbreak in the crown over the roadheader.

FIG. 10. Standley Lake Tunnel (note slickenside and overbreak of claystone in crown

During the excavation and support sequence, it was found that the key to reducing slaking of the claystones and resulting overbreak and raveling was to reduce the unsupported time to approximately three to four hours between excavation and placement of the initial shotcrete support. When the claystones were left unsupported for longer periods, the amount of overbreak on slickensided joints and the raveling increased dramatically.

Convergence of the tunnel opening was regularly measured during construction using tape extensometers. The primary displacement that was measured occurred horizontally as the sides of the tunnel converged at a relatively constant rate of approximately 2.5 millimeters (0.1 inches) per day. This convergence is a result of the over-consolidation of the claystones. The vertical stresses have been largely relieved, but the horizontal stresses have been "locked in" until the tunnel was driven. The convergence stopped as soon as the invert shotcrete was placed, completing the full ring of support.

Although the tunnel was driven immediately downstream of a full reservoir, the water inflows were limited to minor weeps and moist spots on joints and fissures. When the tunnel ventilation was on, the water evaporated as fast as it seeped in.

CONCLUSIONS

The behavior, or rather the misbehavior, of the Laramie claystones when encountered on civil construction projects are several. The physical and engineering properties of the claystones are a result not only of the mineral composition of the claystones, but also the bedrock geologic stress history. The properties are not constant with time. Changing the loading or state of stress and exposure of the claystones to weathering can result in a significant loss of effective shear strength from peak strength to fully softened strength, which often results in slope failures. Many of the slope failures on the Laramie claystones can probably be attributed to this time dependent loss of strength. Peak Laramie claystone strengths should not be used for project design.

The swelling of the Laramie claystones results in significant foundation problems for structures. Numerous approaches have been taken to mitigating the swelling properties of the Laramie claystones. None of the approaches has been completely successful and damages to buildings due to swelling bedrock continues to be a problem.

When exposed in foundations or in underground openings, the claystones need to be protected from exposure to air and water or they will rapidly slake and begin to breakdown in a period of a few hours. In underground openings, the high horizontal stresses that remain in the Laramie claystones from over-consolidation need to be considered in both design and construction.

REFERENCES

Bjerrum, L., (1967). "Progressive Failure in Slopes of Overconsolidated Plastic Clay and Clay Shales." *3rd Terzaghi Lecture Proceedings of the American Society of Civil Engineers*, Vol. 93, No. SM5, September.

CH2M Hill. (2001). "Geotechnical Baseline Report for the Construction of the Standley Lake Dam Improvement Project." *Unpublished report*.

Deere, D.W. (2012). "The 2011 Landslide at Woman Creek Reservoir." *Unpublished report.*

Deere, D.W., Goss, C.M. and Church G.G. (2005). "Roadheader Tunneling and Microtunneling in Low Strength Claystone at Standley Lake, Colorado." *Rapid Excavation and Tunneling Conference Proceedings*, Chapter 97.

Dewoolkar, M.M. and R.G. Huzjak. (2005). "Drained Residual Shear Strength of Some Claystones from Front Range Colorado." *Journal of Geotechnical and Geoenvironmental Engineering*, Paper No. GT-03-23577.

Roberts, S.B. (2007). "Coal in the Front Range Urban Corridor - An Overview of Coal Geology, Coal Production, and Coal Bed Methane Potential in Selected Areas of the Denver, Basin, Colorado," and "Potential Effects of Historical Coal Mining on Development and Land-Use Planning." *Chapter 3 of Petroleum Systems and*

Assessment of Underground Oil and Gas in the Denver Basin Province, Colorado, Kansas, Nebraska, South Dakota, and Wyoming, USGS Province 39, USGS Digital Data Series DDS-69-P.

Sherard, J.L., Woodward, R.J., Gizienski, S.F., and Clevenger, W.A. (1963). *Earth and Earth-Rock Dams*, John Wiley & Sons.

Spitzer, R.H. and Deere, D.W. (2003). "Investigation and Design for Replacement of the Outlet Works, Standley Lake Dam and Reservoir, Jefferson County, Colorado." *Engineering Geology in Colorado, Contributions, Trends and Case Histories*. Association of Engineering Geologist Specialty Publication No. 15.

Stark, T.,D. and Hisham, T. (1994). "Slope Stability Analysis in Stiff Fissured Clays." *Journal of Geotechnical and Geoenvironmental Engineering*, Vol. 123, No. 4, April 1997.

Wildgrass Subdivision Filing No. 2, Geotechnical Testing Summary obtained from the City and County of Broomfield Public Records.

Effective Use of Underdrain System in Construction on Expansive Subsoils

Narender Kumar, P.E., M.ASCE, FACEC

CEO, Kumar & Associates, Inc., Denver, Colorado; nkumar@kumarusa.com

ABSTRACT: This paper examines the practice of geotechnical engineers and design and construction professionals of construction on expansive soil and bedrock in the Colorado Front Range. A common practice is to support structures on deep foundation, generally drilled piers and place slab on grade. Over-excavation of expansive subsoils below the structures is recommended to mitigate the effect of swelling subsoils. Over-excavation creates a bathtub which stores water and results in creation of a perched groundwater condition.

This paper contends that the perched groundwater is more from the interruption of historic flow through the upper bedrock permeable zones than the factors commonly associated with this phenomenon, such as inadequate grading, use of water subsequent to the development, etc. The measurements conducted in the sump pits and discharge from the pumps indicates steady flow of water during all times of the year. This condition should be recognized and steps taken to drain the water by use of properly designed underdrain system.

Continuing movement and distress is experienced in many existing structures constructed on expansive subsoils. Deep underdrain system (DUS) is effective in intercepting the flow of groundwater and preventing the development of perched groundwater which provides moisture to the underlying expansive subsoils and causes continued movement and distress. The paper presents cases where the use of deep underdrain system has prevented the continuing movement and distress of the existing structures. Measurements conducted of groundwater flow in the sump pits confirm the effectiveness of the system.

The geology and hydrogeology of Denver Formation indicates flow of groundwater through the permeable zones in the upper portion of bedrock. The author contends that the flow pattern in the upper bedrock has significant effect in wetting of the subsoils and should be recognized and considered in evaluation of the depth of wetting in this area.

INTRODUCTION

Structures built on expansive soils along the Front Range have experienced hundreds of millions of dollars' worth of damage over the years. Geotechnical engineers and design and construction professionals practicing in the area have adapted by supporting the structures on deep foundation system primarily using piers drilled in bedrock, placing the bottom of the piers at depths unaffected by change in the moisture content or in other words, below the anticipated depth of wetting or active zone.

Procedure to prevent slab movements include construction of structural floors above a void space supported by drilled piers (primarily in residential construction). Structural floor slabs are relatively expensive and rarely used for commercial projects. The alternative is to place the slabs on stabilized fill by over-excavating the subgrade and replacing all or part of the over-excavated ground with moisture conditioned and/or structural fill. Slip joints are recommended for slab support systems to accommodate movement of the slabs.

Over the years, deeper over-excavations are being recommended primarily as a result of litigation and depth of wetting studies. Some firms are routinely recommending 3 to 6 meters (10 to 20 feet) of over-excavation depending on the in-situ swell potential. This is partially from the requirements of building in the Designated Dipping Bedrock Overlay Zone adopted by Jefferson and Douglas Counties. Over-excavation has reduced floor slab heave, however, at a considerable cost to the projects. Additionally, if the fill is not properly controlled, there is a greater potential of settlement should the fill experience an increase in moisture content subsequent to placement.

This paper recommends the use of an underdrain system to prevent development of a perched water condition in the bathtub created as a result of over-excavation, causing the underlying expansive subgrade to swell and cause distress. The cause of development of perched groundwater is primarily due to the interruption of the historical flow in the permeable zones in the upper bedrock along with water usage and surface grading and water drainage issues subsequent to the development. The use of underdrain system is recommended as an effective method to remove accumulated water and build slab-on-grade without overly deep over-excavation.

For existing structures with continuing movement and distress, deep underdrain systems are recommended to intercept the water and route it around the structure to effectively stop the movements. This paper provides examples where the use of DUS has been effective.

Due to the groundwater flow conditions in the upper zones in the bedrock, there is some concern in the author's mind whether depth of wetting concept as currently practiced is truly applicable to the subsurface conditions along the Front Range.

GEOLOGY AND GROUNDWATER CONSIDERATIONS

Geology and Hydrogeology of the Denver Formation

The late Cretaceous age Denver Formation is considered an aquifer by the U. S. Geological Survey, Colorado Geological Survey, and the Colorado Division of Water Resources. The Denver Formation extends through an area of about 9,000 square kilometers (3,500 square miles) and underlies most of the Denver Metropolitan area. The formation is a 250 to 300-meter (800 to 1,000-foot) thick sequence of moderately consolidated, interbedded shale, claystone, siltstone and sandstone, in which coal and fossilized plant remains are common. Water-yielding layers of sandstone and siltstone occur in poorly defined irregular beds that are dispersed within relatively thick sequences of claystone and shale. Individual sandstone and siltstone layers are typically lens-shaped and range in thickness from a few centimeters to as much as 15 meters (50 feet). Because of the interbedded shale and claystone, the thickness of saturated water yielding materials generally ranges from 30 to 100 meters (100 to 350 feet).

Distinctive characteristics of the aquifer are the predominantly fine-grained and discontinuous nature of the sandstone lenses, widespread olive, green and brown coloration, an abundance of fossilized plant remains, and numerous carbonaceous and lignitic beds. Due to the irregular nature of the lenses and beds, it is not possible to correlate them over any distance. Because of this discontinuous nature and interfingering of permeable materials, the Denver Aquifer is considered to be hydrologically connected throughout its entire vertical and horizontal extent with the exception of the continuous confining clays and clay shales which form the top and base of the aquifer.

The competent claystone beds are fractured with iron staining and slickensides evident on the fracture surfaces. These fractures or discontinuities transmit groundwater through the formation connecting the more permeable sandstone and siltstone lenses. Each fracture is under unique hydrologic conditions including aperture, extent, and interconnectivity resulting in a highly variable ability to transmit ground water.

In 1998 a detailed analysis of the Denver Basin Bedrock Aquifers was performed by a project team consisting of the Denver Museum of Nature and Science (coordinating organization); the USGS Water Resources and Geologic Disciplines; Colorado Department of Natural Resources; Office of the State Engineer; Colorado Geological Survey; Elbert County; Colorado State University; University of Colorado at Boulder; New Mexico Institute of Mining and Technology; University of Alaska at Fairbanks; and the Scripps Institution of Oceanography. As part of the “Kiowa Core Project” 42 laboratory permeability tests were performed on Denver Aquifer core samples. The hydraulic conductivity values resulting from the tests ranged from a low of 3.75×10^{-7} cm/sec to a high of 3.21×10^{-3} cm/sec. The higher hydraulic

conductivity values are representative of sandstone beds and the lower values are representative of the claystone units.

Groundwater Flow through Upper Bedrock

Claystone bedrock in this area is frequently considered to be a virtually impermeable "aquiclude"; and the water is considered to build up on the top of the bedrock creating "perched" aquifer. Generally, the perched aquifer is considered to consist of the lower portion of the overburden soils and upper permeable portion of bedrock. The permeable portion of bedrock includes weathered and fractured bedrock, bedding and more permeable zones such as sandstone and siltstone. Overall, the bedrock portion of this upper perched aquifer has much lower permeability and lower effective porosity than the overlying overburden soil, although localized permeable zones can have relatively high permeability. The hydraulic conductivity of the bedrock and, consequently, dewatering rates, will be dependent on the degree of fracturing and the possible presence of more pervious sandstone zones in the bedrock. It is author's experience that the degree of fracturing and occurrence of sandstone lenses, and therefore the effective hydraulic conductivity of the bedrock materials, can be highly variable and difficult to predict. I would expect that some zones of the bedrock may convey little, if any, seepage while other zones may yield significant quantities of water.

Perched Groundwater Table (PGWT)

Site grading cuts interrupt the historical flow of shallow groundwater. The bathtub created by over-excavation recommended in the geotechnical reports, ponds the groundwater resulting in the development of perched aquifer commonly referred to as perched groundwater table (PGWT). PGWT conditions occur even if the over-excavation is backfilled by structural fill or on-site material, as the backfill material does not permit the historic flow and has different permeability and flow characteristics than the original ground. PGWT if not removed from the bathtub, causes further wetting of the underlying expansive subsoils and is the major cause of the movement and in some cases continuing movement of the grade supported slabs and structures. Figure 1 schematically depicts the interruption of the flow of groundwater and development of PGWT.

The contribution to the development of PGWT by inadequate surface drainage and water use subsequent to development has been recognized by the professionals and contractors; however, little attention has been given to the contribution by the interruption of the historic flow in the upper subsoils. The author's experience indicates that in majority of the cases considerably more water is being transmitted in the upper subsoils by the historic flow than by other sources. As an example, a PGWT does not disappear during winters when exterior water use is nonexistent or minimal and the sprinklers are not in use and during extended drought periods. This indicates the water perched under structures is from the flow of groundwater in the general vicinity of the site due to hydrogeologic conditions and not necessarily from

local sources subsequent to development such as excessive watering or other reasons such as broken sprinklers heads etc.

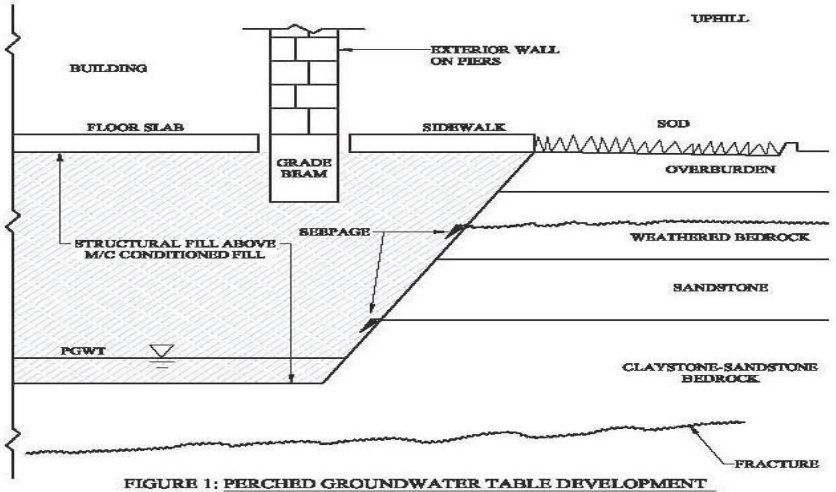

FIGURE 1: PERCHED GROUNDWATER TABLE DEVELOPMENT

Measurements in the underdrain systems indicate continuous flow of groundwater throughout the year and that the amount of flow far exceeds the surface drainage and water use in the area. The author has measured continuous ground water flow between 0.23×10^{-2} m^3/h (0.01 gpm) and 0.45 m^3/h (2 gpm). This flow is sufficient to cause additional expansion of subgrade and distress.

DESIGN CONSIDERATIONS

Underdrain system should be installed at the base of over-excavation below the structures to remove the PGWT or whenever the bottom of the slab is 1.5 meters (5 feet) or closer to the bedrock. Design of the underdrain system should consider the following:

- Slope over-excavation cuts, especially in bedrock towards the perimeter.
- Use rigid perforated plastic pipe to provide the consistent recommended slope and prevent water from ponding in the sags that typically form in the flexible pipes.
- The underdrain should intercept water flow through the permeable zones in the cut.
- Observation and testing of the underdrain system include:
    - Location
    - Slope
    - Elevation
    - Materials used in the construction

Typical section of an underdrain is shown on Figure 2.

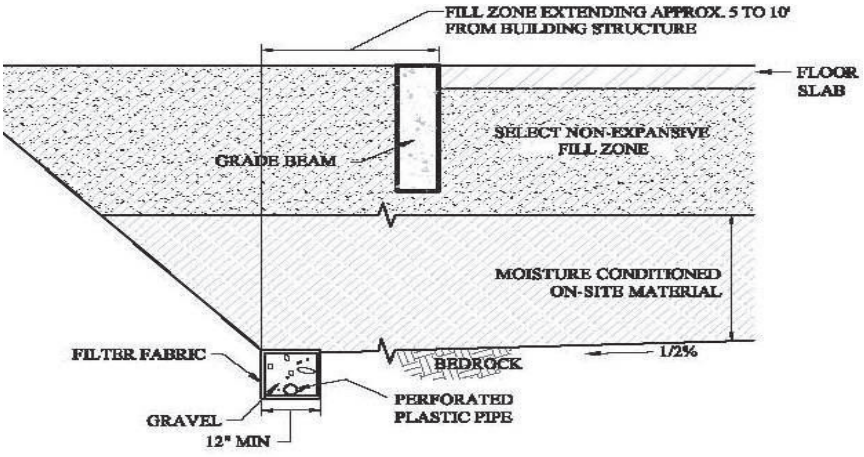

FIGURE 2: CONCEPTUAL DETAIL UNDERDRAIN SECTION

Lack of a properly designed underdrain system is responsible for distress and damage to buildings and structures throughout the Front Range. In many cases floor slabs and partition walls have been reconstructed only to have them experience more movement and distress. The addition of moisture to the previously unsaturated subsoils by the PGWT or other sources is the cause of movement. In some instances, PGWT also causes movement of the drilled piers, especially the ones with light dead loads.

DEPTH OF WETTING CONSIDERATIONS

Geotechnical professionals have been exploring the depth of wetting issue along the Front Range for the last several years. Several papers have been published on the subject and have had effects on the design and construction recommendations. Colorado Association of Geotechnical Engineers (CAGE) generally endorses the work done by Walsh, Colby et al., however, differing opinions remain.

Most of the publications maintain that deep seated moisture changes are rare due to climatic changes. The upper several feet are more likely to be affected by seasonal moisture content changes due to climatic changes or watering subsequent to the development and the resulting water use. The zone over which volume changes occur due to moisture variation is called the active zone due to the depth of wetting.

However, the studies do not consider the pattern of groundwater flow in the upper reaches of the bedrock. Practicing engineers and construction personnel commonly encounter water flow in the deeper excavation of bedrock whereas the upper portion is relatively dry. Lack of homogenous subsurface conditions in the Front Range,

require the theoretical calculation of the depth of wetting consider the subsurface conditions that actually exist in this area.

REHABILITATION USING DEEP UNDERDRAIN SYSTEM

Frequently, continuing movements are experienced by structures and present challenge to geotechnical engineers and design and construction professionals. Although the amount of incremental movement maybe small, the movement is the source of complaints and in some cases affects the usefulness and functionality of the facility.

The author's experience indicates the movement can be effectively eliminated by the use of a properly designed and constructed DUS. The intent of a DUS should be to capture and reroute the groundwater around the structure in the zone that has been affected by the over-excavation and grading during construction. Therefore, the underdrain should wrap around the structure or as a minimum, should be placed upgradient of the structure to intercept the groundwater flow and divert the accumulated water away from the structures.

Photo 1: Floor Slab Damage Retail Store

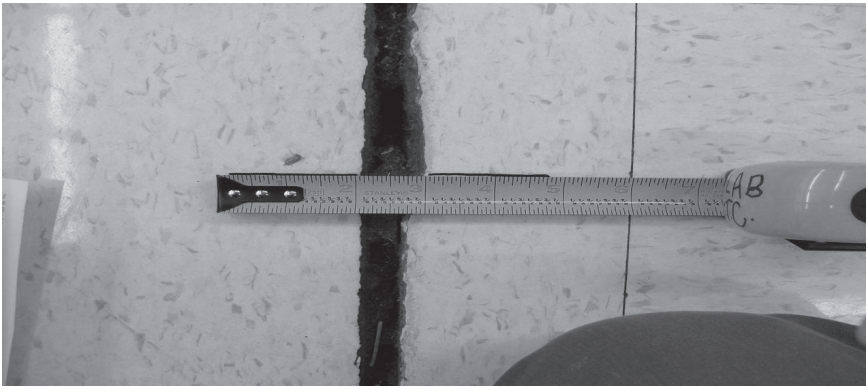

Photo 2: Floor Slab Distress

Design of the DUS for rehabilitation purposes should include the following:

- Subsurface investigation to evaluate the depth of overburden soil and bedrock and stabilized ground water level. Sufficient number of borings should be drilled to penetrate random permeable zones. Perforated plastic pipes should be installed in the bore holes and ground water level should be monitored over a period of time (several weeks, if needed) to determine the stabilized ground water table. Presence of water is the sign that the DUS will be effective.
- Laboratory tests on samples should include; index property tests, swell-consolidation tests, specific gravity tests (needed to determine the degree of saturation) and soil suction.
- Place the perforated underdrain line, preferably rigid plastic pipe, at the bottom of the trench at a consistent slope. Cover the pipe with free draining gravel above the bedrock and saturation zone. Wrap the underdrain with filter fabric to prevent contamination by backfill.

EXAMPLE PROJECTS

The author has installed DUS to eliminate continuing movement on several projects over the last 30 years. The installation of the DUS is relatively expensive and causes disruption to the business and should be carefully studied. The owners and the users of the facility need to be convinced of the benefit of such system and whether the expense is justified. Their rationale to use of the system is based on the functionality of the facility and the expense of continuing maintenance over the years. In one case, the floor slab had heaved over 15 cm (6 inches) with respect to the grade beam and the shopping carts had to be secured inside the store and the distress in the floor slab caused tripping hazards. In another instance critical satellite signals were being interrupted causing communication failures. In all cases the DUS was successful in preventing further movement and the clients are happy with the outcome. The amount of water collected by DUS varies by location and local geo-hydrologic conditions.

Photographs 1 and 2 presented above show damage to floor in a retail facility. The distress was monitored over several months and showed continuing signs of deterioration. Installation of a DUS stabilized the distress and restored the functionality of the building.

The sump pumps can be equipped with devices which document the dewatering times logged by wireless meters. Even a low amount of seepage collected by DUS is sufficient to cause the movement and distress.

Apartment Building, Aurora, Colorado

The development consists of several three story apartment buildings. The subsoils consisted of shallow lean to fat clay with sand overburden above moderately to highly expansive claystone bedrock. The buildings are founded on post-tensioned (PT) slab-on-grade placed on seven feet of over-excavated swelling subsoil placed back below the slab in a moisture conditioned and compacted state. Due to the length of the buildings, two post-tensioned slab sections with 60 cm (24-inch) step in the middle were constructed. Underdrain system was not recommended in the original soil report.

One of the buildings in the development showed signs of distress and significant cracking in the middle. It appeared the two sections of the building had moved differentially causing distress above the step extending from the bottom to the top third story.

The investigation conducted in 2007, about five years after initial construction, indicated development of a PGWT in the bathtub created by over-excavation with no means of readily draining the accumulated water. Water ponded on the expansive subsoils caused the movement and distress.

A DUS was proposed as a means of stabilizing the subgrade (Figure 3). Criteria used was placing the drainpipe at the bottom or below the over-excavated subgrade and extending the free draining gravel layer to the top of bedrock or bottom of the PT slab, whichever was higher. The underdrain intercepted the flow of the groundwater. Pump flow monitored remotely indicated an average rate of 0.68 m^3/h (0.03 gpm). Photograph 3 shows the installation of DUS at the site. Photograph 4 shows accumulation of groundwater in the sump pit.

The exterior building veneer was repaired and interior cracks were patched. Inspection conducted last year (2011) indicated no sign of movement since the repair in 2007.

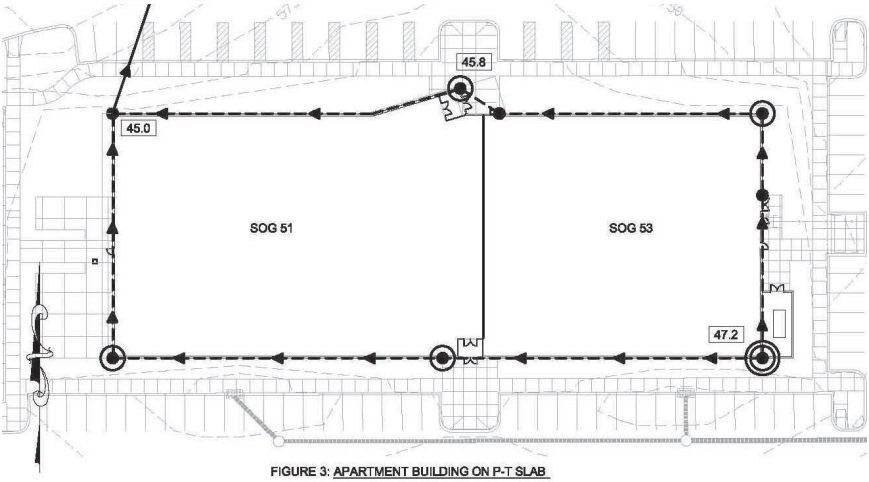

FIGURE 3: APARTMENT BUILDING ON P-T SLAB

Photo 3: Underdrain system installation

Photo 4: Sump pit with water

Industrial Facility, Broomfield, Colorado

The facility consists of several large warehouses; one to two stories tall with slab-on-grade construction, used for manufacturing and a three story headquarters office building built on a 30-acre site. The construction at the site started in late 1970s and has continued through 2010. The site slopes towards the south and southwest. Generally, the subsoil conditions consist of lean clay with sand to sandy clay over claystone and sandstone bedrock. The expansive potential of the overburden soil and bedrock varies between low to high, with majority of subsoils exhibiting moderate swell potential. The buildings are founded on piers drilled into bedrock and the slabs on 1.5 to 3 meters (5 to 10 feet) of reprocessed fill and/or structural non- to low expansive fill.

The buildings experienced continuing floor slab movement over time. The distress generally consisted of cracks in the floor and differential movement at the control joints and dock doors and cracks in the walls. The movement of the floor caused tripping hazards to the workers, jamming of the doors and hazard to the fork lift operations. Exterior walls showed significant distress in one warehouse and the headquarters building had random cracks.

The investigation consisted of drilling exploratory borings and measuring stabilized ground water in perforated PVC pipes over several weeks. The analyses of the subsoils samples indicated a saturated subsurface zone. DUS was recommended as a means of stabilizing the movement. Due to the cost of the procedure, a presentation was made to the management of the company and they approved over one million dollars for the repair using DUS.

Construction of the DUS started in 2007 and completed in January 2008. The DUS consisted of perforated rigid PVC pipe, covered with free draining gravel enveloped by filter fabric. The interceptor DUS was placed uphill of the facility protecting the warehouses and headquarters building. The depth of the underdrain pipe exceeded 8 meters (25 feet) at some locations and manholes with pumps were installed to remove accumulated water. The northern leg of the interceptor drain is mostly dry but drains water following precipitation. The eastern leg of the underdrain is connected to a manhole with pump and drains water continuously at the rate of 0.45 m^3/hr (2 gpm). The water is drained into the previously existing detention pond south of the property. The DUS was strictly for rerouting the groundwater around the buildings. Schematic layout of the DUS is shown on Figure 4, which also presents typical cross sections of the underdrain system. Photograph 5 shows the installation of DUS.

The building distress in the warehouses has been monitored by installation of crack monitors at several locations. In all, over 20 crack monitors were installed and are being monitored by the owner. The author has been informed by the owner that the movements in the buildings have stopped. One crack monitor has shown 0.8 mm (1/32 inch) movement in four years, others have indicated no movement.

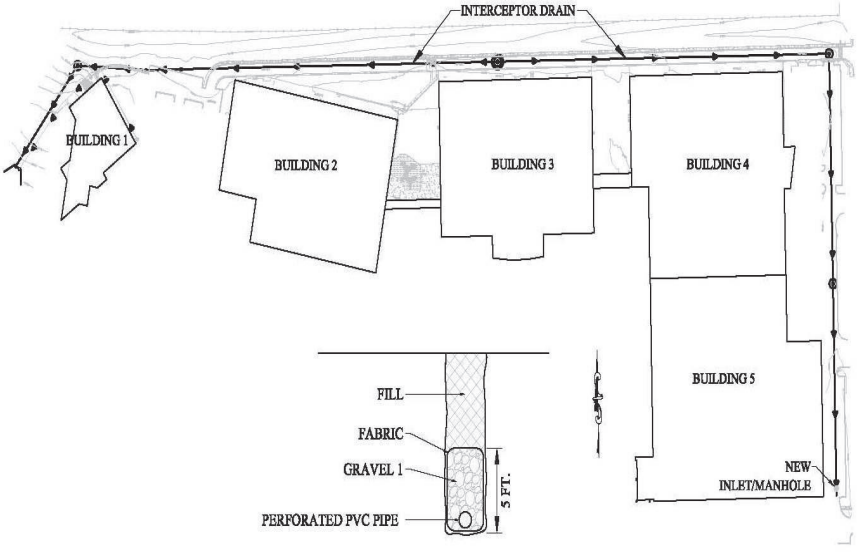

FIGURE 4: INDUSTRIAL FACILITY

Photo 5: Underdrain Systems Installation

CONCLUSIONS

Geotechnical design and construction personnel should consider the effects of shallow ground water flow through the permeable zones in the subsoils including flow in the bedrock when making recommendations for the development of the project. The over-excavation below the floor slab creates a bathtub which collects groundwater which provides moisture to the expansive subsoils, causing expansion of the subgrade and causing building movement and distress. Use of a properly designed and constructed underdrain system is highly recommended to prevent buildup of perched groundwater below the structures. The depth of wetting should consider the flow of groundwater in the upper permeable zones of the bedrock.

ACKNOWLEDGEMENTS

I appreciate the help from Don Ganser, P.G. for his input into the Geology and Hydrogeology in Denver Formation section of this paper and Alan Claybourn, P.E. for his review and technical input in preparation of this paper. Both work for Kumar and Associates, Inc.

REFERENCES

Bara, J., (1969). “Controlling the expansion of Desiccated Clays During Construction" Second International Research Conference on Expansive Clay Soils.

Blight, G., & deWet, J., (1965). “The Acceleration of Heave by Flooding. Butterworths, Australia”.

Chen, F., "Foundations on Expansive Soils", (1975). New York: Elsevier Publishing Company.
Chen, F., "Geotechnical Analysis of Driven Pile Foundations", (not dated). Denver, CO.
Chu, T., & Mou, C., (1973). "Volume Change Characteristics of Expansive Soils Determined by Controlled Suction Tests", Third International Conference of Expansive Soils. Hafia.
Claybourn, A., (not dated). Kumar & Associates Internal Design Memoorandum. "Estimate of Potential Heave using Denver Swell-Consolidometer Test Method. Denver, CO".
Cokca, E., (2000). "Comparison of suction and oedometer methods for the measurement of swell pressure", Quarterly Journal of Engineering Geology and Hydrogeology.
Colorado Division of Water Resources, (1985). "Geology of the Denver Basin Aquifers".
Colorado Association of Geotechnical Engineers, Various Documents
Holtz, R. D., & Kovacks, W. D., (1981). "Introduction to Geotechnical Engineering", Englewood Cliffs, Prentice Hall.
Jefferson County Colorado, (2011). "Designated Dipping Bedrock Area Guide".
Kenneth Walsh; Craig Colby; et al (2009); "Method of Evaluation of Wetting in Residential Areas", Journal of Geotechnical and Geoenvironmental Engineering, American Society of Civil Engineers.
LaForce, R., (1981). "Explosive Treatment to Correct Swelling Shale. Denver", Colorado Department of Highways.
Noe, D. C., Jochim, C.L. & Rogers, W.P., (2007). "A Guide to Swelling Soils for Colorado Homebuyers and Homeowners", Colorado Geological Survey, Special Publication 43, Second Edition.
Nelson, J., & Miller, D., (1992). "Expansive Soils- Problems and Practice in Foundation and Pavement Engineering", John Wiley & Sons, Inc.
Reynolds, Robert G. H., et. al., (2001). "The Kiowa Core, a Continuous Drill Core Through the Denver Basin Bedrock Aquifers at Kiowa, Elbert County, Colorado, U.S". Department. of the Interior, U.S. Geological Survey, Open File Report 01-185.
Robson, S. G. and Banta, E. R., (1995). " Ground Water Atlas of the United States, Arizona, Colorado, New Mexico, Utah", U.S. Geological Survey, HA 730-C.
Seed, H., Woodward, R., & Lundgren, R., (1962). "Prediction of Swelling Potential for Compacted Clays", ASCE, Soil Mechanics and Foundations Division.
Topper, Ralf, et al., (2003). "Ground Water Atlas of Colorado", Colorado Geological Survey Special Publication 53.

Application of Coulomb's Method to Reinforced Soil Structures

Peter Hoffman

1550 Larimer St, #891, Denver, CO 80202 <peter@PreservationEngineeringLLC.com>

ABSTRACT Coulomb's Method can be adapted to reinforced soil structures. The use of this method may provide insight into unexpected behavior of reinforced soils. For example, these structures can support loads satisfactorily although reinforcement is undermobilized,. This fact has been noted in recent literature. Moreover, the original objective was to explain that the observed angle of failure is not the angle calculated using Rankine theory. The conclusion is that ,once the observed angle is known or predicted, more accurate calculations of deformation and capacity might be possible, reducing unexpected behavior. Calculation based on this method is compared with an instrumented test case published by the Federal Highway Administration (FHWA).

INTRODUCTION

Cast-in-place retaining walls have been supplanted by reinforced soil during the last decades. Because of the significantly lower cost of reinforced soil structures, some engineers have moved forward with a technology that is not completely understood. In 2011, the Federal Highway Administration (FHWA) launched the Geosynthetic Reinforced Soil - Integrated Bridge System (GRS-IBS) initiative. Thus, it has become urgent that the engineering community achieve a comprehensive analytical capability and thorough understanding for reinforced soil. Although GRS is the focus of this paper, these comments are also applicable to Mechanically Stabilized Earth (MSE) design.

To reduce risks, FHWA has conducted performance tests on soil masses in the laboratory. These masses or piers have a square footprint and a height roughly twice the breadth. In Adams et al. (2011a), the FHWA has published load-deformation curves for typical performance tests.

The FHWA validated Equation (1) for ultimate capacity of non-cohesive soils with reinforcement (note, this is the analytical method to determine ultimate vertical capacity, the FHWA manual recommends finding the ultimate capacity empirically if possible). (However, the empirical method involves a sub-scale axisymmetric test

with a distributed load whereas the application is a full-scale article in plane strain with concentrated loads.)

$$q_{ult} = K_P \sigma_H = K_P \left(W \frac{T_f}{S_V} \right) \tag{1}$$

where W $0.7^{\left(\frac{S_V}{6d_{\max}}\right)}$, interaction coefficient (soil-reinforcement)
T_f strength of geosynthetic reinforcement
S_V vertical spacing of reinforcement
$d_{\max}$ maximum diameter of aggregate

Equation (1) is not entirely analytical. W is a coefficient of interaction between reinforcement and soil, and it is calibrated with empirical data. It was proposed in Pham (2009) and recognizes that spacing is more important than strength of reinforcement. Equation (1), including the W factor, is validated against a growing list of performance tests in Adams et al. (2011b).

While capacity can be calculated, no analytical method exists for deformation. The original investigation for this paper focused on anecdotal reports that the angle of failure is not the Rankine angle. Explaining this phenomenon, Coulomb's method for retaining walls is adapted to GRS masses. As a by-product of Coulomb analysis, this paper presents a rudimentary method for analyzing deformation.

COULOMB ANALYSIS

Rankine's method is well known; however, it assumes a vertical wall that retains soil with a horizontal compressive force. When a retaining wall provides a non-horizontal compressive force, Coulomb's method is applicable instead. It reproduces Rankine's result as a special case.

One of the challenges is finding β, the apparent angle of the failure surface, i.e., the angle measured relative to the horizontal axis. When ϕ is the angle of internal friction, the angle of the failure surface calculated by Rankine's method is $\alpha_f = 45° + \phi/2$. Coulomb's method shows a decrease, $\beta - \alpha_f$, in the apparent angle of failure. This decrease is associated with rotation of principal axes that is enabled by reinforcement.

This paper adapts Coulomb's method to GRS structures. It is similar to Coulomb's method for retaining walls, described by Terzaghi and Peck (1967). The compressive force due to the retaining wall is replaced by the tensile force, T, due to the reinforcement. The force at the failure surface is the resultant of a shear force and a normal force, and its angle from the horizontal axis is $\beta + (90° - \phi)$; so its angle from the vertical axis is $\beta - \phi$ as shown in Figure 1.

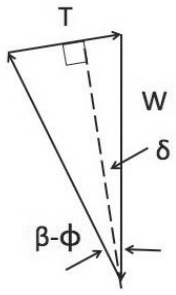

FIG. 1. Forces in Coulomb analysis

After a GRS structure undergoes deformation, the reinforcement and its tensile force are no longer horizontal. Let δ denote the reinforcement's angle with the horizontal axis at mid-height as a failing soil wedge drops.

When the surcharge greatly exceeds the weight of soil, the downward stress, σ_V, can be considered constant[1] throughout the soil mass. Coulomb's downward force, denoted as the W (weight) vector, is now reduced by a vertical component of tension in the reinforcement,

$$W = \sigma_V H \tan(90° - \beta) - T_V \qquad (2)$$

where H height of the GRS mass
σ_V vertical stress associated with load
β angle of failure relative to horizontal axis

T_V is calculated in accord with Figure 2.

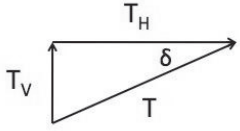

FIG. 2. Vector components of reinforcement tension at mid-height

[1]With small error in center of force, soil weight can be included by setting $\sigma_V = \gamma H/2 + p$, where γ is unit weight of soil and p is surcharge pressure.

A perpendicular (Figure 1) to the reinforcement forms an angle δ with W, so that

$$\sin\delta \approx \left(\frac{\delta}{\beta-\phi}\right) T/W$$
$$= \frac{\left(\frac{\delta}{\beta-\phi}\right)\sigma_H H/\cos\delta}{\sigma_V H\tan(90°-\beta)-\sigma_H H\tan\delta} \qquad (3)$$

where δ angle of deformed fabric from the horizontal axis
ϕ angle of internal friction
σ_H horizontal stress

Rearranging Equation (3) in terms of σ_H/σ_V,

$$\frac{\sigma_H}{\sigma_V}\left(1+(\beta-\phi)\tan\delta\right) = (\beta-\phi)\tan(\frac{\pi}{2}-\beta)\frac{\sin2\delta}{2\delta} \qquad \text{(radians)} \qquad (4)$$

Because $1/(1+x) = 1-x+x^2\ldots$,

$$\frac{\sigma_H}{\sigma_V} \approx \left(1-(\beta-\phi)\tan\delta\right)(\beta-\phi)\tan(\frac{\pi}{2}-\beta)\frac{\sin2\delta}{2\delta} \text{ (radians)} \qquad (5)$$

where σ_H horizontal stress, due to reinforcement
σ_V vertical stress, due to load
β apparent angle of failure, i.e., relative to horizontal axis
δ angle of deformed reinforcement relative to horizontal axis
ϕ angle of internal friction

Coulomb's method corresponds to an energy method and the solution is the extreme point of the curve defined by Equation (5). Using polar coordinates, this paper plots σ_V/σ_H, which is the reciprocal of the expression. Figure 3 shows a family of plots for $\phi = 45°$ and $\delta = 0$, 0.2, 0.4, 0.6, 0.8, and 1.0 radian. The β solution points lie in the valley of the family of curves. Test results are also available for $\phi = 45°$.

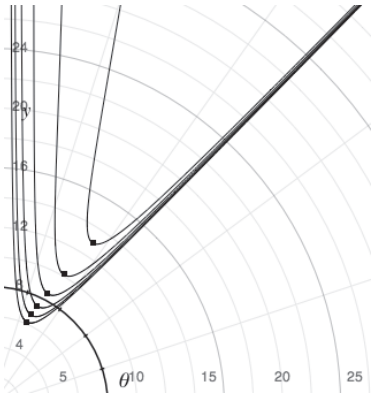

FIG. 3. Polar plot: capacity increases as apparent angle of failure decreases

Rankine's solution corresponds to $\delta = 0$. In Figure 3, the minimum occurs when $\beta = 67.5° = 45° + 45°/2 = \alpha_f$, and $\sigma_V / \sigma_H = 5.8 = \tan^2 \alpha_f$. The latter is K_P, Rankine's coefficient for passive lateral earth pressure. Observe that values for σ_V / σ_H increase as δ increases. At the same time, values for β decrease. In summary, K_P appears to increase while the failure angle appears to decrease; however, these illusory changes are associated with rotation of principal axes enabled by the reinforcement.

For comparison, two additional families of curves are crowded into Figure 4. The family for $\phi = 60°$ is at the top, and the family for $\phi = 30°$ appears at the bottom. The original family for $\phi = 45°$ is shown in the background. Observe that contours become closer as ϕ decreases. This fact is important when analyzing deformation in Section 3.

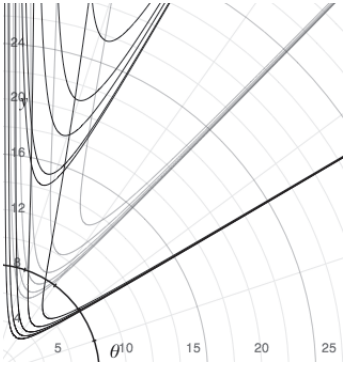

FIG. 4. Polar plots ($\phi = 60°$ family above, $\phi = 30°$ below): contour spacing decreases as ϕ decreases

Because Figure 4 is congested, pertinent information is extracted into Figure 5. It plots σ_V/σ_H as a function of rotation, $\alpha_f - \beta$. Rankine's values prevail prior to rotation; that is, $\beta = \alpha_f$, and $\sigma_V/\sigma_H = K_P$. In summary, the apparent failure angle rotates, and rotation increases as load increases.

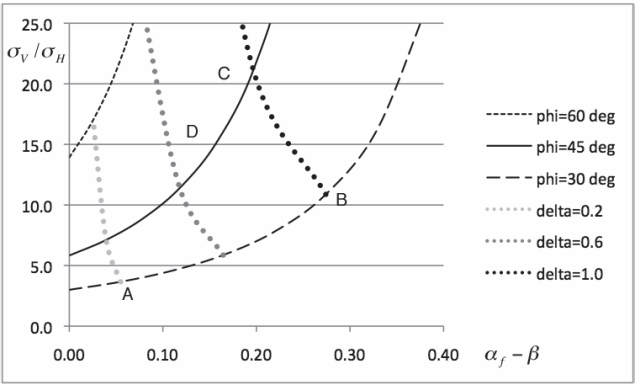

FIG. 5. Capacity increases with rotation of failure angle

Figure 5 also shows contours of constant delta, δ, which are used in Section 3 to calculate deformation.

VERTICAL STRAIN

If reinforcement layers are uniformly spaced throughout the height of the soil mass, and if soil weight is negligible in comparison to the external load, then the reinforcement is represented by a resultant at mid-height, *H/2*.

Let *d* designate the vertical distance that a soil wedge drops during failure. Due to the drop, a fictitious reinforcement layer at mid-height forms an angle, δ, with the horizontal. Figure 6 depicts the situation.

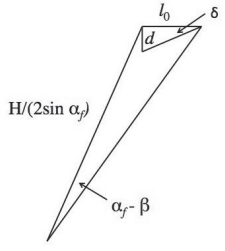

FIG. 6. Deformation is related to rotation of failure angle

Vertical strain, *d/H*, can be calculated because

$$\frac{d}{H}\left(2\sin^2\alpha_f\right)=\delta(\alpha_f-\beta)=A(\alpha_f-\beta)^2 \qquad (6)$$

where β apparent failure angle, measured from horizontal axis (radians)
α_f true or Rankine failure angle, from principal axis (radians)
d vertical movement measured at top of structure
H height of structure
A $A=\delta/(\alpha_f-\beta)\approx 1.6K_P^{0.75}$, where $K_P=1/K_A$

K_P is the coefficient of passive earth pressure. The value $A\approx 1.6K_P^{0.75}$ is merely a curve fit to data calculated with Coulomb's Method in Section 2, but it greatly simplifies Equation (9) below. As a demonstration using Figure 5, observe that $\alpha_f-\beta$ changes by 0.22 radian from Point A to Point B while δ varies by 0.8 radian so that A = 0.8/0.22 = 3.6. For 30 degrees, $1.6K_P^{0.75}=1.6(3)^{0.75}$ is also 3.6, agreeing with the curve fit.

Coulomb's method is an energy method, but it neglects some work. Although the method considers W_1, work done against friction along the failure surface during vertical deformation, it neglects W_2, work during horizontal strain that accompanies vertical deformation. Work done during horizontal strain can be calculated on the assumption of continuous fabric reinforcement and a dry-stacked block facing. Under these conditions, horizontal strain is H/B times vertical strain at the failure surface. This additional work reduces the vertical strain by a factor of $1+\cot\phi$, or approximately two, as follows.

$$W_1=(\text{force})(\text{distance})=\left(\frac{\tau BH}{\sin\beta}\right)\left(\varepsilon_V H\right)=\frac{\tau\varepsilon_V BH^2}{\sin\beta}$$

$$W_2=(\text{force})(\text{distance})=\left(\frac{\tau BH}{\sin\beta\tan\phi}\right)\left(\frac{\varepsilon_V H}{B\sin\beta}(B)\right)=\frac{\tau\varepsilon_V BH^2}{\sin^2\beta\tan\phi} \qquad (7)$$

$$\frac{W_1+W_2}{W_1}=\frac{(\tau\varepsilon_V BH^2/\sin^2\beta)+(\tau\varepsilon_V BH^2/\sin^2\beta\tan\phi)}{\tau\varepsilon_V BH^2/\sin^2\beta}=1+\cot\phi$$

where B breadth
H height
τ shear stress at failure surface

Equations (6) and (7) combine into a simple, useful formula for vertical strain,

$$\varepsilon_V = \frac{d}{H} = \frac{A}{2(1+\cot\phi)\sin^2\alpha_f}\left(\alpha_f - \beta\right)^2 = 0.3K_P\left(\alpha_f - \beta\right)^2 \quad (8)$$

where ε_V vertical strain
K_P coefficient of passive earth pressure, $\tan^2\alpha_f$
$\alpha_f - \beta$ rotation of apparent angle of failure (radians)

When the intermediate expression in Equation (8) is plotted for various ϕ, it is discovered that ϕ-dependence of ε_V / K_P has vanished. The only significant parameter is $\alpha_f - \beta$, rotation of the apparent angle of failure.

VALIDATION

When originally formulated, the ultimate capacity calculation, Equation (1), assumed that the reinforcement tensile load is 100% mobilized and equal to mobilized horizontal soil forces computed using Rankine's active earth pressure theory. On the other hand, Yang, Zornberg, and Bathhurst (2010) found in several field applications that reinforcement strength is only 30% mobilized when peak soil shear capacity is reached.

The Coulomb analysis of Section 2 resolves the discrepancy. According to Figure 5, rotation of the apparent angle of failure allows a value of σ_H / σ_V that is much smaller than the Rankine value, $K_A = 1/K_P$.

Consider an FHWA performance test. A typical configuration is a 100 x 100 x 200 centimeter (40 x 40 x 80 inch) soil mass. The perimeter is formed by dry-stacking concrete blocks.

Adams et al. (2011a) publishes data for a performance test using 70 kN/m (4800 lb/ft) reinforcement spaced 0.2 meter (8 inches). Soil parameters are $\phi = 48°$, c = 0, and $d_{\max} = 1.27$ cm. (0.5 in.). From Equation (1), the ultimate capacity is $q_{\text{ult}} = WK_P T_f / S_V =$ (0.39)(6.8)(70)/(0.2) = 903 kPa (131 psi). So, $\sigma_H = 0.3K_A q_{\text{ult}} = 39.9$ kPa (5.8 psi).

Compaction plays a significant role. According to Jewell (1996), tractor-driven compactors increase σ_H by 14 to 28 kPa (2 to 4 psi). Small compactors provide half as much, perhaps 10 kPa (1.5 psi). Adding 10 to 39.9 gives 49.9 kPa (7.3 psi), so $\sigma_V / \sigma_H = 903/49.9 = 18$.

Figure 5 associates σ_V / σ_H = 18 with rotation $\alpha_f - \beta$ = 0.15, which is 8.6 degrees.

By Equation (8), the vertical strain is $\varepsilon_V = 0.3(6.8)(0.15)^2 = 0.045 = 4.5\%$.

Emphasizing the importance of compaction, Point C becomes Point D in Figure 5, and strain is reduced from 5.8 percent down to 4.5 percent.

The test configuration is summarized as Test 1 in Table 1. Calculations are summarized in Table 2. These tables also summarize three more FHWA tests with non-cohesive soils.

TABLE No. 1 Performance test configurations and parameters

	Test 1	Test 2	Test 3	Test 4
T_f (kN/m)	70	35	70	70
S_V (m)	0.2	0.2	0.2	0.4
$d_{\max}$ (cm)	1.27	1.27	3.30	2.54
ϕ (degrees)	48	48	45	53

TABLE No. 2 Performance test calculations

	Test 1	Test 2	Test 3	Test 4
K_P	6.79	6.79	5.83	8.93
W	0.39	0.39	0.69	0.39
q_{ult} (kPa)	903	451	1392	594
$\sigma_H = q_{\text{ult}}/3K_P$ (kPa)	39.9	20.0	71.7	20.0
$q_{\text{ult}}/(\sigma_H + 10)$	18.0	14.9	17.0	19.6
$\alpha_f - \beta$ (radians)	0.15	0.12	0.17	0.11
ε_V (%)	4.5	2.9	5.1	3.2

Calculated deformations are compared in Figure 7 with data from the four tests. In Adams et al. (2011b), an extensive validation is provided for capacity calculations based on Equation (1). Limited validation of these deformation calculations is consistent with their early stage of development. Nevertheless, this finding supports the assertion by Yang, Zornberg, and Bathurst (2010) that reinforcement strength is only 30 percent mobilized, on average, when peak soil shear capacity is reached.

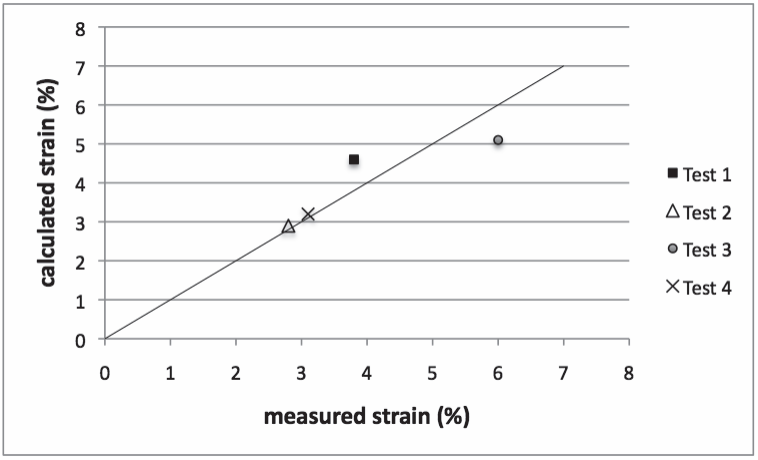

FIG. 7. Validation: calculated strain versus measured strain

CONCLUSIONS

Coulomb's method can be adapted in order to corroborate anecdotal reports that the apparent angle of failure differs from Rankine's angle of failure.

As a corollary, the Coulomb analysis alters the rationale that underlies Equation (1) for capacity, an equation that is well validated. In other words, the capacity equation is accurate but poorly understood. This Coulomb analysis corroborates findings of Yang, Zornberg, and Bathurst (2010).

As another corollary, Coulomb's method provides the means to calculate deformations of GRS structures. Compaction is shown to be a critical factor in deformation. Although the method is in an early stage of development, it provides reasonable accuracy when compared to FHWA performance tests.

ACKNOWLEDGEMENT. The author thanks Professor Jonathan T.H. Wu at the University of Colorado, Denver. He introduced the author to GRS structures and frequently prevented his going astray.

REFERENCES

Adams, M.T., Nicks, J., Stabile, T., Wu, J.T.H., Schlatter, W. and Hartmann, J. (2011a). "Geosynthetic Reinforced Soil Integrated Bridge System – Synthesis Report." *Report No. FHWA-HRT-11-026,* Federal Highway Administration, McLean, VA.

Adams, M.T., Nicks, J., Stabile, T., Wu, J.T.H., Schlatter, W. and Hartmann, J. (2011b). "Geosynthetic Reinforced Soil Integrated Bridge System – Interim Implementation Guide." *Report No. FHWA-HRT-11-027,* Federal Highway Administration, McLean, VA.

Jewell, R.A. (1996). "Soil Reinforcement with Geotextiles." CIRIA Special Publication 123, London.
Pham, T.Q. (2009), "Investigating Composite Behavior of Geosynthetic-Reinforced Soil (GRS) Mass," Ph.D. thesis, University of Colorado, Denver.
Terzaghi, K., and Peck, R.B. (1967), *Soil Mechanics in Engineering Practice*, second edition, Wiley.
Yang, K-H., Zornberg J.G., and Bathurst R.J. (2010). "Mobilization of Reinforcement Tension within Geosynthetic-Reinforced Structures." *Proceedings of the 2010 Earth Retention Conference*, American Society of Civil Engineers.

Bedrock Settlement Beneath a Large Embankment Dam

Robert J. Huzjak[1] P.E., M. ASCE and Adam B. Prochaska[2], Ph.D., P.E., P.G., A.M. ASCE

[1] Project Manager and President, RJH Consultants, Inc., 9800 Mt Pyramid Ct, Suite 330, Englewood, CO 80112; rhuzjak@rjh-consultants.com
[2] Geotechnical Engineer, RJH Consultants, Inc., 9800 Mt Pyramid Ct, Suite 330, Englewood, CO 80112; aprochaska@rjh-consultants.com

ABSTRACT: Predicting deformation of embankment dams and ancillary facilities during and post construction is a critical design consideration. Total and differential settlements of these structures are generally evaluated based on consideration for immediate settlement and consolidation of the embankment materials and the soil foundations, with minimal consideration of bedrock settlement. However, bedrock in many parts of Colorado consists of geologically young (less than about 100 million years old) fine grained sedimentary units. Under loads from moderate to large dams, settlement of this type of bedrock can become a critical design condition.

This paper presents the field and laboratory data, analyses, and design features that were incorporated to accommodate bedrock settlement below Frank Jaeger Dam, a 61-meter-high (200-foot-high) embankment dam that was recently constructed in two phases on a claystone bedrock foundation near Parker, Colorado.

Bedrock settlement was initially computed using one-dimensional manual calculations and two-dimensional finite-element methods. Data obtained from instrumentation and monitoring during and after the first phase of construction were used to calibrate laboratory-obtained settlement properties to observed behavior. These calibrated properties, and the time since completion of the first construction phase, were used to predict the ultimate settlement for the foundation of the completed embankment.

Features incorporated into the embankment and the ancillary facilities to accommodate the predicted construction and post construction bedrock settlement and the performance and reliability of settlement sensors will be described. Bedrock settlement measured during and after completion of the embankment is compared to the predicted settlement.

PROJECT OVERVIEW

For permitting reasons, Frank Jaeger Dam was constructed in two phases. Phase I was constructed from February 2005 to May 2006 and consisted of a 41-meter-high (135-foot-high) embankment dam to create a reservoir that would have an active storage volume of 1,986 ha-m (16,100 acre-feet (ac-ft)). One of the key design criteria for the initial phase was that the dam and ancillary facilities needed to be designed to accommodate construction of a future raise up to the ultimate reservoir capacity of 8,881 ha-m (72,000 ac-ft) without significant lowering of the reservoir pool or interruptions to reservoir operations.

The dam raise (Phase II) was initially anticipated to be completed several decades after completion and filling of Phase I. However, shortly after the start of construction of Phase I, several local water districts requested storage space in the reservoir, and planning and design for the raise began. Phase II was constructed from November 2008 to October 2011.

A general plan of the Phase II dam is provided on Figure 1. The embankment consists of a 61-meter-high (200-foot-high) zoned earth embankment with a crest at Elevation (El.) 1896 m (6,220 feet). The combined outlet works and service spillway are located along the right side of the valley floor, and include two 2-meter-diameter (78-inch-diameter) steel conduits encased in reinforced concrete from the gate tower to the terminal facilities.

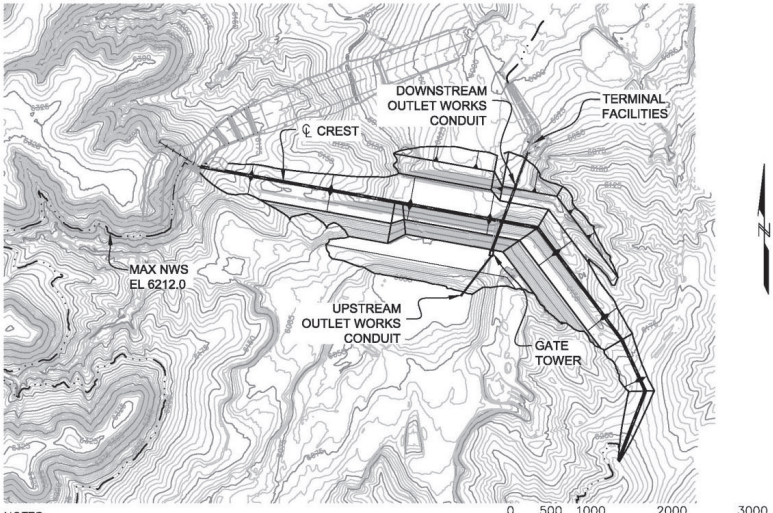

FIG 1. Embankment Plan

INTRODUCTION

Predicting deformation of embankment dams and ancillary facilities during and post construction is a critical design consideration. For dams constructed on soft bedrock, settlement of the bedrock must be considered in addition to settlement of the embankment fill and foundation soils. Frank Jaeger Dam was recently constructed near Parker, Colorado and is founded on soft claystone bedrock. Bedrock deformation analyses were performed to support design of the embankment dam and outlet works conduit. Bedrock deformation properties were developed based on unconfined compression tests, triaxial compression tests, and consolidation tests on core samples of bedrock recovered from subsurface explorations. Construction and post-construction bedrock settlements were computed using one-dimensional and two-dimensional analyses. Field instrumentation and survey data obtained during and after the Phase I construction were used to calibrate deformation properties to observed behavior to develop predictions for the Phase II dam raise. Instrumentation and survey data were also collected during and after Phase II construction. The measured deformation is compared to predicted values and the quality of the measured data is discussed.

GENERAL GEOLOGY AND FOUNDATION CONDITIONS

Frank Jaeger Dam is located within the Colorado Piedmont subdivision of the Great Plains Physiographic Province, which is generally characterized by an ancient, elevated erosional surface. Remnants of this ancient surface are evident by flat mesa tops that surround the site. The site is located within a broad valley that cuts through the surrounding mesas in a southwest to northeast trend.

Bedrock below the dam consists of 70 million-year-old (Cretaceous age) to 45 million-year-old (Eocene age) sedimentary rocks mapped as the Lower Dawson Formation and the Upper Dawson Formation. The 34 million-year-old (Oligocene age) Castle Rock Conglomerate overlies the Upper Dawson Formation and forms resistant mesa tops west and south of the site. A general bedrock geologic map is provided on Figure 2.

The Lower Dawson Formation at the dam is predominately interbedded claystones and sandstones with localized lenses of strongly cemented conglomerate. Generally, the unit is about 60 percent claystone, 25 percent sandstone, and 15 percent conglomerate. The claystones are generally medium to highly plastic with up to about 30 percent narrowly graded fine sand. The sandstones are generally moderately to well cemented, and comprised of narrowly graded, fine to medium grained sand with up to about 35 percent medium to highly plastic fines. The conglomerates are mostly strongly cemented and consist of fine to coarse grained gravel with a fine to coarse sand material. The lenses of strongly cemented conglomerate are present at depths below about El. 1826 m (5990 feet) in the valley.

Sediments that comprise the Lower Dawson Formation consist of materials that were eroded from the Rocky Mountain Front Range uplift and were deposited in non-marine alluvial channels, meandering streams, and floodplain environments. Based on topography surrounding the site, the top of the Lower Dawson sediments were consolidated by an average of about 79 meters (260 feet) of overburden along the maximum section of the dam, prior to erosion of the valley.

The Upper Dawson Formation is predominately sandstone, with local basal conglomerates and interbedded claystone lenses. The sandstones are generally weakly to very weakly cemented and consist of widely graded, fine to coarse sand with up to 15 percent gravel to 3 inches, and less than 20 percent low to medium plastic fines.

The Upper and Lower Dawson Formations are separated based on an ancient erosional surface located below the contact between the two formations. This erosional surface is identified by the presence of intensely weathered and altered bedrock characterized by red or orange sandstone and variegated claystones. The contact between the Upper and Lower Dawson Formations along the dam centerline is at about El. 1849 m (6065 feet) on the right abutment, and El. 1853 m (6080 feet) on the left abutment. The valley floor is at about El. 1838 m (6030 feet). The erosional surface between the Upper and Lower Dawson Formations dips downward at about one degree to the southeast.

In the valley bottom, except for the central clay core, the dam is founded on about 11 to 12 meters (35 to 40 feet) of alluvial soils overlying the Lower Dawson Formation bedrock. The right abutment of the dam is founded on about 6 to 14 meters (20 to 45 feet) of Upper Dawson Formation overlying the Lower Dawson Formation bedrock. The left abutment of the dam is founded on about 7 to 18 meters (20 to 60 feet) of Upper Dawson Formation overlying the Lower Dawson Formation. The dam's central core is founded on the Lower Dawson Formation in the valley bottom and on the Upper Dawson Formation in the abutments. The general geology along the centerline of the dam is shown on Figure 3.

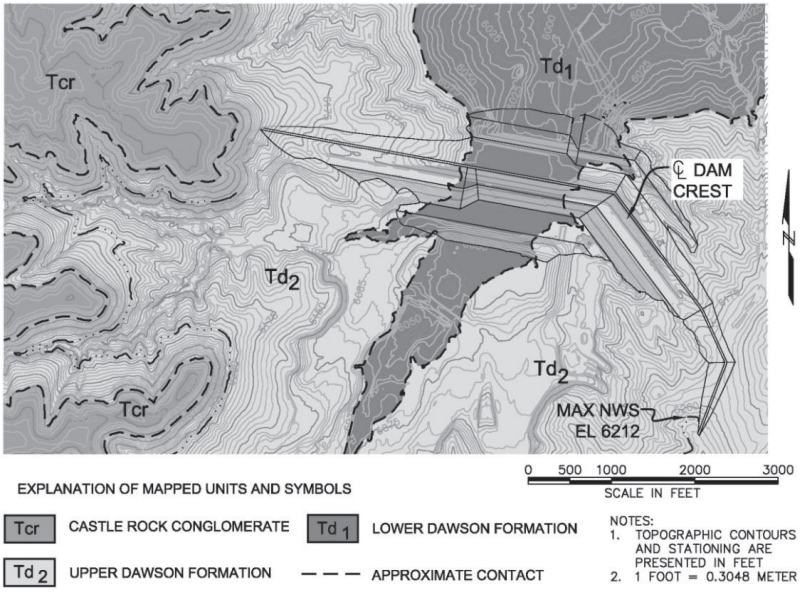

FIG 2. General Bedrock Geology

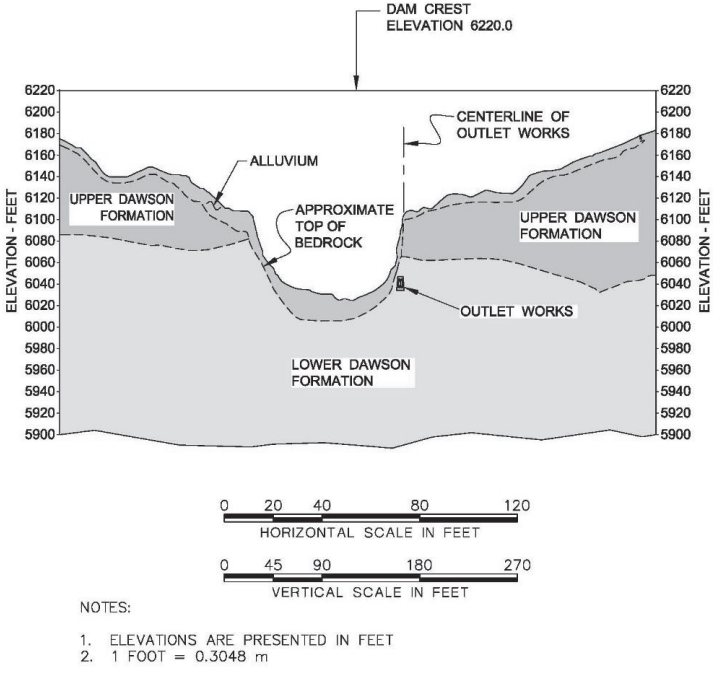

FIG 3. Geologic Section along Dam Centerline

Settlement of the predominantly sandstone Upper Dawson Formation was not a primary concern for embankment deformation analyses because settlement was anticipated to be minor and to occur as elastic deformation simultaneously with construction. Settlement of the predominantly claystone Lower Dawson Formation was a design concern because the total magnitude of settlement was estimated to be significant and because consolidation settlement was expected to continue after completion of construction. About 70 percent of the anticipated consolidation from each phase of construction in the Lower Dawson Formation was estimated to occur after completion of that phase of construction.

Although the Upper and Lower Dawson formations are geologically considered to be rock, they generally consist of weakly cemented, overconsolidated sediments and exhibit properties intermediate between those of soil and rock. Similar to the predominantly fine grained Lower Dawson Formation, weak mudstones are present throughout eastern and western Colorado, primarily in Cretaceous-age sedimentary formations (Santi and Doyle, 1997; Tweto, 1979).

DATA COLLECTION

A series of site investigations was completed during both phases of design within the general area of the proposed dam and reservoir footprint and borrow areas to evaluate stratigraphy, perform in-situ tests, and collect soil and rock samples. A total of 18 boreholes within the general footprint of the dam and 10 boreholes in the general area of the outlet works penetrated into the Lower Dawson Formation. Laboratory tests performed on recovered samples of the Lower Dawson Formation to support development of deformation material properties consisted of:

- 3 unconfined compressive strength tests (ASTM D 2166)
- 2 consolidated undrained triaxial compression tests (ASTM D 4767)
- 10 consolidation tests (ASTM D 2435 and D 4546)

Additional details about the geotechnical data collection for the project are presented by Huzjak and Prochaska (2009).

DEFORMATION ANALYSES DURING PHASE II DESIGN

Initial Settlement Estimates

Deformation analyses were performed during design of the Phase II dam to estimate bedrock settlement beneath the embankment and outlet works conduit. The general procedures used during the deformation analyses were as follows. Additional details are presented by Huzjak and Prochaska (2009).

- Bedrock stratigraphy was developed based on the findings from the subsurface investigations.

- Deformation material properties were developed based on the results of laboratory tests. The material properties used are summarized in Table 1.
- Initial settlement estimates were calculated using the material properties from Table 1. Vertical deformation of the foundation was estimated using one-dimensional analyses and two-dimensional linear elastic finite-element modeling techniques. One-dimensional analyses were completed using Terzaghi's one-dimensional theory of consolidation. Two-dimensional analyses were performed using the SIGMA/W module of the GeoStudio 2004 software package. Results of the predicted foundation deformation for the Phase I and Phase II embankment at the maximum section (STA 7+62 m (25+00 ft)), and along the outlet works are shown on Figures 4 and 5, respectively. As shown on Figure 4, the settlement predicted using the two-dimensional analyses is much greater than using the one-dimensional analyses.

Table 1. Properties for Initial Deformation Analyses

Material Type	Deformation Parameters				
	Recompression Index (c_r)	Coefficient of Consolidation (c_v), m^2/year (ft^2/year)	Initial Void Ratio (e_o)	Elastic Modulus (E), MPa (lb/ft^2)	Poisson's Ratio (μ)
Lower Dawson Claystone	0.049	6.3 (68)	0.72	16.8 (3.5×10^5)	0.27

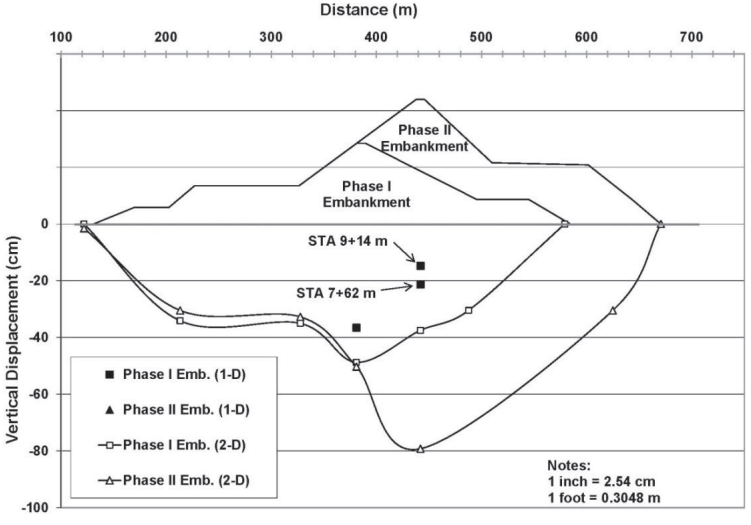

FIG 4. Total Initial Predicted Deformation at Maximum Section

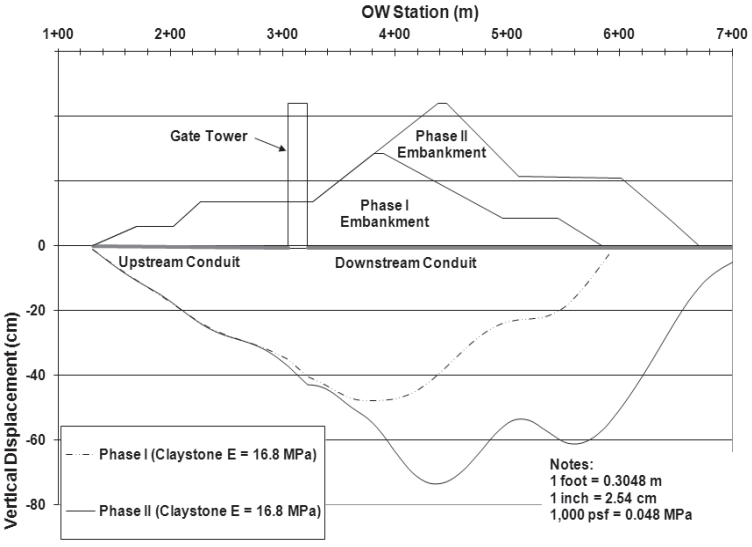

FIG 5. Total Initial Predicted 2-D Deformation for Outlet Works Conduit

Comparison of Settlement Estimates to Settlement Sensor Data

The initial settlement estimates obtained from the one-dimensional analyses were compared to data obtained from settlement sensors installed during Phase I construction. The installed sensors were hydraulic vibrating wire settlement sensors that were installed in boreholes in accordance with manufacturer's recommendations. The bottom of each sensor was grouted in bedrock and the top of each sensor consisted of a settlement plate and fluid reservoir that rested on the top of the stratum in which settlement was being measured. As the settlement plate settled with the top of the stratum, settlement was measured by detecting the change in fluid pressure within tubing in the borehole. The hydraulic vibrating wire settlement sensors were a revision to the original mechanical settlement sensors and were installed to reduce construction time and cost. The locations of the settlement sensors are shown on Figure 6. Settlement sensors S1 and S2 measure the deformation in bedrock between the core/bedrock contact and 41 and 50 feet, respectfully into bedrock, and are located below the core along the Phase I dam centerline and record settlement in bedrock. Sensors S3 and S4 are located about 30 meters (100 feet) downstream of the Phase I dam centerline and monitor settlement in the alluvial foundation soils and bedrock. The subsurface profile along sensor S3 consists of about 4.6 meters (15 feet) of clayey alluvium, underlain by 4.6 meters (15 feet) of granular alluvium, underlain by 14 meters (45 feet) of claystone. Along sensor S4, the subsurface profile consists of about 7 meters (23 feet) of granular alluvium underlain by 16 meters (52 feet) of claystone. Data from Sensor S1 were not used because the data exhibited unrealistic

trends and were considered not to be reliable. Data from these settlement sensors that were available at the time of Phase II design are shown on Figure 7.

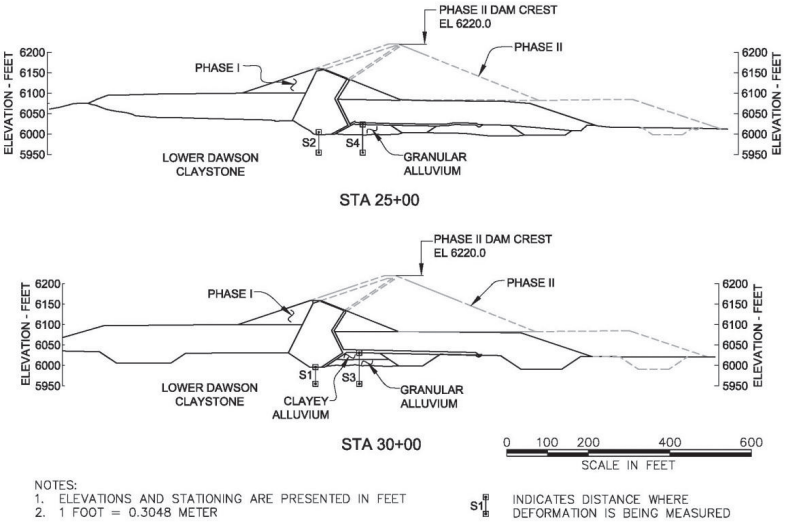

FIG 6. Locations of Phase I Settlement Sensors

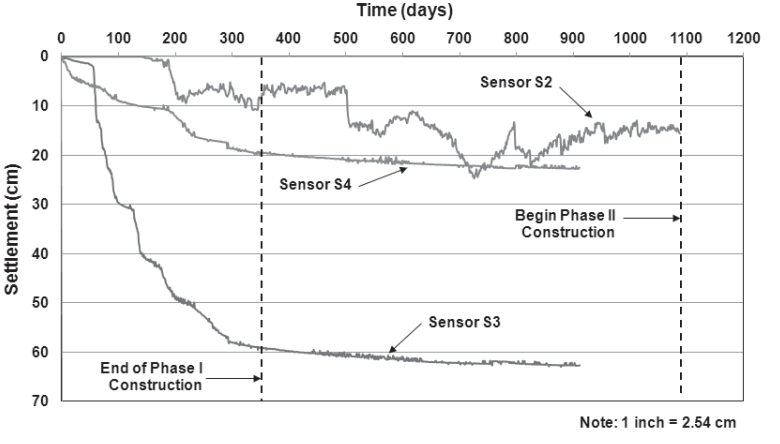

FIG 7. Phase I and Pre-Phase II Settlement Sensor Data

To directly compare the data from the settlement sensors, a time-rate of consolidation analysis needed to be performed. Using the laboratory value of $c_v = 6.3$ m^2/year (68 ft^2/year), approximately 22 percent of the total deformation in the

bedrock was estimated to have occurred by the completion of the Phase I construction, which was a time length of about 24 months. This percentage of consolidation was then compared to the settlement readings taken at the end of Phase I construction. Predictions versus instrumentation readings are presented in Table 2. The predicted settlements from the one-dimensional analyses, using values for recompression index (c_r) and initial void ratio (e_o) for the claystone developed from laboratory data, correlated well with the recorded data from the settlement sensors.

Table 2. Comparison of Instrumentation to Predicted Settlement

End of Phase I Total Foundation Settlement				
Instrument Identification	**Approximate Location**	**Instrumentation Data[a], cm (inches)**	**1-D Analyses[b], cm (inches)**	**2-D Analyses[b], cm (inches)**
S2	Centerline Phase I Dam Crest (STA 7+62 m (25+00 feet))	6.9 (2.7)	8.1 (3.2)	48.8 (19.2)
S3	30 m (100 feet) Downstream of Phase I Dam Crest (STA 9+14 m (30+00 feet))	59.2 (23.3)	73.9 (29.1)	42.4 (16.7)
S4	30 m (100 feet) Downstream of Phase I Dam Crest (STA 7+62 m (25+00 feet))	19.8 (7.8)	26.2 (10.3)	42.4 (16.7)

Notes:

a) Total recorded settlement at end of Phase I, includes bedrock and alluvium.
b) Total computed settlement in alluvium and 22 percent of total predicted consolidation settlement in bedrock.

Calibration of Elastic Modulus Based on Outlet Works Conduit Survey

The vertical alignment of the outlet works conduit was surveyed during installation and the first post-construction survey was performed in July 2007, which was about 300 days after the end of the Phase I construction. The conduit alignment elevations were designed to generally correspond to the maximum estimated foundation settlements and to provide a positive downstream slope along the entire conduit. The survey of the conduit was an optimal method to check construction elevations and to check the predicted deformation behavior of the foundation materials.

The vertical alignment of the conduit surveyed in July 2007 was compared to the computed alignment of the conduit from the two-dimensional deformation model for the Phase I dam using the laboratory value for elastic modulus. Based on analyses completed for the embankment, consolidation of the claystone under Phase I loading was estimated to be about 30 percent complete at the time of the July 2007 survey. The survey data were then adjusted to represent total anticipated settlement (consolidation at 100 percent complete). These elevations are provided on Figure 8.

The two-dimensional analysis of the outlet works conduit was re-computed, varying the elastic modulus of the claystone bedrock in the finite-element model from the initial value of 16.8 MPa (3.5 x 10^5 lb/ft^2) until the predicted settlement profile for the Phase I embankment approximated the data from the adjusted July 2007 survey. We concluded that an elastic modulus in the claystone bedrock of 23.9 MPa (5.0 x 10^5 lb/ft^2) resulted in a predicted profile that most closely matched the survey data and was adopted for design. The computed two-dimensional vertical settlement of the outlet works conduit using an elastic modulus of 23.9 MPa (5.0 x 10^5 lb/ft^2) and the survey data from July 2007 is presented on Figure 8.

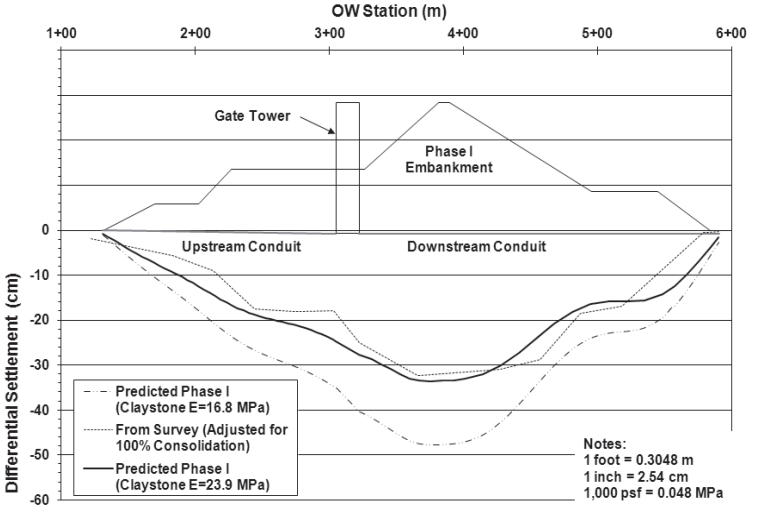

FIG 8. Comparison of Predicted and Measured Vertical Deformation for Phase I Outlet Works Conduit

Final Settlement Analyses

Final deformation analyses were completed using the adjusted elastic modulus of 23.9 MPa (5.0 x 10^5 lb/ft^2) to support design of the Phase II dam and outlet works conduit, and to confirm the adequacy of the outlet works components constructed during Phase I. The computed maximum deformations for the Phase II dam below the maximum section of the embankment and along the outlet works conduit for both the initial analyses and the final analyses are presented on Figures 9 and 10, respectively.

The revised deformations in the bedrock for the Phase II dam, using the calibrated elastic modulus values, are generally about 25 percent less than originally predicted. The predicted deformations were used to: a) compute the forces in the conduit to confirm that the previously constructed components were adequate for the applied loads, b) to design the additional Phase II components of the outlet works, and c) to design the Phase II embankment camber.

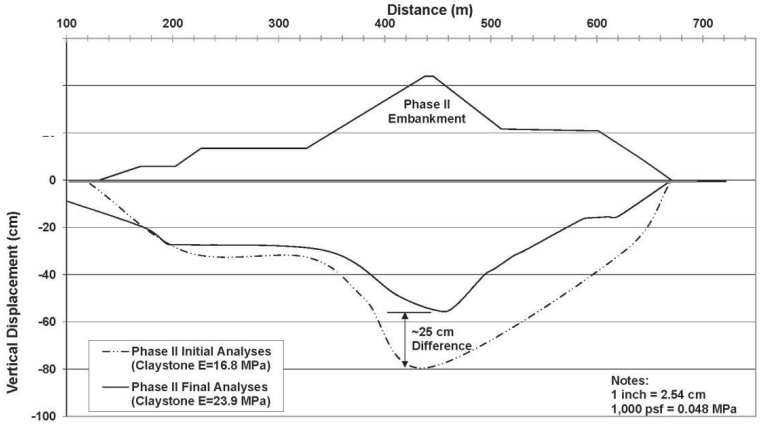

FIG 9. Predicted Phase II Embankment Deformation

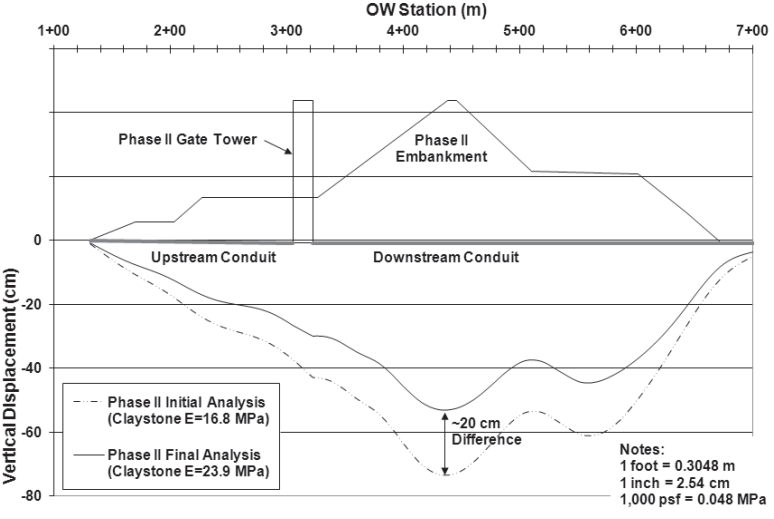

FIG 10. Predicted Phase II Outlet Works Conduit Deformation

Design Features to Accommodate Settlement

Total and long-term consolidation of the bedrock impacted design of both the embankment and the outlet works. The following features were included in the design of the project to mitigate the impacts from deformation of the bedrock.

The primary impact to design of the embankment was the amount of additional crest camber needed to accommodate bedrock settlement in addition to settlement of the embankment fill and foundation soils. Sixty one centimeters (24 inches) of camber were included at the maximum embankment section; 36 cm (14 inches) of these were included to compensate for post-construction consolidation of the bedrock foundation.

The magnitude and variable deformations of the foundation bedrock below the outlet works presented a greater design challenge than deformations below the embankment. Typically, the connections between an outlet works conduit and a gate tower are designed as rigid connections. One result of these variable deformations between the gate tower and the conduit was that the use of a typical design connection concept would not be possible because the resulting bending moment from a rigid connection would be extreme. The following elements were included in the design of the outlet works to accommodate expected short- and long-term deformation of the bedrock:

- The design elevation of the conduit included a non-uniform slope (camber) that was based on the computed deformations. The design slope was selected to maintain a positive downstream slope along the entire conduit for both the Phase I and Phase II dam. This camber should maintain the conduit in compression.
- The connections between the gate tower and the conduit were designed as a pinned connection instead of a rigid connection. The connection was designed to allow axial movement of the joint and limited rotational movement.

POST-DESIGN SETTLEMENT MONITORING

Settlement sensors continued to measure settlement and periodic outlet works conduit surveys continued to be performed throughout and after Phase II construction. The following sections present a summary of the data collected since Phase II design and compare the measured settlement to predictions.

Settlement Sensors

Settlement sensor data collected since their installation are shown on Figure 11. Data presented previously on Figure 7 were an enlargement of the early data collected from sensors S2, S3, and S4.

Sensor S1 was not considered reliable and was not used during the deformation analyses. S1 recorded episodes of almost 25 cm (10 inches) of cyclic settlement and

heave after Phase I construction and recorded accelerating heave during Phase II construction.

Data presented on Figure 11 for S2 are the raw data collected. The data presented in Figure 7 for S2 had been purposely inverted because, at the time of the Phase II deformation analyses, it appeared that the inversion was necessary to properly display a reading of settlement. Now that additional data have been collected (Figure 11), a different trend appears from the raw data. Sensor S2 measured about 25 cm (10 inches) of heave from February 2006 to August 2007, and since then has been measuring settlement. From February 2006 to July 2011, sensor S2 has measured almost no net deformation.

Measurements from sensors S3 and S4 have been following expected trends. Increased settlement has repeatedly occurred under applications of load (fill placement), and after each load application, the rate of settlement eventually lessens. Sensor S4 did record some unexplained "noise" in the summer of 2009, but has since reverted to an expected trend.

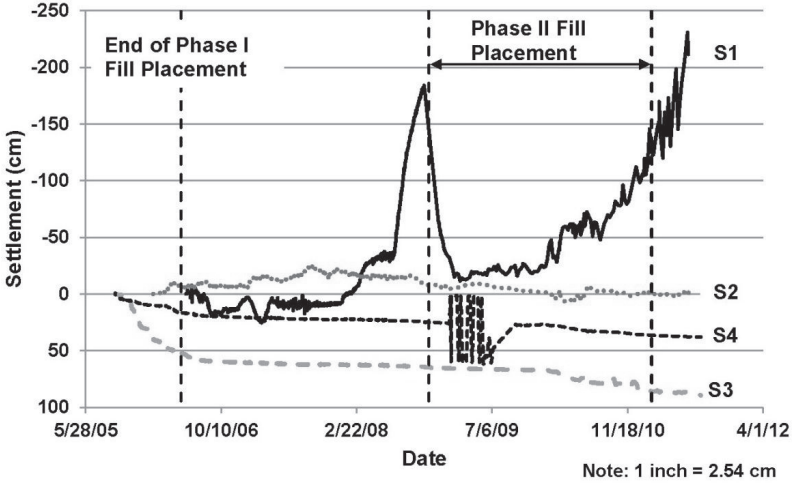

FIG 11. Settlement Sensor Data. Negative Values Represent Heave Measured by Malfunctioning Instruments

As presented previously, sensors S1 and S2 were installed entirely within bedrock and sensors S3 and S4 were installed partly in alluvium and partly in bedrock. It is not known why the two sensors installed entirely within bedrock show erratic results and the two sensors installed partly in alluvium follow expected trends. After observing the anomalous settlement data, research was performed on the reliability of hydraulic vibrating wire settlement sensors. The general result of this evaluation was that a magnetic settlement sensor would have been a more reliable sensor for a long-term application where large deformations are expected. Hydraulic vibrating wire

settlement sensors are better suited for short-term applications where large deformations are not expected because of concerns with air bubbles and other fouling in the tubing. According to data provided during construction, the claim was that air bubbles and fouling typically do not occur in tubing installed underground. However, after further evaluation, hydraulic vibrating wire settlement sensors can malfunction if large settlement occurs rapidly and the tubing becomes pinched.

The total settlement that is expected to occur in the bedrock and alluvial foundation materials at the maximum embankment section after completion of Phase I construction is about 64 to 97 cm (25 to 38 inches). This range includes settlement after Phase I construction caused by Phase I loads, settlement during Phase II construction caused by Phase II loads, and settlement after Phase II construction caused by Phase II loads. The foundation settlement that was predicted to occur between the end of Phase I construction and July 2011 was about 44.5 to 47.2 cm (17.5 to 18.6 inches), which is about 46 to 74 percent of the anticipated total settlement. During this same time period, sensors S3 and S4 recorded 36.5 and 21.7 cm (14.4 and 8.5 inches) of settlement, respectively. The predicted settlements for this time period were conservative with respect to the measured settlements; the measured settlements were about 50 to 80 percent of the predicted settlements.

Outlet Works Conduit Surveys

The elevation of the outlet works conduit alignment has been surveyed approximately monthly since July 2007. A plot of settlement over time at selected stations is shown on Figure 12. The outlet works stationing relative to the gate tower and embankment is shown on Figure 5.

Prior to Phase II construction, the settlement at each of the stations shown on Figure 12 had been similar in magnitude and in trend. Since Phase II construction, settlements at outlet works stations STA 4+42 m and 5+49 m (14+50 and 18+00 ft) have accelerated and increased relative to the settlements at STA 1+52 m and 3+81 m (5+00 and 12+50 ft). This is to be expected, because all of the additional Phase II fill placement occurred downstream (downstation) of the Phase I crest (Figure 5).

Figure 12 also illustrates frequent spikes and dips within the settlement trend, which generally occurred at the same date for each station. These anomalies were likely caused by consistent surveying errors on various dates.

Table 4 provides a comparison between the actual settlement at the different stations and the settlement that was estimated to occur in bedrock throughout the period of the conduit surveys. The estimated settlements agree well and were conservative with respect to the measured settlements. In general, the estimated settlements are up to about 5.1 cm (2.0 inches) greater or 100 percent more than the measured settlements.

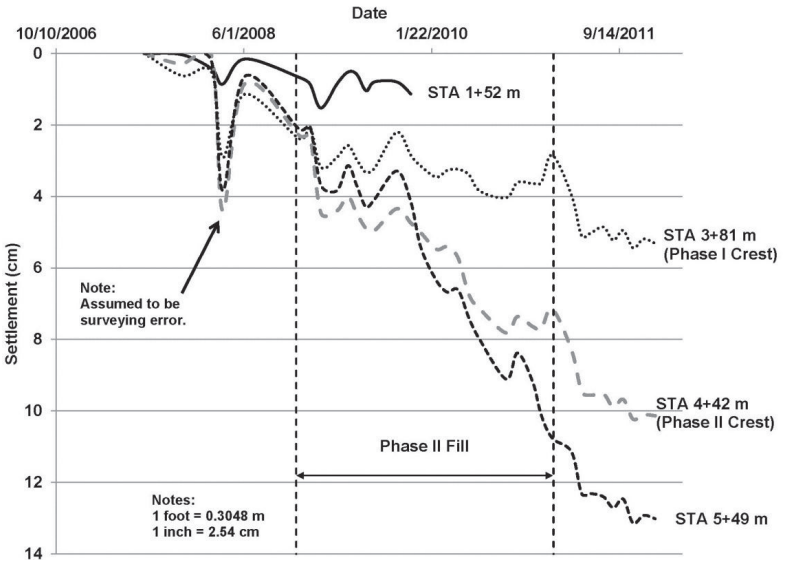

FIG 12. Outlet Works Conduit Settlement Over Time. Settlement is Relative to the Conduit Elevation from July 2007

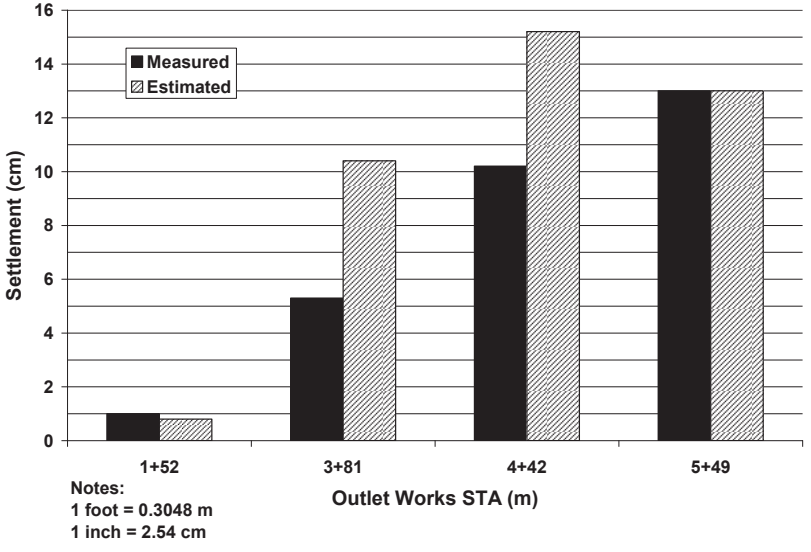

FIG 13. Settlement of Outlet Works Conduit. Settlements Are for the Period of July 2007 to January 2012, Except for STA 1+52 m (5+00 ft), Which is July 2007 to February 2010

CONCLUSIONS

Evaluation of deformation is required to support design of any type of dam. However, caution needs to be used when analyses are based on an assumption that deformation of bedrock does not need to be considered. Bedrock settlement can be a significant issue for medium to large embankment dams and the potential deformation of the bedrock should be evaluated early in design. This paper described deformation analyses that were completed to evaluate bedrock settlement to support design of a large embankment dam constructed in two phases and how settlement of the soft claystone bedrock impacted the design of the project. Outlet works conduit surveys were used to calibrate material properties and assist in dam deformation analyses. The initial development of modulus provided a value that generated a safe and conservative design; however, using survey data to calibrate the modulus value resulted in a more value-engineered design. Predicted deformations during and after construction were conservative and have been similar to settlement measured by settlement sensors and outlet works surveys. Two of the four settlement sensors installed during Phase I do not appear to be providing meaningful results, and based on our evaluation, we would recommend that magnetic settlement sensors be used for future projects where it is not possible to replace the hydraulic vibrating wire instruments and where large settlements are expected. Soft, geologically-young claystone bedrock exists in many parts of Colorado and it is important early in the design of a new dam to identify what types of data are needed to investigate not only the strength but also the deformation properties of the foundation bedrock.

REFERENCES

Huzjak, R.J. and Prochaska, A.B. (2009). "Settlement of embankment dams – don't forget about the bedrock." *Proc., Association of State Dam Safety Officials, Dam Safety Conference* (CD-ROM), ASDSO, Lexington, KY.

Santi, P.M. and Doyle, B.C. (1997). "The locations and engineering characteristics of weak rock in the U.S." In Santi, P.M. and Shakoor, A., eds., *Characterization of Weak and Weathered Rock Masses, Association of Engineering Geologists Special Publication #9:* Association of Engineering Geologists, Sudbury, MA, pp. 1-22.

Tweto, O. (1979). "Geologic map of Colorado." U.S. Geological Survey.

Drilled Shaft Responses under Pre-Torsion Lateral or Vertical Loads

Brian Volmer[1] and Nien-Yin Chang[2], Ph.D., P.E., M.ASCE

[1] Student of Civil Engineering, University of Colorado Denver, 1200 Larimer Street, Denver, Colorado, 80204; brian.volmer@ucdenver.edu
[2] Professor, University of Colorado Denver, Department of Civil Engineering, 1200 Larimer Street, Denver, Colorado, 80204; Nien.Chang@ucdenver.edu

ABSTRACT: Drilled shafts are frequently designed with single load consideration. Insufficient research attention has been rendered to the effects of load sequence under combined loading (Abdel-Rahman and Achmusand, 2006). The effects of load sequence under combined loading on the performance and design capacity of drilled shafts are important, however, and warrant focused research consideration. Over the last decade and a half, the University of Colorado Denver (UCD) has devoted considerable research effort in deep foundations, driven piles, and drilled shafts, including the subject matter addressed in this paper (Volmer, 2011).

Volmer (2011) performed a study on the effects of combined loading relative to the torsional response of drilled shafts, using a developing nonlinear finite element analysis (FEA) program, SSI3D, for both cohesive and cohesionless soils. This study finds the influences of combined loading to be significant in some cases and highly dependent upon the soil type.

These research findings, in terms displacement and capacities, aim at providing scientific input for the service and strength limits in load resistance factor design (LRFD) in the current AASHTO Bridge Design Specifications.

INTRODUCTION

Deep foundations are used in supporting critical infrastructures, like bridges, hospitals, etc. and, for public safety during their design lives, have to be designed to resist the most critical loading combination of all potential load types. To date few studies are available on the effects of combined loading. Loading on deep foundations can be complex and involves loads from all degrees of freedom resulting from artificial loads like machine vibration, vehicular loading, etc. and natural loads, like those from earthquake, earth pressures, wind and waves, etc. Recent UCD studies involved the combination of loads, including vertical, lateral, overturning, and torsion. The results of these studies reflect important effects of combined loading and the sequence of load applications, which should be considered in deep foundation design.

In fact, Gonzales (2010) performed a numerical study of drilled shafts under combined vertical-lateral and lateral-vertical loading. The study demonstrated that the responses of deep foundations are dependent upon the magnitude and staging of loading.

Soon afterward, Volmer (2011) performed a numerical study of the torsional

response of drilled shafts subjected to prior and sustained application of lateral or vertical loading in both sand and clay. It was found that the soil type is a very important factor in the response of shafts under combined loading.

NUMERICAL ANALYSES

Computer Code and Model Geometry

To study the effects of combined loading relative to the torsional response of drilled shafts, the newly developed non-linear FEA code SSI-3D (Volmer, 2011; Nghiem, 2009) was used. This code is quite capable, well verified, and well validated against full-scale testing as shown by Nghiem (2009).

Two hypothetical cases designed to be typically representative of those cases encountered in reality were created in SSI-3D. One consisted of a 10-meter-long, 1-meter-diameter drilled shaft in a typical cohesive (clay) soil and the other consisted of the same configuration t in a typical cohesionless (sand) soil.

Figure 1 shows the 10-m-long, 1-m-diameter drilled shaft embedded in 9 m of soil (either sand or clay). To avoid boundary effects, the model boundaries were set at 9 m from the pile center in the radial direction and 9 m beyond the pile tip. These boundary distances from the modeled pile were initially based upon those used for model validations (Nghiem, 2009). And the fully deformed models did not indicate that boundary effects at these distances were of concern. Three dimensional (3D) solid elements were preferred for the analyses performed and used to model the soils and shaft.

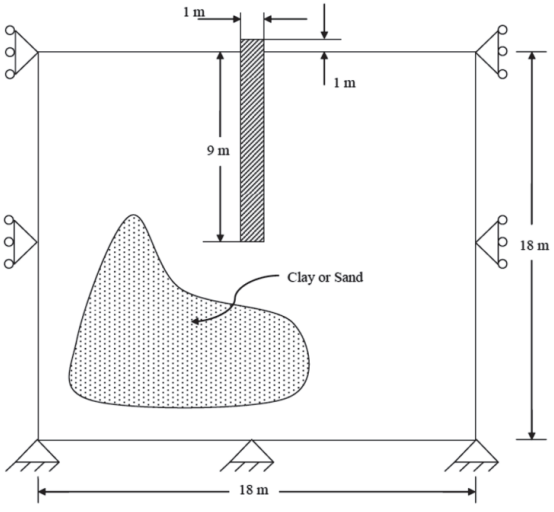

FIG. 1. Geometric Layout of Research Model

Material Models and Properties

While more sophisticated constitutive models are available in the SSI-3D program for the static analysis of drilled shaft behavior, relatively simple models were used. The reinforced concrete shafts were modeled with linear elasticity, while the soil and pile-soil interfaces were modeled with Mohr-Coulomb. It is believed that there is no need for the more complex and increasingly popular material models in that SSI-3D is well validated against full-scale testing using these models.

The relevant material parameters used are shown in Table 1. As may be seen, the values chosen may be considered somewhat typical of reinforced concrete, clay, and sand materials from such sources as the American Concrete Institute (2008), Bolton (1986), McCarthy (2007), and Kulhawy (1990). The clay was created to be representative normally consolidated (NC) material in undrained conditions. Knowing, however, that undrained cohesion is a function of effective stress, the undrained cohesion (c_u) is assumed to increase linearly with depth from 35.9 kPa to 68.9 kPa, as shown in Table 1, in accordance with that given by Ladd (1974). The sand was created as a typical and homogeneous cohesionless soil.

Table 1. Material Parameters (Volmer, 2011)

Material Parameters							
				Strength Parameters			
Material	Unit Weight (γ) kg/m^3	Young's Modulus (E) Mpa	Poisson's Ratio (ν)	Cohesion (c_u) kPa	Friction Angle (φ) deg.	Dilatancy Angle (ψ) deg.	Lateral Earth Pressure Coefficient (K_0)
Reinforced Concrete	[-]	27600	0.2	[-]	[-]	[-]	[-]
Clay	1920	7.18	0.45	35.9 68.9	0	0	0.9
Sand	1890	33.5	0.3	0	35	2.5	0.5

LOADING SCHEMES AND ANALYSIS RESULTS

In order to investigate the effects of lateral and vertical loading on the torsional response of shafts, one load type, either lateral or vertical, was applied until a certain displacement, as a percentage of 2.5 cm, was reached. This load was sustained while torsion was applied. Figures 2 through 9 show the results of this analysis.

Lateral then Torsional Loading Response in NC Clay

Figure 2 shows the torsion versus rotation angle curves of the modeled drilled shaft in clay under different pre-torsion lateral loads causing 25 percent (0.25 L-T), 50 percent (0.5 L-T), and 100 percent (1 L-T) of 2.5 cm pile top displacement. As is readily seen, these curves are nearly identical to the curve under torsion alone (Pure T). This implies the negligible effect of the pre-torsion lateral loading on the torsional response of drilled shafts in NC clay.

Vertical Then Torsional Loading Response in NC Clay

Figure 3 shows the torsion versus rotation angle curves of the drilled shaft in NC clay under different pre-torsion vertical loads causing 25, 50 and 100 percent of 2.5

cm pile top vertical displacement. As is seen, these responses are quite different from the pure torsional response. The difference increases with an increase in the vertical pre-torsion load. And the torsional response after 2.5 cm of vertical deformation is quite different from the pure torsional response. This implies the significant effect of the pre-torsional vertical loads on the torsional response of drilled shafts in NC clay.

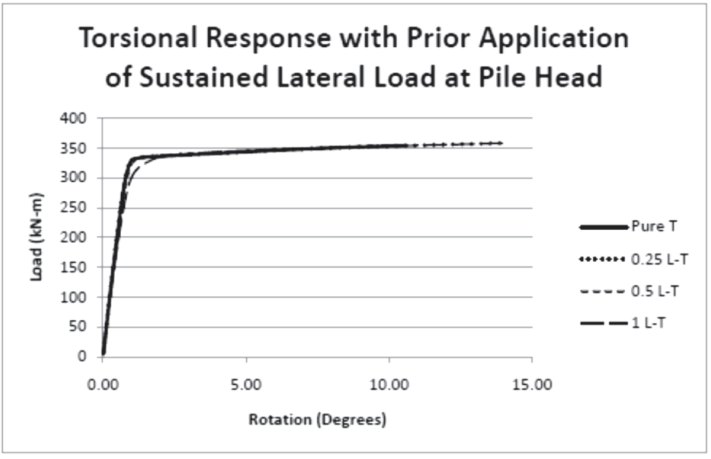

FIG. 2. Lateral then Torsional Loading in NC Clay (Volmer, 2011)

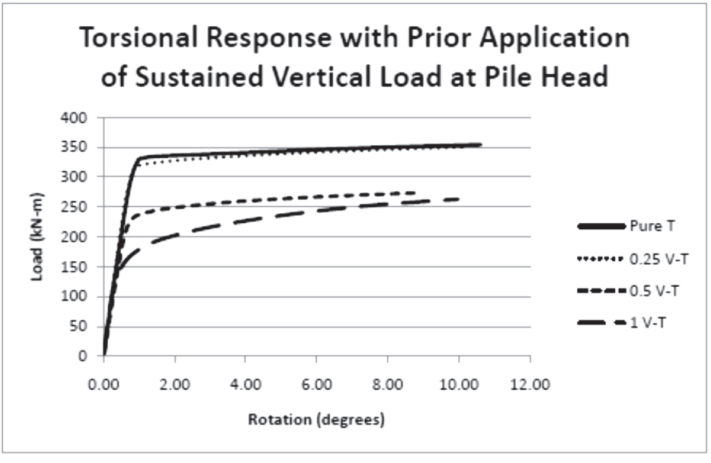

FIG. 3. Vertical then Torsional Loading in NC Clay (Volmer, 2011)

Lateral then Torsional Loading Response in Sand

Figure 4 shows a much stronger torsional response, when the drilled shaft in sand is subjected to lateral load before the application of torsion. Soil dilatancy, more specifically dilation rather than compression, may explain this behavior. The dilation of sand under lateral load causes normal stress to increase under high confinement and, thus, strengthen the torsional response. Here it is important to mention that difficulties in attaining convergence with the developing FEA program made it difficult to maintain the series of 25, 50, and 100 percent of 2.5 cm prior lateral displacement for this case. The "Lax L-T" curve corresponds to a pre-torsional lateral displacement of approximately 40 percent of 2.5 cm with relaxed convergence. The un-relaxed or rather more accurate solution to the lateral-torsional response after prior application of lateral loading is believed to be significantly strengthened beyond what is shown for this case.

Vertical then Torsional Loading in Sand

Figure 5 shows the torsional responses of drilled shaft in sand under pre-torsion vertical loads at 25, 50, and 100 percent of 2.5 cm vertical displacements. Here the differences are less significant.

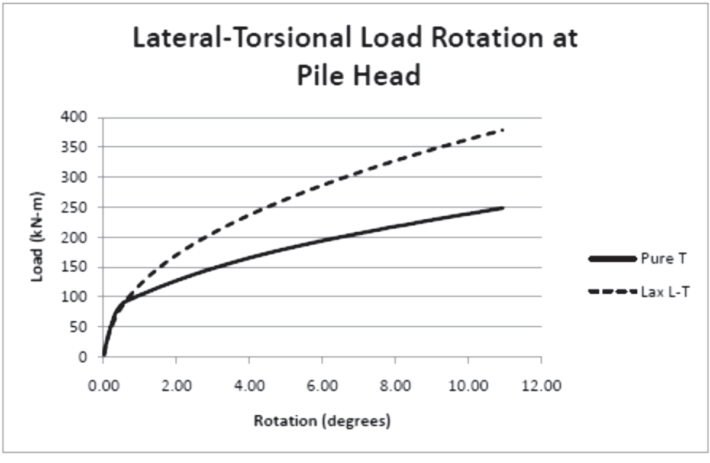

FIG. 4. Lateral then Torsional Loading in Sand (Volmer, 2011)

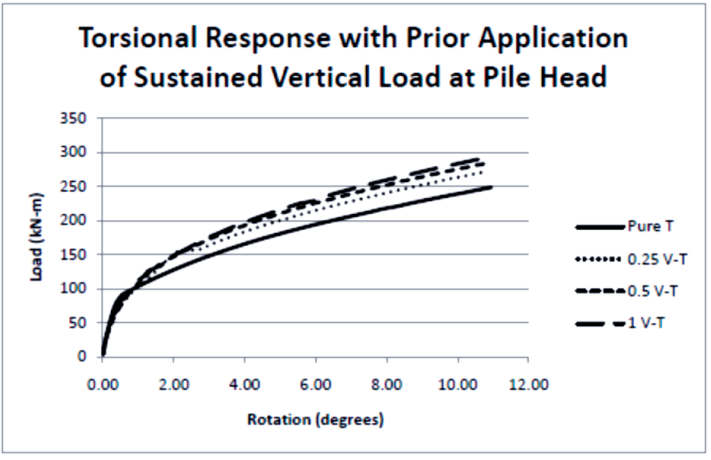

FIG. 5. Vertical then Torsional Loading in Sand (Volmer, 2011)

Lateral Displacement Due to Torsion in NC Clay

Figure 6 shows the lateral displacement of the drilled shaft in NC clay due to the addition of torsional load. That is, the lateral displacement due to the increasing torsional load after the initial application of sustained lateral loading. It is interesting to show that this curve somewhat represents what was shown in the corresponding Figure 2, whereas torsion increases, very little additional lateral displacement takes place until it reaches the yield point. At the yield point, a sudden increase in lateral displacement occurs for a small increment of torsion. As shown in Figure 2, this yielding point is fairly constant for various amounts of sustained lateral loads.

Vertical Displacement Due to Torsion in NC Clay

Figure 7 shows the vertical displacement of the drilled shaft in NC clay due to the addition of torsional load. It is interesting to show that this curve somewhat represents that shown in corresponding Figure 3, whereas torsion increases, very little additional vertical displacement takes place until it reaches a yielding point when a sudden increase in vertical displacement occurs for a small increment of torsion. The yielding torsion load decreases with the increase in vertical displacement and the rate of vertical displacement increases with the amount of pre-imposed vertical displacement.

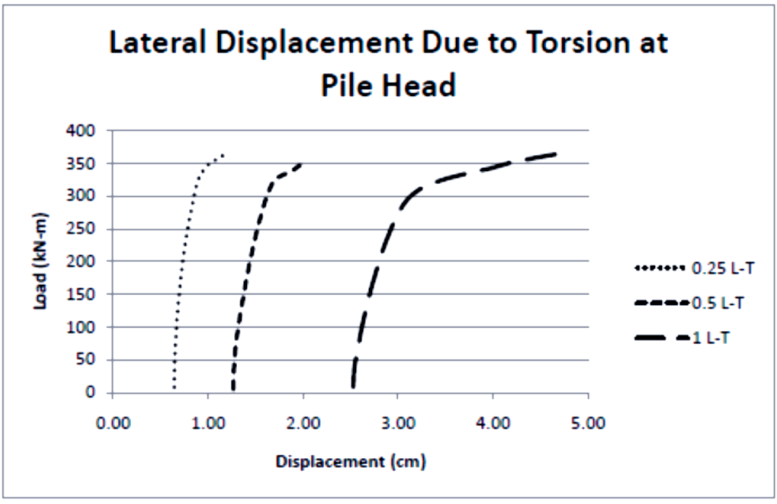

FIG. 6. Lateral Displacement Due to Torsion in NC Clay (Volmer, 2011)

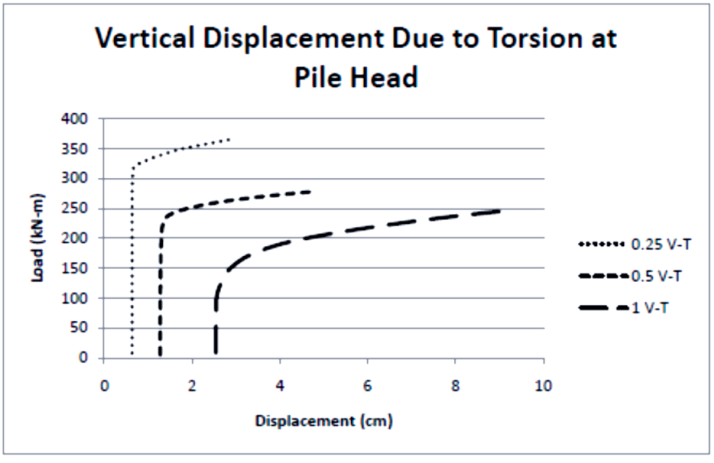

FIG. 7. Vertical Displacement Due to Torsion in NC Clay (Volmer, 2011)

Lateral Displacement Due to Torsion in Sand

Figure 8 shows that the torsion versus lateral displacement curve is somewhat soft overall for the drilled shaft in sand. This is also true for the corresponding torsion versus rotation curve of Figure 4. Unfortunately, because of the numerical difficulties aforementioned, little else may be reasonably learned from this specific curve.

Vertical Displacement Due to Torsion in Sand

Figure 9 shows that for the drilled shaft in sand, the torsion versus vertical displacement curve is again somewhat representative of the corresponding torsion versus rotation curve of Figure 5. In comparison with that of NC clay, the yielding torsion in sand is much smaller and is about the same for all cases with different initial vertical displacements. And the torsion required to cause additional vertical displacement in sand is much larger.

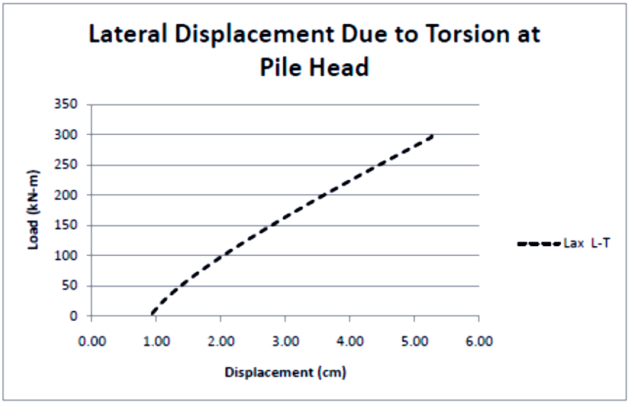

FIG. 8. Lateral Displacement Due to Torsion in Sand (Volmer, 2011)

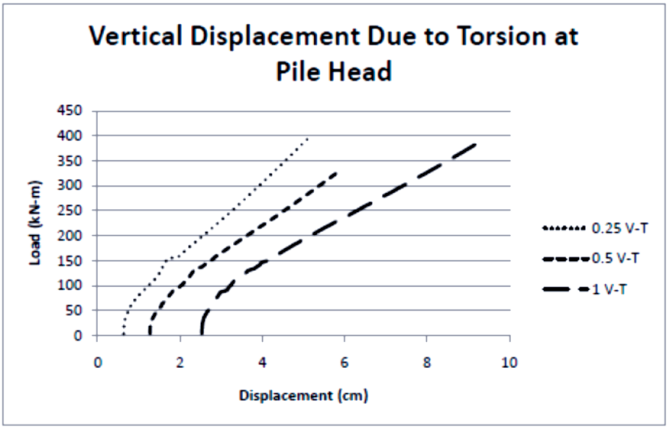

FIG. 9. Vertical Displacement Due to Torsion in Sand (Volmer, 2011)

DISCUSSION OF NUMERICAL RESULTS

Clayey Foundation Soils

Analysis of the results shows that combined loading significantly influences the behavior and capacities of drilled shafts, particularly when the foundation soil is NC clay. When a lateral load is applied ahead of torsion, the influence of the combined

lateral-torsional loading is insignificant, as shown in Figure 2. However, the torsional stiffness and capacities are significantly decreased when a vertical load is applied ahead of torsion for vertical-torsional loading, as shown in Figure 3. Furthermore, the yielding torsion in NC clay was found to decrease with an increase in vertical load for the combined vertical-torsional loading and the rate of vertical displacement increased with the magnitude of pre-imposed vertical displacement as shown in Figure 7.

Sandy Foundation Soil

The pre-imposed lateral load in sand significantly stiffens the torsion versus rotation response as shown in Figure 4. This is believed to be caused by the dilation of sand in the front of the pile under lateral loading. Similarly, the sand dilation might have contributed to the slight strengthening of the torsion versus rotation relationship as shown in Figure 5 for combined vertical-torsional loading.

When a vertical load is pre-imposed, the drilled shaft in sand experiences an additional vertical displacement under torsion, as shown in Figure 9. This indicates that there exists a coupled relationship between vertical and torsional behaviors of drilled shafts in sand under combined vertical-torsional loading.

The above observations are summarized in Tables 2 and 3. A significant mutual influence indicates the coupling effects when the drilled shaft in sand is under combined loading. In the following tables, (θ) signifies rotation, (x) signifies lateral displacement, and (z) denotes vertical displacement.

Table 2. Drilled Shaft Behavior under Combined Loads in NC Clay

Response to Combined Lateral-Torsional and Vertical-Torsional Loading		
Loading Sequence		**Drilled Shaft in NC Clay**
Lateral then Torsion		
	T vs θ Response	Negligible Effect
	T vs x Response	Stiff Behavior Until Yielding When Large Lateral Displacements are Given for a Small Increase in Torsion
Vertical then Torsion		
	T vs θ Response	Significant Reduction
	T vs z Response	Virtually No Effect Until Torsional Yielding When Large Vertical Displacements are Given for a Small Increase in Torsion

Table 3. Drilled Shaft Behavior under Combined Loads in Sand

Loading Sequence		Drilled Shaft in Sand
Lateral then Torsion		
	T vs θ Response	Significant Increase
	T vs x Response	Soft Response Overall. Lateral Displacements Increase with Increasing Load.
Vertical then Torsion		
	T vs θ Response	Slight Increase
	T vs z Response	Stiff Behavior Until Yielding When a Somewhat Softer Response is Witnessed and Vertical Displacements Increase with Increasing Torsion.

CONCLUSIONS

Drilled shaft behavior was numerically evaluated using a non-linear 3-D finite element computer code. Four main cases were analyzed to investigate the drilled shaft behavior under various combined loads, including lateral, vertical, and torsional loads, with different loading sequences and in two different foundation soil types (NC clay and sand). Analysis findings are summarized as follows:

- Combined loading and loading sequence can significantly influence the drilled shaft behaviors in terms of load and deformation relation and load capacity. The influence can be different with drilled shafts in NC clay and sand.
- Coupling effects exist for different load types, while the strength of coupling varies. Drilled shaft behavior is generally nonlinear and the superposition principle might not be applicable.

- Comprehensive study is needed for the full understanding of the drilled shaft behavior under combined loads with different loading sequences. Determinations of both displacements and bearing capacities are needed to meet the contemporary trend of using load and resistance factor design.

Future plans for additional research into the topic of this paper are being made. This paper presents some theoretical deep foundation behavior under combined loading. Unfortunately, it is currently difficult to verify these numerically developed responses, because few large scale physical observations exist. Hopefully, the authors' research plans for experimentation and further numerical analyses will soon be able to give a better picture of overall deep foundation response under combined loading.

REFERENCES

Abdel-Rahman, K., Achmusand, M. (2006). "Numerical modeling of the combined axial and lateral loading of vertical piles." *Sixth European Conference on Numerical Methods in Geotechnical Engineering*, Austria: 575-581.

American Concrete Institute. (2008). "Building Code and Commentary." (ACI

318-08), *American Concrete Institute*.
Bolton, M. D. (1986). "The strength and dilatancy of sands." *Geotechnique* 36, No. 1: 65-78.
Gonzalez, Cesar (2010). "Drilled shafts under combined axial and lateral loads." *Master's Thesis*, University of Colorado Denver.
Kulhawy, F. H., and P. W. Mayne. (1990). "Manual on Estimating Soil Properties for Foundation Design." Ithaca, New York: Hollister Hall.
Ladd, C. C. (1974) "New design procedure for stability of soft clay." *Journal of the Geotechnical Engineering Division, ASCE* 100, GT7: 763-786.
McCarthy, D. F. (2007). "Essentials of Soil Mechanics and Foundations." 7th ed. New Jersey: Pearson Prentice Hall.
Nghiem, H. M. (2009). "Soil-pile-structure interaction effects on high rises under seismic shaking." *Ph. D. diss.*, University of Colorado Denver.
Volmer, B. P., (2011). "A study of static torsional loading on drilled shafts." *Master's Thesis*, University of Colorado Denver.

Behavior of Full-Scale Energy Foundations in Denver, Colorado

Kyle D. Murphy[1], S.M. ASCE and John S. McCartney[2], Ph.D., P.E., M. ASCE

[1]Graduate Research Assistant, University of Colorado Boulder, Dept. of Civil, Environmental, and Arch. Eng., UCB 428 Boulder, CO 80309; kyle.murphy@Colorado.edu.
[2]Assistant Professor and Barry Faculty Fellow, University of Colorado Boulder, Dept. of Civil, Env., and Arch. Eng., UCB 428 Boulder, CO 80309; john.mccartney@colorado.edu.

ABSTRACT: This paper focuses on the thermo-mechanical response of two energy foundations installed at the new Denver Housing Authority Senior Living Facility in Denver, Colorado. Heat exchanger tubes within the foundations are coupled together with a conventional ground source heat pump system to evaluate the heat exchange response of the foundations as well as any thermo-mechanical effects. The thermal strains measured during heat exchange are within acceptable limits, and the temperature changes within the foundations appear to be stable during heating and cooling operations. The results indicate that energy foundations can sustainably provide the base heating and cooling load for buildings, and that they have strong potential for application in new buildings in Colorado with little added cost.

INTRODUCTION

Energy foundations are drilled shafts that incorporate ground-source heat exchange elements, which can be used to transfer heat to or from the ground to the building (Brandl 2006; McCartney 2011). Ground-source heat exchange systems exploit the relatively constant temperature of the ground to improve the efficiency of heat pump systems for heating and cooling of buildings. Traditional geothermal systems typically require a series of small-diameter, deep boreholes, which are installed outside of the building footprint. The additional drilling costs of these boreholes can be prohibitive (Hughes 2008). To counter this problem heat exchange elements can be incorporated into deep foundation elements, which are already being installed, to avoid this additional installation cost. Although energy foundations may not provide the full amount of energy required to heat and cool residential and commercial buildings, they may provide sufficient heat exchange to cover the base heating and cooling load for the building, which is typically 10 to 20 percent of the peak heating or cooling load. In this case, a conventional heating or cooling system would not be required except during peak heating or cooling events.

To better understand the behavior of energy foundations during building operation, this study presents the results from a pair of full-scale energy foundations installed in a building in Denver, Colorado. The issues under investigation in this paper include the typical temperature variations within the foundation during heating and cooling operations along with the thermally-induced strain distributions.

BACKGROUND

As a structural element is heated and cooled, thermal strains are superimposed onto already existing mechanical strains. Limited knowledge has been collected regarding thermo-mechanical strains in energy foundations under thermal loading conditions. Several experimental studies have been performed in the laboratory using centrifuge-scale models of energy foundations in order to identify mechanisms of soil-structure interaction in energy foundations (McCartney et al. 2010; McCartney and Rosenberg 2011; Stewart and McCartney 2012). Several full-scale energy foundations have been installed throughout Europe and Asia, although there have only been two well-documented thermo-mechanical tests on full-scale foundations to date (Laloui et al. 2006; Bourne-Webb et al. 2009). In these studies, proof load tests along with heating/cooling tests were used to evaluate the thermo-mechanical stress-strain response in the foundations. Data from these tests were used to develop soil-structure interaction design tools (Knellwolf et al. 2011) Other studies on full-scale foundations included evaluations of the efficiency of energy extraction (Ooka et al. 2007; Wood et al. 2009; Adam and Markiewicz 2009) and system thermal conductivity tests (Ozudogru et al. 2012). However, these studies did not evaluate the performance of energy foundations under typical building operation conditions.

FOUNDATION SYSTEM AND INSTRUMENTATION DESCRIPTION

Building Description

Two of the sixty drilled shaft foundations installed as part of the construction of the new Denver Housing Authority Senior Residential Facility were converted into energy foundations. The goal of this conversion is to demonstrate the feasibility of this new technological approach from the perspectives of constructability, thermal performance, and thermo-mechanical performance. Construction of this eight-story building started in the summer of 2010 and lasted through December 2011. A plan view of the foundation layout is shown in Fig. 1.

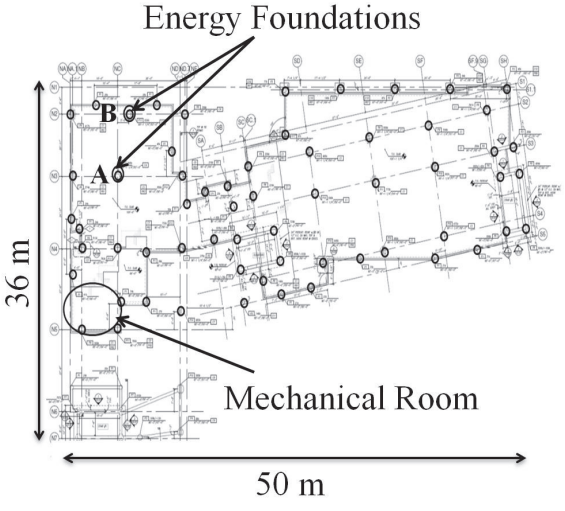

FIG. 1. Plan view of foundation layout noting the energy foundation locations

Subsurface Conditions

Site characterization was performed by Koechlein Consulting Engineers, Inc. in April, 2010. A series of 10 exploratory borings extending to depths ranging from 8.8 m (29 ft) to 11 m (36 ft) below finished grade was performed throughout the site. The conditions encountered in each of the borings were similar, with a typical profile shown in Fig. 2. Fill extends from grade to a depth of approximately 3 m (9.8 ft) and consists of slightly moist, medium dense, clayey sand with gravel. Beneath the fill, non-expansive, medium dense, silty, sand and gravel extended to a depth of approximately 7.6 m (25 ft) below grade. Following the sands and gravels, to the maximum depth explored of 11 m (36 ft), the subsurface conditions consisted of hard sandy claystone bedrock from the Denver formation. Perched ground water was encountered at three of the ten boreholes at depths ranging from 6.4 m (21 ft) to 8.2 m (27 ft), although these borings were not in the vicinity of the energy foundation locations. Because of the potential for caving during drilling through the overburden and possible perched ground water conditions, a cased-hole method was chosen for installation of the drilled shaft foundations at the site.

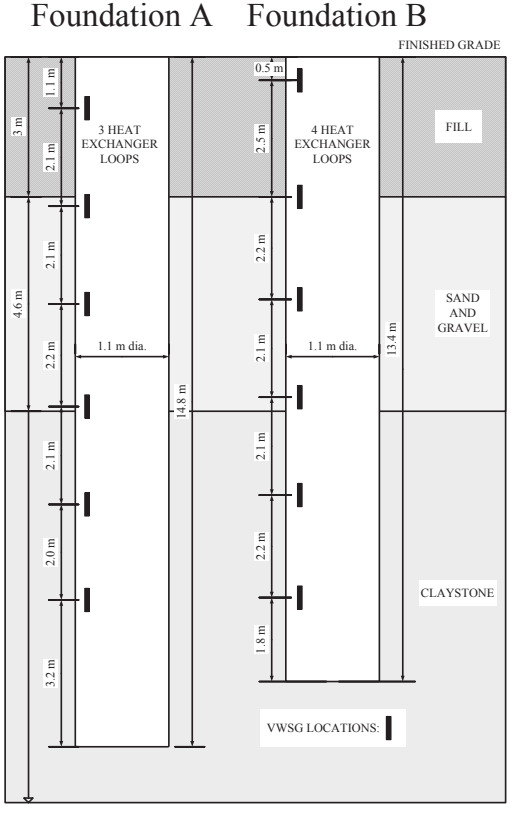

FIG. 2. Soil stratigraphy and foundation instrumentation layout

Energy Foundation System

The locations of the two energy foundations evaluated in this study are shown in Fig. 1. Foundation A is located below an interior column while Foundation B is located directly under an exterior wall. Foundations A and B are both 1.1 m (42 in) in diameter and extend to depths of 14.8 m (48.7 ft), and 13.4 m (44 ft) respectively, and are bearing in the Denver formation, as shown in Fig. 2. The foundations at the site functioned as rock-socketed, end-bearing elements in the bedrock as shown in Fig. 2. Foundation A is expected to carry a load of 3.84 MN (865 kips) and Foundation B is expected to carry a load of 3.65 MN (820 kips). Although the rock socket for Foundation B is shorter than that of Foundation A because of difficulty in drilling in the wet claystone, both are within their design depth tolerance. Each shaft consists of a full-length reinforcing cage 0.91 m (36 in) in diameter with nine #7 vertical reinforcing bars tied to #3 lateral reinforcing hoops spaced 0.36 m (14 in) on center.

The energy foundations were coupled with a traditional deep borehole geothermal system which was already being installed to provide heating and cooling for the building, in order to demonstrate the feasibility of energy foundations. The heat exchanger system in each energy foundation consists of 4.4 cm (1.75 in) diameter polyethylene tubing attached to the inside of the reinforcing cages. Foundation A contains a total of 82.3 linear m (270 linear ft) of tubing configured into three loops running the length of the reinforcing cage, as shown in Fig. 3(a). Similarly, Foundation B contains of a total of 109.7 linear m (360 linear ft) of polyethylene tubing arranged in four loops running the length of the reinforcing cage, shown in Fig. 3(b).

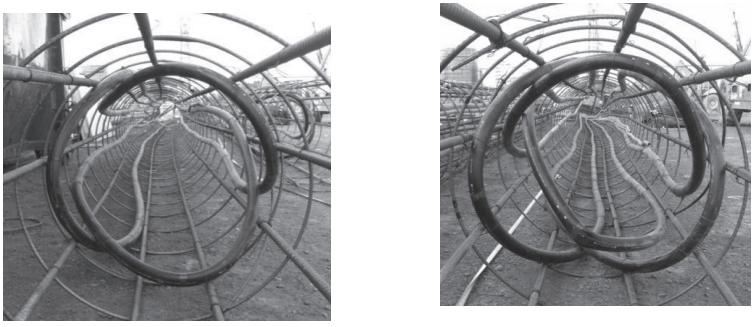

(a) **(b)**

FIG. 3. Heat exchanger tubing attached to reinforcing cages: (a) Foundation A, (b) Foundation B

The heat exchanger tubing was attached to the interior of the reinforcing cage using wire ties connected at every other hoop along the length of the reinforcing cage. The heat exchanger tubing was routed along the inside perimeter of the reinforcing cage to avoid crossing the diameter of the cage, which could block concrete flow or cause segregation of concrete. Equal angular spacing of the tubing was maintained to ensure relatively uniform temperature along the circumference of the shafts. The tubing was installed away from the vertical reinforcement to ensure an adequate bond between the concrete and reinforcement and to ensure good contact between the concrete and the tubing itself. The supply and return lines for each loop were arranged on opposite sides of the reinforcing cage to reduce thermal short-circuiting, which occurs when

heat flows directly from the inlet of the tube to the outlet of the tube before the fluid has circulated through the entire foundation.

Assuming 152 linear m (499 linear ft) of heat exchanger tubing are required to supply 1 thermal ton (3.5 kW or 12000 BTU/hr) (McCartney et al. 2010), Foundation A is expected to be able to supply 0.54 thermal tons (1.89 kW) and Foundation B is expected to be able to supply 0.71 thermal tons (2.49 kW). The impact of the number of heat exchange loops in a foundation has not been quantified. Long-term evaluation of the data from this project may help ascertain if the greater length of heat exchanger tubing in Foundation B leads to the expected increase in heat exchange. A thermal ton is the heat which must be exchanged over time to cool or heat approximately 120 m^2 (250 ft^2) of floor space. If all 60 foundations shown in Fig. 1 had been converted to energy foundations having 3 loops, and the heat exchanger loops extend to a depth of 13.7 m (45 ft) in the foundations, the energy foundation system should be able to supply up to 32 thermal tons (112 kW). This is close to half the required peak thermal load for the building of 75 thermal tons (263 kW). If only a single loop were installed in each foundation, the length of heat exchanger tubing would still be able to supply 10.5 thermal tons (37 kW), which is close to the base thermal load for the building.

Primary Ground-Source Heat Pump System

The primary ground-source heat pump (GSHP) system into which the two energy foundations were integrated consists of a total of 40 boreholes outside of the building footprint, each extending to depths of 143.3 m (470 ft) below grade. Each 100 mm (4 in) diameter borehole contains a heat exchanger loop composed of 44 mm (1.75 in) diameter polyethylene tubing formed in a U-shape extending to the bottom of the borehole. After the installation of the U-tube, the borehole is backfilled with sand-bentonite grout. The network of borehole heat exchangers is capable of providing approximately 75 thermal tons (263.5 kW) to the heat pump. To absorb this thermal load, the heat pump was designed to circulate a supply line fluid temperature through the borehole network of 32.2 °C (90 °F) during cooling operations or 1.7 °C (35 °F) during heating operations. The fluid within the heat exchange system consists of a 10 percent methanol to water mixture to prevent freezing during cooling operations. The supply and return lines from the borehole field are connected through a set of two manifolds that run to the inlet and outlet lines of the heat pump. The supply and return lines for each of the energy foundations were also connected to the manifolds for the ground-source heat pump. However, in order to avoid preferential flow through the foundations (which are much shorter than the deep boreholes), ball valves were used to restrict the flow of heat exchanger fluid to the foundations to approximately 50 percent of the flow going through the borehole heat exchangers.

Instrumentation

An instrumentation system was incorporated into the two foundations to monitor the distributions of temperature and axial strain with depth, as well as the supply and return temperatures of the heat exchanger fluid. Six vibrating wire concrete-embedment strain gauges were installed in each energy foundation at the locations shown in Fig. 2. The concrete embedment vibrating wire strain gauges (VWSG) (Model 52640299 from Slope Indicator of Mukilteo, WA) were oriented longitudinally and attached to the lateral reinforcing hoops then cast in concrete during construction. The VWSGs were positioned at depths within the shaft so that the cumulative strain distribution throughout the entire shaft length could be characterized. Each VWSG contained a thermistor to monitor temperature in the concrete at each

sensor location. Cables from each sensor were routed from the energy foundations to the mechanical room prior to casting of the floor slab. A Geokon, Inc datalogger (Model 8002-16 LC-2×16) was used to record data hourly from December 29, 2011 to April 18, 2012. During installation, a VWSG located at 3.2 m (10.5 ft) below grade in Foundation A was damaged. Although the VWSG at this depth did not function, the corresponding thermistor remained operational.

In addition to the instrumentation in the foundations, four pipe-plug thermocouples were installed in the plumbing manifold to record inlet and outlet fluid temperatures for each of the two energy foundations. Fluid temperature measurements were recorded every five minutes using Lascar EL-USB-TC data loggers to capture the intermittent and long-term operation of the ground source heat pump system.

RESULTS

Thermal Behavior

Seasonal variations in ground temperature beneath the building were characterized prior to operation of the GSHP system, as the foundations were installed in October 2010 but the heat pump was not fully operational until March 2012. Typical temperature profiles at different times throughout the year shown in Fig. 4 indicate a decrease in seasonal variability of temperature with increasing depth and a relatively constant ground temperature below a depth of 6 m (20 ft), which is consistent with observations of Moel et al. (2010). Foundation A exhibited less seasonal variability due to the location within the building footprint and was relatively insulated by the concrete floor slab. Foundation B was located at the outer edge of the building and consequently the temperature in the upper portion of the foundation was more susceptible to fluctuations in outside ambient air temperature. These observations demonstrate that ground temperatures in the winter months will be warmer than surface air temperatures and can be used as a source of heat. Conversely, the subsurface ground can be used as a heat sink in warm months when ground temperatures are lower than surface air temperatures.

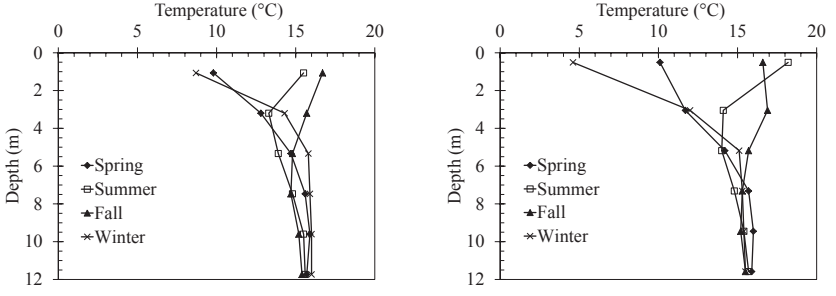

(a) **(b)**

FIG. 4. Seasonal ground temperature fluctuations measured after installation of the foundation but before operation: (a) Foundation A, (b) Foundation B

The supply and return line fluid temperatures were monitored over the duration of the study using pipe-plug thermocouples installed on the inlet and outlet heat exchanger tubes for each of the two energy foundations. The fluid temperatures are

shown in Figs. 5(a) and 5(b) for Foundations A and B, respectively. The difference in inlet and outlet temperatures, $\Delta T_{out\text{-}in}$, also shown in Fig. 5, indicates the magnitude of heat exchange. Further, the sign of $\Delta T_{out\text{-}in}$ reflects whether the GSHP system is in heating or cooling mode. Although Foundation A appears to be in cooling mode during the winter months, the building was not occupied until March 2012. Further, the pipe-plug thermocouples in the manifold were not insulated until February 23, 2012, before which they were affected by the temperature of the mechanical room. After March 2012 the two foundations show similar results, which are consistent with normal operation of conventional heat pump systems. Typical of spring weather conditions in Denver, the system transitioned frequently from heating to cooling.

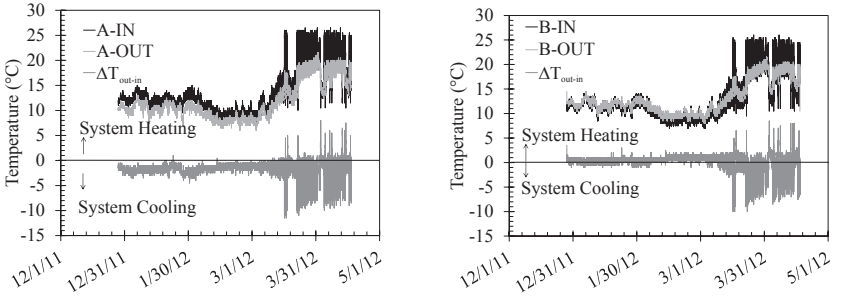

(a) **(b)**

FIG. 5. Inlet and outlet temperatures of the fluid circulating within the heat exchange loops in the foundations: (a) Foundation A, (b) Foundation B

Thermistors at different depths within each of the energy foundations were used to monitor temperature on an hourly basis. Seasonal fluctuations of temperature in each of the energy foundations are shown in Figs. 6(a) and 6(b) for Foundations A and B, respectively. The upper portion of the energy foundations experienced greater fluctuations in temperature than the lower portions. The results in Fig. 6(b) indicate that Foundation B, which is at the edge of the building, is more sensitive to changes in outside ambient air temperature because it is less insulated by the building than the interior Foundation A. After typical operation of the heat pump in March 2012, the temperature distributions within both energy foundations were more uniform, as shown in Figs. 6(c) and 6(d) for Foundations A and B, respectively. The uppermost thermistor in Foundation B is still sensitive to variations in outside ambient air temperature, but not as significantly as before heat pump operation started. Changes in temperature after the heat pump became operational closely mimic fluctuations in the inlet and outlet fluid temperatures shown in Fig. 5.

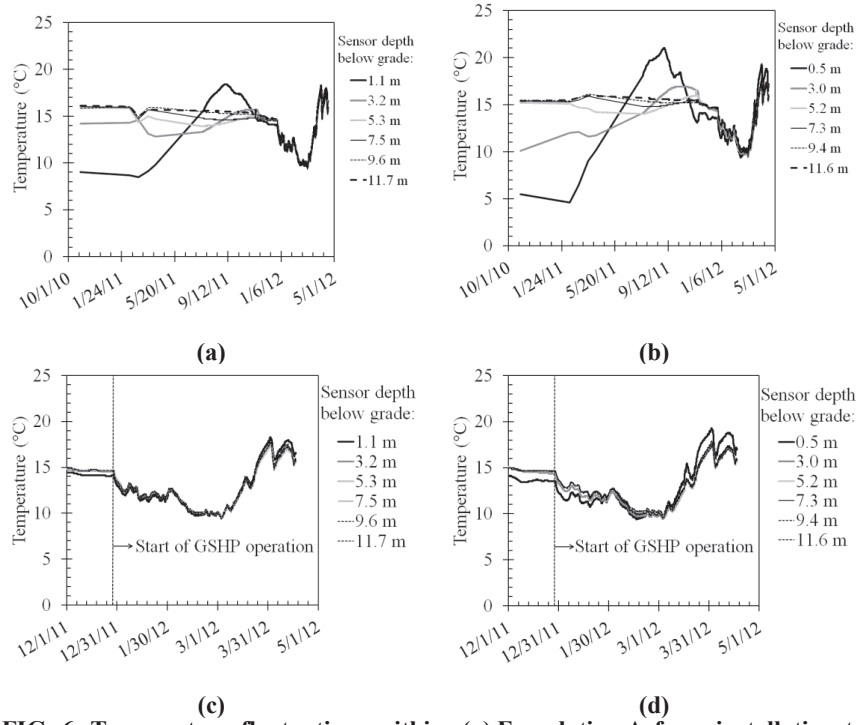

FIG. 6. Temperature fluctuations within: (a) Foundation A from installation to present, (b) Foundation B from installation to present; (c) Foundation A during heat exchange; (d) Foundation B during heat exchange

The heat exchange capacity of the energy foundation can be assessed by evaluating the values of $\Delta T_{out\text{-}in}$ observed in Fig. 5 and the temperatures within the energy foundation. Thermal energy is withdrawn from the ground to heat the building by introducing a cold fluid to the heat exchange loops within the energy foundation, which absorbs heat from the ground and returns to the heat pump at a warmer temperature. Larger values of $\Delta T_{out\text{-}in}$, depending on whether positive or negative, reflect a greater amount of heat either withdrawn from or dumped into the ground, respectively. Typically, a temperature difference of $\Delta T_{out\text{-}in} = 2°C$ between supply and return flow temperature of the heat exchanger fluid is sufficient for normal operation of a heat pump, as long as the temperature of the ground does not start to change significantly (Brandl 2006). The data in Fig. 5 indicates that the maximum differences in inlet and outlet temperatures observed in this project were approximately 10°C, which shows potential for good heat exchange. Further, the data in Figs. 6(c) and 6(d) indicate that during heating operations for the building in January to March 2012 the temperature of the energy foundation tended to stabilize at 10°C, indicating steady flow of heat from the ground into the energy foundation. It appears that the energy foundation reached a steady value during the later months, which are dominated by cooling operations. The inlet and outlet temperatures of the two energy foundations are similar after March even though Foundation B had one more heat exchange loop. This indicates that the number of loops may lead to a more uniform temperature distribution in the energy foundation, but may not improve heat exchange.

Thermo-Mechanical Behavior

An important aspect of this study was to evaluate thermally induced strains in the energy foundations caused by temperature changes. The structure was completed in October 2011 (i.e., the dead load was fully applied), and no further significant changes in mechanical strain are expected after this time (i.e., the live load is a small fraction of the dead load). It is assumed that there is negligible drift in the mechanical strain over time. At this point, the measured strain values ε_m were zeroed by subtracting the mechanical strain $\varepsilon_{mechanical}$, and were corrected to account for thermal effects on the gauge to define the actual thermal strain ε_T in the foundation, as follows:

$$\varepsilon_T = (\varepsilon_{m} - \varepsilon_{mechanical}) + \alpha_s \Delta T \quad (1)$$

where α_s is the coefficient of linear thermal expansion of steel wire (-12 με/°C) and ΔT is the change in temperature of the foundation. This correction is needed because heating causes the vibrating wire to expand, which causes the VWSG gauge to appear to go into compression instead of correctly showing expansion.

Next, the thermal strains were evaluated to assess if they were less than the free expansion strain of reinforced concrete, given by:

$$\varepsilon_{T,free} = \alpha_c \Delta T \quad (2)$$

where α_c is the coefficient of linear thermal expansion of reinforced concrete, which is assumed to be similar to that of the steel wire (-12 με/°C). It is not possible for the foundation to expand or contract more than given by Eq. (2), although it is possible for the thermal strains in the foundation to be less than this, because of soil-structure interaction. A global thermal correction factor of 0.5 was applied to all of the different gauges, which corrects the magnitudes to realistic values but does not affect the trends with depth. The correction factor was defined so that the maximum absolute value of the thermal strain observed in both foundations was less than given by Eq. (2), and empirically corrects for the different thermal responses of the gauge and surrounding concrete. The corrected thermal strains $\varepsilon_{T,c}$ are shown in Figs. 7(a) and 7(b) for Foundations A and B, respectively. In Figs. 7(a) and 7(b), positive strains indicate compression (shortening of the foundation) while negative strains indicate expansion (lengthening of the foundation).

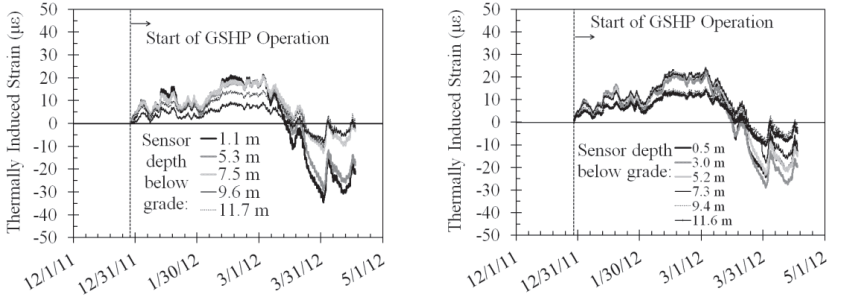

(a) **(b)**

FIG. 7. Thermal axial strain vs. time: (a) Foundation A, (b) Foundation B

In order to define profiles of thermal strain representative of the energy foundation performance, instances in time at which the energy foundations had experienced average changes in temperature of 1°C increments were identified. The temperature profiles for these increments are shown in Figs. 8(a) and 8(b) for Foundations A and B, respectively. The maximum extents of temperature change corresponded to ΔT = -5°C during building heating and ΔT = 3°C during building cooling, with respect to the initial temperature of the foundation at startup of the heat pump. Slight deviations in temperature at the top of the foundations are likely due an influence of warm outside ambient air temperature when the building was in cooling mode.

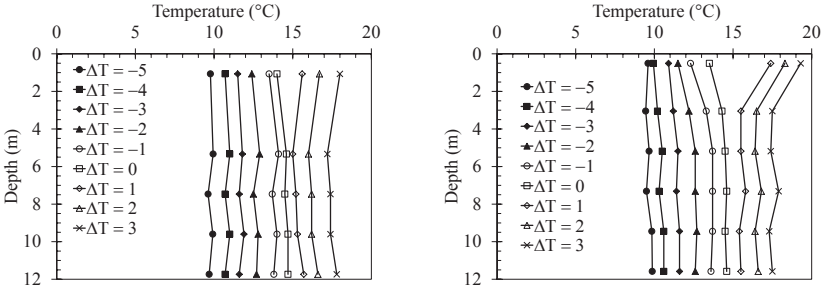

FIG. 8. Temperature profiles within the energy foundations for different average changes in foundation temperature: (a) Foundation A; (b) Foundation B

The profiles of thermally induced axial strain corresponding to the average changes in temperature from Fig. 8 are shown in Figs. 9(a) and 9(b) for Foundations A and B, respectively. If the shafts were free to move during cooling of the energy foundations (i.e., heating of the building), axial contraction occurs as reflected in the positive sign of the strain measurements. Conversely, during heating of the energy foundations (i.e., cooling of the building), axial expansion occurs as reflected in the negative sign of the strain measurements. The maximum thermally induced axial strain was 24.0 με in Foundation B during a temperature change of ΔT = -5°C, while the minimum thermally induced axial strain is -30.81 με in Foundation A under a temperature change of ΔT = 3°C. Because the strain data was corrected empirically to ensure that the measured values would all be less than the free thermal expansion of the foundation given by Equation (2), the strain values are all less than $\alpha_c \Delta T$ for the given change in temperature at a particular depth. The shapes of the thermal strain profiles in both energy foundations are similar to those observed by Stewart (2012) for end-bearing foundations tested in the centrifuge. Specifically, the smallest strain is observed at the bottom of the foundation, indicating that the foundations are expanding upwards from the relatively rigid bedrock. For the maximum change in temperature of 3°C during heating of the foundation observed in the data collected to date, a maximum axial displacement of 0.003 mm (0.00001 in) is expected, which is unlikely to cause damage to the building.

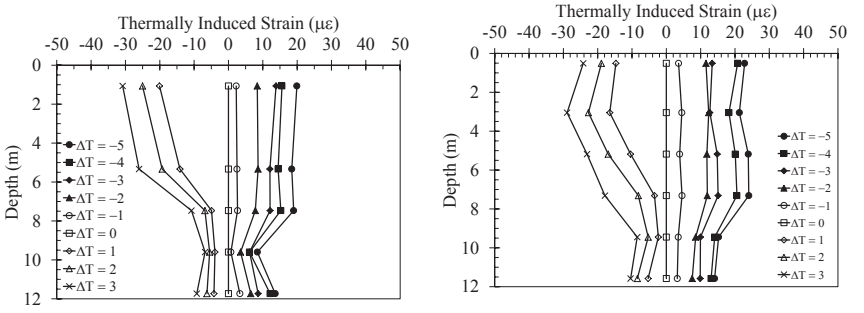

(a) **(b)**

FIG. 9. Thermal axial strain profiles for different average changes in energy foundation temperature: (a) Foundation A; (b) Foundation B

The maximum compressive and tensile profiles of thermally induced strain observed during heating and cooling of the energy foundation were superimposed upon the strains due to mechanical loading to define the total thermo-mechanical axial strains, as shown in Figs. 10(a) and 10(b) for Foundations A and B, respectively. The mechanical strain profiles are difficult to interpret; it was expected that the greatest axial strain would be observed near the top of the foundation, and would either decrease with depth if there was side shear resistance or remain uniform with depth if there was negligible side shear resistance. However, both foundations show an inconsistent mechanical strain profile with depth. This is attributed partially to the impact of curing on the calculation of the mechanical strains in the foundations from the raw VWSG readings. Nonetheless, the magnitudes of the average mechanical strains are consistent with the design axial loads for the foundations, assuming a Young's modulus of 30 MPa. Regardless of the shapes of the mechanical strain profiles, it is clear that heating and cooling operations lead to a shift in the thermo-mechanical strain profiles to the left or right. The thermal strains are not as significant as those generated due to the self-weight of the building, with magnitudes well below those which may cause structural damage. Further monitoring is needed to see if thermal strains during cooling lead to tensile strains near the bottom of the foundations.

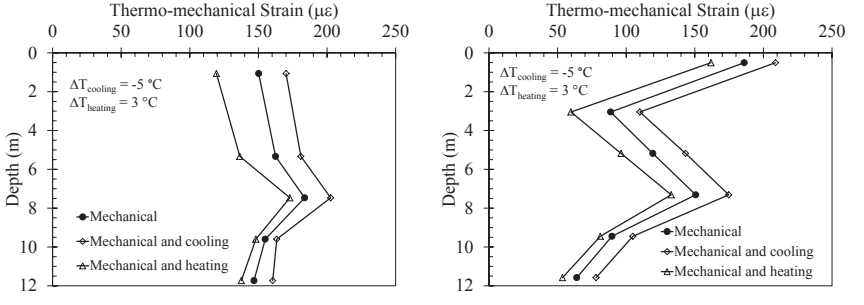

(a) **(b)**

FIG. 10. Thermo-mechanical axial strain profiles: (a) Foundation A; (b) Foundation B

The thermal stresses σ_T induced in the foundation by temperature changes can be calculated as follows:

$$\sigma_T = E(\varepsilon_T - \alpha_c \Delta T) \quad (3)$$

where E is the Young's modulus of reinforced concrete which is assumed to be 30 MPa (4.35 ksi), ε_T is the measured thermal strain after correction, and $\alpha_c \Delta T$ is the free expansion strain of the reinforced concrete. The thermal stress profiles calculated from the data in Figure 9 are shown in Figures 11(a) and 11(b) for Foundations A and B, respectively. The locations of the smallest strain in the energy foundation correspond to the locations of the maximum thermal stress. Compressive (positive) thermal stresses occur during heating when the axial expansion of the foundation is restrained by the overlying building, underlying bedrock, or the side shear resistance of the soil surrounding the foundation. With the exception of the high thermal stresses noted at the top of Foundation B during heating, which are likely due to the higher ambient temperature at this time, the stress profiles indicate that the highest stresses are at the bottoms of both foundations. The decrease in compressive stress with height is due to resistance from side shear stresses during thermal contraction or expansion. It is also possible that the smaller stresses noted in Foundation B between depths of 2 and 6 meters may have occurred due to residual stresses encountered during cooling of the foundation, which deserves further study.

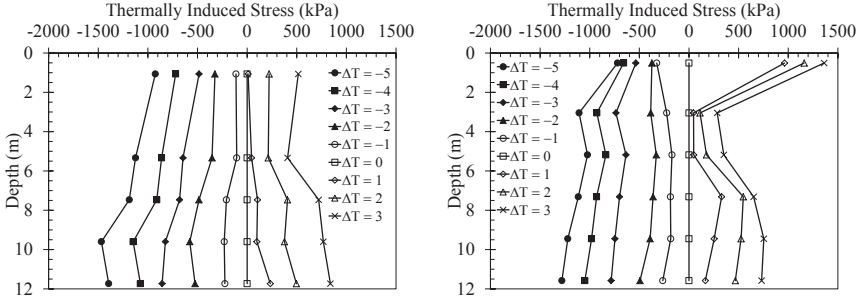

FIG. 11. Thermal axial stress profiles: (a) Foundation A; (b) Foundation B

CONCLUSIONS

The results from a thermo-mechanical evaluation on two full-scale energy foundations in a building in Denver, Colorado during typical building heating and cooling operations indicate potential for energy foundation technology in Colorado. The heating and cooling operation indicates that the energy foundation can sustainably provide the base heating and cooling loads for buildings. Further, analysis of data collected from strain gauges embedded in the energy foundations indicates that the magnitudes and trends of thermal axial strains and stresses are consistent with end-bearing foundations and are not expected to lead to structural issues.

ACKNOWLEDGEMENTS

The authors acknowledge the support of Milender-White Construction Company, AMI Mechanical, Rocky Mountain Geothermal, and the Denver Housing Authority

for incorporating the energy foundations into the building. Financial support from National Science Foundation grant CMMI 0928159 is gratefully acknowledged.

REFERENCES

Adam, D. and Markiewicz, R. (2009). "Energy from Earth-Coupled Structures, Foundations, Tunnels and Sewers." *Géotechnique*. 59(3), 229–236.

Bourne-Webb, P., Amatya, B., Soga, K., Amis, T., Davidson, C. and Payne, P. (2009). "Energy Pile Test at Lambeth College, London: Geotechnical and Thermodynamic Aspects of Pile Response to Heat Cycles." *Geotechnique* 59(3), 237–248.

Brandl, H. (2006). "Energy Foundations and other Energy Ground Structures." *Géotechnique*. 56(2), 81-122.

Hughes, P.J. (2008). *Geothermal (Ground-Source) Heat Pumps: Market Status, Barriers to Adoption, and Actions to Overcome Barriers*. Report ONRL-2008/232.

Knellwolf, C. Peron, H., and Laloui, L. (2011). "Geotechnical Analysis of Heat Exchanger Piles." *ASCE Journal of Geotech. and Geoen. Eng*. 137(10). 890-902.

Laloui, L., Nuth, M., and Vulliet, L. (2006). "Experimental and Numerical Investigations of the Behaviour of a Heat Exchanger Pile." *IJNAMG*. 30, 763–781.

McCartney, J.S., LaHaise, D., LaHaise, T., and Rosenberg, J.E. (2010). "Feasibility of Incorporating Geothermal Heat Sinks/Sources into Deep Foundations." *ASCE GSP 198*. M. Hussein, W. Camp, and J. Anderson, Eds. 12 pg.

McCartney, J.S. and Rosenberg, J.E. (2011). "Impact of Heat Exchange on the Axial Capacity of Thermo-Active Foundations." *GeoFrontiers 2011*. Dallas, TX. 10 pg.

McCartney, J.S., Rosenberg, J.E., and Sultanova, A. (2010). "Engineering Performance of Thermo-Active Foundation Systems." *GeoTrends 2010*. ASCE GPP 6. Goss, Kerrigan, Malamo, McCarron, and Wiltshire, eds. pg. 27-42.

McCartney, J.S. (2011). "Engineering Performance of Energy Foundations." *2011 PanAm CGS Geotechnical Conference*. Toronto, Canada. October 2-6, 2011. 14 pg.

Moel, M., Bach, P., Bouazza, A., Singh, R., and Sun, J. (2010). "Technological Advances and Applications of Geothermal Energy Pile Foundations and their Feasibility in Australia." *Renewable and Sust. Energy Rev*. 14(9), 2683-2696.

Ozudogru, T., Brettmann, T., Olgun, G., Martin, J., and Senol, A. (2012). "Thermal Conductivity Testing of Energy Piles: Field Testing and Numerical Modeling." *GeoCongress 2012*. Oakland, CA. Mar. 25-29 2012. 10 pg.

Stewart, M.A. (2012). *Centrifuge Modeling of Strain Distributions in Energy Foundations*. MS Thesis. University of Colorado Boulder. 110 pg.

Wood, C. J., Liu, H. and Riffat, S. B. (2009). "Use of Energy Piles in a Residential Building, and Effects on Ground Temperature and Heat Pump Efficiency." *Géotechnique.* 59(3), 287–290.

Geotechnical Challenges for the South Coast Water District Tunnel Rehabilitation and Sewer Pipeline Replacement Project

David Jurich[1], P.E., M. ASCE, Joseph McDivitt[2], and Tim Lawson[3], C.E.G., G.E.

[1]Manager, South Central West, Hatch Mott MacDonald, 198 Union Boulevard, Suite 200, Lakewood, CO 80228; david.jurich@hatchmott.com
[2]Director of Operations, South Coast Water District, P.O. Box 30205, Laguna Niguel, CA 92607-0205; jmcdivitt@scwd.org
[3]Geotechnical Engineer, LGC Geotechnical, Inc., 120 Calle Iglesia, Suite A, San Clemente, CA 92672, tlawson@lgcgeotechnical.com

ABSTRACT: The South Coast Water District Sewer Tunnel was constructed in 1954 and contains a 61 cm (24 in) gravity sewer pipeline critical to the District's South Laguna Beach, California sewer system. Timber supports in the 1.8 m (6 ft) high by 1.8 m (6 ft) wide, 3,192 m (10,474 ft) long tunnel are deteriorated and jeopardize the pipeline that conveys an average of 4.73 million liters (1.25 million gallons) of wastewater per day within a highly sensitive coastal environment. Emergency repair were completed to a 122 m (400 ft) long interval of the tunnel in 2007. Planning and design are underway for the rehabilitation of the balance of the tunnel and replacement of the pipeline. The District is proactively addressing and mitigating geotechnical risks, securing additional easements and access rights, and planning the rehabilitation to ensure continued service during construction. As part of a risk management strategy, the District has implemented an innovative project delivery approach of early contractor involvement coupled with a Target Price contract. This paper will review how lessons learned and an innovative contracting project delivery strategy can be applied to the rehabilitation of aging Rocky Mountain water conveyance tunnels.

INTRODUCTION

South Coast Water District (District) operates the Sewer Tunnel in South Laguna Beach, Orange County, California between the community of Three Arch Bay and Aliso Beach (Figure 1). The 3,192 m (10,474 ft) long tunnel was constructed in 1954 and houses a 61 cm (24 in) gravity sewer interceptor pipeline critical to the District's sanitary sewer collection system. Periodic inspections since the 1990s have documented deterioration of large intervals of the tunnel with failing timber supports and an increasing frequency of rock falls that endanger the sewer pipeline. Pipeline

flows average 4.73 million liters (1.25 million gallons) per day and a rupture would result in discharge of untreated sewage onto the beach and a potentially catastrophic environmental event. Therefore, the District made rehabilitation of the tunnel and pipeline replacement a priority. The District has adopted proactive measures to identify and manage the operational, environmental, community, and geotechnical risks associated with the project. This paper describes the District's alternative project delivery strategy to addressing high risk geotechnical challenges of deteriorating tunnel support, poor quality rock, low ground cover, and slope stability concerns all of which are typical risks for mountainous water conveyance tunnels.

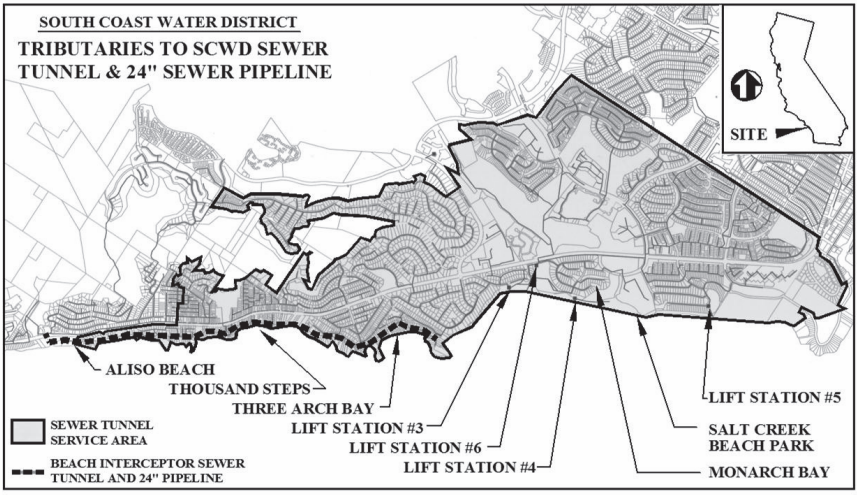

FIG. 1. Location of Beach Interceptor Tunnel

PROJECT DESCRIPTION

Project Setting

The tunnel is situated in a seaside community on a coastal terrace. The terrace is generally level and terminates at wave cut sea cliffs that range in height from a few meters to nearly 43 m (140 ft) above sea level and provide some of the most desirable and exclusive home sites along the California Coastline. Constructed in 1954 when the project alignment was sparsely populated, the tunnel and sewer have operated in relative obscurity while home development has completely occupied the surface above. The original vitrified clay pipeline was replaced with a Techite pipeline and limited structural repairs were made to the tunnel in 1974. Altogether more than 200 oceanfront homes are now located above or adjacent to the tunnel.

Geological Setting

The tunnel is located within a coastal bluff comprised of marine and non-marine terrace deposits which directly overlie the wave-cut platform of an elevated marine terrace in the Laguna Beach area. The wave-cut platform was created by prolonged wave erosion just below sea level into the Tertiary San Onofre Breccia bedrock. The wave-cut platform was formed during high sea-level interglacial periods of the Pleistocene Epoch. Deposition of the non-marine terrace material on the wave-cut platform occurred as the sea-level fell and during low sea-level glacial periods. The platform was further exposed to non-marine deposition as a result of regional uplift of the San Joaquin Hills, which continues today.

The lower approximately two thirds of the coastal bluff is generally comprised of steep to near vertical exposures of the San Onofre Breccia ($Tso_)$. The upper approximately one third of the coastal bluff is comprised of steep to more subdued exposures of the terrace deposits (Qt). Variable amounts of fill are present above the terrace deposits and adjacent to portions of the bluff. Isolated landslides are also evident along the bluff face. Beach sands (Qb) are typically present at the base of the bluff.

Generally, the San Onofre Breccia consists of massive to thickly bedded weakly cemented sandstone and breccia. Locally the breccia is thickly interbedded with massive to well-bedded siltstone, conglomerate, and shale. The angular clasts of the breccia are derived from the Catalina Schist source basement rock offshore to the west. Occasional silt and clay beds are also observed within the breccia. The San Onofre Breccia is generally considered one of the more resilient bedrocks within Orange County.

Bedding within the San Onofre Breccia dips generally between 10 to 25 degrees. The orientation of the bedding is variable, with the variability appearing to be controlled by faulting. Bedding within the terrace deposits typically mimic the trend of the underlying wave-cut platform, which is typically found to dip from 5 to 15 degrees in a southwesterly direction.

Joints have not been observed and fractures are rarely present in the San Onofre Breccia. When fractures are observed in the tunnel they occur as a single discontinuity and do not form wedges.

Faulting

While faults have been identified on the site, no active or potentially active faults have been mapped transecting the tunnel alignment. However, the San Joaquin Hills Blind Thrust is estimated to be located approximately 2.7 km (1.7 mi) to the north of the site, and the offshore portions of the Newport Inglewood fault are located approximately 3.2 km (2.0 mi) to the south. These faults are predicted to be capable of magnitude 6.6 and 7.1 earthquakes. Inactive minor faults and shears were mapped

at several locations along the bluff face. The orientations of these features are variable and the dips are typically moderate to steep. The largest faults trend approximately north to south and are near vertical.

Original Tunnel Construction

The tunnel was hand mined and blasted with access through adits and portals located at public and private beaches. Several adits and one portal have collapsed and are now abandoned. Most of the tunnel is horseshoe shaped and unsupported, but approximately 914 m (3,000 ft) is supported by timber struts and wooden lagging. Typical tunnel cross sections of the unsupported and timber supported intervals are presented in Figures 2.

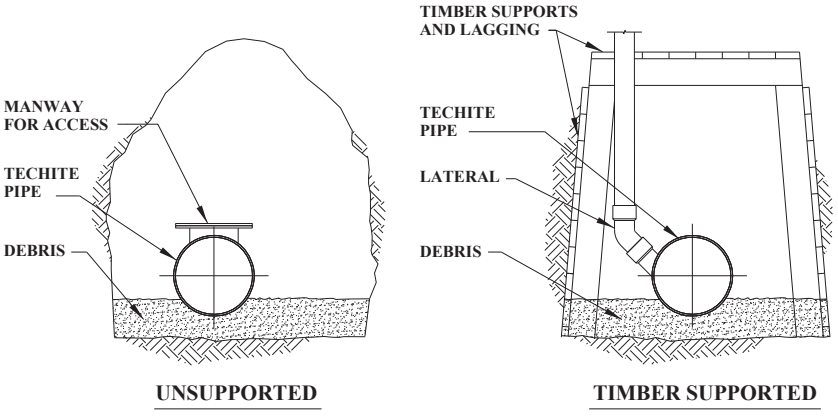

FIG. 2. Typical Cross Sections of Unsupported and Timber Supported Tunnel

GEOTECHNICAL HAZARDS

The geotechnical hazards for this tunnel, described below, are familiar to those who have worked on tunnel projects in mountainous terrain. Detailed geotechnical investigations, as completed for this rehabilitation project, are recommended to identify and thoroughly characterize project specific geotechnical risks.

Slope Stability

Both liquefaction zones and zones of potential earthquake-induced landslides exist along portions of the tunnel alignment as depicted on the State of California Seismic Hazard Zones for Dana Point, Laguna Beach, and San Juan Capistrano 7.5 Minute Quadrangles. These zones are general indications of areas where the general conditions suggest the potential of such hazards. These maps were prepared by the State to raise awareness of the potential for such hazards and to prompt appropriate

investigation to evaluate these potentials on a site-by-site basis. The District engaged LGC Geotechnical, Inc. to review published geotechnical reports, interpret project-specific aerial photographs and conduct surface mapping along the entire tunnel alignment to investigate potential landslides, including those identified on the referenced regional geologic map.

A total of six landslides were mapped along the coastal bluff in the vicinity of the tunnel alignment, the following three of which could potentially impact the tunnel. A moderate-sized landslide was mapped on the coastal bluff descending to the beach near the northern end of the tunnel. Most of the area of the landslide is located on private property and is obscured by development and vegetation. Access from the beach was limited and field geologic mapping did not provide any conclusive indication with regard to the potential presence of this landslide. Failure of this landslide could potentially damage one of the construction staging area and therefore impact tunnel construction.

A large, partially repaired, landslide is present in the southern third of the tunnel alignment. The failure was at least partially stabilized through grading and mechanical methods for homes constructed on top of it. It is not clear whether the western portion of the failure was stabilized or remains unstable. The landslide has generally been mapped above and to the north and west of the tunnel and therefore is not anticipated to threaten the stability of the tunnel.

A moderate-sized landslide was identified and mapped near the southern end of the tunnel. Shoring systems have been installed for some of the properties above but no indication of stabilization efforts is apparent for the landslide itself. The portal door to an access adit located within the landslide has been displaced and racked. It appears that a minor cave-in has occurred in the adit where the portal structure has separated from the adit. Based on the assumed geometry of the landslide failure in the overlying soils, the tunnel it is not anticipated to be threatened by additional movement of the landslide. However, additional movement within the access adit due to continued landslide movement is expected.

Groundwater

Groundwater seepage is a persistent condition along the bluff. The groundwater is believed to be the result of rain and irrigation water infiltration into the sandy terrace soils from the higher elevations east of the project area. A perched groundwater condition has developed as the infiltrated water builds up on the less permeable San Onofre Breccia at the base of the terrace deposits. The water is believed to migrate along the base of the terrace, at the terrace/bedrock contact, towards the bluff. Groundwater seepage along the terrace/bedrock contact and through fractures and permeable zones in the underlying bedrock is present year-round. Groundwater levels and rates of inflow into the tunnel fluctuate with the seasons and in response to intense precipitation events.

Much of the tunnel is dry to damp with groundwater seepage present where drainage courses cross the tunnel alignment and at properties with irrigation systems where the ground cover is low. The observed seepage ranges from minor drips from the tunnel crown and sidewalls to small concentrated inflows of less than 0.3 l/s (5 gpm). Groundwater seeping into the tunnel flows along the tunnel invert and collects at the low point where it is removed by pumping.

Low Ground Cover and Rock Quality

While the San Onofre is generally massive, there are intervals where the rock mass is poorly cemented and subject to deterioration. In the first few years after original tunnel construction, the District entered the tunnel several times to install additional timber sets in intervals of spalling ground. Eventually, the District erected bulkheads at two intervals of the tunnel due to ongoing rock deterioration and backfilled the intervals with sand. These intervals have not been entered or investigated since being sealed. District records of the remedial timber work include descriptions of intervals where the tunnel crown has raveled 2-3 m (7-10 ft) above the timber supports. The extent of overbreak and the quantity of cribbing that has been installed in the sealed intervals is unknown.

Recent site investigations completed for the rehabilitation revealed that short intervals of the tunnel are very close to the ground surface. These areas of low cover are composed of soils and/or weathered rock with the tunnel supported by closely spaced timbers and represent a risk of tunnel roof collapse during rehabilitation. Special construction methods were developed for these intervals to provide additional support and mitigate the risk of collapses and daylighting the tunnel.

EMERGENCY REPAIR

Emergency Repair

A preliminary inspection of select portions of the tunnel was performed in 2005 to assess the condition of ground support measures at documented locations of significant rock falls and failure of timber supports. As a result of this inspection, the District authorized emergency repair to a 213 m (700 ft) interval of the tunnel in the middle third of the alignment. The emergency repair completed in 2007 included the following:

- Rehabilitation of portal structure and enlargement of an access adit;
- Encasement of the Techite pipe in concrete;
- Enlargement of the tunnel; and
- Installation of a shotcrete structural lining.

A schematic diagram of the emergency repair is illustrated in Figure 3.

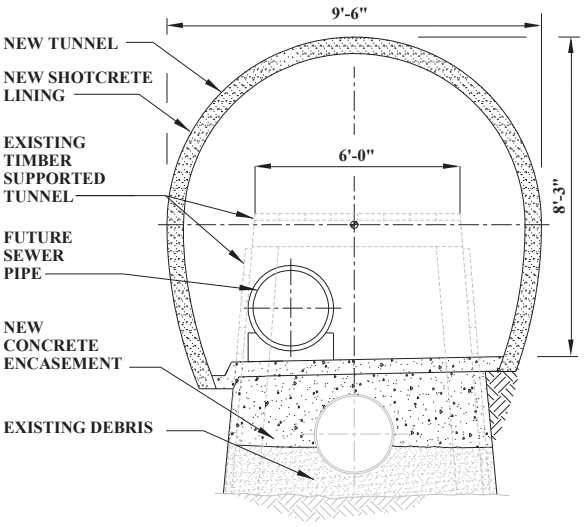

FIG. 3. Schematic of Emergency Tunnel Repair

Ground Behavior

Ground behavior of the deteriorated tunnel was a key concern when planning the emergency repair. Therefore, the design included a "tool box" of various ground support measures from which the contractor could choose as ground conditions changed. Also, an experienced tunnel inspector was on site full time to evaluate the rock as the timber sets and lagging were removed and confirm with the contractor initial ground support measures to be installed. The San Onofre Breccia did not behave as a brittle fractured rock mass but rather could be carved with little to no overbreak and typically exhibited standup time of at least one week with no indications of overstressing or deformation. When exposed, the rock was generally self supporting but there were intervals with up to 1.8 m (6 ft) of deteriorated rock in the crown of the tunnel that either fell out or were barred down with minimal effort. Limited areas of the sidewalls were subject to localized spalling to a depth of 10 cm (4 in) due to partings on weak bedding planes but did not pose a risk of destabilizing the excavation.

Groundwater was present throughout the interval repaired but did not adversely impact construction activities or the stability of the tunnel excavation. Small drips appeared within days of shotcrete lining installation but inflow remained very low. The shotcrete liner was designed with weep holes to prevent buildup of excessive groundwater pressure.

Boulders, up to 1.8 m (6 ft) in diameter, were encountered and required special construction methods. The boulders had significantly higher strength than the surrounding matrix and could not be broken into smaller pieces without causing

significant disturbance to the immediate surroundings. Therefore, the most effective approach was to first build up a spoil pile on the tunnel invert to provide added protection to the concrete encased Techite sewer pipe. The contractor would then loosen and pluck the boulder out of the matrix, remove the boulder and spoil, and shotcrete the excavated profile locally thickening the application in the boulder void.

A photograph of the completed emergency repair is given in Figure 4.

FIG. 4. Completed Emergency Tunnel Repair

Lessons Learned

In addition to protecting the Techite pipe and stabilizing a deteriorated interval of the tunnel, the repair successfully demonstrated the validity of the design and construction methods, yielding several benefits relevant to the full rehabilitation project. These benefits included: a better understanding of environmental constraints; issues associated with community impacts; confirmation of ability to operate tunnel construction equipment over a live concrete encased sewer, characterization of the occurrence of boulders, and observation of ground behavior during excavation in what was considered to be an interval of the tunnel with the poorest quality rock.

While the District and its consultants made every effort to identify and plan for all issues prior to implementation of the emergency repair, valuable data was collected on impacts and the effectiveness of geohazard and public impact mitigation measures. For example, it was surprising to learn that beach visitors did not appreciate the safety risk posed by mobile construction equipment and refused to move out of the way

when construction crews were moving equipment and materials on the beach. As a result, the District implemented two mitigation measures 1) engaging life guards whose direction the beach goers followed, and 2) requiring the contractor to position several additional construction workers as flaggers during movements. As a result of this and other lessons learned, several refinements were incorporated into the planning of the full tunnel rehabilitation, all of which better defined the scope and cost of the work and resulted in a more robust rehabilitation plan with reduced risk. Similar behavior of residents and recreational visitors should be anticipated and mitigation measures identified during planning of water conveyance tunnel rehabilitations.

MITIGATION OF GEOTECHNICAL HAZARDS

The District employed a phased approach to tunnel and geotechnical site investigations. This approach allowed an initial geological characterization, identification of potential areas of concern and subsequent detailed investigations at specific locations. This information was used to design mitigation measures for each of the identified geotechnical hazards. The investigations completed in support of the design of full tunnel rehabilitation provided additional data regarding conditions in the tunnel and at access portals, intervals of low cover, and identified the presence of potentially running sand at the interface between the terrace deposits and the San Onofre Breccia at the new access shaft.

Detailed Tunnel Inspection

A detailed inspection of the entire tunnel was conducted at the time of the emergency repair. A structural engineer and a geotechnical engineer walked all of the accessible intervals of the tunnel and made detailed observations of the ground conditions, support elements, and groundwater occurrences. Table 1 summarizes the percentages of ground support types in the tunnel documented during the preliminary inspection.

Table 1. Summary of Pre-Emergency Repair Support Types

Support Type	Total Distance m (ft)	Percentage of Total Distance
Trenched	117 (384)	3.7
Unsupported	1,665 (5,464)	52.2
Timbers, <3 ft spacing	121 (397)	3.8
Timbers, 4 to 7 ft spacing	1,081 (3,547)	33.8
Shotcrete	184 (603)	5.7
Steel Sets	18 (60)	0.6
Adit 16 Ravine (daylight)	6 (19)	0.2
Total Length	**3,192 (10,474)**	**100**

Documentation of rock conditions included descriptions of features or characteristics expected to impact (good and bad) ground behavior during rehabilitation including:

- Approximately 50 percent of the tunnel has stood unsupported for more than 50 years with minor rock fall outs and no documented collapses.
- Several boulders of Catalina Schist up to 152 cm (60 in) in maximum dimension are exposed in the tunnel and appear ready to fall out.
- The presence of a "rind" of softened rock on the excavated walls of the tunnel. This rind of weathered material, typically 5 cm (2 in) in depth and easily excavated with a geo-pick, was evident on most of the exposed rock surfaces.
- Dipping siltstone, sandstone, and claystone inter-beds of the San Onofre Breccia have delaminated along bedding planes and fallen out creating local areas of overbreak in the sidewalls and crown.

Additional Investigations

Subsequent to the inspection additional adverse geotechnical and man-made conditions were identified at specific areas along the tunnel alignment that required design modifications, special construction methods, and instrumentation and monitoring during construction. These project-specific geotechnical and subsurface hazards include:

- Intervals of low cover (less than 7.6 m (25 ft) of ground above the crown of the rehabilitated tunnel) were identified at a limited number of locations.
- Construction of residential properties after the tunnel was put into service included the installation of several caisson foundation systems. Caisson foundations of a condominium complex are in close proximity to the tunnel and there are no accurate as-built construction drawings. Additional investigations are required to confirm the location and depth of the caissons.
- The concrete slab foundation at the corner of a condominium building is less than 3 m (10 ft) above the crown of the existing tunnel.

The design team worked closely with the geotechnical consultant to develop engineering solutions to address geotechnical hazards. For example, enlarging the tunnel in close proximity to a coastal cliff system required the team to demonstrate the enlarged tunnel would not destabilize the cliffs and consequently the multi-million dollar residences above. In order to demonstrate this numerous geologic cross-sections were analyzed along the length of the tunnel alignment (see Figure 5).

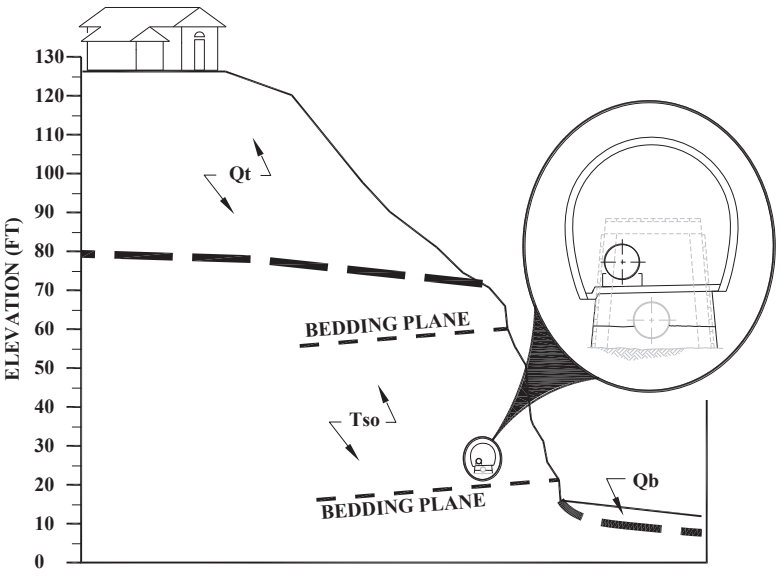

FIG. 5. Typical Cross section of the Coastal Cliff and Tunnel Analyzed for Slope Stability

For each section the geologic and groundwater conditions were carefully depicted and slope stability analyses were performed using the computer program GSTABL7 with STEDwin version 2.002 for both static and pseudo-static (seismic) loading conditions. For seismic analysis, a coefficient of 0.15 was used to model potential seismic loading conditions. Potential rotational and block failure modes were analyzed using Bishop's Modified Method and Janbu's Simplified Method, respectively. The results of the analysis indicated the following:

- Where the tunnel is set back from the bluff, a theoretical failure plane through the tunnel has a very high factor of safety, and widening the tunnel has no significant effect on bluff stability.
- In general the most critical failure surface at each section analyzed is a shallow failure close to the bluff and above the tunnel, mimicking the observed landslides along the tunnel alignment.
- Where the tunnel is close to the bluff, and failure planes are artificially forced through the tunnel, there is a small but measurable decrease in the overall stability of the bluff for the enlarged tunnel with no structural liner
- The enlarged tunnel with a structural liner increases the slope stability factor of safety. In essence the structural liner replaces and increases the strength of the removed rock.

Additional engineering solutions to eliminate or mitigate geotechnical hazards include:

- A combination of pre-excavation support, detailed excavation methods, and additional reinforcing in the shotcrete lining for enlargement of the tunnel in low cover areas.
- Seepage drains to limit the buildup of groundwater pressure on the shotcrete lining.
- Specification of modified low impact tunneling methods and additional support elements where caissons are in close proximity to the tunnel.
- Realignment of the tunnel to avoid conflict with shallow concrete foundations and excessive settlement.

EARLY CONTRACTOR INVOLVEMENT AND TARGET PRICE CONSTRUCTION CONTRACT

Tunnel rehabilitation projects can have a relatively low risk profile due to a generally well defined scope, known ground conditions, and good access to the work. However, in this case, construction activities in the immediate vicinity of a live high-risk sewer pipeline, work within a sensitive environmental setting with multiple geotechnical hazards, and long term construction activities in or near high value communities present a unique set of risks that justified consideration of an alternative to time-and-materials or a low-bid project delivery. The District selected a project delivery strategy that combines Early Contractor Involvement with a Target Price Construction Contract as part of it's a risk mitigation strategy.

An early constructability review during preliminary engineering identified contractor means and methods as critical to mitigating geotechnical risks and justified early contractor involvement during final design. In order to maintain a competitive environment, the District adapted a unique variation of Early Contractor Involvement for the final design:

- Prequalify and select two contractors at the 60 percent design milestone to work with a project design team to complete constructability reviews and prepare an Estimated Target Price.
- Each contractor will work independently with a separate project design team to maintain a competitive environment until a contractor has been selected and an Agreed Target Price is negotiated.

Early contractor involvement during design allows the engineer to understand how the contractor perceives the project risks and tailor the design, where possible, to the contractor's preferred means and methods. Early contractor review also eliminates design ambiguity and "or-equal" options. This collaborative design process reduces the risk of defective design, uncertainty during pricing, and change orders during construction. The specific benefits of this process became evident early in the

constructability review process with both contractors offering innovative cost effective approaches to address high risk elements of the project.

The District recognized that design/bid/build and design/build, while proven project delivery methods for underground construction, could result in contractors carrying substantial contingency money in their pricing for the rehabilitation project in anticipation of hard-to-quantify issues such as complicated access and working around a live high-risk sewer. The District considered several contracting options and selected the Target Price Contract.

The Target Price Contract includes: explicate definitions of direct and indirect costs, open book accounting of all costs, a fair negotiated profit, a clearly defined mechanism for gain and pain sharing, and allowance for changes in scope and pricing. The benefits of a Target Price Contract include reduced risk for the contractor and elimination of built in contingencies and reduced risk of cost overruns to the District due to the gain/pain sharing terms.

CONCLUSIONS

Owners and engineers must be proactive in developing an understanding of the geohazards risks for any underground construction or rehabilitation project being considered. A well conceived and executed approach to planning, investigation, and design should utilize several tools to identify, quantify, and mitigate geohazards risks. Three effective risk management tools employed by the South Coast Water District for its Tunnel Rehabilitation & Sewer Pipeline Replacement Project include:

- Comprehensive multi-phased geotechnical site investigation to identify and characterize geohazards;
- Test Section of a small interval of the tunnel to demonstrate constructability and gains hands on experience with ground behavior; and
- Early Contractor Involvement and Target Price project delivery strategy to obtain contractor input on constructability and control costs.

Regardless of the geotechnical risk management tools employed, sufficient time must be allowed for data gathering, risk identification, development of mitigation measures, and adaptation of a comprehensive Work Plan.

Design and construction of initial ground support measures and lining systems for tunnel rehabilitation projects present unique challenges that must address variable rock conditions, presence of groundwater, and timber supports and lining systems of questionable condition. Water conveyance tunnel owners planning a rehabilitation project should consider specifying an assortment of materials, equipment, and methods and be ready to adapt to changing conditions. Similarly, using a contract that limits large contingencies and fairly compensates the contractor provides the greatest opportunity to cost effectively complete a rehabilitation project within budget and on schedule.

REFERENCES

Hatch Mott MacDonald, (2006). "Tunnel Inspection Report, Sanitary Sewer Interceptor Tunnel, Laguna Beach, California." prepared for South Coast Water District.

LGC Geotechnical, Inc. (2009). "Geotechnical Assessment of the Coastal Bluff Paralleling the South Coast Water District Laguna Beach Sanitary Sewer Interceptor Tunnel, City of Laguna Beach, California, Project No. 081058-01

LGC Geotechnical, Inc. (2010). "Updated Geotechnical Assessment of the Coastal Bluff Paralleling the South Coast Water District, Laguna Beach Sanitary Sewer Interceptor Tunnel, City of Laguna Beach, California." prepared for Hatch Mott MacDonald.

Sancon, Inc., (2003). "Tunnel Inspection and Lateral Survey Report, Sanitary Sewer Interceptor Tunnel, Laguna Beach, California." prepared for South Coast Water District.

South Coast Water District, (2006). "Beach Interceptor Tunnel Emergency Stabilization and Sewer Pipe Protection, South Laguna Beach, California, Design Drawings and Specifications." prepared by Hatch Mott MacDonald.

South Coast Water District, (2007). "Work Plan – Beach Interceptor Tunnel Emergency Stabilization and Sewer Pipeline Protection, South Laguna Beach, California." prepared by eGIS and Hatch Mott MacDonald.

South Coast Water District, (2010). "Recirculated Draft Environmental Impact Report –Tunnel Stabilization & Sewer Pipeline Replacement Protection, South Laguna Beach, California." prepared by eGIS.